Developing the Understanding of Air Pollutant Emissions in Urban Areas:

Using New Analysis and Measurement Approaches

Rebecca L. Wagner

Doctor of Philosophy

University of York

Chemistry

August 2023

Abstract

Volatile organic compounds (VOCs) and nitrogen oxides (NO_x = NO + NO_2) play an important role in the formation of ozone and particulate matter, which can both have detrimental effects on human health. Current understanding of urban air pollution largely relies on fixed monitoring sites, most of which do not include the measurement of VOCs and our understanding of the temporal and spatial variation of air pollutants is limited. Furthermore, there is limited understanding of the contribution made by vehicle exhaust emissions under real-world driving conditions. This thesis aims to develop the understanding of air pollutant emission sources through the development of a mobile laboratory using a selected-ion flow-tube mass spectrometer (SIFT-MS) and other trace gas instrumentation to provide on road, high spatial and temporal resolution measurements of VOCs, NO_x and other trace gases. Two principal approaches are developed: point sampling, where fast response measurements are made of individual dispersing vehicle plumes, and mobile measurements that provide spatial information. New data analysis approaches are developed and tested to quantify vehicle emissions and other emission sources under a range of conditions. Emissions of NO_x and VOCs are quantified for individual classes of vehicles using point sampling data from Milan and motorcycles and mopeds are identified as high emitters of NO_x and VOCs, representing a source type that is currently less stringently regulated. Finally, emission patterns and sources in contrasting urban areas are quantified using mobile measurements collected in York, Manchester and Milan.

Contents

List of Figures

List of Tables

Acknowledgements

Firstly, I would like to thank my supervisors, David Carslaw and Marvin Shaw. Thank you both for always giving me great support, encouragement and guidance. Thank you Marv for being a SIFT wizard and thank you David for always coming up with the best ideas!

Thanks to everyone at the Wolfson Atmospheric Chemistry Laboratories (WACL) who made my PhD so enjoyable. There was always someone there when I needed help and for that I am very grateful. A particular thank you to my row who were always the first ones to offer guidance and who were also pretty fun to be around- thanks for making the day-to-day office life so enjoyable.

Special thanks to Shona and Naomi for always being there for me, entertaining me during field work and just generally being the best gals ever! I am so thankful that I met you both at WACL and I can't wait for lots more fun together in the future.

Thank you to my friends, particularly Jess, Jen and Katie for always being there for me and taking my mind off research whenever I was in need of a break! Thank you to my family, Nana, Gramps, Matt and the rest, for all supporting and encouraging me during my PhD and my academic journey.

To Mum, thank you for being the most supportive Mum out there, for always being my biggest cheerleader and for always believing in me. Thank you so much for all the love, the gardening and the dogsitting, I can't thank you enough for everything you have done for me.

Finally, thank you TJ, for all the love and support that you have given me over my academic life and for always encouraging me to go for that next step. Thank you for cheering me up when I needed it and for always making me laugh. I can't wait for some great adventures together in the future!

Author's declaration

I declare that this thesis is a presentation of original work and I am the sole author. This work has not previously been presented for an award at this, or any other, University. All sources are acknowledged as References. Some of the contained work is based on peer reviewed publications with myself as the lead author or as a co-author the details of which are provided below:

Ch 2 + 5: **Wagner, R. L.**, Farren, N. J., Davison, J., Young, S., Hopkins, J. R., Lewis, A. C., Carslaw, D. C., and Shaw, M. D (2021). **Application of a mobile laboratory using a selected-ion flow-tube mass spectrometer (SIFT-MS) for characterisation of volatile organic compounds and atmospheric trace gases.** *Atmospheric Measurement Techniques* 14, 9, 6083–6100
url: https://doi.org/10.5194/amt-14-6083-2021

Ch 3: Farren, N. J., Schmidt, C., Juchem, H., Pöhler, D., Wilde, S. E., **Wagner, R. L.**, Wilson, S., Shaw, M. D. and Carslaw, D. C (2023). **Emission ratio determination from road vehicles using a range of remote emission sensing techniques.** *Science of the Total Environment* 875, 10, 162621
url: https://doi.org/10.1016/j.scitotenv.2023.162621

Davison, J., Rose, R. A., **Wagner, R. L.**, Wilde, S.E., Wareham, J. V. and Carslaw, D. C (2022). **Gasoline and diesel passenger car emissions deterioration using on-road emission measurements and measured mileage.** *Atmospheric Environment: X* 14, 100162
url: https://doi.org/10.1016/j.aeaoa.2022.100162

Farren, N. J., Davison, J., Rose, R. A., **Wagner, R. L.** and Carslaw, D.C (2021). **Characterisation of ammonia emissions from gasoline and gasoline hybrid passenger cars.** *Atmospheric Environment: X* 11,

100117
url: https://doi.org/10.1016/j.aeaoa.2021.100117

Davison, J., Rose, R. A., **Wagner, R. L.**, Murrells, T. P. and Carslaw, D. C (2020). **Verification of a National Emission Inventory and Influence of On-road Vehicle Manufacturer-Level Emissions**. *Environmental Science and Technology* 55, 8, 4452-4461
url: https://doi.org/10.1021/acs.est.0c08363

Farren, N. J., Davison, J., Rose, R. A., **Wagner, R. L.** and Carslaw, D. C (2020). **Underestimated Ammonia Emissions from Road Vehicles**. *Environmental Science and Technology* 54, 24, 15689–15697
url: https://doi.org/10.1021/acs.est.0c05839

Chapter 1

Introduction

1.1 The importance of air pollution

The largest environmental threat to human health is air pollution, which is defined as *the presence in or introduction into the air of a substance which has harmful or poisonous effects*. Air pollution has been attributed to 6.7 million deaths worldwide in 2019 and is the 4th leading risk factor for early death worldwide, surpassed only by high blood pressure, tobacco use and poor diet[6]. Air pollution can be separated into two categories: indoor (household) and outdoor (ambient), with the latter estimated to cause 4.2 million deaths worldwide in 2019[6] and impacting the majority of humans around the world.

There is much agreement in the scientific community that both short- and long-term exposure to air pollution can cause adverse health effects. Short-term exposure can aggravate asthma and cause spikes in hospitalisations or deaths of other respiratory and cardiovascular diseases[7]. Long-term exposure to air pollution can cause increased risk of illness and death from heart disease, lung cancer, chronic obstructive pulmonary disease, lower-respiratory infections, stroke and type 2 diabetes[7]. There is also growing scientific evidence that exposure to air pollution can cause adverse birth

outcomes[8] and dementia[9]. It is estimated that health damages associated with exposure to air pollution have a global cost of $8.1 trillion[10], which can have detrimental effects on the economic and social development of countries around the world.

In order to combat air pollution, governments around the world have introduced legalisation and regulations to limit the amount of certain air pollutants (which will be discussed in subsection 1.2.2). Over the last few decades, air pollution in many high income countries (e.g the United States and many European countries) has improved due to developments in reduction technologies and the tightening of air pollution-related regulations[11]. Whereas, many developing and low-income countries still struggle to combat various air pollution-related health issues. Many countries in western and eastern sub-Saharan Africa, most countries in south Asia and most of China suffer from the highest attributable air pollution burden. The overall health burden of air pollution in these countries is estimated to contribute between 10-15% to the total burden from all diseases[6]. Global inequalities in the burden of air pollution are clearly evident, but they are also present in developed countries, such as the UK where areas with the poorest households experience the highest concentrations of traffic-related pollution[12]. Furthermore, in most countries around the world air pollutant limits are often not met and high pollution events are common in many urban areas due to high population densities and concentrated emission sources. Therefore, despite vast amounts of evidence highlighting the adverse health effects of air pollution, it still remains a central issue in society today.

1.2 Air pollutants and air pollution legislation

1.2.1 Air pollutants

Air pollution occurs as a direct result of pollutant species in the air, which can have a variety of sources. Sources of air pollutant species can be natural, such as plants and wildfires, and/or anthropogenic (man-made), such as traffic and industry[13]. Furthermore, the presence of pollutants in the air can be a result of primary emissions, where air pollutants are produced and released directly from a particular source, or secondary formation, where air pollutants are formed through chemical reactions between chemical species in the atmosphere. Health and environmental problems related to air pollution are often a result of primary anthropogenic emissions and the resulting production of secondary pollutants, particularly in urban areas where emission sources are concentrated.

As discussed above, air pollutants can have detrimental health effects by increasing the risk of multiple respiratory and cardiovascular disease. Air pollution can also have serious impacts on the environment and ecosystems. Reactions between air pollutants can cause the formation of acid rain and photochemical smog, which can affect plant growth and have serious consequences on diversity in ecosystems[14].

Furthermore, many air pollutants have important climate effects. A common way to examine the climate change effects of atmospheric species is radiative forcing (RF), which evaluates the net change in the energy balance of the Earth's system[15]. A positive RF value indicates that a species reduces the outgoing radiation from the Earth's surface, which can lead to climate warming and climate change effects. Many air pollutants have a positive RF and therefore can play an important role in global warming.

There is a vast number and variety of air pollutant species, but the species that will be discussed below are central to air pollution issues and are often

targeted by legalisation to limit their amount in the air.

1.2.1.1 Volatile organic compounds (VOCs)

Volatile organic compounds (VOCs) are a group of carbon-containing compounds present in mixing ratios at levels of parts per trillion (ppt)-parts per billion (ppb). This excludes carbon dioxide (CO_2), methane (CH_4) and carbon monoxide (CO), which are present at much larger mixing ratios. Examples of VOCs include toluene, benzene, ethanol and isoprene. Exposure to VOCs can cause eye and respiratory irritation and damage to internal organs, such as the liver and kidneys[16]. Furthermore, some VOCs are known carcinogens and can cause cancer, including benzene and 1,3-butadiene[17,18]. VOCs also play an important role alongside NO_x in the formation of tropospheric O_3[19] and PM[20,21] (Section 1.3).

VOCs are emitted from a wide range of sources. Natural sources of VOCs are called biogenic emissions, where VOCs are emitted by plants and soils[22]. Major biogenic VOCs include isoprene, monoterpenes and pinene. This work focuses on VOC emissions from anthropogenic sources. Anthropogenic sources of VOCs include road transport, solvent use, agriculture, volatile chemical products (VCPs) and other industries[23]. VCPs are commonly used consumer and industrial items, including personal care products, cleaning agents, adhesives and pesticides[24,25]. VOCs from road vehicles can be emitted from the vehicle exhaust (tailpipe) or from evaporative emissions, such as from a fuel tank. Vehicular VOC emissions have historically been important, but VOC emissions from vehicle exhaust have been aggressively reduced over the past few decades in Europe through the introduction of technologies such as three-way catalysts on gasoline vehicles, they still present an important source of emissions, accounting for 4% of total UK VOC emissions in 2017[26]. Nevertheless, the reduction in vehicular emissions means it is likely that other sources of emissions, such as VCPs, solvent use, cooking, residential wood burning and industry, have become more important. Mass

balance analysis by McDonald et al. [24] concluded that emissions from VCPs now account for half of the fossil fuel VOC emissions in industrialised cities. Lewis et al. [26] estimated that in 2017 in the UK, solvent use and industrial processes account for 63% of total VOC emissions. This agrees well with NAEI estimates, which estimated that in 2020 in the UK, industrial processes and product use account for 58% of the UK total VOC emissions. Other important VOC sources included agriculture (17%), extraction and distribution of fossil fuels (14%), transport and mobile sources (6%) and stationary combustion plants (5%)[27]. However, the composition and sources of these species in urban areas is highly complex, and it is still difficult to determine the role played by VOCs from road vehicles relative to other sources, particularly due to a lack of measurements of VOCs around the UK.

1.2.1.2 Nitrogen oxides (NO_x)

Nitric oxide (NO) and nitrogen dioxide (NO_2), collectively known as nitrogen oxides (NO_x), are a group of gases primarily formed during the combustion of fuels. The majority of NO_x is emitted as NO and then converted into NO_2 via chemical reactions in the atmosphere (Section 1.3). NO_2 is harmful to human health as it is an irritant of the respiratory system and increases the susceptibility to respiratory infections and diseases[17,28]. NO_x contributes to a wide range of environmental effects including the formation of acid rain, which causes the acidification of soil and water, negatively impacting aquatic organisms and the growth of forest trees and crop plants[29]. Furthermore, NO_x plays an important role in the formation of tropospheric ozone (O_3)[30] and secondary particulate matter (PM)[31](Section 1.3), which have important health and environmental effects and these will be discussed later.

There are various emission sources of NO_x, including many natural and anthropogenic sources. Natural sources of NO_x include lightning and biogenic emissions from soil[32]. However, the majority of NO_x is emitted from anthropogenic sources related to the combustion of fuels, including road

vehicles, other transport and energy and manufacturing industries[33]. Emissions of NO_x from different sources in the UK are estimated by the National Atmospheric Emissions Inventory (NAEI). In 2020, the NAEI estimated that sources that involve the combustion of fuels are responsible for 95% of total UK NO_x emissions in 2020. Road transport was the most important source of NO_x in the UK, accounting for 28% of total UK NO_x emissions in 2020 and the majority of road transport vehicle emissions of NO_x is from diesel vehicles. Other important sources of UK NO_x emissions include other forms of transport (19%), industrial sites (12%) and energy production (10%)[33].

1.2.1.3 Tropospheric ozone (O_3)

Ground-level/tropospheric O_3 is a secondary pollutant formed through photochemical reactions between NO_x and VOCs[19] (Section 1.3). Exposure to O_3 can cause adverse respiratory health effects, such as difficulty in breathing and inflammation of the airways[19,34]. O_3 can aggravate lung diseases and contribute towards the development of asthma[19]. In 2019, exposure to ambient O_3 was estimated to attribute to 365,000 deaths worldwide[6]. O_3 also damages vegetation as it reduces plant growth, which can decrease the diversity of ecosystems[28,35]. Furthermore, the negative impact that O_3 has on plant growth can result in reduced crop yields. The lifetime of O_3 in the atmosphere is approximately 20 days, therefore O_3 can travel long distances to suburban and rural areas and across national boundaries[36]. Therefore, high O_3 levels can be observed far from the emission sources that contribute to its formation. Tropospheric O_3 is an important greenhouse gas, with the 3rd largest positive RF value, surpassed only by CO_2 and CH_4[15], meaning that it contributes significantly to global warming. Furthermore, O_3 plays an important role to the oxidising capacity of the atmosphere and can contribute to greenhouse gas levels (discussed in Section 1.3). Therefore, it is important that emission sources and the chemistry of O_3 precursors are fully understood.

1.2.1.4 Particulate matter (PM)

PM is a type of air pollutant consisting of solid particles and liquid droplets found in the air, which vary in size and composition. The health effects of PM depend on its size as this determines where the particles can deposit in the respiratory system. Particles with a size of 10 micrometers or less in diameter (PM_{10}) deposit in the upper respiratory tract, whereas particles less than 2.5 micrometers in diameter ($PM_{2.5}$) are able to penetrate deep into the lungs and can reach lung alveoli[17]. Studies have shown that exposure to high concentrations of $PM_{2.5}$ over several years has been the most consistent and robust predictor of resulting mortality caused by air pollution[36]. Exposure to $PM_{2.5}$ can cause many adverse health effects as the small size of the particles means that they can enter the bloodstream and travel to vital organs, causing cardiovascular disease and mortality, diabetes and adverse birth outcomes[37]. There is also growing scientific evidence that exposure to $PM_{2.5}$ can cause cognitive decline, leading to cognitive diseases such as dementia[9] and Alzheimer's[38]. $PM_{2.5}$ has been identified as the leading air pollutant of concern with regards to human health and was estimated to be attributable for 4.14 million deaths worldwide in 2019[6]. PM also has important climate effects and can have cooling or warming effects depending on it's composition. Black carbon, from anthropogenic combustion, contributes to warming, but particulate sulphates, from volcanic eruptions or secondarily produced through oxidation of sulphur dioxide, can cool the earth's atmosphere[15].

PM can be primarily emitted and also produced via secondary chemistry. Natural primary sources of PM include sea salt, dust, airborne soil and volcanic ash[39]. Anthropogenic primary sources of PM include road traffic, coal-burning power plants, industrial activities, waste burning and cooking[39]. Road traffic exhaust emissions have historically been of central importance to PM emissions, but this has declined in most of the developed world as vehicle emission control technology has developed[40]. This had led

to emerging sources of $PM_{2.5}$ including non-exhaust emissions from road traffic (brake and tyre wear), cooking and domestic wood combustion[39]. Secondary PM is formed from photochemical reactions of VOCs in the presence of NO_x[21] (Section 1.3 or other chemical reactions between air pollutant species, such as NH_3[41]). Secondary PM is composed of both inorganic and organic compounds. Measurements of secondary inorganic PM are well-established due to formation pathways of secondary inorganic PM being well understood[42]. However, it is difficult to determine primarily emitted to secondarily produced organic PM, due to formation pathways being less understood. The secondary component of organic PM can be estimated using measurement of tracers or precursors, alongside the understanding of formation pathways that can be obtained from laboratory measurements[42]. Yin et al. [43] estimated that 19% of organic PM resulted from secondary production during a London winter measurement campaign in 2012[43]. The contribution of secondary PM is likely to be much higher in summer, with higher ambient temperatures and solar intensity, which encourage photochemical reactions. Furthermore, it is important that the emission sources of PM precursors are well understood in order to combat health and environmental issues related to PM.

1.2.2 Legislation and regulation of air pollution

Air pollution has been of central importance for many decades in the UK due to the negative impacts it can have on human health and the environment. Therefore, a vast amount of legalisation has been introduced to regulate or limit levels of air pollution in the UK.

Air pollution issues in the UK came to the forefront with the industrial revolution during 1750-1950. The industrial revolution was a period of rapid growth in developing cities with major scientific and technological development, fuelled by increased coal combustion. Rapid growth led to

increased emissions of sulphur dioxide (SO_2), NO_2, ammonia (NH_3) and smoke and the degradation of air quality in urban areas or areas close to large industrial sources[44]. Air pollution was accepted as a consequence of industrial activity, until the great smog of London in 1952. In early December 1952, there was increased coal burning due to cold weather in London. The meteorological conditions at the time were low wind speed and cold surface air, which greatly reduced the dispersion of air pollution and resulted in thick smoke/smog across London for five days. The London smog event has been estimated to have resulted in approximately 12,000 premature deaths[45]. The smog event led to the introduction of the Clean Air Act in 1956 in the UK, which established smoke-free areas in cities, led to the relocation of power stations to more rural areas[46] and resulted in reductions of SO_2 and smoke in urban areas. However air quality still remains a leading problem decades later and legislation has been updated to combat new air pollution issues.

Governments around the globe introduce and develop legislation to mitigate health and economic effects resulting from air pollution. The World Health Organisation (WHO) sets out air quality guidelines, which proposes concentration limits for specific air pollutants including PM, O_3, NO_2, SO_2 and CO. Limits for air pollutants are evidence-based recommendations and are expressed as upper limits occurring over a period of time (annual, daily, hourly). WHO air quality guidelines were first released in 1987 and the most recent updates have been in 2005 and 2021. The 2021 guidelines significantly reduced the suggested limits of air pollutants and highlighted health effects of air pollutants even at low concentrations. Details of WHO air pollutant limit guidelines from 2005 and 2021 are included in Table 1.1. Air quality guidelines set by the WHO are not legally binding, but are designed to offer guidance to national, regional and local governments in reducing the health impacts of air pollution[47]. Not all countries around the world will be able to fully implement the guidelines as they may not be feasible given

their economic or technological capabilities.

The UK's limits for air pollutants are set by the Department for Environment, Food and Rural Affairs (DEFRA). Details of the current limits for air pollutants in the UK are shown in Table 1.1. Air quality limits for the UK were last updated in 2010 and are lagging behind the more stringent guidelines set by the WHO. The current limits for $PM_{2.5}$, PM_{10} and SO_2 in the UK are higher than the 2005 WHO guideline values and limits for NO_2 are higher than the 2021 WHO guideline values. Under the Environment Act 2021, the air quality strategy for the UK must be updated at least every five years, with a review of the current strategy expected in 2023[48]. $PM_{2.5}$ targets have recently been reduced to 12 μg m^{-3}, with this target aiming to be met by 2028[49]. Air quality limits in the UK are likely to be reduced, but how effective the reductions will be is unknown. In addition to the air pollutants shown in Table 1.1, the UK also has specific limit values for benzene and 1,3-butadiene. The annual average for benzene should not exceed 5 μg m^{-3} and the running annual meal of 1,3-butadiene should not exceed 2.25 μg m^{-3}[50].

PM and O_3 have relatively long lifetimes in the atmosphere and they can travel across regional and national borders. Therefore, air quality in the UK can be affected by the emissions from nearby countries and UK action alone to control their emissions will have a limited effect. Furthermore, international action is required to address trans-boundary air pollution issues. Historically, legislation in the UK has been driven by international agreements and European legislation. Air quality limits set by the UK government in 2010 were introduced to meet legislation created by the European Union (EU). In 2008, the EU created the Air Quality Directive, which set limit values for specific air pollutants[51] and these values are still used today in the UK.

The EU directive created legally binding targets and allowed for exceedances of target values a certain number of times in a specific time period.

			WHO Guidelines	
Pollutant	**Averaging**	**UK**	**2021**	**2005**
$PM_{2.5}$	Annual	20	5	10
	24-hour	—	15	25
PM_{10}	Annual	40	15	20
	24-hour	50	45	50
O_3	Peak season	—	60	—
	8-hour	100	100	100
NO_2	Annual	40	10	40
	24-hour	—	25	—
	1-hour	200	200	200
SO_2	24-hour	125	40	20
	1-hour	350	—	—
	15-minute	266	—	—
	10-minute	—	500	500
CO	24-hour	—	4	—
	8-hour	10	10	—
	1-hour	—	35	—
	15-minute	—	100	—

Table 1.1: UK National air quality limits[50], alongside the World Health Organisation (WHO) air quality guidelines (2005 and 2021)[47]. All limit values of air pollutants are in micrograms per cubic meter of air (μg m^{-3}). "Peak season" is defined as the "average of daily maximum 8-hour mean O_3 concentration in the six consecutive months with the highest six-month running- average O_3 concentrations".

For example, the 1 hour limit value of 200 μg m^{-3} for NO_2 cannot be exceeded by more than 18 times per year[51]. In 2014, the EU Commission launched legal proceedings against the UK government for its failure to meet air quality targets for NO_2, as set by the Air Quality Directive[52]. The UK was found to have broken air pollution law by the Court of Justice of the European Union on the 4th March 2021 by "systematically and persistently" exceeding annual limits for NO_2 and for failing to put plans into place to address the problem in the shortest possible time[53]. With the UK leaving the EU in 2018, the role that EU institutions play in monitoring and enforcing air quality targets will be lost. The UK government has proposed the creation of a new independent environmental watchdog to hold the government to account on its environmental obligations[54].

In addition to limits for specific values of air pollutants, there is also legislation related directly to the emission of air pollutants. In the UK, the National Ceiling Regulations 2018 sets total national, UK wide, emission limits for SO_2, NO_x, NH_3, non-methane VOCs and $PM_{2.5}$[55]. The emission limits closely follow those agreed under the internationally approved Gothenburg Protocol, which aims to reduce the impacts of air pollution and to control long range trans-boundary pollution. The National Ceiling Regulations 2018 also sets emission reduction commitments, for which the UK in 2020 met for NO_x, SO_2, non-methane VOCs and $PM_{2.5}$, however it did not meet emission reduction commitments for NH_3[56]. There is other legislation targeting individual emission sources, such as Euro emission standards for road vehicles which can play an important role in contributing to total emissions in urban areas (Section 1.5).

1.3 Chemistry of air pollutants

The troposphere is the lowest layer of the Earth's atmosphere and it is the region that contains the air we breathe. Therefore, it is important that

the chemistry that occurs in this region is well understood, particularly if the regulation of air pollutant emissions is to be effective in reducing air pollution. The major constituents of the troposphere are nitrogen and oxygen (99% collectively), but much of the chemistry is driven by trace gases which make up less than 1% of the troposphere. The concentration of an air pollutant in the atmosphere depends on its emissions from particular sources or production through chemical reactions. But, an air pollutant concentration can also be reduced through chemical reactions with other species, leading to their destruction. The next sections will discuss important chemistry of relevant air pollutants to this thesis.

1.3.1 Tropospheric oxidant species

Atmospheric oxidation is the process that leads to the removal of trace gases through reactions with oxidant species. Atmospheric oxidation leads to the formation of secondary species, such as O_3 and PM, which as discussed in subsection 1.2.1 can be harmful to human health and damage the environment. Oxidant species are very important in the atmosphere as they determine the composition of the troposphere and the amount of secondary pollutants. There are a number of different oxidant species in the atmosphere including hydroxyl radicals (OH), nitrate radicals (NO_3), ozone molecules (O_3) and chlorine atoms (Cl).

1.3.1.1 OH radical

The OH radical is an important oxidant species and is thought to be responsible for the majority of oxidation in the troposphere. OH is the dominant daytime oxidant[57] and a major pathway for its formation is the photolysis of O_3 (Equation 1.1). The photolysis of O_3 produces excited $O(^1D)$ atoms which can react with water vapour to form OH radicals (Equation 1.2).

$$O_3 + hv \longrightarrow O(^1D) + O_2 \qquad (\lambda<340\,nm) \tag{1.1}$$

$$O(^1D) + H_2O \longrightarrow 2\,OH \tag{1.2}$$

In urban environments, the photolysis of nitrous acid (HONO) (Equation 1.3) is considered to be the dominant source of OH, particularly in the morning[58,59]. HONO can be directly emitted from soil, biomass burning and vehicle exhausts. HONO can also be formed through chemical reactions, including the reaction of NO with OH, the reaction of NO_2 on surfaces in the presence of water, the photolysis of particulate nitrate or the oxidation of NO_x[60,61].

$$HONO + hv \longrightarrow OH + NO \qquad (\lambda<400\,nm) \tag{1.3}$$

1.3.1.2 NO_3 radical

During the daytime, NO_3 is rapidly photolysed and it has a lifetime of around 1 minute. However, at night-time the lifetime of NO_3 is much longer and it is considered to be the dominant night-time oxidant[62]. During night-time, NO_3 is produced by the oxidation of NO_2 by O_3[63] (Equation 1.4). The rate constants for oxidation by NO_3 are much lower than the equivalent reactions with OH, however night-time concentrations of NO_3 are 10-100 times higher than OH[64], resulting in NO_3 contributing significantly to night-time oxidation. The oxidation potential of NO_3 depends on the concentrations of nitrogen containing species, as NO_3 can be removed by reactions with NO_2 and NO[65] (Equation 1.5 and Equation 1.6). During daytime hours, NO_3 is photolysed by sunlight (Equation 1.7) and does not contribute significantly to daytime oxidation.

$$NO_2 + O_3 \longrightarrow NO_3 + O_2 \tag{1.4}$$

$$NO_3 + NO_2 + M \rightleftharpoons N_2O_5 + M \tag{1.5}$$

$$NO_3 + NO \longrightarrow 2\,NO_2 \tag{1.6}$$

$$NO_3 + h\nu \longrightarrow NO_2 + O(^3P) \qquad (\lambda < 590\,nm) \tag{1.7}$$

1.3.1.3 O_3 molecule

O_3 is one of the most abundant oxidant species in the atmosphere and it is formed via the photochemical oxidation of VOCs, which will be discussed in detail in subsection 1.3.2. O_3 molecules have a large bond energy and are relatively unreactive, with reaction rates with most VOCs being much lower than those with OH or NO_3[62,66]. However, there are fairly large atmospheric concentrations of O_3 compared to other oxidant species and therefore it can still contribute significantly to the atmospheric oxidation of VOCs[66].

1.3.1.4 Cl atom

There is increasing evidence that Cl atoms can be important atmospheric oxidant species. The main source of Cl atoms is the photolysis of nitryl chloride ($ClNO_2$) in sunlight[67,68] (Equation 1.8). $ClNO_2$ is formed at night through the reaction of chloride-containing aerosols (Cl^-) and di-nitrogen pentoxide (N_2O_5)[69].

$$ClNO_2 + h\nu \longrightarrow Cl + NO_2 \qquad (193\,nm < \lambda < 248\,nm) \tag{1.8}$$

Cl atoms can also be produced through the reaction of hydrochloric acid (HCl) with OH radicals (Equation 1.9)[70]. HCl is directly emitted from industrial processes or through reactions of chloride-containing aerosols with nitric acid (HNO_3)[71]. Another source of Cl atoms is the photolysis of

chlorine molecules (Equation 1.10), which can be emitted from industrial processes, produced from reactions involving chlorine-containing species[72] or from coal combustion and waste incineration[73].

$$OH + HCl \longrightarrow Cl + H_2O \tag{1.9}$$

$$Cl_2 + h\nu \longrightarrow 2\,Cl \qquad (308\,nm < \lambda < 351\,nm) \tag{1.10}$$

The OH radical is considered the most important daytime atmospheric oxidant due to its high reactivity and high atmospheric concentration, when compared to Cl atoms[74]. However, rate coefficients for reactions of Cl atoms with some VOCs have been shown to be up to 200 times faster than equivalent reactions with OH[68]. Furthermore, Cl atom concentrations reach their maximum much earlier in the morning than OH, due to rapid photolysis of accumulated $ClNO_2$ produced over-night[75]. Therefore, high levels of Cl atoms occur when other oxidant concentrations are low and therefore it has the potential to be a significant morning oxidant.

1.3.2 Oxidation of VOCs and formation of O_3

As previously mentioned, O_3 is an important air pollutant because of its adverse health and environmental effects. O_3 is not directly emitted, but formed through a series of chemical reactions in the atmosphere between NO_x and VOCs. The production of O_3 directly relies on the photolysis of NO_2, which is the sole known anthropogenic source of tropospheric O_3[76]. The photolysis of NO_2 produces NO along with an oxygen atom, $O(^3P)$ (Equation 1.11), which then reacts with O_2 to produce O_3 (Equation 1.12). O_3 reacts rapidly with NO (Equation 1.13) to form NO_2 and O_2. Therefore an equilibrium between NO, NO_2 and O_3 is reached with no net formation or loss of O_3- this is called the photostationary state (PSS).

$$NO_2 + hv \longrightarrow NO + O(^3P) \qquad (\lambda{<}420\,nm) \tag{1.11}$$

$$O(^3P) + O_2 + M \longrightarrow O_3 + M \tag{1.12}$$

$$O_3 + NO \longrightarrow NO_2 + O_2 \tag{1.13}$$

However, in the presence of VOCs the conversion of NO to NO_2 is catalysed, resulting in net O_3 formation and the PSS is perturbed. This process is illustrated in the following reaction schemes using OH, as it is the dominant atmospheric oxidant due to its high reactivity and concentration in the atmosphere. VOCs (including CO and CH_4) can be oxidised by atmospheric oxidants to form reactive peroxy radical intermediates (RO_2 or HO_2). VOCs can react with OH in the presence of O_2 to form RO_2 through the abstraction of a hydrogen atom (Equation 1.14). OH can also react with CO to produce HO_2 (Equation 1.15).

$$VOC + OH \xrightarrow{O2} RO_2 + H_2O \tag{1.14}$$

$$CO + OH \xrightarrow{O2} HO_2 + CO_2 \tag{1.15}$$

The peroxy radicals (RO_2 and HO_2) can then oxidise NO to NO_2, whilst producing an alkoxy radical (RO) (Equation 1.16). NO_2 is created without the destruction of an O_3 molecule (as is shown in Equation 1.13), facilitating net O_3 production through the photolysis of NO_2 (Equation 1.11 and Equation 1.12). RO reacts rapidly with O_2 to form a carbonyl (RCHO) and HO_2 (Equation 1.17). In polluted conditions, where there is an abundance of NO_x, there is an additional peroxy radical-catalysed oxidation of NO to NO_2 and the regeneration of OH (Equation 1.18), leading to further increases the production of O_3.

$$RO_2 + NO \longrightarrow RO + NO_2 \tag{1.16}$$

$$RO + O_2 \longrightarrow RCHO + HO_2 \tag{1.17}$$

$$HO_2 + NO \longrightarrow OH + NO_2 \tag{1.18}$$

In cleaner environments, where there is low concentrations of NO, reactions of O_3 with OH and HO_2 radicals lead to losses of tropospheric O_3 (Equation 1.19 and Equation 1.20)[77].

$$O_3 + OH \longrightarrow HO_2 + O_2 \tag{1.19}$$

$$O_3 + HO_2 \longrightarrow OH + 2\,O_2 \tag{1.20}$$

Furthermore, in regions with high VOC and low NO_x concentrations, cross reactions between peroxy radicals can dominate over the reaction with NO (Equation 1.16), which leads to the chain termination of radical cycling (Equation 1.21). Alkyl nitrates are also formed in a minor branch reaction of NO with organic peroxy radicals (Equation 1.22), which become increasingly important as the alkane chain length increases[78].

$$RO_2 + RO_2 \longrightarrow ROOH \tag{1.21}$$

$$RO_2 + NO + M \longrightarrow RONO_2 + M \tag{1.22}$$

As discussed above, OH can play an important role in the oxidation of VOCs in the presence of NO_x, facilitating the net production of O_3. However, at high NO_x concentrations the amount of OH present can be reduced due to the reaction between OH and NO_2 forming nitric acid (Equation 1.23)[79].

$$OH + NO_2 + M \longrightarrow HNO_3 + M \tag{1.23}$$

There is a balance between the formation and loss of tropospheric O_3, which are both highly dependent on the concentration of NO_x and VOCs. The influence of NO_x and VOC mixing ratios on the production of O_3 is illustrated using O_3 isopleth diagrams, as shown in Figure 1.1. The isopleth diagram shows the initial mixture compositions which give rise to the same peak O_3 concentrations and these are connected by the appropriate isopleth. The isopleth diagram shows that O_3 formation is a highly non-linear process in relation to NO_x and VOC mixing ratios[80].

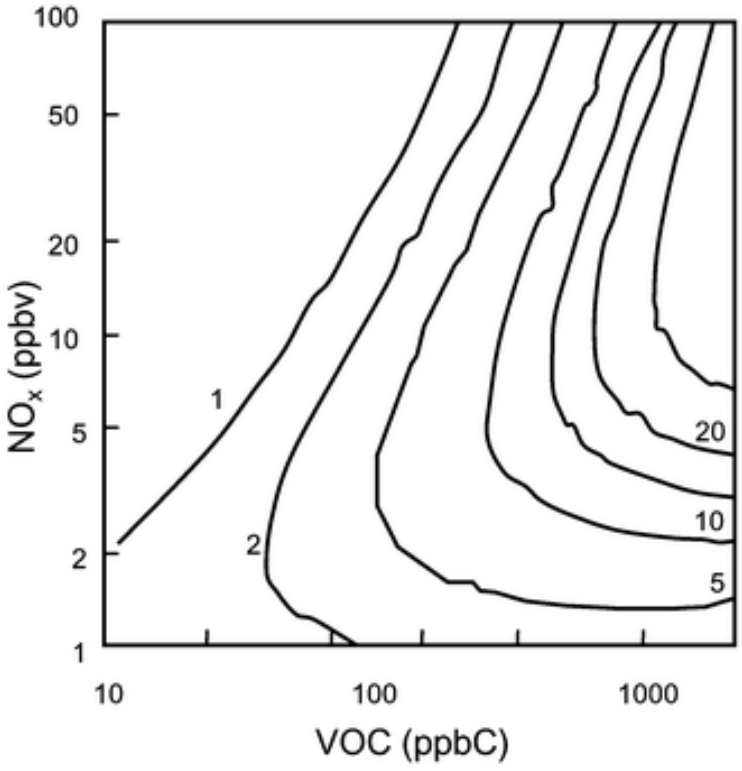

Figure 1.1: O_3 isopleth diagram showing the net rate of O_3 production in ppb h^{-1} as a function of NO_x and VOC mixing ratios. Figure taken from Monks [1].

Figure 1.1 highlights two different photochemical regimes, which are separated by the characteristic ridge line: VOC limited and NO_x limited

regimes. To the left of the ridge line is the VOC limited regime, where VOC/NO_x ratios in this region are typical of highly polluted urban environments. In this regime, lowering VOCs at constant NO_x results in lower peak O_3 concentrations. The same is also true if VOCs and NO_x are decreased proportionately and at the same time. However, lowering NO_x whilst keeping VOCs constant will result in increased peak O_3 concentrations until the ridge line is reached, where the O_3 concentrations begin to decrease[81]. Increased O_3 production when NO_x is lowered and VOCs are kept constant is a result of the chemical reactions discussed above. When NO_x is high, NO_2 competes with VOCs to react with OH radicals (Equation 1.23), slowing the production of peroxy radicals through VOC oxidation. As NO_x is decreased, more OH is available to react with VOCs and O_3 production is increased (Equation 1.14 to Equation 1.18).

To the right of the ridge line is the NO_x limited regime, where VOC/NO_x ratios are characteristic of those in rural and suburban areas downwind of cities. Lowering NO_x either at a constant VOC concentration or in conjunction with lowering of VOCs results in lower peak concentrations of O_3[81]. In this region of high VOC/NO_x ratios, there is a sufficient amount of available peroxy radicals to convert NO to NO_2, therefore reducing VOCs at a constant NO_x has no effect on peak O_3 concentrations. However, the photolysis of NO_2 is an important source of O_3 and therefore reducing NO_x directly leads to a decrease in O_3.

It is important that isopleth diagrams are considered in order for legislation to be effective in improving air quality and reducing the impact of related health and environmental effects. NO_x is often a target for air quality policies due to its emission from vehicles in urban areas, but the effectiveness of NO_x reductions will be highly dependent on the VOC/NO_x ratio in a particular area. Therefore, it is necessary that both VOC and NO_x emission sources in urban areas are well-understood.

1.3.3 VOC chemistry

VOCs play an important role in the formation of O_3 and SOA through reactions with atmospheric oxidants. The oxidation of VOCs forms alkyl radicals (Equation 1.24), which go on to form peroxy radicals in the presence of O_2 (Equation 1.14). The main types of reaction pathways of VOCs include H-atom abstraction from C-H bonds by atmospheric oxidants (OH, NO_3 and Cl), addition of atmospheric oxidants to C=C double bonds (OH, NO_3 and Cl) and OH radical addition to the carbon ring of aromatic compounds[82] and a brief discussion of these reaction pathways is included here.

$$\mathrm{VOC + OH \longrightarrow R^{\bullet} + H_2O} \tag{1.24}$$

The H-atom abstraction reactions occur from C-H bonds in alkanes (Equation 1.25)[83], including C-H bonds in CHO groups in aldehydes (Equation 1.26)[84] and C-H bonds in substituent groups in alkenes and aromatic compounds. H-atom abstraction from vinylic C-H bonds and from C-H bonds in aromatic rings is too slow to be of any significance. H-atom abstraction can also occur from O-H and N-H bonds in the case of alcohols and amines. In the following reaction equations, X = OH, NO_3 or Cl, and R/R' represent substituent groups.

$$\mathrm{X + RCH_2R' \longrightarrow HX + RC^{\bullet}HR'} \tag{1.25}$$

$$\mathrm{X + RCHO \longrightarrow HX + RCO^{\bullet}} \tag{1.26}$$

Atmospheric oxidants can add across C=C double bonds, as is shown in Equation 1.27. Reactions of O_3 with VOCs containing C=C double bonds are complex and lead to the formation of Criegee intermediates, which can undergo further reactions to produce OH[85].

$$X + RCH{=}CHR' \longrightarrow RC^{\bullet}H{-}CH(X)R' \quad (1.27)$$

OH radicals can add to the carbon ring of aromatic compounds to form an OH-aromatic adduct, which is the dominant reaction pathway (90% of the overall OH-aromatic reaction), or to substituent groups attached to the aromatic ring[86].

1.3.4 Secondary organic aerosol formation

The oxidation of VOCs in the presence of NO_x is important for the formation of O_3, but also for the formation of secondary organic aerosol (SOA). SOA is PM formed by the chemical transformation of atmospheric organic compounds[87]. As discussed in subsection 1.2.1, PM is responsible for the majority of air pollution-related health effects and it also has important environmental and climate effects. A substantial proportion of atmospheric $PM_{2.5}$ is made up of organic compounds and is estimated to account for 20-90% of aerosol mass in the lower troposphere[88]. In the Northern Hemisphere, SOA can account for between 64-95% of the total organic aerosol in urban and remote regions[89].

The most important formation pathway of SOA is the oxidation of VOCs, resulting in the formation of products of a lower volatility which can then partition into aerosol particles[82]. VOC precursors of SOA can be emitted from both biogenic and anthropogenic sources. It has been reported that 90% of global SOA resulted from the oxidation of biogenic VOCs[88]. However, field studies have suggested that SOA formed from anthropogenic VOCs can also contribute significantly. Anthropogenic SOA has been reported to contribute 20-25%[57] and over 75%[90] to total organic aerosol, depending on the measurement location. SOA formation is dominated by mainly monoterpenes and aromatic VOCs, which produce high SOA yields[87]. Road vehicles are important sources of SOA precursors in urban areas and emissions from

diesel vehicles may contribute significantly to SOA precursors[91]. However, the understanding of SOA precursor emissions from on-road vehicles is fairly limited and there is a need for vehicular VOC emissions to be studied further.

1.4 Measurements of air pollution in urban areas

1.4.1 Current air pollution measurements in the UK

As discussed in subsection 1.2.2, air pollution and its effects on human health and the environment became an increasingly serious problem after the Industrial Revolution. A variety of legislation targeting the emission of specific air pollutants has been introduced over the last few decades and limits for air pollutants have become increasingly stringent. In the UK, a network for the monitoring of air pollution has been developed over the same time period to determine the effectiveness of this legislation. The measurement and monitoring of air pollutants in the UK was first introduced in 1961 and air pollutants monitored included black smoke and SO_2[92], which were the main air pollutants of concern at the time.

Over the last few decades, the levels of black smoke and SO_2 have been reduced as legislation has been effective in reducing their emission sources. This has resulted in other air pollutants becoming more important from a human health perspective, including PM and O_3. Whilst the most important air pollutants have changed, the air pollutant monitoring network in the UK has developed to provide necessary information on air pollution. In the UK, the Automatic Urban and Rural Network (AURN) is the main air pollution monitoring network. The AURN is used for compliance reporting against the air quality limits and it consists of 171 sites across the UK. The network includes automatic air quality monitoring stations which are located across a variety of sites across the UK, including rural, suburban and urban sites and

the sites are used to represent background, industrial or traffic dominated emissions.

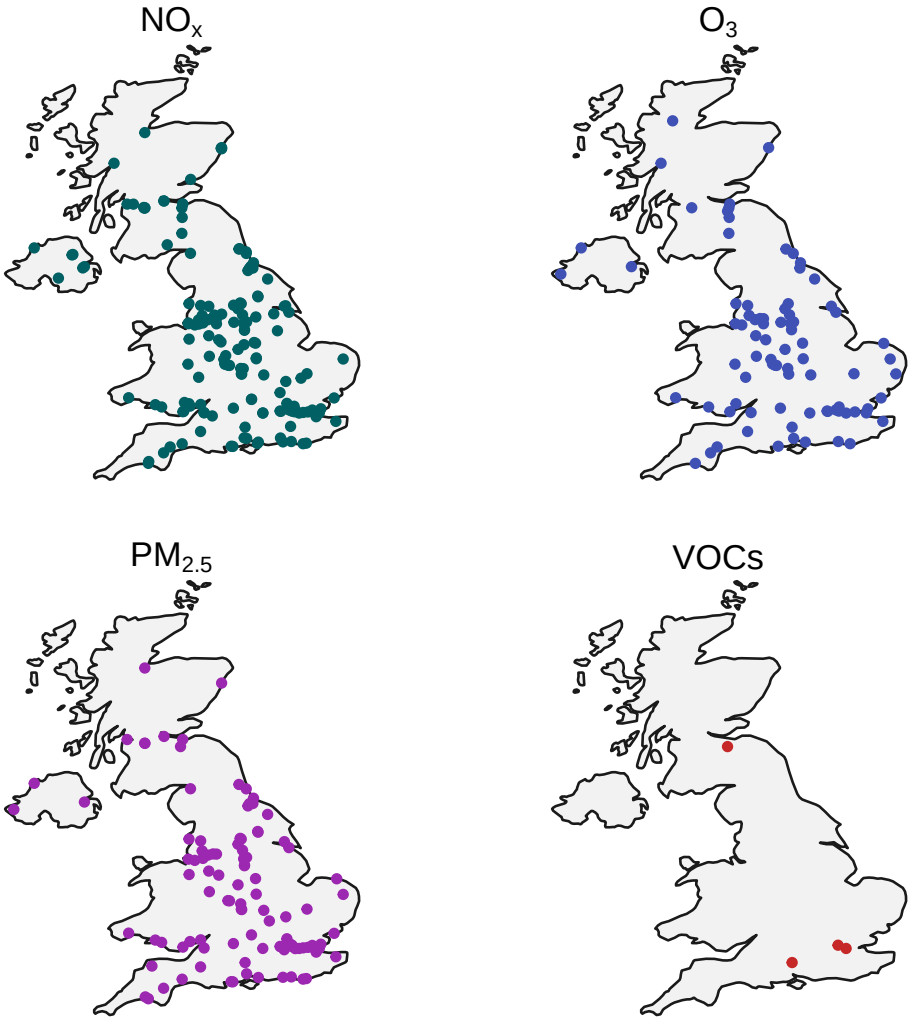

Figure 1.2: Map of the UK with the location of AURN sites for measurements of NO_x, O_3, $PM_{2.5}$ and VOCs.

The air pollutant species measured by the AURN include: NO_x, SO_2, O_3, CO and particles (PM_{10} and $PM_{2.5}$). NO_x is measured at 158 sites, O_3 at 86 sites and $PM_{2.5}$ at 103 sites. There are also online measurements of VOCs, but only at 4 sites around the UK. The sites that measure VOCs are: London Eltham, London Marylebone Road, Chilbolton Observatory and Auchencorth Moss. Figure 1.2 shows the location of AURN measurement

sites of NO_x, O_3, $PM_{2.5}$ and VOCs in the UK. Figure 1.2 shows that the AURN monitoring sites are mainly concentrated in England, particularly in the South of England, with very few in Wales, Scotland and Northern Ireland. Therefore, the spatial resolution of current air pollution measurements in the UK is fairly poor. Furthermore, there is a lack of urban VOC measurements, two of the measurement sites are located in London, one by the roadside and the other representing an urban background, whilst the other two measurement sites are located in rural environments, one in the South of England (Chilbolton) and one in Scotland (Auchencorth). Therefore, important VOC emission sources in urban areas could potentially be missed. Furthermore, even at sites where a VOC measurement is present, only 13 of the 20 most significant VOCs in the UK are measured[26]. This is because set-up of VOC measurements took place around 30 years ago when road transport was the dominant VOC emission source and current measurements do not reflect the change in the contribution of VOC emissions from different sources. In order to overcome current limitations of measurements sites, new urban air pollution research observatories (supersites) in central Manchester, Birmingham and London have been installed in recent years. The supersites monitor key species in atmospheric processes, including NH_3, VOCs, trace metals and particle composition using highly sophisticated measurement instruments[93].

At AURN measurement sites, air pollutants are measured using standardised techniques and operating procedures, ensuring that measurement data from different sites is comparable. NO_x is measured using the chemiluminescence technique[94] and VOCs are measured using an advanced automatic gas chromatograph[95]. The chemiluminescent measurement technique is described in detail elsewhere[96], but a brief description is included here. NO in the sample air stream reacts with O_3 in an evacuated chamber to produce activated NO_2. As it returns to its ground state, a photon is emitted and the intensity of the chemiluminescent radiation produced depends upon the

amount of NO in the sampled air. This light is measured and the detector output voltage is proportional to the NO concentration. The ambient air sample is divided into two streams. In one of the streams, NO is measured directly using the method described above. In the other stream, NO_2 is reduced and converted to NO (with at least 95% efficiency) by passing over a catalyst before the reaction with O_3. The measurement of the second stream represents the sum of NO and NO_2 and therefore the NO_2 concentration is calculated by the difference between the two streams[97]. A problem with this measurement method is NO_2 is not directly measured. During NO_2 conversion to NO, other nitrogen-containing species can also be oxidised by the catalyst and therefore the NO_2 measurement can be overestimated[98].

Automated gas chromatography is used alongside flame ionisation detection to measure VOCs[99]. Gas chromatography is a technique that separates compounds in a gaseous mixture. Gas chromatography involves the use of a separation column, through which the sample mixture flows. The different compounds in a sample mixture are separated as they all have different retention times, so will pass through the column at different rates. Once the compounds are separated they can pass through to the flame ionisation detector, where the amount of individual compounds is quantified. Flame ionisation detection uses a flame to ionise sample compounds, which are then detected using an electrode. The count of the generated ions is proportional to the concentration of the species sampled from the ambient air[100]. Measurements made by the AURN are useful, however they are limited in their spatial resolution (as shown in Figure 1.2) and also in their temporal resolution. AURN measurements of air pollutants are often reported hourly and therefore the temporal variation of pollutants cannot be fully captured by current monitoring in the UK.

Furthermore, in developing and low-income countries, the measurement of air pollutants is less common due to technological and economical barriers. For example, Martin et al. [101] reported that global $PM_{2.5}$ measurements are

so poor that it is difficult to determine which city in the world suffers from the highest concentrations of $PM_{2.5}$. Only 24 out of 234 countries in the world have more than 3 monitors per 1 million inhabitants and 141 countries have no regular $PM_{2.5}$ monitoring at all[101]. Areas in the world that have poor air pollution measurements are likely to be the same areas that suffer from the heaviest health burden as a result of air pollution. Gaps in the measurement of air pollution are often filled in with satellite measurements and modelling. However there is still a need for better ground measurements and the new measurement techniques presented in this thesis are able to provide useful information on a variety of air pollutants and emission sources.

1.4.2 Mobile measurements in urban areas

As mentioned above, the current understanding of urban air pollution relies mostly on hourly or daily measurements of a limited amount of atmospheric pollutants recorded at stationary monitoring sites. These measurements are unable to represent relative contributions of different source types and complex temporal and spatial variations of pollutants. Therefore, there is a need for measurement methods that are able to provide new information on emission types and sources, particularly in urban areas. A measurement method which has been developed is mobile measurements. This approach involves equipping a moving vehicle, typically a van or a car, with fast response instrumentation for measurements of air pollutants. Mobile air pollutant measurements are performed by driving the equipped vehicle around a particular target measurement area, which could be a point source of interest or a variety of possible emission sources in urban areas. Mobile laboratories have been used in many studies for high temporal measurements at fine spatial scales of a variety of air pollutants, including gaseous pollutants[102–108] and particles[102,103,105,109–111].

In recent years, mobile laboratories have been equipped with instruments

to allow for mobile measurements of VOCs. VOCs in urban areas are emitted from a wide range of sources, as discussed in subsection 1.2.1. The measurement instruments that are used in mobile laboratories for quantification of VOCs are mass spectrometers, as will be discussed below. Mass spectrometry is explained in detail elsewhere[112,113], but a brief description of the principles will be included here. Mass spectrometers are analytical instruments used to quantify compounds in a sample mixture. Firstly, analyte compounds are converted into gaseous ions through reaction with reagent ions generated from an ion source within the instrument. The ions are separated in the mass spectrometer according to their mass-to-charge ratio (m/z) and the number of product and reagent ions are measured. The ratio between the product and reagent ions can be used to calculate the amount of the analyte compounds in the sample mixture. The main components of mass spectrometers are an ion source, a mass analyser and a detector.

Studies utilising real-time mass spectrometry in a mobile laboratory use Proton Transfer Reaction Mass Spectrometers (PTR-MS). PTR-MS instruments use the hydronium ion (H_3O^+) as the reagent ion. Early on-road measurements of VOCs using PTR-MS in a mobile laboratory were carried out by the Aerodyne Research Institute in vehicle plume chase experiments[114,115]. More recent measurements carried out by Aerodyne have focused on spatial mapping of petrochemical emissions[116,117]. VOC emissions from the oil and gas industry, such as benzene, toluene and other aromatics have also been investigated using PTR-MS in a mobile laboratory[118]. More recent studies by the NOAA Chemical Science Laboratory research group have used Proton Transfer Reaction Time-of-Flight Mass Spectrometers (PTR-TOF) in mobile laboratories to measure VOCs in urban areas in the US. A PTR-TOF can detect and resolve product ions at much higher mass resolution. Measurements by the NOAA group revealed a variety of VOC emission sources, including VCPs[119–123], livestock farming[124] and residential and crop residue burning[125].

1.5 Vehicle emission legislation and measurements

1.5.1 Background of road vehicle emissions

Road vehicles have played an important role in the development of modern societies, enabling the movement of people and goods. However, they have also been of historical importance to the deterioration of air quality through emissions of air pollutants.

Road vehicles are mostly powered by internal combustion engines fuelled by hydrocarbon-based fuels, such as gasoline (petrol), diesel or natural gas. Combustion is a chemical process of releasing energy from a fuel and air mixture and internal combustion engines operate on this principle. Air is drawn into a fixed cylinder, where it is compressed with fuel and the mixture is ignited. The expanding combustion gases push a piston, which rotates the crankshaft and induces motion in the vehicle. Gases produced from combustion are driven out of the engine through the exhaust (tailpipe) and into the atmosphere- these are exhaust emissions from a road vehicle.

Exhaust emissions from road vehicles include a variety of air pollutants: CO_2, CO, PM, VOCs and NO_x. CO_2 is an important GHG as it has the largest positive RF value and therefore contributes the largest amount towards climate change and global warming. CO_2 is emitted from road vehicles as a by-product of complete combustion (sufficient O_2) of fuel and road transport is the largest emitting sector in the UK, accounting for 24% of the UK's total CO_2 emissions in 2020[126]. CO is a poisonous gas and also plays an important role in O_3 formation (Equation 1.15) and it is produced when incomplete combustion of fuels occur (insufficient oxygen)[127]. As mentioned previously, PM has detrimental health and environmental effects. The contribution of emissions from road vehicles to PM has been declining due to advances in technologies aimed at reducing air pollutant emissions

from vehicle exhausts. However, they remain an important source of PM, particularly in urban areas with high vehicle usage. An important component of PM directly emitted from vehicles is black carbon, which can contribute towards health effects of PM and to global warming and it is formed during incomplete combustion[128], similar to CO.

Combustion engine road vehicles are mostly fuelled by either gasoline or diesel. Both fuels are composed of mixtures of hydrocarbons and both are obtained from the refining and processing of crude oil. Gasoline is more volatile and consists of shorter-chain (5-12 carbon atoms) and aromatic hydrocarbons, whereas diesel is less volatile and consists of longer-chain hydrocarbons (10-21 carbon atoms)[129]. The different fuels are used alongside different engines in road vehicles. The engines used in gasoline-fuelled vehicles are spark ignition engines. In spark ignition engines, gasoline is mixed with air, compressed and ignited using a spark plug, with the amount of air throttled to control the fuel to air ratio. The engines used in diesel-fuelled vehicles are compression ignition engines. In compression engines, diesel is injected into already compressed non-throttled air, the heat of which causes it to spontaneously ignite. Diesel engines are considered more efficient as they produce a higher amount of power and are therefore used in heavier vehicles such as vans, heavy goods vehicles (HGVs) and agricultural equipment. Gasoline engines are typically used in lighter vehicles, such as passenger cars and motorcycles. However, in the UK and Europe there are many diesel passenger cars as a result of diesel vehicles being encouraged by European governments (through monetary incentives, e.g. road tax) in an attempt to mitigate climate change effects, as diesel vehicles emit lower amounts of CO_2[130]. However, the increase in diesel vehicles resulted in the exacerbation of air pollution problems due to higher emissions of NO_x and PM.

Diesel engines operate at higher temperatures and pressures compared to gasoline engines and also run lean, with an excess of air. Due to higher

temperatures and excess air during combustion, diesel engines emit higher amounts of NO_x[131] and diesel vehicles can dominate NO_x emissions in urban areas[132]. PM emissions from diesel engines are considerably higher (6-10 times) than from gasoline engines[133]. As diesel fuel is injected into the engine, it is not completely mixed with air and therefore incomplete combustion can occur, resulting in the formation of black carbon[134].

Another important class of air pollutants emitted from road vehicles are VOCs, which play an important role in O_3 and SOA formation. A variety of VOCs are emitted from vehicles as unburnt/partially burnt fuel, combustion products or evaporative emissions (from the fuel tank). Whilst improvements in reduction technologies of vehicles have succeeded in reducing emissions of VOCs from vehicles, there is a lack of real world VOC measurements from individual vehicles. Therefore it is difficult to determine whether vehicles are significant contributors to VOC emissions and also to identify possible high VOC emitting vehicle and fuel types.

1.5.2 Vehicle emission legislation and reduction technologies

There is a vast amount of evidence that road vehicles contribute significantly to poor air quality, particularly in urban areas where there is a concentrated number of vehicles[135,136]. Therefore, specific legislation related to the regulation of air pollutant emissions from road vehicles has been introduced to reduce the role vehicle emissions play in contributing to poor air quality.

Since 1992, all new road vehicles in the UK and Europe must meet European "Euro" emission standards. Euro standards are set by the European Union and they are a set of regulations which define limits on the acceptable amount of exhaust emissions from vehicles. The aim of the standards is to reduce the emissions of CO, NO_x, HCs and PM. The emission standards are updated every few years and with a new Euro class, the emission limits

tend to become more stringent. Details of Euro standards for passenger cars and motorcycles/mopeds are provided in Appendix B. The next emission standard to be introduced is Euro class 7, which will become mandatory for all new passenger cars in July 2025. The proposed limits for Euro 7 could be expanded to include additional species such as NH_3 and formaldehyde[137].

To combat poor air quality in urban areas many cities have introduced Low Emission Zones (LEZs), which restrict certain vehicle types based on their emissions[138]. A LEZ may cover a few roads or a large inner city area and involves a ban or a charge for certain vehicles, typically older vehicles that emit high concentrations of air pollutants, whilst newer, less-polluting vehicles do not have to pay a charge. The aim of LEZs is to discourage high-polluting vehicles in these areas, resulting in a vehicle fleet with lower overall emissions and an improvement in air quality. The largest LEZ in the world is in London, which was first introduced in 2008, targeting commercial vehicles and aiming to reduce PM concentrations. In April 2019, the Ultra Low Emission Zone (ULEZ) was introduced in central London and was further expanded across all London boroughs on 29th August 2023[139]. The London ULEZ includes a charge for vehicles that do not meet the minimum emission standards, which are Euro class 4 for petrol vehicles and Euro class 6 for diesel vehicles[139]. An assessment of the London ULEZ in 2023 found that it had been successful in drastically reducing air pollutant emissions across London, with emissions of NO_x reduced by 23% and emissions of $PM_{2.5}$ reduced by 7%[140].

In order to reduce the emission of air pollutants and to meet the limits set by Euro emission standards, vehicles are fitted with a range of emission reduction technologies. The aim of the technologies is to either remove or convert emissions after production within a vehicle engine, but before they exit into the atmosphere through the vehicle tailpipe.

The most commonly used reduction technology in gasoline engines is the three-way catalyst (TWC), which effectively became mandatory in 1992 in

the UK with the introduction of Euro 1 standards. TWCs simultaneously oxidise CO and HCs to CO_2 and water and reduce NO_x to N_2[141]. In TWCs, the promotion of oxidation or reduction is highly dependent on the amount of oxygen present in the system. In lean conditions (excess air), the oxidation of CO and HCs is enhanced and the reduction of NO_x is poor. The reverse is true when the TWC is operating under rich conditions (low air), the reduction of NO_x is promoted and the oxidation of CO and HCs is low[142]. TWCs operate efficiently in a narrow air to fuel ratio window and therefore, TWCs are not used in diesel vehicles which operate in lean conditions.

Despite the effective implementation of the TWC in gasoline vehicles to reduce CO, HCs and NO_x, TWCs can form NH_3 as an unwanted by-product[143,144]. NH_3 can be produced during the reduction of NO_x, when the reduction does not stop at N_2 but continues to NH_3[145]. NH_3 contributes significantly to the formation of $PM_{2.5}$[41], which has important adverse health and environmental effects (subsection 1.2.1). NH_3 also plays an important role in nitrogen deposition to ecosystems[146], causing detrimental ecosystem problems such as eutrophication and reductions in plant diversity.

The control of emissions from diesel engines has proved more difficult than gasoline engines. An early technology used to control NO_x emissions from diesel engines was exhaust gas recirculation (EGR). EGR reintroduces part of the cooled engine exhaust back into the combustion chamber, which reduces the oxygen concentration, slows the combustion process and decreases the temperature, therefore reducing NO_x formation[147]. Another diesel emission control technology introduced in the mid-2000s was the diesel oxidation catalyst (DOC). DOCs oxidise CO, HCs and other VOCs to CO_2 and water, whilst also oxidising NO to NO_2[141]. Therefore, DOCs do not reduce overall NO_x emissions and can increase the proportion of NO_2 in NO_x emissions, which is considered to be the more harmful component.

However, the use of DOCs with other diesel emission control technologies can improve their efficiencies. Optimising the ratio of NO to NO_2 using a

DOC supports the performance of selective catalytic reduction (SCR) systems and promotes passive regeneration of diesel particulate filters (DPFs), which are positioned downstream of the DOC[148]. SCR is an after-treatment reduction technology which was introduced to reduce NO_x emissions. SCR systems reduce NO and NO_2 to N_2 using urea as a reductant[149]. During the injection of urea, NH_3 is produced and this can lead to excess NH_3 emissions, commonly termed as an "ammonia slip"[145]. As mentioned above NH_3 has important atmospheric and wider environmental impacts, therefore emission limits for NH_3 have been proposed for the upcoming Euro 7 emission standard. DPFs were introduced to reduce PM emissions and to meet the PM emission standards. A DPF is a structure through which the exhaust gas travels and to which PM adsorbs. As PM is trapped on the filter, DPFs have to be regenerated, which happens by burning off of the particulates[150]. Regeneration can occur when the exhaust reaches high temperatures (motorway driving) or using an active regeneration system which forces an increase in exhaust temperature when the DPF reaches a certain capacity.

The emission control systems discussed above are commonly used in passenger cars. It is worth commenting on the emission control systems present on motorcycles and mopeds as they are an important vehicle type in this work. The majority of motorcycles and mopeds are gasoline vehicles and are therefore fitted with a TWC[151].

1.5.3 Vehicle emission measurement techniques

To test the compliance with emission standards, vehicles undergo laboratory tests on chassis dynamometers. Chassis dynamometers are often called “rolling roads" and are designed to simulate driving in a controlled environment. Vehicles undertake fixed drive cycles which should generate repeatable emission measurements and simulate real driving conditions. Whilst vehicles are driving on the rolling roads, the exhaust gas is output to gas

analysers for emission measurements of the target air pollutants. Chassis dynamometer tests are limited as the tests are time consuming, meaning that a limited number of vehicles can be measured. Furthermore, the "Dieselgate" scandal highlighted discrepancies between laboratory and real-world vehicle emission measurements of NO_x. The Dieselgate scandal is related to the use of a "defeat device" by vehicle manufacturers. A defeat device detects when a car is undergoing an emissions test and optimises the engine performance to minimise air pollutant emissions to meet stringent emissions regulations during tests[152].

As differences between laboratory and real world emissions measurements became apparent, the real driving emissions (RDE) test was introduced. The real driving emissions tests uses a Portable Emissions Measurement System (PEMS) and is used to complement in-laboratory chassis dynamometer tests[153]. PEMS is attached to the tailpipe of a test vehicle and emissions are sampled and analysed as the vehicle is driven. This provides emissions information of a specific vehicle over a period of time and a range of driving conditions. However, it is time consuming and expensive to obtain useful emissions information from a large number of vehicles using PEMS, as only one vehicle can be sampled at a time. Furthermore, whilst PEMS is less susceptible to cheating than in-laboratory tests, it is still possible that vehicles can detect when they are being tested by PEMS and react by changing engine calibration and emission controls[154], resulting in distorted emissions measurements.

Other measurement techniques can also address discrepancies between laboratory and real world vehicle emissions by providing non-intrusive emission measurements under real driving conditions. One of these measurements techniques is cross-road remote sensing. The principles of operation of remote sensing have been described in detail elsewhere[155–157], but a brief overview is provided here. Remote sensing is a non-obtrusive, kerbside method for measuring real-world vehicle emissions. As a vehicle drives

through the remote sensing setup, each individual module of the remote sensing device simultaneously activates. These are an ultraviolet/infrared (UV/IR) source and detector to measure exhaust emissions, optical speed-acceleration bars to capture instantaneous driving conditions, a camera to photograph number plates, and sensors to record ambient conditions such as temperature, pressure and relative humidity.

Positioned on the kerbside is the UV/IR detector and the detecting speed bar, with the light source and emitting speed bar positioned directly opposite across a single lane carriageway. Pollutants in the exhaust plumes of passing vehicles interact with the collinear beam of non-dispersive IR and dispersive UV light produced by the source, permitting the measurement of CO, CO_2, hydrocarbons (HC), SO_2, NH_3, NO, NO_2 and a background reference. Based on the blocking and unblocking of the two parallel lasers, the speed bars allow for the speed and acceleration of the vehicle to be calculated. Number plate photographs are cross referenced with vehicle databases to obtain further vehicle technical information. Large samples of snapshot emission measurements (typically 0.5 s) can be collected in a short period of time and aggregated to generate emissions information for different vehicle characteristic groups such as vehicle type, fuel type or manufacturer. Remote sensing has been used for a variety of applications, including emission factor verification[143,144,158] and the surveillance of vehicle emission trends[4,159–162].

Whilst remote sensing is a useful measurement technique, it is limited in the type of pollutants that can be measured or the driving conditions that can be sampled. Other real world vehicle emission measurement techniques include tunnel measurements, plume chase and point sampling. Tunnel measurements involve the measurement of pollutant concentrations at the tunnel's entrance and exit and the measurement of the number of vehicles passing through the tunnel. Average emission factors of vehicle fleets can be estimated using the difference in pollutant concentrations[163].

Plume chase and point sampling allow for real world emissions measurements of individual vehicles. Plume chase uses a vehicle equipped with fast-response instrumentation to follow a vehicle of interest and measure the emissions within its dispersing plume[164,165]. A specific vehicle can be monitored over several minutes to obtain detailed emissions information over a range of driving conditions. The point sampling measurement technique involves the use of fast-response air quality instruments positioned at the side of the road to perform extractive sampling of pollutants from individual dispersing vehicle exhaust plumes[166–168]. Similar to remote sensing, the point sampling measurements are performed alongside a vehicle number plate camera, which is used to obtain vehicle characteristics for each passing vehicle. Furthermore, the point sampling measurement technique can be used to obtain a vast amount of emissions information from a wide variety of vehicles within a relatively small time period. All of these approaches offer the potential to broaden the suite of pollutants that can be monitored, as theoretically any species can be measured, provided the accuracy and time resolution of the measurement is sufficient.

1.6 Thesis outline

The overall aim of this thesis is to develop new measurement and data analysis techniques to obtain useful information on air pollutant emission sources in urban areas. The measurement techniques used in this study include vehicle point sampling and repeat mobile measurements in urban areas. The work focuses on emission sources of NO_x and VOCs, with a particular focus on vehicular emissions.

Chapter 2 presents an overview of the mobile laboratory and the instrumentation used for high temporal and spatial measurements of air pollutants. The operation and calibration of a selected-ion flow-tube mass spectrometer (SIFT-MS) are discussed in detail. Details of the mobile measurement and

point sampling campaigns carried out in York, Manchester and Milan are also included.

Chapter 3 presents the development of analysis methods for point sampling and mobile measurement data sets, which can be complex. The point sampling analysis method ensures the alignment of pollutant species associated with passing vehicles and extraction of combustion-related plumes, before the calculation of emission ratios of NO_x and VOCs from individual vehicles. The mobile measurement analysis method uses a distance-weighted regression approach, which overcomes arbitrary splitting of road segments and can be used to reveal spatial patterns of air pollutants or emission sources. A rolling-regression analysis approach is also presented which allows for the extraction of combustion-related emissions from mobile measurements, which can then be compared to point measurements. The chapter also includes a discussion of the importance of different regression approaches for the calculation of emission ratios.

Chapter 4 presents results from the point sampling measurements carried out in Milan, Italy. The chapter uses the analysis methods outlined in Chapter 3 to extract combustion-related emissions of NO_x and VOCs from individual vehicles. The results are then grouped by vehicle characteristics, including vehicle type, fuel type and euro class to identify vehicles that could play an important role in the emissions of NO_x and VOCs. The results are compared to corresponding results from remote sensing to assess the agreement between the two measurement methods.

Chapter 5 presents results from mobile measurements made in York, Manchester and Milan. The mobile measurement data sets are analysed using the analysis methods outlined in Chapter 3 to reveal the spatial distribution of air pollutants and possible emission sources. The chapter also presents the comparison between point and mobile measurements made in Italy and aims to determine the spatial contribution of vehicle-related emissions of air pollutants. A new application of mobile measurements is developed where

the temperature dependence of air pollutant emissions is explored using measurements made during different seasons in Manchester. The results from mobile measurements made in Milan and Manchester are compared to investigate differences in emission sources and intensities in the two measurement locations.

Chapter 6 provides a summary of the work and discusses potential future directions for this research.

Chapter 2

Experimental methods: Mobile laboratory, instrumentation and measurement campaigns

2.1 Abstract

Over the last two decades, the importance of emission source types of air pollutants in urban areas has undergone significant change. Understanding the role played by different source sectors is important if effective air pollution control is to be achieved. Currently, atmospheric measurements in the UK are made at fixed monitoring sites, which do not represent the spatial and temporal variation of pollutants. Furthermore, the variety of species measured at UK monitoring sites is often limited and the overwhelming majority of sites do not measure VOCs. Recent technological advances have resulted in declining VOC emissions from vehicles, however it is still difficult to determine the contribution of vehicles to total VOC emissions due to limited measurements of vehicle-related VOC emissions in real-world conditions. This chapter will describe the application of a mobile laboratory

using a Selected-Ion Flow-Tube mass spectrometer (SIFT-MS) and other trace gas instrumentation to provide on-road, high temporal and spatial resolution measurements of multiple VOCs, CO_2, NO_x and other trace gases.

2.2 Introduction

As discussed in Chapter 1 mobile measurements and vehicle point sampling are new measurement methods which can be used to provide further information about air pollutant emission sources. In recent years, mobile laboratories have been developed and used for high spatial and temporal measurements of gaseous pollutants and particles[102,103,105–107,169–172]. These studies highlight the use of mobile laboratories for spatial mapping of air pollutants and also emission source identification and quantification. However these studies tend to focus on the measurement of common pollutants (CO_2, NO_x and CH_4), which typically represent specific emission source types in urban areas, such as road transport or gas leakages.

VOCs in urban areas are emitted from a complex range of sources and knowledge on their emission sources is limited. In order to both identify and characterise VOC emission sources, their spatial distribution in urban areas has to better resolved. To achieve this, recent work has involved the incorporation of real-time mass spectrometers into mobile laboratories for direct measurement of VOC species at high spatial resolution. Previous studies involving mobile measurements using mass spectrometry have used a Proton-Transfer-Reaction Mass Spectrometer (PTR-MS) to map the spatial distribution of VOCs[116–118]. PTR-MS is a mass spectrometry technique which consists of an ion source that is directly connected to a drift tube and a mass analysing system, which either consists of a quadrupole or time-of-flight mass analyser (TOF). Standard PTR-MS instruments are a Proton Transfer Reaction Quadrupole Mass Spectrometer (PTR-QMS), which can detect and resolve product ion masses at single unit mass resolution. Mobile

measurements carried out using PTR-MS have been used for mapping and hot spot detection of air pollutants in urban areas[117] and to investigate specific emission sources, including petrochemical emissions[116] and the oil and gas industry[118].

More recent studies use a Proton Transfer Reaction Time-of-Flight Mass Spectrometers (PTR-TOF) in mobile laboratories to measure VOCs. A PTR-TOF can detect VOCs at concentrations as low as a few parts per trillion (ppt) and at high mass resolutions (greater than 4000 m/δm)[173]. Previous mobile measurements carried out using PTR-ToF-MS have been used to reveal important emission sources of VOCs in urban areas. Many studies have revealed the importance of VCPs as a major source of petrochemical VOC emissions in US cities. Some studies have analysed temporal patterns of mobile measurements to determine VOC emission events related specifically to VCP usage and to identify tracer compounds for different VCP categories[119,120,123]. Other studies have concluded that VOC emissions from VCP usage are as important as VOC emissions from fossil fuels[119,174] and Gkatzelis et al. [121] concluded that VOC emissions from VCP usage in some US cities account for the highest fraction of urban VOC emissions. Mobile VOC measurement studies have highlighted other important VOC emission sources, including farming[124], biomass burning[125] and other industrial facilities[175], however these emission sources are less important in urban areas. These studies exhibit the potential of mass spectrometry in a mobile laboratory to distinguish and examine varying emission sources of VOCs in urban areas.

Roadside vehicle point sampling is a new measurement technique for quantifying vehicle emissions and involves high temporal sampling from dispersing vehicle exhaust plumes. The point sampling method has been used to determine emissions of particles and gases from on-road vehicles[166–168,176,177] and more recently the method has been used alongside mass spectrometry for measurement of organic and inorganic gases from heavy-duty trucks[178].

Whilst these measurements highlight the success of the measurement method, they are typically carried out in fairly controlled conditions with limited influence from other road vehicles or emission sources, and tend to focus on larger vehicle types, such as buses and trucks. Therefore, there is a need for sampling of individual vehicles in real-world conditions to determine detailed information from a variety of vehicle types. Furthermore, many existing studies focus on measurements of common pollutants, such as CO_2 and NO_x, and real-world measurements of VOC emissions from individual vehicles is limited. Additional measurements of VOCs directly from vehicle exhausts are needed to determine the importance of vehicles as a source of VOC emissions in urban areas.

The work described here differs from previous studies by using a Selected-Ion Flow-Tube Mass Spectrometer (SIFT-MS) to target selected VOCs, which has some important advantages when compared to other types of mass spectrometry. The Voice200 ultra SIFT-MS (used in this study) provides easy to use software and is therefore suitable for a wide range of users, compared to other mass spectrometers which can require considerable expertise. Therefore the method described in this chapter could be used by non-research organisations, such as regulators or governments. Another difference is that SIFT-MS uses multiple reagent ions, which can be switched in real-time (discussed in Section 2.4). Some PTR-TOF instruments also utilise selective reagent ionisation, with the use of multiple reagent ions, but these have reagent ion switching times typically in the order of tens of seconds compared to SIFT-MS switching times of milliseconds. The use of multiple reagent ions also allows for measurement of a wider range of species and separation of isomeric compounds[179]. Lehnert et al. [179] concluded that SIFT-MS is sensitive enough to perform trace gas measurements in ambient air and it also performs well when analysing complex mixtures at varying humidities.

A limitation of SIFT-MS when compared to PTR-TOF is that it cannot measure as many compounds in the same time resolution as it utilises a

quadrupole mass analyser. A PTR-TOF can potentially measure hundreds of VOCs every second, but SIFT-MS can be used with careful selection of compounds, which ensures that target emission sources can be investigated at an appropriate time resolution. Previous studies have utilised multiple reagent ions for measurements of VOCs and trace gases across a wide range of applications such as breath analysis[180,181], analysis of emissions from consumer products[182,183] and measurements of ambient air quality[184,185]. These studies present successful measurements of a wide range of VOCs and atmospheric trace gases, showing that SIFT-MS is suitable for measurements in urban areas.

This chapter will describe a mobile laboratory equipped with SIFT-MS and other trace gas instrumentation to provide high spatial and temporal resolution measurements of multiple air pollutants. The chapter includes a detailed description of the SIFT-MS instrument, which was used for the measurement of multiple VOCs, and details on its performance in the mobile laboratory. The chapter also describes details of the mobile measurement campaigns that took place in York, Manchester and Milan and the vehicle point sampling measurements that were carried out in Milan.

2.3 Mobile laboratory set-up

Figure 2.1 shows the platform used for trace gas measurements- the WACL Air Sampling Platform (WASP). The WASP is a Nissan NV400SE L3H2 van with interior dimensions of length 3450 mm, width 1650 mm, height 1750 mm and a payload of 1000 kg. In the rear of the van, the walls and floor are overlaid with 50 mm of insulation and there is an air conditioning system, which can be controlled from the driver cab and maintains a constant temperature, overcoming any instrumental heating. Aircraft-style L-tracks are built into the flooring and the ceiling of the rear of the van, which allow for the SIFT-MS instrument and the instrument rack to be secured. The instrument

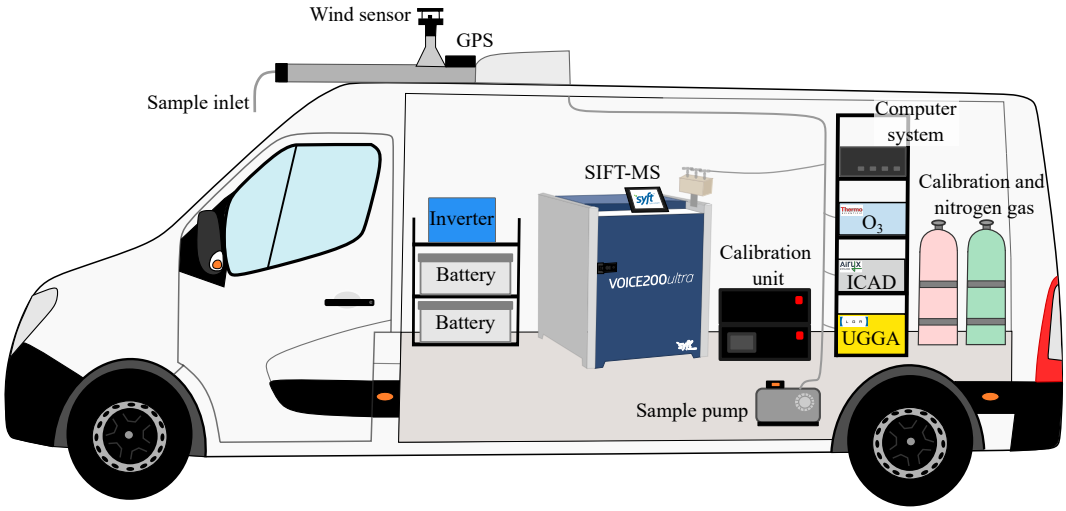

Figure 2.1: A graphic of the WACL Air Sampling Platform (WASP) and trace gas measurement instrumentation.

rack holds the computer system and other trace gas instrumentation (shown in Figure 2.1). Detailed information of air pollutant measurement instruments, including time resolution and targeted measurement compounds is shown in Table 2.1.

The power in the van is supplied by two 12VDC 230Ah batteries that are charged whilst driving by a 240VAC inverter or by an external mains power port when stationary. The total battery life when powering the instruments and air conditioning is approximately 3 hours whilst driving. Air is sampled from a front-facing inlet constructed from 6 m of PTFE tubing with an outside diameter of 12.5 mm (1/2 inch). During mobile measurements, the sample line is located 2.25 m above the ground, at windscreen height of the WASP, this minimised sampling of vehicle exhaust emissions in the nearby vicinity when making on-road measurements to allow for a variety of emission sources to be sampled. Furthermore, the height of the sample line minimised self-sampling of exhaust emissions from the WASP. Details of the placement of the sample inlet for point sampling measurements is included in Section 2.6. Sample air is distributed to the instruments by drawing air through the inlet at a flow rate of 40 SLPM using a pump mounted in the rear

Instrument	Time resolution	Compounds	Precision	Detection limit
Voice200 ultra Selected-Ion Flow-Tube Mass Spectrometer (SIFT-MS)	1-2.5	Multiple VOCs	0.08-4.96 ppb (dependent on compound)	2-35% (dependent on compound)
Ultraportable Greenhouse Gas Analyser (UGGA)	1	CH_4, CO_2 and H_2O	2 ppb (CH_4), 500 ppb (CO_2)	3 ppb (CH_4), 800 ppb (CO_2)
Iterative Cavity enhanced Differential Optical Absorption Spectrometer (ICAD)	1	NO_x, NO_2, NO and CO_2	0.33 ppb (NO_x), 0.26 ppb (NO_2), 0.40 ppb (NO), 1.21 ppm (CO_2)	0.49 ppb (NO_x), 0.39 ppb (NO_2), 0.60 ppb (NO), 1.82 ppm (CO_2)
Thermo 39i Ozone analyser	10	O_3	1 ppb	–
Gill 2D Ultrasonic wind sensor	1	Wind speed and direction	–	–
Garmin GPS 18x PC	1	Vehicle speed, direction and location	–	–

Table 2.1: Details of the air pollutant measurement instrumentation housed in the WASP and the corresponding time resolution (in seconds), measurement compounds, precision and detection limit. Further detail of precision and detection limit of individual compounds measured by the SIFT-MS is shown in Table 2.3.

of the van. Real-time location of the WASP is recorded by a Garmin GPS 18x PC and a measurement of wind speed and direction is made using a Gill 2D Ultrasonic Wind Sensor, both of which are fitted on the roof of the WASP at a height of 2.5 m. Data outputs of the GPS, wind sensor, the O_3 analyser and the UGGA are stored on the computer system and the outputs of the SIFT-MS and the ICAD are stored in the internal system of the instrument and the measurements from all of the instruments can be visualised in real-time. It is worth noting that the instrument fit in the WASP is flexible and can be easily altered due to the relatively large size and payload of the WASP. Further details on air pollutant measurement instrumentation are provided in Section 2.4 and Section 2.5.

2.4 Selected-Ion Flow-Tube Mass Spectrometer (SIFT-MS)

2.4.1 Principles of operation

Selected-Ion Flow-Tube Mass Spectrometry (SIFT-MS) is a mass spectrometry instrument used for direct quantification of VOCs and other trace gases. The SIFT-MS principles of operation are discussed in detail elsewhere[186,187], but a brief outline is included here.

The instrument consists of a switchable reagent ion source capable of rapidly switching between multiple reagent ions: H_3O^+, NO^+ and O_2^+, which are generated in a microwave plasma ion source, from a mixture of air and water at a pressure of approximately 440 mTorr. The reagent ions are extracted into the upstream quadrupole chamber, which is maintained at a pressure of approximately 5×10^{-4} Torr using a 70 L s^{-1} turbo pump, and then pass through an array of electrostatic lenses. The reagent ions then pass through the upstream quadrupole mass filter and reagent ions not rejected by the mass filter are injected into the flow tube, where they are

thermalised in a stream of nitrogen. The thermalised reagent ions selectively ionise target analytes and form product ions. The product ions flow into the downstream quadrupole mass filter and the secondary electron multiplier detector, where the ions are separated by their mass-to-charge ratios (m/z) and the ion counts are measured.

The mixing ratios of analyte compounds in the flow tube are calculated using the ion-molecule reactions that take place within the SIFT-MS, shown by Equation 2.1:

$$[A] = \gamma \frac{[P^+]}{[R^+]t_r k} \tag{2.1}$$

where

- $[A]$ is the analyte mixing ratio
- γ is the instrument calibration factor
- $[P^+]$ is the product ion
- $[R^+]$ is the reagent ion
- t_r is the reaction time
- k is the rate constant

2.4.2 Voice200 ultra SIFT-MS

A Voice200 ultra SIFT-MS manufactured by Syft Technologies (Christchurch, New Zealand), was used to quantify VOCs and inorganic gases in this study. Figure 2.2 shows the SIFT-MS inside the WASP, suspended in a rope-shock mounted rack, which reduces 3-dimensional vibration that the instrument may be subjected to during mobile measurements. The SIFT-MS has an in-house multi-port sample inlet which is capable of autonomously selecting between sample, zero and calibrant gases using the instrument software (Labsyft 1.6). The multi-port inlet uses 3 PTFE internally coated solenoid

valves (12VDC, Gems). The SIFT-MS was operated using a flow tube pressure of 460 mTorr, a nitrogen carrier gas (Research grade, BOC) with a flow rate of 0.6 Torr L s^{-1} and a sample flow rate of 100 SCCM.

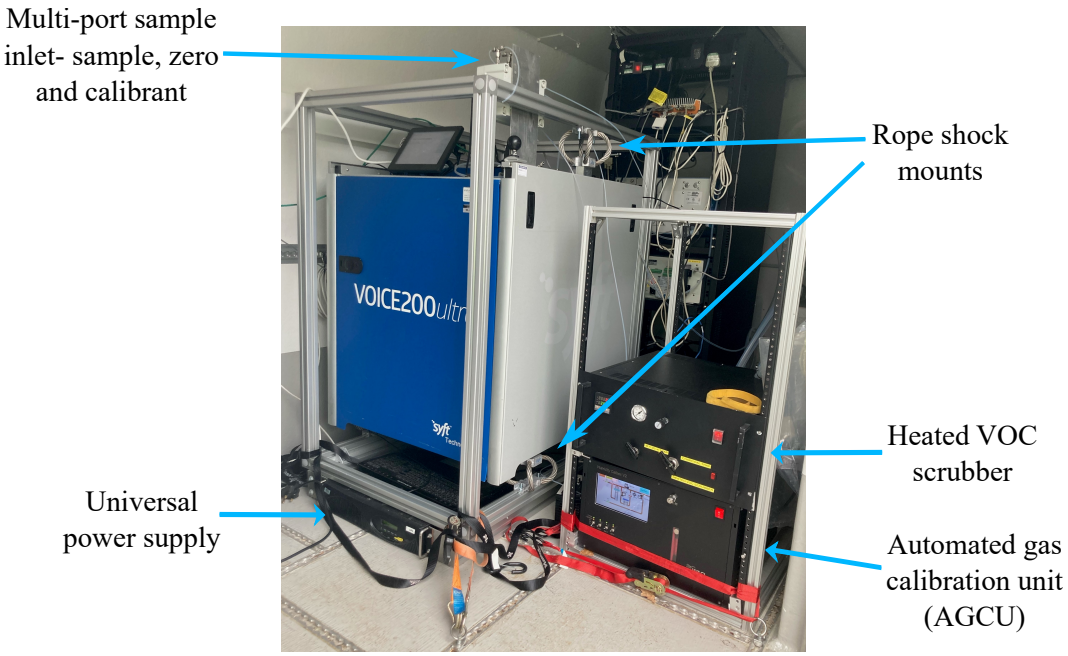

Figure 2.2: The Voice200 ultra SIFT-MS in a rope-shock mounted case with in-house built multi-port sample inlet (left). The custom built automated gas calibration unit (AGCU) and heated VOC scrubber (right).

The right hand side of Figure 2.2 shows the custom built automated gas calibration unit (AGCU) and heated VOC scrubber. The heated VOC scrubber consists of palladium-coated alumina pellets heated to 380° C which produces zero air whilst maintaining the humidity of the sample gas. The AGCU allows for controlled dilution of a VOC standard (1ppm certified National Physics Laboratory, UK) in the ppt-ppm range. Mass flow controllers (MFCs, Alicat) control the flow of the diluent zero air and the VOC standard and a simplified schematic of the internal gas flows in the AGCU is shown in Figure 2.3. Automated step-wise changes to the dilution ratios are made, generating a multi-point calibration curve for routine external calibration of the SIFT-MS. Further discussion relating to the calibration of

the SIFT-MS measurement compounds is included in subsection 2.4.3.

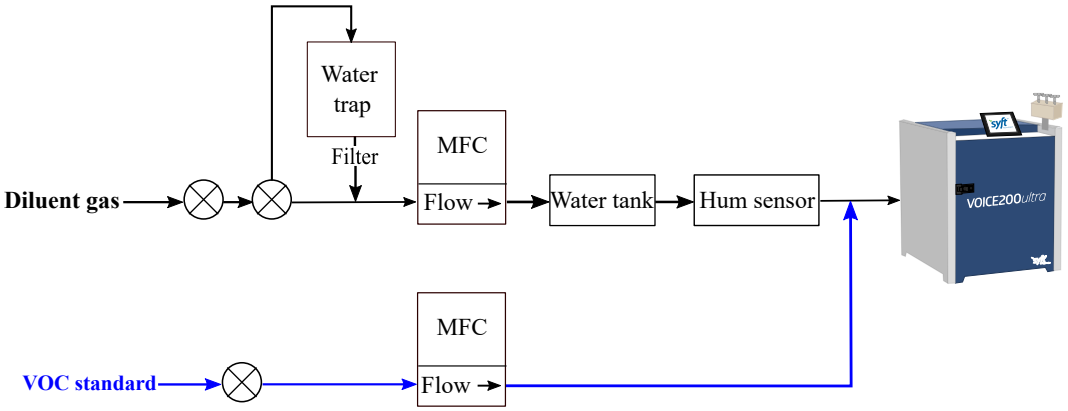

Figure 2.3: Schematic of the internal gas flow paths in the automated gas calibration unit (AGCU).

The SIFT-MS was operated at a time resolution of 1-2.5 s, depending on the number of measurement compounds selected. Details of the SIFT-MS measurements during each measurement campaign, including time resolution and the target compounds is included in Section 2.6.

2.4.3 Calibration of SIFT-MS

The mixing ratios of all of the SIFT-MS measurement compounds are dependent on the instrument calibration factor (ICF, γ) and the compound specific rate constant, as shown in Equation 2.1. The ICF value validates the mass dependent ion transmission of the instrument and a daily ICF value was generated using a 2 ppm gas standard, details of the gas standard are shown in Table A.1. Additionally, a zero offset was applied to all of the compounds, which was determined from measurement of zero air for VOCs and from measurement of a nitrogen blank for other compounds that would not be removed by the VOC scrubber. In the case of the compounds that would not be removed by the VOC scrubber, their mixing ratios were determined directly from the daily ICF.

The remaining compounds were externally calibrated using the AGCU and a 1 ppm 14-component VOC gas standard (National Physical Laboratory). These compounds include: acetone, benzene, butadiene, ethanol, isoprene, methanol, m-xylene (C_2-alkyl benzenes), toluene and trimethlybenzene (C_3-alkyl benzenes). Figure 2.4 shows the multi-point calibration of these compounds which was carried out at before and after mobile measurements (pre- and post-drive). Both pre- and post-drive calibrations were performed to ensure specific VOC compound sensitivities did not change during mobile operation. The calibrations were performed at VOC mixing ratios of 10, 5, 1 and 0 ppb and each of the mixing ratio steps lasted for 3 minutes. In order to assess daily both intra- and inter-calibration reproducibility, duplicate calibration steps were carried out both before and after mobile operation.

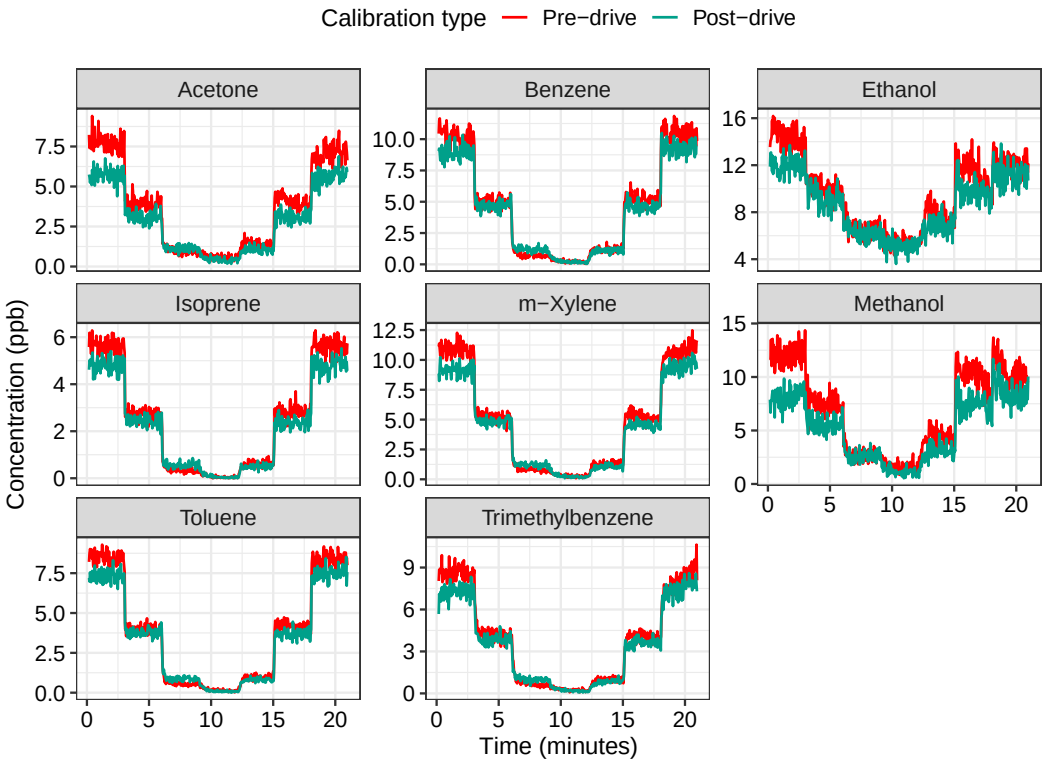

Figure 2.4: An example of a multi-point calibration for VOC gas standard compounds over 10, 5, 1 and 0 ppb performed pre-drive and post-drive.

In general, Figure 2.4 shows good agreement between the left- and right-

hand steps of the calibrations. The left-hand steps were used to condition the internal surfaces and SIFT-MS inlet and were not used for calibration of the measurement data. Compound specific calibration curves were obtained from averaging the last 1.5 minutes of each of the right-hand steps of the post-drive calibrations- this removed data influenced by mixing ratio transitions. Calibrations were carried out daily and calibration slopes were applied to the mixing ratio data obtained during mobile measurements. Figure 2.4 also shows good agreement for the majority of the compounds between the pre- and post-drive calibrations. Larger differences in the mixing ratios are observed for the alcohols, ethanol and methanol, and this may have been due to changes in ambient temperature, as pre-drive calibrations were performed in the morning when temperatures were lower. This may have lead to the alcohols sticking on the sample lines or mixing with condensation in the line during calibrations.

Figure 2.5 shows the noise in the SIFT-MS measured concentrations for each of the calibration concentration steps and the associated noise with the measurements. For the majority of the compounds, the noise for each of the calibration steps is relatively small, however for the alcohol compounds (ethanol and methanol) there is a lot more variation. The higher amount of variation in the calibration of ethanol and methanol is likely due to sticking of alcohols to the sample lines, as discussed above.

When static measurements were carried out (roadside point sampling in Milan), calibrations of the SIFT-MS were performed every 2 hrs. The same multi-step calibrations were performed (10, 5, 1 and 0 ppb) and the calibration slopes were calculated using the same method (averaging of the last 1.5 minutes of the right-hand steps).

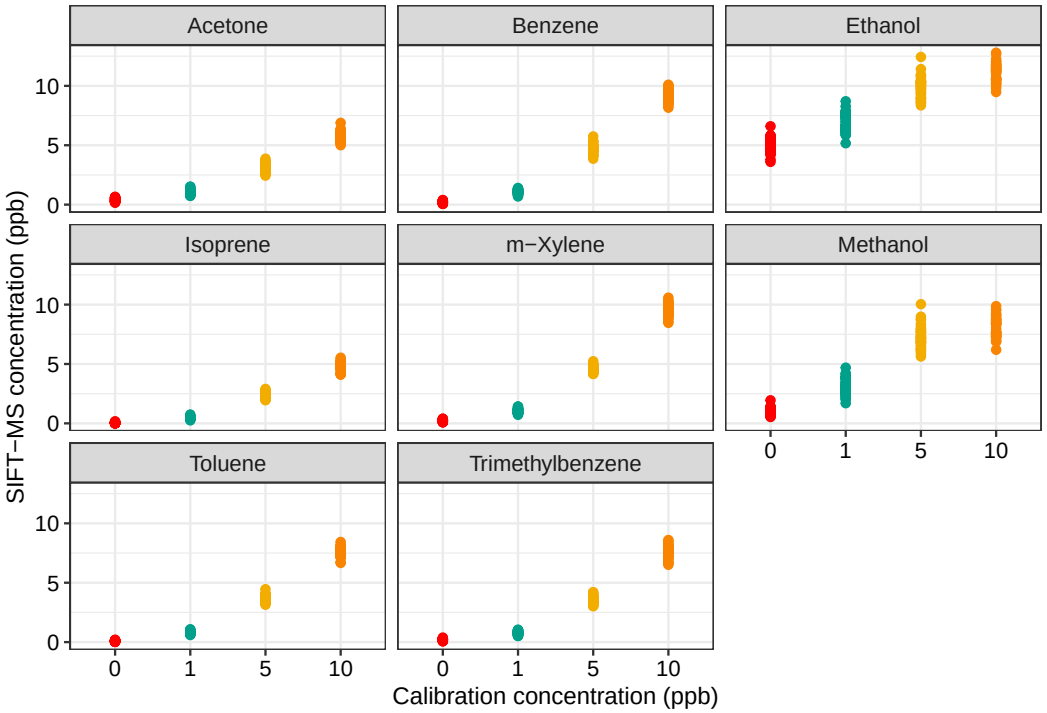

Figure 2.5: An example of the concentration for each calibration concentration step and the corresponding concentration measured by the SIFT-MS for each calibrated compound.

2.4.4 Data quality assurance

To ensure that VOC mixing ratios measured by the SIFT-MS were independent of instrumental noise, instrument dark counts using the H_3O^+ reagent ion, (m/z 25) were routinely measured during mobile operation. Figure 2.6 shows an example of measurements of m/z 25 alongside the corresponding counts of the product ion for benzene (m/z 78) and the benzene mixing ratio during a 40 minute period of mobile measurements.

Figure 2.6 shows that during mobile measurements, minimal instrumental noise of 0 to 40 cps (m/z 25) was recorded. Corresponding increases in the mixing ratio of benzene and the counts of the benzene product ion (m/z 78) is also shown in Figure 2.6, therefore displaying that mixing ratio increases in benzene were due to real increases in ambient concentrations.

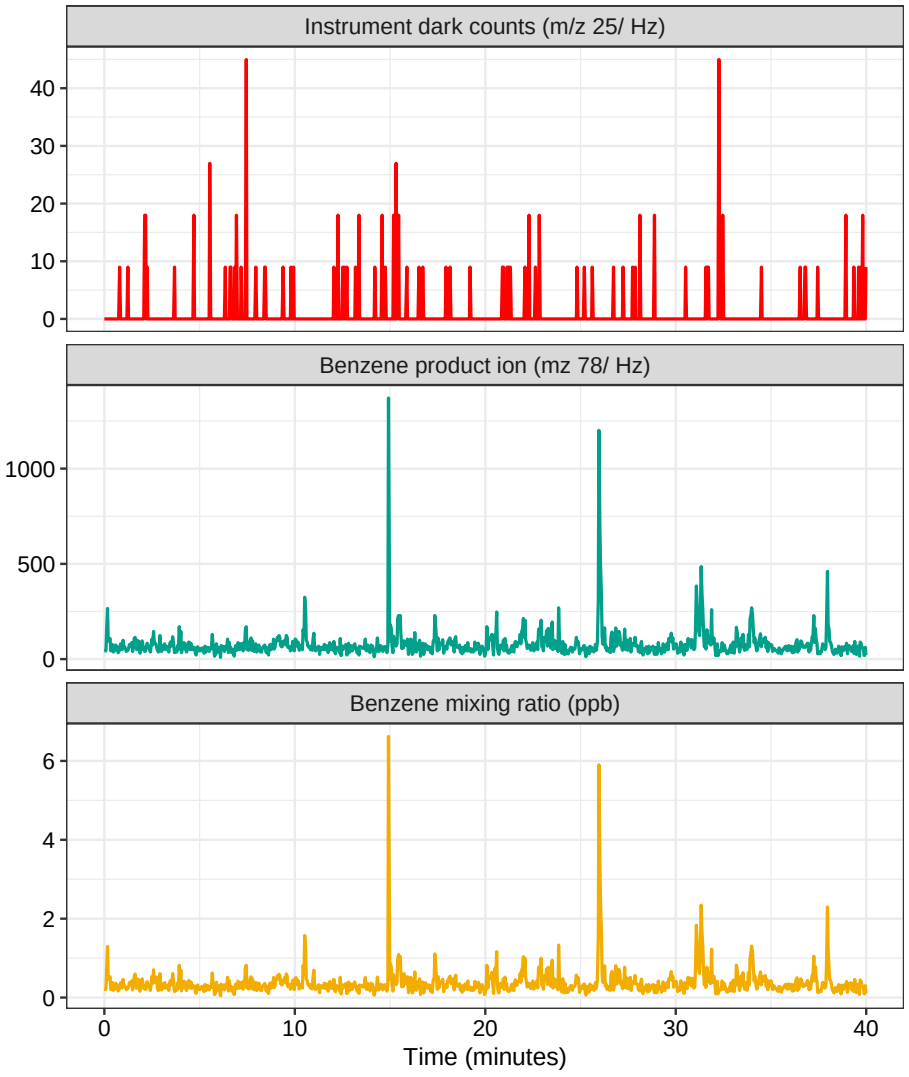

Figure 2.6: An example of measurements of instrument dark counts (m/z 25, in Hz), the corresponding benzene product ion counts (m/z 78, in Hz) and the benzene mixing ratio (in ppb) during a 40 minute period of mobile measurements.

Any periods of elevated instrument noise (m/z 25 >100 cps) were routinely removed to improve measurement accuracy, these periods may have been due to extreme vibrations or movement when driving. Further investigation of vibration and movement effects on instrument noise were carried out by sampling the SIFT-MS instrument on nitrogen only during mobile

measurements.

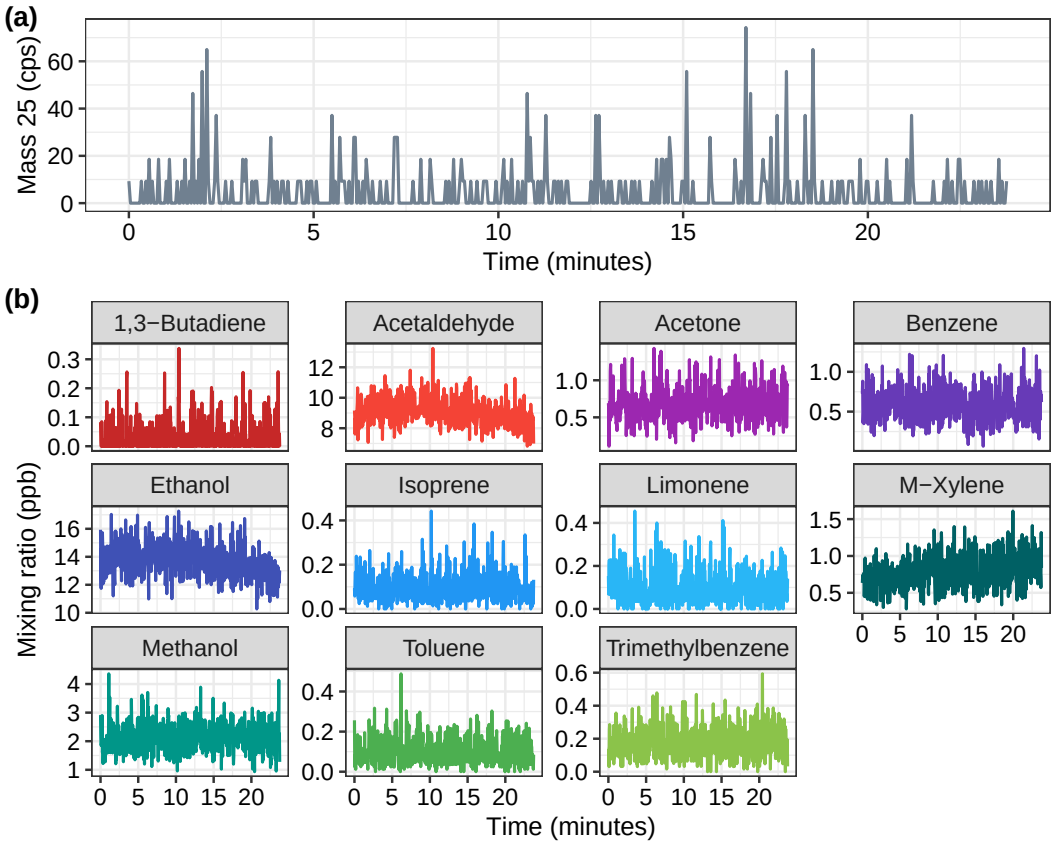

Figure 2.7: (a) Counts per second of mass 25 (instrument dark noise) and (b) mixing ratios of the compounds (in ppb) during a nitrogen-only mobile SIFT-MS measurement.

Figure 2.7 shows the results of nitrogen-only mobile SIFT-MS measurements and that there were no observed significant changes in instrument noise and in compound mixing ratios whilst driving. This shows that the driving motion had a minimal or negligible effect on measurement accuracy.

2.5 Other air pollutant instrumentation

2.5.1 Iterative Cavity Enhanced Differential Optical Absorption Spectroscopy (ICAD)

An Iterative Cavity enhanced Differential Optical Absorption Spectrometer (ICAD), developed by Airyx (Eppelheim, Germany), was used to quantify NO_x (NO_2 + NO) and CO_2. Detailed information on the iterative cavity-enhanced differential optical absorption spectroscopy approach is provided in Horbanski et al. [188], but a brief description is included here. The instrument uses optical absorption spectroscopy in the spectral range between 430 to 465 nm to provide a direct measurement of NO_2. In a second optical cavity, NO is converted to NO_2 by gas phase titration with a NO_x-free O_3 source, and a measure of total NO_x concentration is obtained. NO concentration is calculated by subtracting the NO_2 concentration measured in the first optical cavity from the total NO_x concentration. The instrument is installed with an IR sensor for parallel measurements of CO_2. The NO_2 measurements are time aligned to the corresponding NO_x and CO_2 measurements by applying a constant time offset of 3 s.

The instrument offers 1 second time resolution, sub-ppb precision, and a fast response time ($t_{90} < 2$ s). The ICAD is suitable for field measurements as it is lightweight (< 10 kg), has low power requirements (< 30 W at 12 V), and is installed in compact, waterproof housing. An algorithm is used to separate the absorption structure of NO_2 from overlapping absorptions such as water vapour and glyoxal. The instrument is practical to use for mobile applications since consumable gases are not required for instrument operation and it is insensitive to mechanical vibrations and temperature variations. The ICAD was used at a 1 s time resolution. The precision of the ICAD over 2 seconds is 1.21 ppm for CO_2, 0.33 ppb for NO_x, 0.26 ppb for NO_2 and 0.40 ppb for NO. The detection limit of the ICAD over 2 seconds is

1.82 ppm for CO_2, 0.49 ppb for NO_x, 0.39 ppb for NO_2 and 0.60 ppb for NO. The precision and detection limit of the ICAD was calculated using 2σ and 3σ, respectively, of gas canister-only laboratory measurements.

2.5.2 Ultra-portable Greenhouse Gas Analyser (UGGA)

An Ultra-Portable Greenhouse Gas Analyser (UGGA) developed by Los Gatos Research was used to quantify CO_2, methane (CH_4) and water vapour (H_2O). The UGGA instrument uses off-axis Integrated-Cavity Output Spectroscopy (off-axis ICOS) to quantify mixing ratios of gaseous species, which has been described in detail by Gupta [189], but a brief description is included here. Off-axis ICOS uses a laser and an optical cavity in an off-axis configuration[190], which enhances the measured absorption of light by a sample by creating an effective optical path length of several thousands of meters. The measured absorption spectra is recorded and when this is combined with the measured gas temperature and pressure in the cell, effective path length and known line strength, it can be used to determine a quantitative measurement of mixing ratio.

The UGGA was used at a 1 s time resolution, with a response time of 10 seconds. The precision of the UGGA over 1 second is 2 ppb for CH_4 and 500 ppb for CO_2 and the detection limit is 3 ppb for CH_4 and 800 ppb for CO_2. The precision and detection limit of the UGGA was calculated using 2σ and 3σ, respectively, of gas canister only measurements made whilst driving.

2.5.3 Ozone analyser

A model 39i ozone analyser developed by Thermo Scientific was used to quantify O_3. The model 39i uses UV photometry and operates on the principle that O_3 absorbs UV light at a wavelength of 245 nm. The degree to which the UV light is absorbed is directly related to the ozone concentration. The O_3 analyser was used at a 10 s time resolution and has a precision of 1

ppb (value taken from instrument user manual).

2.6 Measurement campaigns

Measurements used in this work were made using two different measurement techniques: mobile measurements and vehicle point sampling. A description of the measurement techniques is included below.

Mobile measurements can be used to increase the knowledge surrounding the temporal and spatial variation of air pollutants and for determination of important emission sources in urban areas. For mobile measurements, measurement routes were designed to capture a variety of possible emission sources and to also be a reasonable length in order to be repeated multiple times. It was important that the same measurement route was sampled multiple times as some sources may not be detected with every passing due to the sources being intermittent or being affected by meteorological conditions. Compounds of interest measured by the SIFT-MS also had to be carefully selected in order to help with source apportionment. Some compounds are emitted as a result of particular sources or relationships between compounds (such as benzene and toluene) can be indicative of particular sources. For this study, mobile measurements were carried out in all 3 measurement locations and the aim was to investigate emission sources in these areas.

Point sampling is a measurement method used for the determination of vehicle-specific emissions of air pollutants. It involves fast-response measurements at the roadside as vehicles pass by and this method was carried out in Milan. The use of the SIFT-MS allowed for measurement of selected-speciated VOCs, which, to our knowledge, has never been carried out for on-road, individual vehicle plumes. The SIFT-MS measurement compounds were carefully selected to ensure high time resolution measurements and the compounds selected were indicative of vehicle emissions.

The next sections will discuss each of the measurement campaigns (York, Manchester and Milan) in detail.

2.6.1 Mobile measurements in York

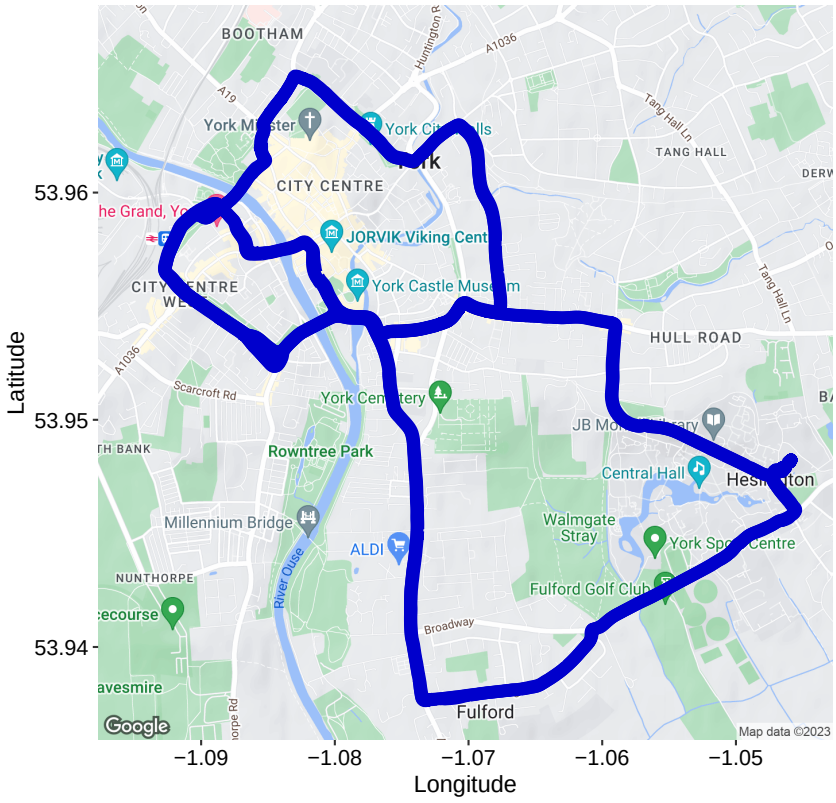

Figure 2.8: Measurement route sampled by the WASP for mobile measurements around York (© Google). Visualised by the *ggmap* R package [3].

Mobile measurements were carried out in the summer of 2020 around the city of York, UK. Figure 2.8 shows the measurement route, which starts at the University of York and then passes into and around the inner ring road of the city. York has a population of approximately 200,000 people and air pollution in the city is thought to be dominated by vehicle emissions, especially around the inner ring road due to congestion. The measurement route has a total distance of 15.1 kilometers and it was designed to capture a

variety of potential emissions sources, such as beauty salons, dry cleaners and eateries, to determine dominant sources. Measurements were carried out for a total of 10 days, between the 30th June 2020 and the 23rd July 2020, during daytime hours (09:00-17:00), weekdays and periods of dry weather. The aim was to sample the measurement route as many times as possible, in order to develop the mobile measurement analysis method and to determine the usefulness of mobile measurements. Therefore, the measurement route in York was sampled 30 times in total.

It should be noted that during the measurement period the Covid-19 stringency index in the UK was 64.35 (taken from: [191]), indicating reduced economic and traffic activity. The stringency index is a measure based on indicators relating to Covid-19 restrictions including school closures, workplace closures and travel bans. The stringency index value is a number between 1-100, with 100 being the strictest. This could affect both the concentration and detection of different VOC species due to possible decreased emissions.

The WASP was used for mobile measurements and it was fitted with the SIFT-MS, UGGA and O_3 instruments. The SIFT-MS was used at a 2.5 s time resolution. Further details on the SIFT-MS selected compounds for each of the measurement campaigns is shown in Section 2.7.

2.6.2 Mobile measurements in Manchester

Mobile measurements were carried out in Manchester, UK during the summer of 2021 (June-July) and the winter of 2022 (January), as part of the Integrated Research Observation System for Clean Air (OSCA) campaign. The Covid-19 stringency index in the UK during the summer of 2021 was 51.39 and during winter 2022 was 38.18 (taken from: [191]). Figure 2.9 shows the Trafford park measurement route sampled by the WASP. The measurement route in Manchester has a total distance of 12.4 km and it was

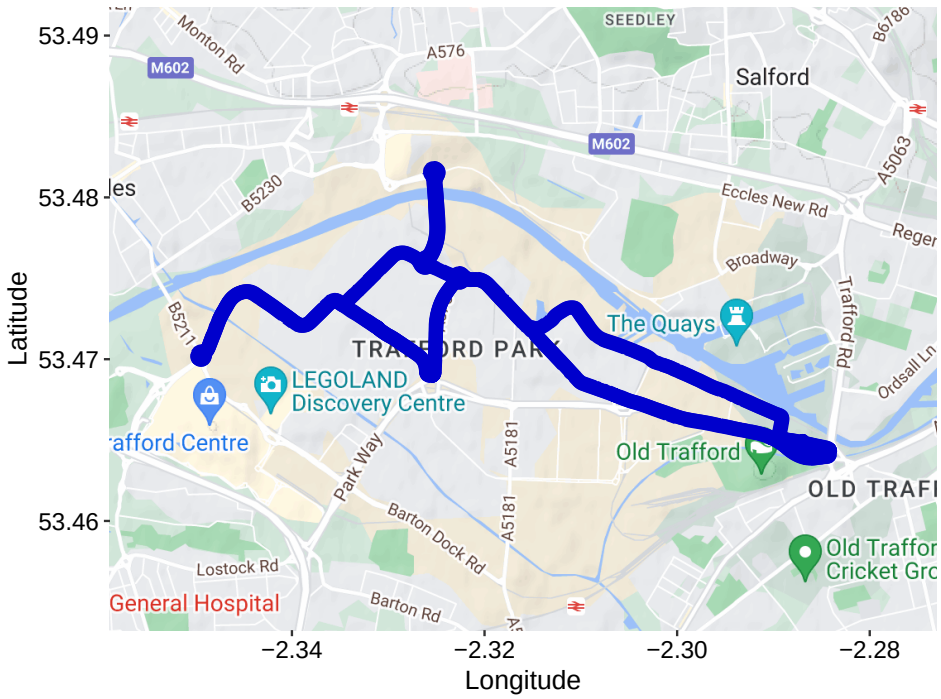

Figure 2.9: Measurement route sampled by the WASP for mobile measurements around Trafford Park, Manchester (© Google). Visualised by the *ggmap* R package [3].

designed to target the large industrial area Trafford park, which contains large amounts of industry. Trafford park contains around 1,330 businesses including cleaning products supplier, food manufacturers, car repair centres and many others. This industrial area was a good contrasting location to York, which contains very little industry. Summer measurements were carried out for a total of 4 days, between 28th June 2021 and 1st July 2021 and winter measurements were carried out for a total of 5 days, between 19th January 2022 and 26th January 2022. Both measurements were carried out during daytime hours (09:00-17:00) and periods of dry weather. The route

was driven for a total of 28 times, 12 times during summer 2021 and 15 times during winter 2022.

The WASP was used for mobile measurements and it was fitted with the SIFT-MS, ICAD, UGGA and O_3 instruments. The SIFT-MS was used at a 2 s time resolution. Further details on the SIFT-MS selected compounds for each of the measurement campaigns is shown in Section 2.7.

2.6.3 Point sampling and mobile measurements in Milan

A vehicle emission measurement campaign was carried out in Milan, Italy during September and October 2021, as part of the CARES (City Air Remote Emission Sensing) project. The CARES project involved multiple other European universities/institutions and the aim of the project was to test new methods of direct vehicle exhaust emission measurements. Milan has a population of approximately 1.4 million people and air pollution in the city is thought to be dominated by vehicle emissions.

A combination of both point sampling and mobile measurements were carried out between the 27th September and 2nd October 2021. The Covid-19 stringency index in the Italy was 56.55 (taken from: [191]). Figure 2.10 shows the site of the point sampling measurements (Via Madre Cabrini, in red) and the route driven for the mobile measurements (in blue). The aim of the point sampling measurements was to test the new method of vehicle emission measurements and to also investigate if the SIFT-MS could be used to derive VOC emission ratios from individual vehicles. The aim of the mobile measurements was to investigate the effects of differing vehicle fleets/emissions sources (compared to UK measurements in York and Manchester) and to complement the point sampling measurements. An overview of the point sampling and mobile measurements will be discussed below.

Point sampling measurements were carried out at Via Madre Cabrini (shown in Figure 2.10), which was a road located within the low emis-

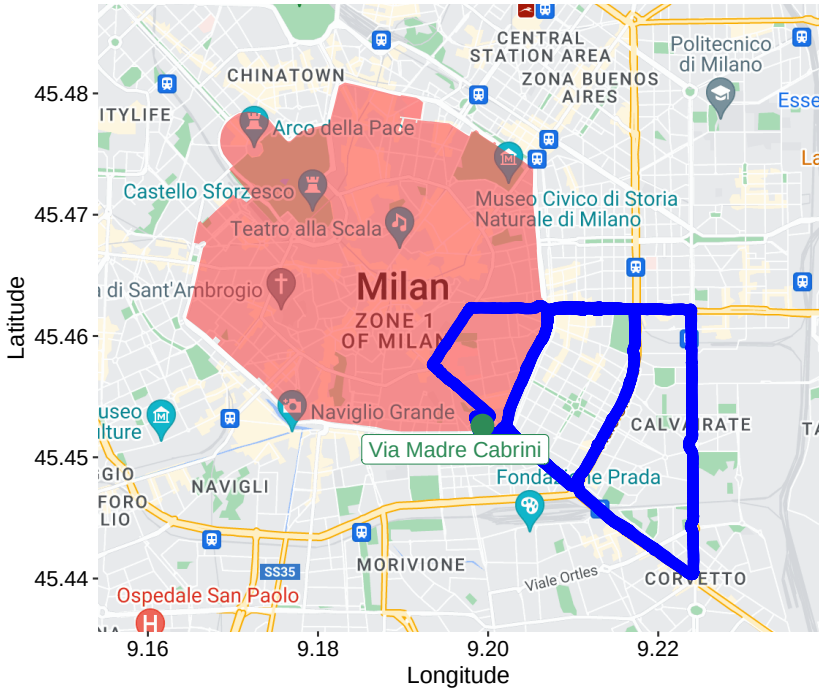

Figure 2.10: Map of the roadside site (Via Madre Cabrini, in green) and the mobile measurement route driven in Milan (in blue) (© Google). The red shape represents the boundary of the Area C low emission zone. Visualised by the *ggmap* R package [3].

sions zone of Milan. The measurement location was suitable for vehicle exhaust emission measurements due to vehicles accelerating whilst passing the sample inlet after turning into the road, therefore producing a plume large enough for measurements. Figure 2.11 shows the set-up of the WASP and other measurements during vehicle point sampling in Milan. Other measurements included an EDAR remote sensing instrument (HEAT), which works in the same way as a remote sensing detector, measuring CO_2, NO_x and total HC. There were also particle measurements (University of Graz), measurements of CO_2 and NO_x using an ICAD (Airyx) and an air quality station (Milan institutions). The sample inlet for the WASP was placed underneath the HEAT remote sensing equipment, at the height of passing vehicle exhausts and sample air could then be distributed to the various

measurement instruments housed in the WASP. Information for passing vehicles was recorded using an automatic number plate recognition camera placed on the dashboard of the University of Graz/Airyx van. The camera photographs vehicle number plates and these can be cross referenced with vehicle databases, from the Italian Ministry of Transport, to obtain technical information about the passing vehicles. Vehicle technical information could then be used to distinguish between different vehicle classifications, for example vehicle type and fuel type).

A total of 108 hours of point sampling measurements were conducted (~4.5 days), between 27th September and 2nd October. The point sampling data collection was paused between approximately 09:00 and 16:00 local time on 30th September and 1st October to conduct the mobile measurements.

Figure 2.11: Set-up of the vehicle point sampling measurements in Milan.

Mobile measurements were carried out on the 30th September and the 1st October 2021 during daytime hours (09:00-15:00). The measurement route is shown in Figure 2.10 and the total distance is 13.2 km, covering a variety of areas of Milan- including inside and outside of the low emissions zone and inside and outside of the city centre. There are a series of ring

roads surrounding the city of Milan which form an expanding circle from the centre (Area C) outwards into Area B. Area B covers most of the city of Milan and it is a limited traffic area with no access for the most polluting vehicles. Area C is a combined Urban Road Toll and LEZ, where vehicles need to pay to enter and only the less polluting vehicles may enter and is present in the centre of Milan (shown in Figure 2.10). Both Area B and C are active from 07:30 to 19:30 on Monday to Friday. The measurement route was designed to capture a 'slice' of the circular ring roads, to capture potential changes in vehicle fleet, congestion levels and other emission sources. The route was driven a total of 7 times, resulting in ~13 hours of mobile measurements.

The WASP was used for point sampling and mobile measurements and it was fitted with the SIFT-MS, ICAD, UGGA and O_3 instruments. The SIFT-MS was operated at a data acquisition rate of 1 s for point sampling measurements and 2 s for mobile measurements. Further details on the SIFT-MS selected compounds for each of the measurement campaigns is shown in Section 2.7.

2.7 SIFT-MS measurement details

Table 2.2 shows details of the SIFT-MS measurement compounds and which campaigns each compound was selected for. It is worth noting that for the Milan campaign, additional compounds were selected for the mobile measurements in order to assist with emission source apportionment. Additionally, for the point sampling measurements most of the SIFT-MS compounds were measured with the NO^+ reagent ion in order to minimise the data acquisition rate for point sampling (1 s).

Further details on the SIFT-MS measurements, including the branching ratios, rate constant and structural formula targeted by the MM (shown in Table 2.2) are included in Appendix A (Table A.2).

Table 2.3 shows details of the limit of detection (LoD), precision and

Reagent Ion	**Compound**	**MM**	**Campaigns**
O_2^+	Ethane, propane and butane (C_2-C_4 alkanes)	28	Milan
	NO_2	46	York
NO^+	Acetaldehyde	45	Milan (PS)
	Ethanol	47	Milan (PS)
	1,3-Butadiene	54	Milan (PS)
	Isoprene/Furan	68	York, Manc, Milan (M)
	Benzene	78	York, Manc, Milan
	Acetone	88	York, Manc
	Toluene	92	York, Manc, Milan
	C_2-alkyl benzenes	106	York, Manc, Milan
	C_3-alkyl benzenes	120	York, Manc, Milan
	Total Monoterpenes	136	York, Manc, Milan (M)
H_3O^+	Methanol	33	York, Manc, Milan (M)
	Acetaldehyde	45	York, Manc, Milan (M)
	Ethanol	47	York, Manc, Milan (M)
	1,3-Butadiene	54	York

Table 2.2: The compounds measured by the SIFT-MS, their corresponding reagent ions, molecular masses (MM, in g mol^{-1}) and which campaigns they were selected for. Campaign abbreviations: Manchester (Manc), Milan point sampling (Milan (PS)) and Milan mobile (Milan (M)).

uncertainty for each of the SIFT-MS measurement compounds. The LoD and precision were calculated using 3 and 2 times, respectively, the standard deviation (σ) of measurements made when sampling zero air or nitrogen gas. The LoD and the precision were calculated over 2.5 s, which is the acquisition rate of the SIFT-MS during mobile measurements. The uncertainty for

the calibrated SIFT-MS measurement compounds was calculated using the method described by Reimann et al. [192] and the details are included in Appendix A. For the SIFT-MS compounds that were not calibrated, an uncertainty of ±35% can be expected due to systematic errors, details are described by Syft Technolgies [193] and included in Appendix A. Mixing ratios of SIFT-MS measurement compounds that were below the LoD values shown in Table 2.3 were set to half of the LoD value for each measurement compound. Giskeodegard and Lydersen [194] states that this method is acceptable if no more than 20% of the values are below the limit of detection, which is the case for each of the compounds measured by the SIFT-MS.

Species	**LoD**	**Precision**	**Uncertainty**
Acetone	0.22	0.15	6%
Benzene	0.20	0.13	8%
1,3-Butadiene	0.06	0.04	7%
C_2-alkyl benzenes	0.33	0.22	6%
C_3-alkyl benzenes	0.14	0.09	4%
Ethanol	0.27	0.18	9%
Isoprene	0.04	0.02	2%
Methanol	0.17	0.11	7%
Toluene	0.11	0.08	3%
Acetaldehyde	0.41	0.27	35%
C_2-C_4-alkanes	7.44	4.96	35%
Monoterpenes	0.11	0.07	35%
NO_2	2.48	1.65	35%

Table 2.3: The limit of detection (LoD) and precision of compounds measured by the SIFT-MS (in ppb) for every 2.5 second measurement. Compounds in the upper part of the table were externally calibrated.

2.8 Conclusion

A mobile laboratory was equipped with a variety of trace gas instrumentation and has been used for high temporal and spatial measurements of a suite of air pollutants. The SIFT-MS has been shown to be a suitable measurement instrument for high time resolution measurements of multiple speciated VOCs during mobile sampling which, to the best of our knowledge, is the first time that this has been performed. The mobile laboratory has been used to perform point and mobile sampling methods in a variety of urban areas. The data sets acquired from these measurements will be analysed to provide useful insight into emission sources in urban areas.

Chapter 3

New analysis techniques for vehicle point sampling and mobile measurements

3.1 Abstract

Vehicle point and mobile sampling are measurement techniques, which can provide useful information on emission sources of air pollutants. Existing analysis methods for point sampling data rely on the subtraction of a background before emission ratios/factors can be calculated, which is often quite complex and the definition of a background varies between studies. Existing data analysis methods of mobile measurement data often rely on discrete road segments to provide information about the spatial variation or hot-spots of air pollution. These analysis methods are useful but limit the types of analysis that can be applied to spatial data which could lead to important emission sources being missed.

In this work, methods for analysing point sampling and mobile measurement data have been developed. The point sampling analysis method ensures

the extraction of combustion plumes from vehicles and then calculation of emission ratios by regression. The mobile measurement analysis method incorporates regression-based approaches and applies them to mobile data for the quantification of emission sources spatially and extraction of vehicle-related emissions. The work also includes a discussion on the importance of different regression approaches, which are important for determination of emission sources in urban areas.

3.2 Introduction

Both vehicle point sampling and mobile measurements are techniques which can provide useful information about emission sources or spatial variations of air pollutants. However, both of the measurement techniques produce high temporal and large data sets for which the analysis can be challenging.

Point sampling measurements involve extractive sampling from dispersing vehicle exhaust plumes using fast-response instruments at a fixed roadside location, which can be used to increase our understanding of tailpipe emissions from vehicles. Many studies report information related to vehicular emissions as emission ratios, which represent the ratio between the enhancement in a pollutant species and the corresponding enhancement in a tracer gas, typically CO_2. Emission ratios from point sampling studies are typically calculated by subtracting background concentrations. Background concentrations have to be estimated as it is impossible for the background to be measured in the same location. Current methods to calculate emission ratios include quantifying background concentrations before and after a target vehicle pass and then integrating the area of the concentration peaks[166–168,176–178]. This approach is useful, but the definition of the background value is somewhat arbitrary. Furthermore, determination of background levels from point sampling data do not perform well in urban settings where there are high traffic flows and complex emission source

types.

Mobile measurements have been used to provide useful information on a variety of complex emission source types in urban areas. Many mobile measurement studies make multiple repeat measurements of a sample area to derive statistics such as mean or median mixing ratios of air pollutants across the road network. The results have been used to provide information on the spatial variation of air pollutants through spatial mapping and hot spot identification of pollutants[105,106,117,170,171,174]. Spatial mapping of pollutants is useful, but many of these studies often use arbitrary distances to split up the road network into discrete segments. Apte et al. [106] splits up the road network into 30 m segments, whereas other studies use larger grid cells (approx. 100 m^2) to separate the sample area[117,170,172].

Splitting up the road network and taking the mean/median will down-weight the contribution from less frequent, higher concentrations such as evaporative emissions. Using this approach when investigating consistent emissions sources is useful. However there is potentially important information and intermittent sources that may be missed. Further analysis of mobile measurements has been carried out using complicated techniques, such as principal component analysis or positive matrix factorisation, which can be used to explore relationships between variables and provide information on potential emission sources[107,121,195]. Whilst these techniques can be used to distinguish emission sources, they are complex techniques and often rely on existing knowledge about the spatial distribution of sources in urban areas, which is limited in current emission inventories.

Determining the importance of air pollutant emission sources is difficult and calculating emission ratios between pollutants has widely been used to identify source types[196,197]. Emission ratios are defined as the ratio between the enhancement in a species concentration compared to a coinciding enhancement of a reference species. The reference species is typically a tracer for a specific emission source, such as CO_2 for vehicular emissions[167,168,177].

The ratio between species which are co-emitted from a source should remain constant if both of the species are similarly affected by dilution and air mass mixing[166,198]. Therefore, the emission ratio can be used to represent the ratio at the point of emission. However, if photochemical processing does impact the ratio, it can be related to the air mass age, assuming the major removal mechanism is reaction with the hydroxyl radical (OH)[196,199]. The calculation of an emission ratio from a particular source is important as they are used in the calculation of emission factors. Emission factors for particular air pollutants and emission sources are used in emission inventories, which can be used to assess the effectiveness of air quality reduction strategies or for air quality modelling and predictions. Therefore, it is important that they are accurately calculated.

The work discussed below includes development of analysis methods for point sampling and mobile measurement data. The point sampling analysis method aims to ensure alignment of air pollutant species associated with a passing road vehicle and extraction of combustion-related vehicle plumes. Furthermore, the point sampling analysis method aims to remove the requirement of complex background determination and subtraction through the application of regression analysis. The mobile measurement analysis method aims to remove arbitrary splitting of the road network through the use of a distance-weighted approach to quantify concentrations and emissions spatially. Furthermore, we aim to extract combustion-related emissions and separate these from other sources in a complex urban environment. The work discusses different regression approaches and their importance when used for the determination of emission sources in urban areas.

3.3 Vehicle point sampling analysis

3.3.1 Challenges to overcome

Point sampling measurements are used to determine the emission of air pollutants from vehicle exhausts and this is typically done by calculating emission ratios. Combustion-related emissions are determined by calculating the ratio of a pollutant to CO_2 as this represents the amount of a pollutant emitted per unit of fuel burnt[167,168]. Therefore, the alignment of measurement data to a vehicle pass and the alignment between pollutants is important. Initial alignment of air pollutant measurements was carried out using daily lighter tests. The lighter tests involved holding a lighter flame by the sample line and noting the time the lighter was lit. The difference between the lighter test and the time that the maximum of a pollutant was reached represented the lag time. During the lag tests, propane was measured by the SIFT-MS, CO_2 and NO_x by the ICAD and CO_2 by the UGGA, these compounds were selected as they would increase due to the lighter flame. The SIFT-MS had the shortest lag time of 1 s, the ICAD had a lag time of approximately 6 s and the UGGA had a lag time of approximately 8 s. Vehicle pass times were aligned to air pollutants measurements by applying the average amount of time it took for the vehicle to pass from the sample inlet to the ANPR camera, which was placed slightly further up the road.

An example of two vehicle passes and corresponding pollutant peaks measured by the SIFT-MS and the ICAD after manual alignment, using lag times obtained from lighter tests, are shown in Figure 3.1. Increases in CO_2 and NO_x are shown for both of the vehicle passes and increases in the selected VOC compounds are shown for the first vehicle pass. The pollutant peaks associated with the first vehicle reach a maximum slightly before the vehicle pass time, however, pollutant peaks associated with the second vehicle pass reach a maximum slightly after the vehicle pass time.

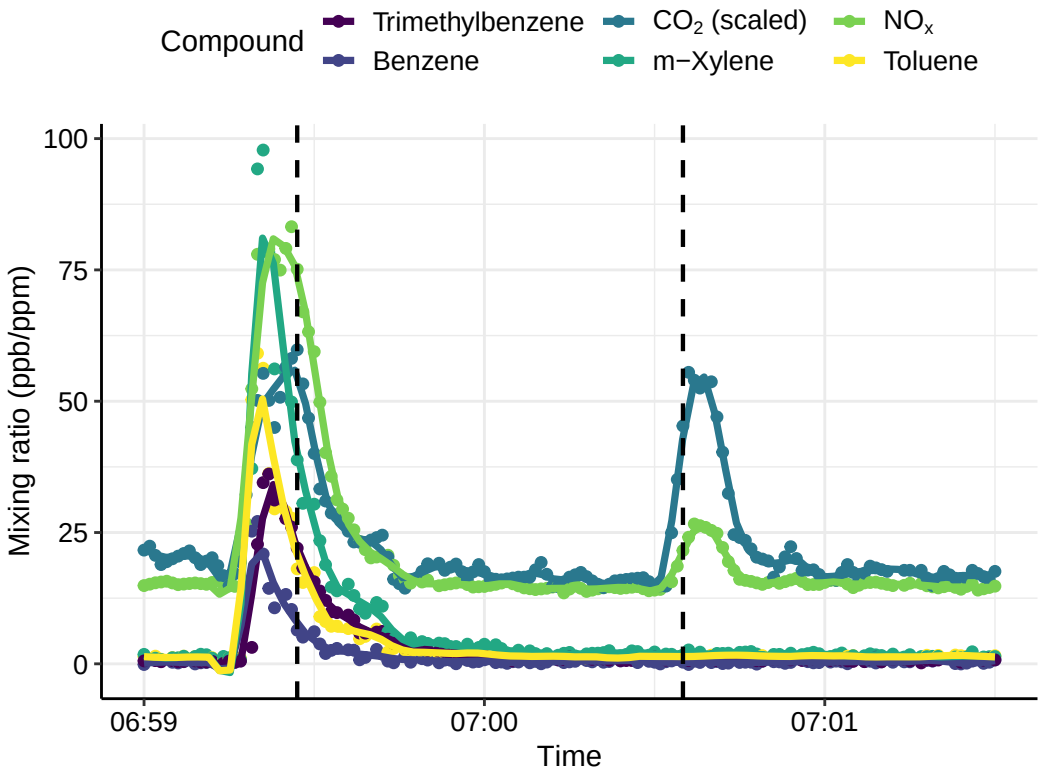

Figure 3.1: An example of 2 vehicle passes (dashed lines) and corresponding pollutant peaks from the SIFT-MS (trimethylbenzene, benzene, m-xylene and toluene (all in ppb)) and the ICAD (CO_2 (in ppm) and NO_x (in ppb)). CO_2 has been scaled by -475 ppm for data visualisation.

There are a multitude of reasons as to why the pollutant measurements associated with the vehicle passes show different behaviour. These reasons include meteorological effects, such as varying wind speed and direction which can affect the vehicle plumes. Another reason could be varying vehicle speeds along the measurement road as the sample inlet and ANPR camera were placed slightly apart, so the time of the vehicle taken to travel between the inlet and the camera would vary with vehicle speed. Therefore, in order to calculate accurate emission factors and associate them with individual vehicles, it is important that any differing response times in pollutant measurements and vehicle passes are taken into account.

A further challenge that is important to address is ensuring that combustion emissions related to vehicles are extracted from point sampling measurements. This is difficult as measurements are being carried out in a highly complex emissions environment. The point sampling measurements for this study were carried out in Milan and in a highly populated urban environment where it is possible that there is a broad range of emission sources, particularly for VOCs. Therefore, it is important that only vehicle-related emissions are extracted from the data before further analysis is performed and emission ratios are calculated.

The next section describes the development of an analysis method which takes into account the differing response times for individual vehicle measurements and ensures the alignment of measurement data related to a particular vehicle pass. The analysis method includes identification of a combustion plume, which ensures that combustion-related vehicle emissions are extracted from a complex source area. The next section also includes a discussion on the investigation of other methods used to extract vehicle plumes and methods to calculate emission ratios of individual vehicles.

3.3.2 Alignment of pollutant species

It is important that pollutant species associated with a vehicle pass are well-aligned to each other, ensuring accurate calculation of emission ratios. In order to align species to each other, an observation window for each vehicle pass was created. An observation window was created by considering the time before and after a vehicle pass. The observation windows that were created contained a third of the time between vehicle passes with a maximum of 20 observations (10 s either side of the vehicle pass). The observation windows created for each vehicle pass could then be treated individually and pollutants within the windows could be aligned. The observation windows for each vehicle pass are represented by the black points in Figure 3.2.

Once the observation windows for each vehicle pass has been created, the optimum offset for each species can be calculated and applied. The offset for each species was determined by calculating the correlation between each species and CO_2. CO_2 was used as the pollutant species that other species would be aligned to as it is directly related to fuel consumption and can be used as a tracer for combustion[167,168,177]. The measurement of CO_2 from the ICAD was used for alignment and further analysis as the ICAD CO_2 measurement had a much faster time response than the UGGA CO_2 measurement (1 s (ICAD) and 10 s (UGGA)). It was important that the measurement of CO_2 was fast response to distinguish individual vehicle plumes and reduce the possible effects of vehicles passing close to one another.

The correlation between each pollutant species and CO_2 was calculated within an offset time range of ±5 seconds and the time offset that gave the best correlation between the species and CO_2 was applied to the data. Each observation window and pollutant species was treated individually. For some of the vehicle passes there was no improvement in the correlation within the time range and in this case no time offset was applied. Once the measurements of different pollutants within the vehicle pass window were aligned, further analysis can be investigated before emission ratios are calculated.

During the creation of the observation windows, vehicle passes were flagged if they appeared too close to one another. Vehicle passes were flagged if they occurred within 5 s of another vehicle pass and these could then be removed from further data analysis if required. A period of 5 s was selected as the time between vehicles as it has been reported that this is the minimum time needed between vehicles for background levels to be reached[167,177] and this was also supported by the point sampling measurement data. Figure 3.2 shows an example of vehicle passes during a busy and quiet time period, their corresponding observations of NO_x and they are coloured by their

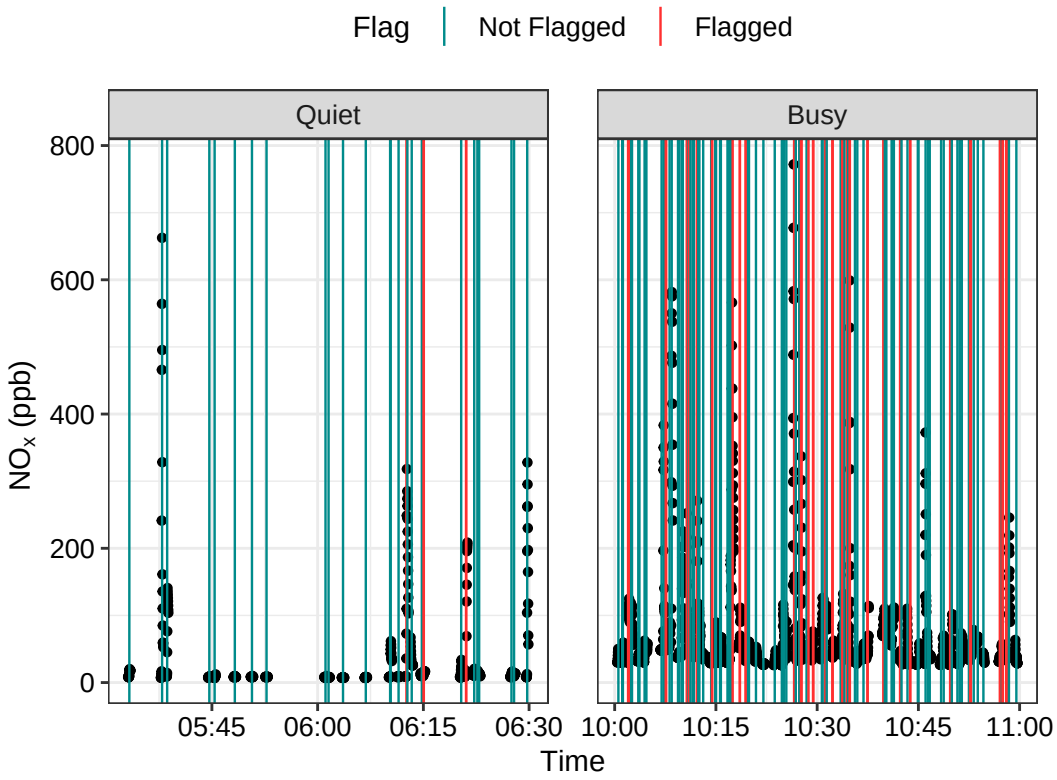

Figure 3.2: An example of vehicle passes during a "quiet" and a "busy" period on the 29th October 2021 and the extracted NO_x observations (from each vehicle pass window). Vehicle passes are coloured depending on if they are too close to another vehicle- not flagged (blue) means they are far apart from another vehicle pass and flagged (red) means that another vehicle pass occurs within 10 s.

flagging.

During the quiet morning period, which occurred between the hours of 5:30 - 6:30am, there were a total of 31 vehicle passes and 19% were flagged. Whereas during higher traffic hours, typically between the hours of 10:00 to 11:am, there were 150 vehicle passes and 43% were flagged. For all of the point sampling data collected in Milan (approximately 9000 vehicles), 44.3% of the vehicle passes were flagged, which is a significant amount of the total number of vehicles. Therefore, filtering for flagged vehicle passes

will remove a large amount of the data and investigation into the effect of time between vehicle passes is considered below.

The functions used to create the observation windows and align the measurement data are available in the **mobilemeasr** R package[200].

3.3.3 Calculating emission ratios

In order to be confident in emission ratios calculated for individual vehicles, it is important to make sure that only vehicle plume measurements are extracted, particularly combustion-related plumes. In order to extract combustion-related vehicle plumes, different requirements of the measurements have been investigated and are discussed below, including time between vehicle passes, correlations between species, statistical results of the regression (such as standard errors or p-values).

Emission ratios shown below were calculated for each individual vehicle pass and were derived using linear regression, which does not require a background determination as the intercept derived from the regression represents the background.

3.3.3.1 Time between vehicle passes

The first requirement for extracting vehicle plumes that was investigated was excluding vehicle passes that were too close to another. A vehicle pass was flagged if it occurred within 5 s of another vehicle pass, as shown in Figure 3.2. Excluding the flagged vehicle passes would ensure that ratio calculations for individual vehicles would be exempt from interference from other vehicles plumes as there is a significant time between each vehicle pass. However, as 44.3% of the total vehicle passes were flagged, simply removing these would remove a significant amount of the total data. Therefore, investigation was carried out as to what effect filtering for flagged passes would have on the average ratios of different vehicle categories.

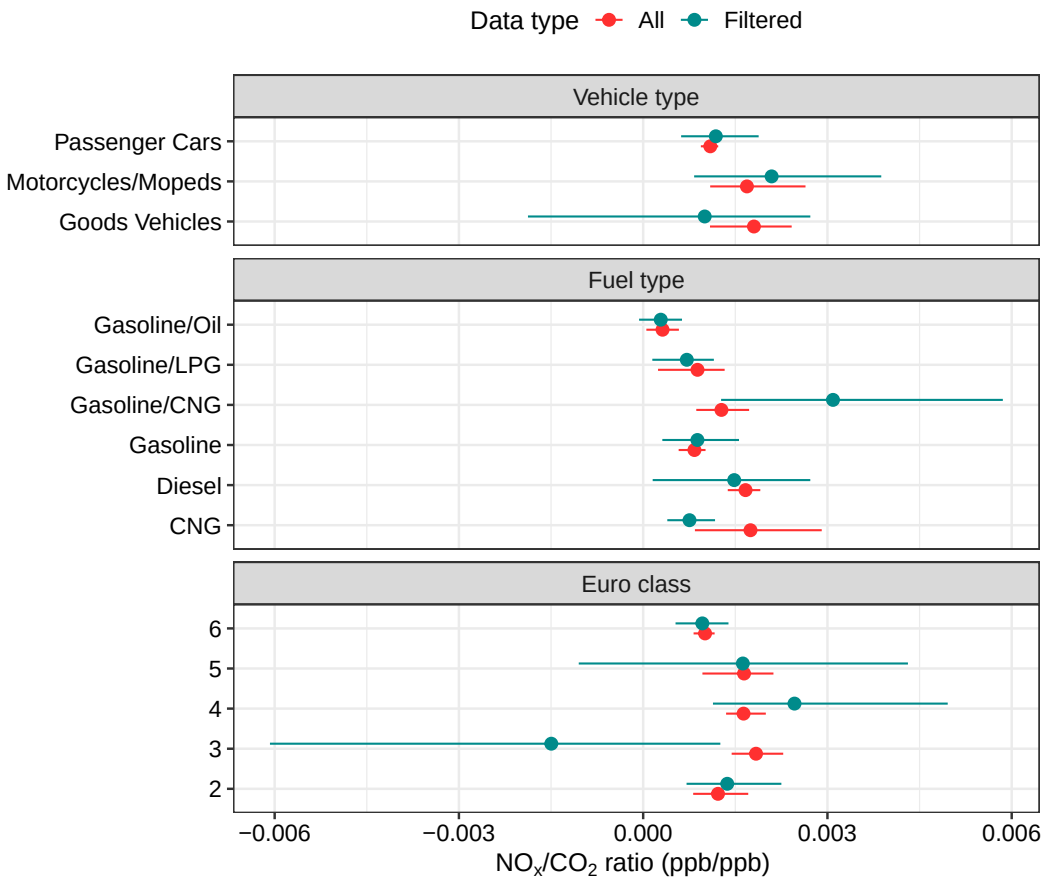

Figure 3.3: Average NO_x/CO_2 ratios (ppb/ppb) grouped by fuel type, vehicle type and euro class for the data including (all, red) and excluding (filtered, blue) flagged data. The error bars represent the 95% confidence interval calculated for each mean value.

Figure 3.3 shows the comparison of excluding/including the flagged vehicle passes when calculating average NO_x/CO_2 ratios for diesel and gasoline fuel types grouped by vehicle type and euro class (vehicle classification information was obtained using the methods described in Section 2.6). For the majority of the vehicle groups, excluding the flagged data does not make a significant difference in the ratio values and the majority of ratio calculations have good agreement. There are some grouped ratios that have larger differences between the different ratio calculations, however the pattern

of the difference is not always the same (e.g filtered ratios are not always higher), which suggests that time between vehicle passes may not be the best requirement. Furthermore, excluding flagged vehicle passes removes almost half of the data (44.3%), does not seem to alter the average ratio values by a large amount and also results in larger associated confidence intervals.

Flagged vehicle passes represent data in which the separation between vehicles is less clear and the vehicle plumes may overlap. These vehicle passes could be removed, but Figure 3.3 shows that removing these vehicles does not have a large effect on the results and therefore using these vehicles could still provide valuable emissions information. For example, if a clean Euro 6 vehicle is often overlapping with another vehicle, the average ratio may be a bit higher than reality. The same is true for a high emitting vehicle that would be mixed in with lower emitting vehicles and the ratio would tend to be a bit lower than average. However, with many samples the effect is to compress the range of emissions with multiple measurements, which is what is seen in Figure 3.3. Furthermore, a large enough sample of measurements will include different combinations of overlapping vehicles and any possible biases will be significantly reduced. Therefore a requirement based on time between vehicle passes may not be the most effective as much of the data is removed and alternative methods have been considered and described below.

3.3.3.2 Different ratio calculations

A possible improvement to the ratio calculation that has been investigated has been using different regression approaches. Different regression approaches would allow for all of the data to be included, compared to filtering by time between vehicle passes which removes a significant amount of the data. The different regression approaches investigated include weighted linear regression and reduced major axis (RMA) regression.

Weighted regressions were carried out by weighting the linear regression

by the standard error of the slope, as this would down-weight vehicle plumes with larger standard error and possibly provide a better estimate of ratios. Including a weighting of the regression by error, rather than a flag depending on the time between vehicle passes, allows all of the data to be included in ratio calculations. The different weightings investigated were weighting by 1/standard error (reciprocal) and the error/slope (proportional).

Another approach is RMA regression. Standard linear regression assumes that there is no error in the X-axis variable, which is true for categorical variables, however it is not the case for measurements of air pollutants because they have an associated measurement uncertainty. Atmospheric trace gas measurement instruments have associated errors in the measurements which are usually a result of instrumental or measurement noise. Therefore, using standard linear regression to calculate ratios between pollutants could result in an underestimation of ratios due errors in the X-axis measurements not being considered. RMA regression considers the error in both of the variables and gives a more accurate ratio calculation. Further discussion on the importance of different regression approaches is included in Section 3.5.

Figure 3.4 shows the comparison between the different regression approaches for NO_x/CO_2 ratio calculations of grouped vehicles: normal linear regression, linear regression weighted by the proportional and the reciprocal of the error and RMA regression. Figure 3.4 shows that for the majority of the grouped ratios, the RMA regression calculated ratio (in blue) is the highest ratio value. This is because it is likely that standard linear regression is under-estimating slope values. Both of the regressions weighted by error have large variation compared to standard linear regression and it is likely that these are not an accurate way to calculate emission ratios. Therefore the ratio calculated by RMA regression is likely to be the most accurate method for calculation of ratios from point sampling measurement data and this will be the method used for final data analysis.

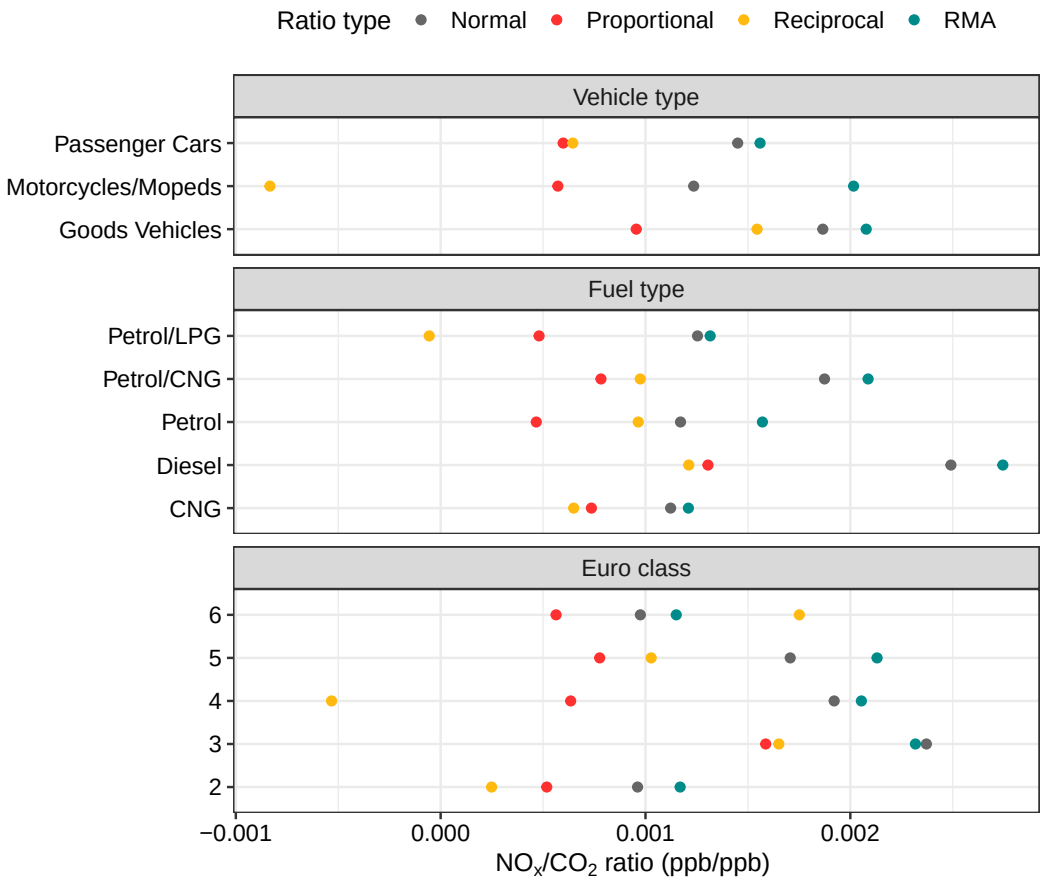

Figure 3.4: Average NO_x/CO_2 ratios (ppb/ppb) grouped by fuel type, vehicle type and euro class for the different ratio calculations. The different ratio calculation types are standard linear regression (grey, normal), regression weighted by 1/standard error (red, proportional), regression weighted by slope/standard error (yellow, reciprocal) and reduced major axis regression (blue, RMA).

3.3.3.3 Other requirements

Further investigation was carried out to determine if other requirements were need for the extraction of vehicle plumes, particularly extraction of combustion-related plume measurements. These other requirements included a minimum change in CO_2 and ensuring that the emission of a pollutant was related to a combustion source.

To be confident that combustion-related vehicle plumes were being extracted, a requirement of a delta change in CO_2 was investigated. CO_2 is directly related to fuel consumption and can be used as a tracer for combustion[167,168,177]. A delta change in CO_2 of 20 ppm was selected as a reasonable value as it exceeded the measurement noise and variation in the background of CO_2. Therefore, vehicle plume measurements used in final ratio calculations had to meet this threshold and this ensured that emission ratios were related to combustion from vehicles. Including a requirement of a delta CO_2 of greater than 20 ppm resulted in the extraction of 3546 vehicle passes (40% of all vehicle passes).

Statistical metrics calculated from the regression were also investigated to ensure that the relationship between pollutants was statistically significant and that an emission event was related to a combustion source. The two metrics that were investigated were R-squared (R^2) and p-values. R^2 values represent how much influence a particular independent variable has on the dependent variable (X and Y variables) and how much variation is explained by the regression model. An R^2 value greater than 0.7 suggests that there is a strong effect on the dependent variable. P-values are used to determine whether relationships between variables are statistically significant and the threshold typically used for this is a p-value less than 0.05.

After some investigation, it was decided that filtering the regression results for a p-value less than 0.05 ensured that there was a good relationship between the variables in the regression calculation. A p-value was chosen over R^2 values as the p-value is a better indicator of the relationship between variables. For example, sometimes the R^2 value may be low, but the corresponding p-value may be high, which suggests that the regression model doesn't fit the data very well and that there is greater variation but that the result is still statistically significant. Low R^2 values are not always problematic, as greater variation may be a result of pollutants not being co-emitted, however it is still important that these results are included when

calculating emission ratios. Including a requirement of a p-value less than 0.05 alongside the requirement of a delta CO_2 of 20 ppm resulted in the extraction of 3100 vehicle passes (36% of total vehicle passes).

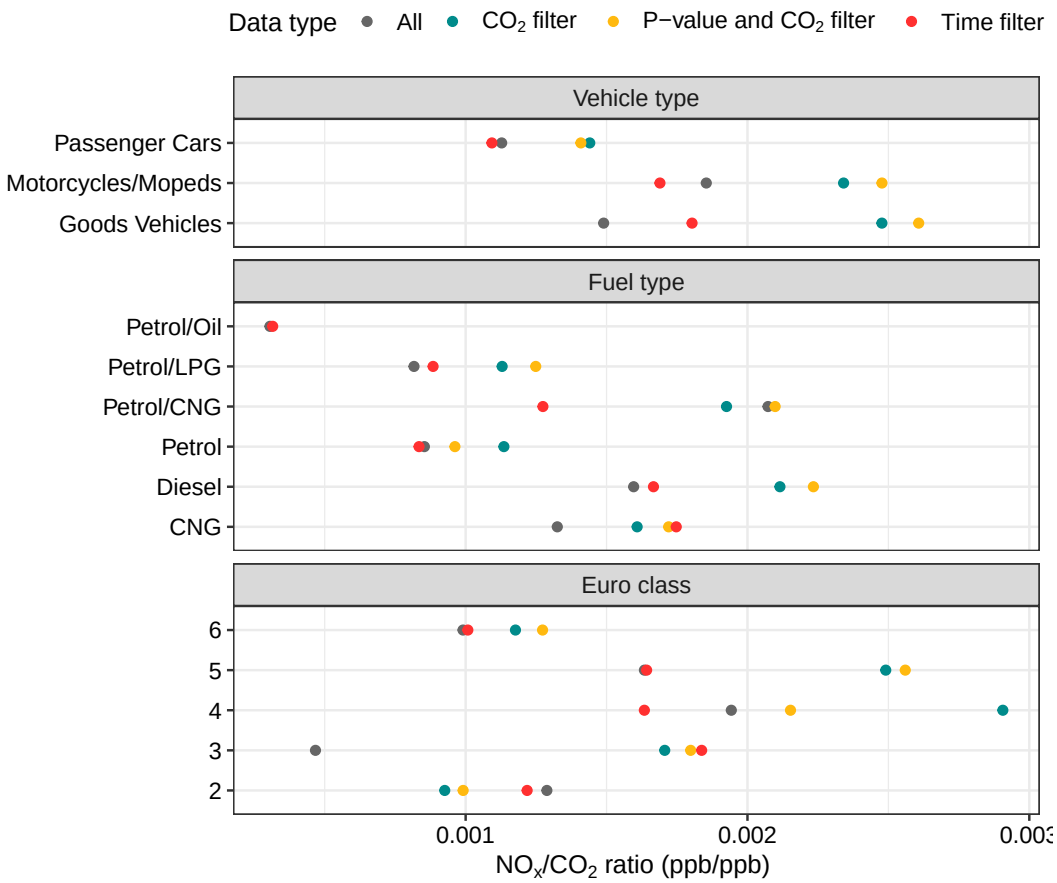

Figure 3.5: Average NO_x/CO_2 ratios (ppb/ppb) grouped by fuel type, vehicle type and euro class for the ratios calculated using different requirements/filters. The data types are all of the data (grey, all), filtered vehicle passes that have a delta CO_2 of 20 ppm (blue, CO_2 filter), filtered vehicle passes that have a p-value of less than 0.05 and a delta CO_2 of 20 ppm (yellow, p-value and CO_2 filter) and filtered vehicle passes that occur greater than 5 s apart (red, time filter). Ratios for all different categories were calculated using RMA.

A combination of RMA regression with these requirements (delta CO_2

of 20 ppm and a p-value less than 0.05) will then lead to the most accurate estimate of ratios between pollutants calculated from point sampling measurements. A comparison of the ratios that result from different requirements/filters is shown in Figure 3.5. Figure 3.5 shows that including a requirement for a delta CO_2 of greater than 20 ppm (in blue) increases the majority of the ratios compared to ratio calculations using all of the data or the data filtered by time between vehicle passes. This would be expected as combustion-only plumes are extracted. Including a further requirement of a p-value of less than 0.05 (in yellow) slightly increases some of the ratios further, but this ensures that the regression results are valid and that there is a good relationship between the two variables in the regression.

3.3.4 Summary of the point sampling analysis method

The text above discusses the development of the analysis method applied to the point sampling data from Milan and will be summarised here. Firstly, the measurements from the ICAD and SIFT-MS are merged to produce a time series with a time averaging of 1 second, with the ICAD measurements interpolated from 1.5 seconds to 1 second. The measurements were then manually time aligned by applying lag times calculated for each pollutant using lighter tests. To further align pollutants, an observation window for each vehicle pass was created. The observation window created contained a third of the time between vehicle passes, with a maximum of 20 observations. Vehicle passes could then be treated individually and air pollutants could be further aligned. The offset for each species and each observation window was determined by calculating the correlation between each species and CO_2. The offset time range was ±5 s and the time offset that gave the best correlation between the species and CO_2 was applied to the data. Once the measurements for each vehicle pass were well aligned, then emission ratios could be calculated. Firstly, vehicle passes were filtered to ensure

that they had an associated delta CO_2 change of 20 ppm, which ensured that combustion-related emissions were extracted. Emission ratios were calculated using RMA regression as this takes into account uncertainty in both of the variables. Finally, the regression results were filtered by a p-value of less than 0.05, to ensure that the regression results were statistically significant. These steps were applied to the point sampling data from Milan and ensured that combustion-related emission ratios were extracted.

The method development was carried out using NO_x/CO_2 ratios as these are well-established results and results can be compared to corresponding results from the remote sensing EDAR system, allowing for the effectiveness of the point sampling measurement and analysis method to be evaluated. Furthermore, extracting vehicle-related plumes of NO_x is less challenging than VOCs due to fewer sources of NO_x compared to VOCs in a busy urban environment, and higher emissions of NO_x from vehicles compared with VOCs. The method can then be applied to calculate VOC ratios to CO_2 for individual vehicles, which will represent the amount of a particular VOC emitted per unit of fuel burnt. The vehicle characteristic groups for VOC ratios may be broader than NO_x/CO_2 ratios (such as only fuel or vehicle type) due to the more difficult nature of measuring VOCs from vehicles. Results from point sampling including emissions of NO_x and VOCs as ratios to CO_2, comparisons to the remote sensing EDAR measurements and a discussion surrounding the measurement technique will be included in Chapter 4.

3.4 Mobile measurement analysis

3.4.1 Background determination and correction

Calculation of emission ratios requires the determination and subtraction of background mixing ratios. This allows for isolation of the local exhaust component of the measurements by separating the most recently emitted plumes

from the urban background. To calculate background mixing ratios, we apply the concept outlined by Padilla et al. [201], where the measured concentrations are defined as a mixture of an urban background concentration and a local enhancement superimposed upon that background.

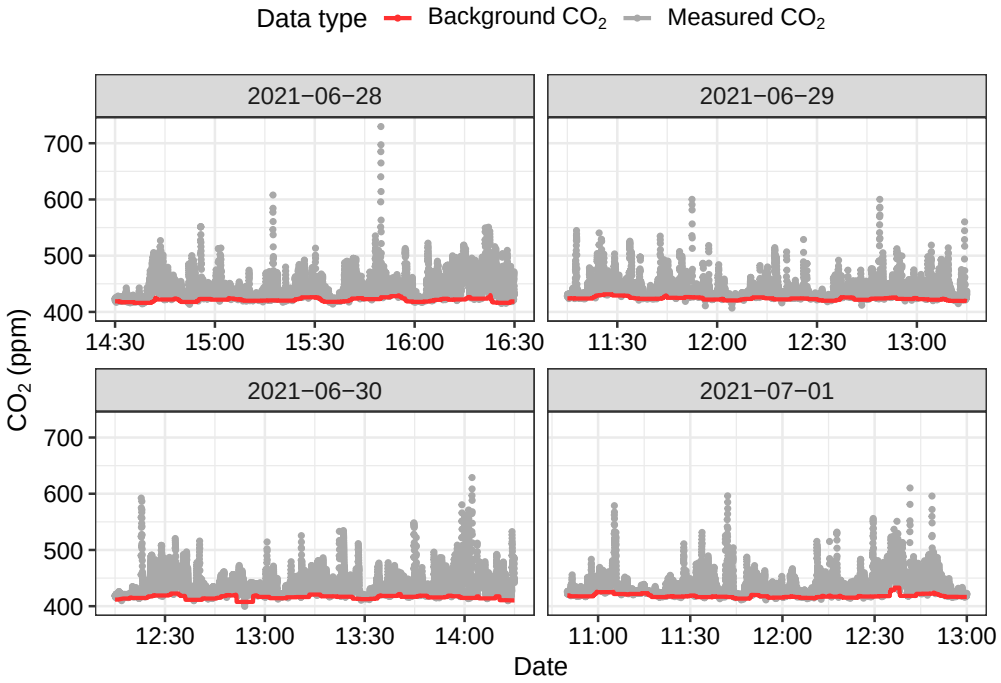

Figure 3.6: Time series of 1 Hz measurements of CO_2 measured by the ICAD (in grey) and the determined background CO_2 concentrations (in red), which were calculated using the 1st percentile of concentrations within a 5 minute rolling window. The time series shown are from mobile measurements carried out in Manchester during Summer 2021.

Background concentrations for NO_x and CO_2 were calculated as the 1st percentile of concentrations within a rolling 5 minute window. The 5 minute windows were centred around each 1 Hz mobile measurement and all data 2.5 minutes before and after each 1 s measurement. Background concentrations represent older pollution, which is a mix of "aged" local emissions and emissions transported to the measurement site from further away sources. Subtracting the background concentration separates the local, recent emis-

sions from other sources. Remaining concentration enhancements represent local, recent emissions which are emitted largely from road transport but also from other non-road sources. Figure 3.6 shows an example of 1 Hz measurements of CO_2 measured by the ICAD and determined CO_2 background concentrations. Figure 3.6 shows that the method described above was able to pick out temporal variations of CO_2 background concentrations from the 1 Hz measurements of CO_2. Background corrected concentrations for all mobile measurements of CO_2 and NO_x were calculated by subtracting the determined background value for each 1 Hz measurement.

3.4.2 Distance-weighted approach

As discussed in Section 3.2, using average or median values of emissions ratios within road segments, as used by Apte et al. [106], will down-weight the contribution from less frequent and higher concentrations. The use of this approach could potentially result in missing intermittent sources and important emissions information. In this work, rather than dividing the road network into discrete, non-overlapping segments to calculate concentrations and emission ratios, a Gaussian kernel smoother is used to weight the mean and regression within a continuous moving window.

The Gaussian kernel smoother is described by by Equation 3.1, where: $K(x, x')$ represents the value of the Gaussian kernel, $\|x - x'\|^2$ is the squared Euclidean distance between the regression point x, and observation x', and σ is the standard deviation that controls the width of the Gaussian curve. The Gaussian kernel represents geographical weights and is a distance decay function, which determines how quickly weights decrease with distance. A Gaussian weighting scheme never reaches zero and therefore every measurement contributes to the regression result, but more weight is given to data close to the location of interest, while down-weighting data collected further away. The use of a distance-weighted approach reduces the influence of out-

liers or measurements with a high uncertainty. Additionally, the Gaussian kernel can be used as a weighting variable in quantile regression modelling or other statistical models, effectively providing a continuous estimate of emission ratio spatially.

$$K(x, x') = \frac{1}{\sqrt{2\pi}\sigma} \exp\left(-\frac{\|x - x'\|^2}{2\sigma^2}\right) \tag{3.1}$$

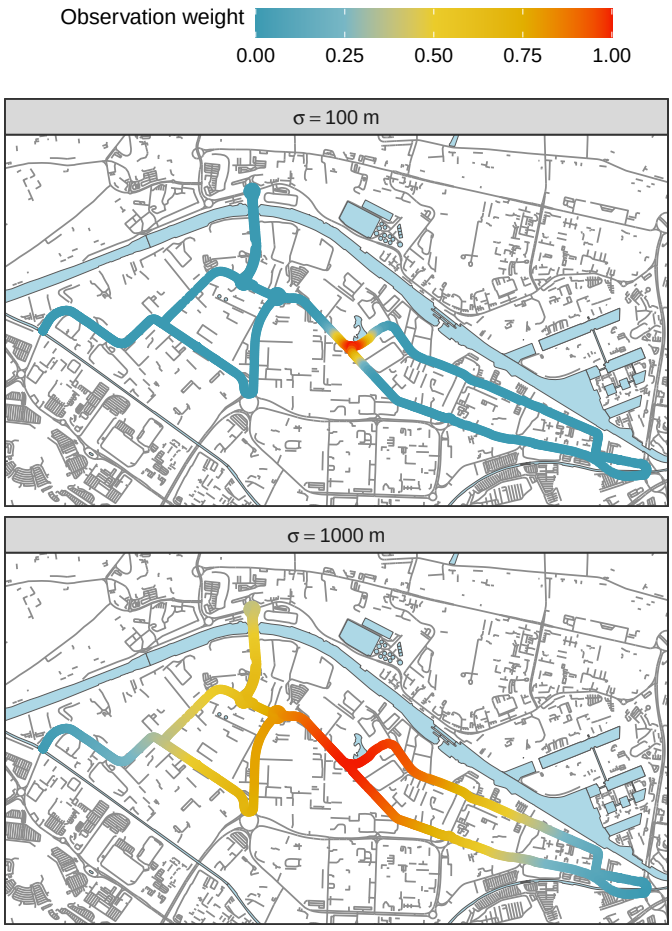

Figure 3.7: Example maps showing the effect of sigma (σ) on the observational weightings used in the distance-weighted approach around the Manchester measurement route (© OpenStreetMap).

The approach also avoids arbitrarily dividing the road up into sections, whereby it can be difficult to determine an appropriate section length. Instead, the spatial scale over which the original data is aggregated can be

controlled by varying the width of the kernel, which is determined by the sigma (σ) value. Figure 3.7 shows an example of the spatial effect that varying the size of the σ value has on observational weightings for a single regression point. A small σ (100 m) can be used to focus on localised effects at a fine spatial scale. A larger value of σ (1000 m) extends the range over which measurements influence the regression and would therefore be useful in studying patterns on a broader, regional scale.

To apply the distance-weighted approach to the mobile measurement data, firstly the road network was split into equally spaced 10 m points. This was selected as an appropriate resolution, given that at an average speed of 20 mph the monitoring platform would cover a distance of 9 m in each 1 Hz measurement. The results were computed at every point within 10 m of any observations. The functions used to perform the analysis are available in the **mobilemeasr** R package[200]. In this analysis, σ was set at 100 m in order to show focus on localised effects at a fine spatial scale.

Results using the distance-weighted approach for spatial mapping of pollutants and quantification of emission ratios will be included in Chapter 5.

3.4.3 Rolling regression to extract combustion events

A distance-weighted regression is useful to identify emission sources spatially, but it still requires a background determination and represents a mixture of a variety of sources. Another approach that has been developed is a rolling regression which can be used to extract combustion events from diluting vehicle plumes[202].

The short-term rolling regression method is represented by Figure 3.8, which shows a scatter plot produced from simultaneous measurements of NO_x and CO_2 in a dispersing plume emitted from a single vehicle exhaust emission event. The red data points are generated from three consecutive measurements at 1 s time resolution. Fitting a regression line through

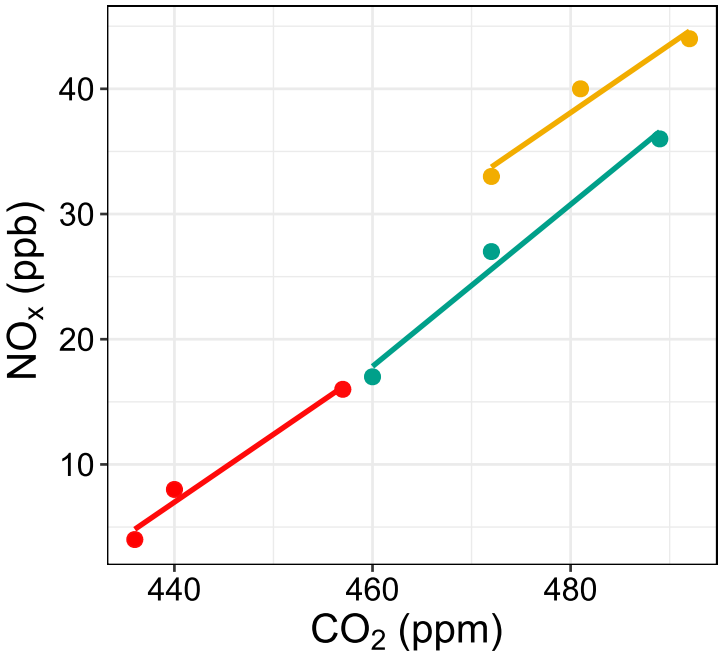

Figure 3.8: NO_x vs CO_2 scatter plot generated from 1 Hz measurements of a dispersing plume emitted from a local combustion event, e.g. vehicle exhaust emissions. The different colour data points represent measurements from three distinct 3 s intervals and the associated regression lines are shown.

these points and determining the value of the slope provides a NO_x/CO_2 emission ratio for the 3 s interval. The NO_x/CO_2 ratio simply represents the change in the concentration of NO_x (ΔNO_x) divided by the change in the concentration of CO_2 (ΔCO_2). The blue and yellow data points and their associated regression lines are generated from measurements of the same plume, made at different 3 s intervals. The slopes of the three regression lines are approximately the same, as the lines are parallel on the scatter plot. This is expected for measurements of a dispersing plume emitted from a single vehicle exhaust emission event, as the ratio of the co-emitted species should be representative of the ratio at the point of emission, and remain constant as the plume dilutes. A 3 s interval is selected, as a minimum of 3 data points are required for the regression- this takes 3 s to obtain using an

instrument with 1 Hz time resolution. The interval is kept to the minimum width required, to retain as much temporal resolution and information on plume dynamics as possible.

The coefficient of determination (R^2) provides a measure of how close the data points are to the regression line. A high R^2 value means that the NO_x/CO_2 ratio remains constant within the 3 s interval, providing strong evidence that the measurements made within that time frame are from the same source. The length of the regression lines gives an indication of how much the pollutant concentrations change within a particular interval. For example the yellow regression line shown in Figure 3.8 is shorter than the blue and red lines and is associated with smaller ΔNO_x and ΔCO_2 values. ΔCO_2 is a useful parameter since a CO_2 enhancement is required to identify a combustion event.

Generating multiple short-term, overlapping regressions from 1 Hz time series data of two co-emitted pollutants and filtering by high R^2 values provides a way to detect dispersing plumes from local combustion events and quantify the associated emission ratios. Regressions are run over short time periods and it is not necessary to account for varying background concentrations. The regressions represent an increment above local background levels and the timescale of changes in background concentrations are negligible relative to the regression timescale (3 s). Subtraction of background NO_x and CO_2 concentrations would slide the position of a regression line on the X-Y coordinate plane, but the slope value would remain unchanged.

To apply the rolling regression approach to the Milan mobile measurements, the ICAD and SIFT-MS measurements were interpolated into a 1 second time series, then the approach was applied to the data to provide a time series of 3 s regression lines. Then a number of filtering steps were applied to ensure that combustion events are extracted. Firstly, the regression lines were filtered by an R^2 value of greater than 0.95, which provides a way to detect dispersing plumes from local combustion events. Secondly,

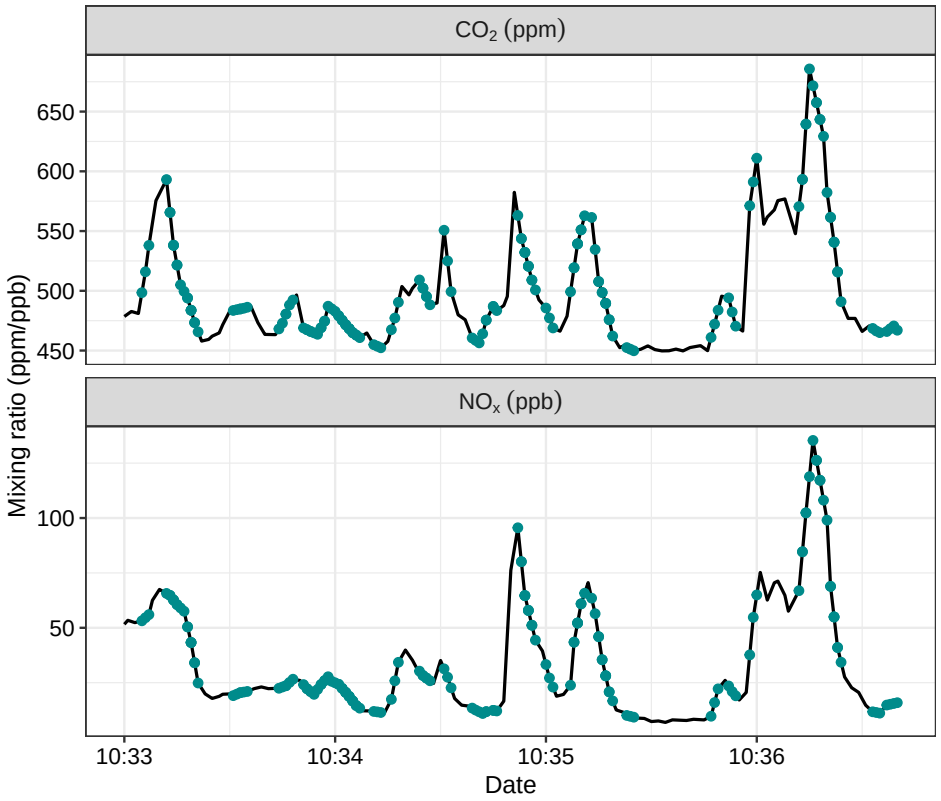

Figure 3.9: Example of a time series of CO_2 and NO_x measurements from mobile sampling in Milan. The black line represents all of the measurement data and the blue points represent the data points that are extracted when the rolling regression and filtering approach has been applied.

the regression lines were filtered for a delta (Δ) CO_2 change of greater than 10 ppm. A Δ CO_2 of greater than 10 ppm was chosen as due to the short regressions, it ensures that any background change in CO_2 is exceeded. Furthermore, it ensures that the high correlation is driven by real covariance and provides a way to extract combustion-related emission events. Finally, the regression lines are filtered for a slope value of greater than 0, which ensures that the high correlation is driven by positive correlation, since co-emitted species in a plume must simultaneously increase or decrease with time. Figure 3.9 shows an example of CO_2 and NO_x measurements during a 3.5 minute mobile measurement sampling period in Milan. The rolling

regression and filtering steps were applied and the blue points represent data points that contribute to the regression lines.

An advantage of this approach is that it can be used to extract combustion-related events from mobile measurement data which is carried out in complex urban environments with a variety of possible emission sources, and still extract local plume dilution events. The approach could be used to quantify the spatial contribution of vehicle emissions to urban air quality.

Results of combustion-related emissions extracted using the rolling regression approach will be discussed in Chapter 5 and there will also be a comparison with the point sampling extracted results to quantify the importance of vehicle emissions spatially.

3.5 The importance of different regression approaches

3.5.1 Different regression approaches

Ratios between pollutants are often used to identify important emission sources or to quantify emission ratios from a specific source or of a particular pollutant. Ratios are calculated using linear regression, which is a linear approach for modelling the relationship between independent and dependent variables (X and Y).

The most widely used regression approach for the calculation of emission ratios is ordinary least squares (OLS). In OLS, it is assumed that the independent variable (X) is error-free and only considers the error associated with the dependent variable (Y). It is achieved by minimising the sum of squares (S) in the Y residuals (vertical deviations), shown by the distance AB in Figure 3.10 and represented by Equation 3.2:

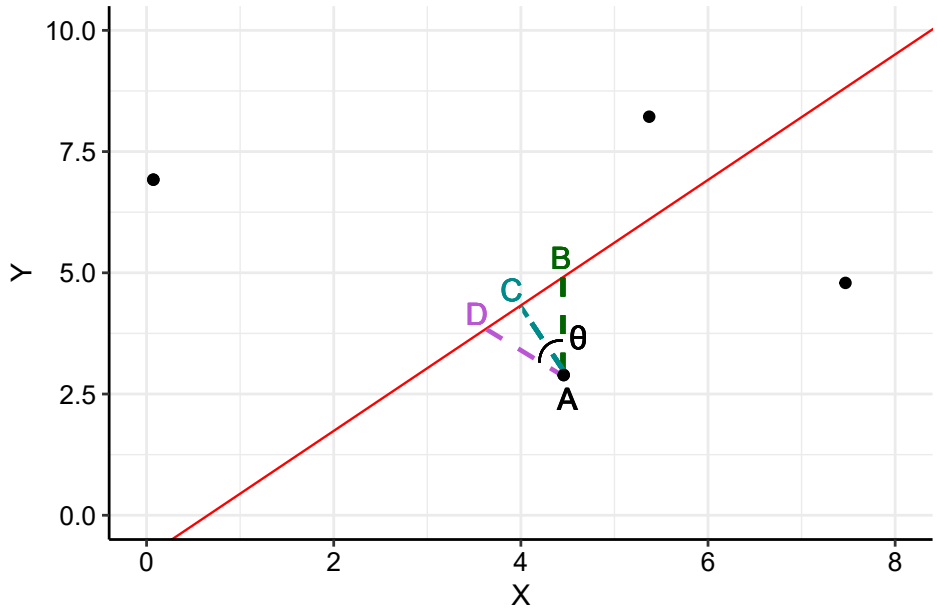

Figure 3.10: Relationships between data point A and the line of best fit (in red). Fitting the line by OLS minimises the distance of AB (AB is perpendicular to the x axis). Fitting the line by RMA minimises the distance of AC (AC is perpendicular to L). Fitting the line by York regression minimises the distance of AD. AD has a θ degree angle relative to AB and the θ depends on the weights of measurement errors in Y and X. Adapted from Wu and Zhen Yu [2].

$$S = \sum_{i=1}^{N} (y_i - Y_i)^2 \tag{3.2}$$

where

- Y_i are the observed data points
- y_i are the regressed data points of the regression line
- N is the number on data points used for the regression

In the case of measurements of atmospheric pollutants, both the X and Y variables are likely to have associated errors[2,203]. Therefore, the use of

OLS regression to calculate ratios between pollutants, could lead to a biased result and the slope value is likely to be underestimated, as is described below.

To overcome the limitation of OLS regression, further regression models can be utilised which consider errors in both of the variables. The reduced major axis (RMA) regression technique, considers the errors of both the X and Y variables. RMA minimises the sum of the squared orthogonal distances (vertical and horizontal deviations) from all data points to the regressed line, shown by the distance AC in Figure 3.10:

$$S = \sum_{i=1}^{N} \left[(x_i - X_i)^2 + (y_i - Y_i)^2 \right] \tag{3.3}$$

where

- X_i are the observed data points
- x_i are the regressed data points of the regression line

A further improvement is the York regression technique[204,205], which calculates the slope using actual error values in the X and Y variables. The error values can be determined from calibrations performed during measurements. York regression introduces the correlation coefficient of errors in X and Y into the minimisation function, shown by the distance AD in Figure 3.10:

$$\begin{aligned} S = \sum_{i=1}^{N} \Big[& \omega(X_i)(x_i - X_i)^2 - 2r_i \sqrt{\omega(X_i)\omega(Y_i)} \\ & (x_i - X_i)(y_i - Y_i) + \omega(Y_i)(y_i - Y_i)^2 \Big] 1/(1 - r_i^2) \end{aligned} \tag{3.4}$$

where

- $\omega(X_i)$ and $\omega(Y_i)$ are weighted data points based on the standard deviation of the error in X and Y, respectively:

$$\omega(X_i) = 1/(\sigma_{X\,i})^2, \omega(Y_i) = 1/(\sigma_{Y\,i})^2 \tag{3.5}$$

- r_i is the correlation coefficient between measurement errors in (X_i) and (Y_i)

This section discusses the importance of different regressions approaches by comparing ratios calculated using the OLS, RMA and York regression techniques. This section also discusses the effect of including measurement uncertainties in ratio calculations.

3.5.2 Examples

3.5.2.1 Simulated data

Comparisons of the different regression techniques for the calculation of pollutant ratios have been carried out with simulated data and the effect of different regression techniques on the resulting slope values has been investigated. Simulated data was generated for 50 X and Y variables, where higher errors are associated with the X variable. Error values for X span between 1 and 20, for Y between 1 and 2 and they were generated in uniform distribution. The simulated data was generated so that the slope value is equal to 1.

The slope and intercept was calculated for the simulated data using the different regression approaches and the results are shown in Figure 3.11. The OLS calculated slope is 0.52 and there is a clear deviation between the lines of best fits for RMA and York regression. RMA regression increases the slope value to 0.71 and York regression increases the slope value even further to 1.07. The effect of the angle (θ) is clear, as the York regression line of best fit is closer to the Y-axis. In the simulated data, the errors of the X variable are higher, making the X data points less reliable and therefore the line tends to be further away from the X-axis. OLS significantly underestimates the ratio

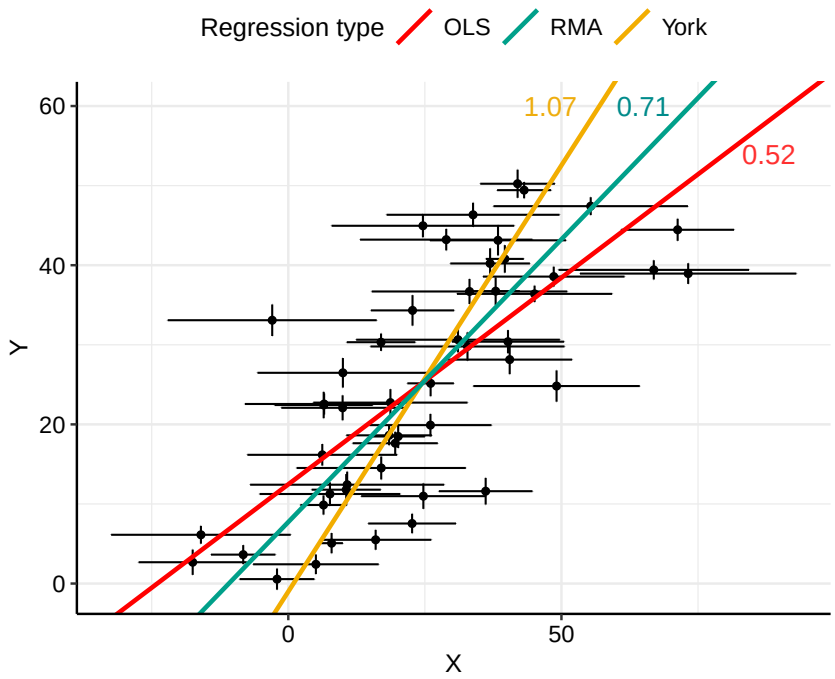

Figure 3.11: An example of simulated data for X and Y variable values with varying error, simulated to have a slope value of 1. The regression slopes and values correspond to results using different regression approaches- OLS (red), RMA (blue) and York (yellow).

by calculating a slope half of the one that was expected. RMA regression increases the slope, but the value is still underestimated. On the contrary, York regression predicted the slope value the most accurately.

The example shown in Figure 3.11 of the X variable having a significantly larger error than the Y variable could be true for the ICAD data. Gas-cylinder only measurements were performed using the ICAD and during this measurement period the CO_2 value had a standard deviation of 4 times higher than the corresponding NO_x value. The CO_2 measurement is likely to have a higher error as the measurement is performed with a sensor, compared to the NO_x measurement which is performed using absorption spectroscopy. The effect of ignoring errors associated with the X variable will tend to result in an underestimated slope, therefore it is important that these errors are

accounted for in the regression calculation.

3.5.2.2 Mobile measurements in York

The effect of the different regression methods has been investigated using measurements of toluene and benzene carried out by the SIFT-MS. This section investigates mobile measurements carried out in York, specifically the toluene-to-benzene (T/B) ratio along Hull road, which was used in Wagner et al. [206] to reveal evaporative emissions and is discussed more in details in Chapter 5. Figure 3.12 shows the T/B ratio along Hull road calculated using the different regression methods.

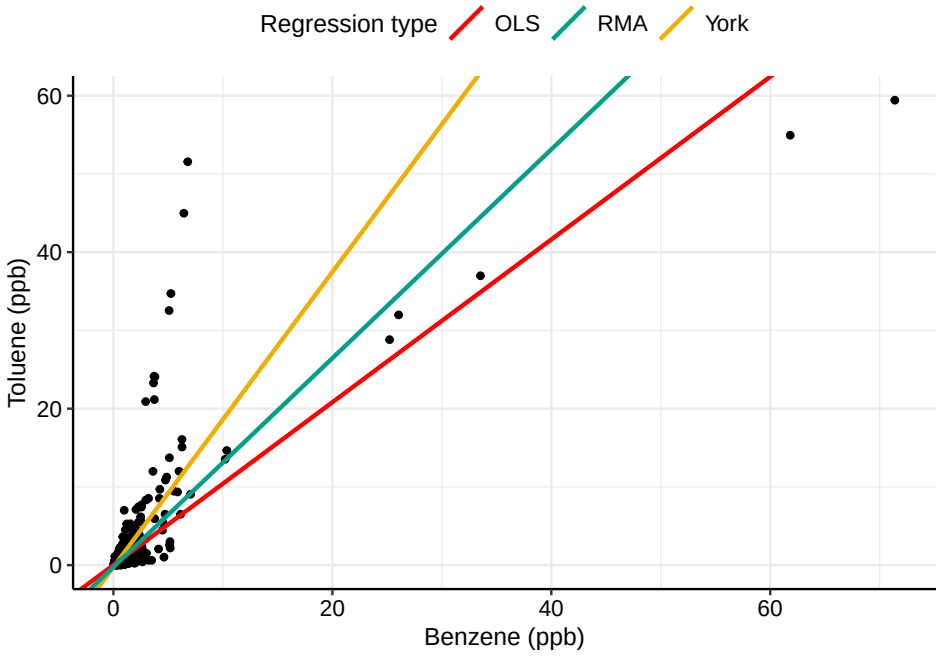

Figure 3.12: Toluene and benzene values (in ppb) along Hull road with the toluene-to-benzene (T/B) ratio calculated using the different regression methods- OLS , RMA and York.

The error values used in the York regression for the benzene and toluene measurements were obtained from the error in the calibration slopes, which were performed daily. The average error in the calibration slopes during the

measurement period was 70% higher for benzene than toluene. Figure 3.12 shows that the use of RMA and York regression significantly increase the ratio value compared to OLS regression. Compared to the OLS regression calculated T/B value of 1.04, RMA regression increased the ratio value by 28% to 1.33 and York regression increased the ratio value by 82% to 1.89. This is a significant increase, which could be important in the identification of emission sources with the use of emission ratios between pollutants.

3.5.2.3 Point sampling in Milan

The effect of different regression techniques has also been investigated using the point sampling measurements carried out in Milan. The T/B ratios were calculated for individual vehicle passes using the methods described in Section 3.3- vehicle passes were extracted if there was an associated Δ CO_2 change of greater than 20 ppm and the regression had a p-value of 0.05. The T/B ratios could then be grouped together by different vehicle characteristics and here we use vehicle type as an example.

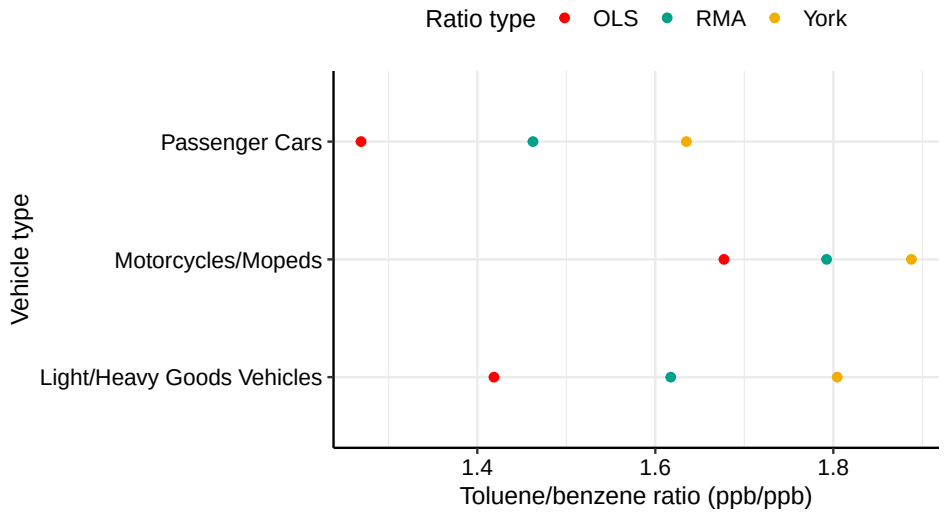

Figure 3.13: The toluene-to-benzene ratio for vehicle types during Milan point sampling measurements. The plot also shows ratio values for different regression methods- OLS, RMA and York.

Figure 3.13 shows the average T/B ratios for different vehicle types calculated by the different regression methods (OLS, RMA and York). Compared to OLS regression ratio values, the RMA regression increases ratio values by 11% on average and York regression increases ratio values by 21% on average. The T/B ratios for passenger cars and goods vehicles show large increases when the RMA and York regression methods are used compared to OLS. The T/B ratios for motorcycles and mopeds show smaller increases when the different regression approaches are used, suggesting that the measurements may have less uncertainty associated with them.

3.5.3 Application to measurement data

As shown above, it is important to consider different regression approaches as OLS underestimates calculated ratio values because it does not take into account errors in both the X and Y variables. When calculating ratios for point sampling measurements, the RMA regression approach was used (results shown in Chapter 4) as this approach takes into account errors in both X and Y variables, which is likely to be true for atmospheric gas measurements. York regression is an important approach and further improves the accuracy of ratio calculation, but it was not used in this work as calibrations of the ICAD instrument were not regularly carried out. A future improvement would be to ensure that all instruments/measurements were regularly calibrated.

3.6 Conclusion

Analysis methods for analysing complex point and mobile sampling measurement data sets have been developed. The new analysis methods aim to obtain useful emissions information that cannot be determined from existing data analysis methods.

The data analysis method developed for point sampling measurements ensures that measurements associated with individual vehicles are extracted and then aligned to CO_2. Requirements of a (Δ) CO_2 value of greater than 20 ppm and a P-value of less than 0.05 ensured that combustion-related vehicle plumes were extracted and that any increases in the pollutant of interest were as a result of combustion. The calculation of emission ratios of individual vehicles was carried out using linear regression, therefore removing the need for background determination, which can be difficult in a complex urban environment. RMA regression was used to calculate emission ratios, which takes into account measurement errors of the pollutants and results in a more accurate calculation of the ratio.

Data analysis methods have been developed for mobile measurements and these methods incorporate regression-based approaches to quantify spatial emission sources. A distance-weighted approach has been developed which can be used to provide spatial distribution of pollutants or a continuous estimate of emission ratios spatially. The distance-weighted approach avoids arbitrarily dividing the road network into discrete segments and reduces the influence of outliers or measurements with a high uncertainty, ensuring an accurate estimation of spatial emissions. A rolling regression / plume dilution method has also been developed, which can be used to extract combustion-related vehicle emissions from mobile measurements. This enables vehicle-related emission ratios calculated from mobile measurements to be compared to emission ratios calculated from point sampling, therefore the importance of vehicle emissions on a spatial scale can be determined.

The importance of different regression approaches for the determination of emission ratios has also been discussed. OLS regression does not consider the errors associated with the X variable and the use of OLS regression to calculate emission ratios may lead to a biased result. RMA and York regression approaches take into account error associated with both variables and lead to a more accurate emission ratio calculation. RMA regression

will be the regression technique used in Chapter 4 for the calculation of emission ratios from individual vehicles. York regression is the most accurate approach, but regular calibrations of the ICAD instrument were not carried out and therefore this approach cannot be applied to the measurement data. A future improvement would be to ensure error values for all instruments were obtained regularly so the York regression approach can be used for regression analysis.

Chapter 4

Roadside vehicle point sampling

4.1 Abstract

Volatile organic compounds (VOCs) and nitrogen oxides (NO_x = NO + NO_2) play an important role in the formation of ozone and particulate matter, which can both have detrimental effects on human health. It is widely known that vehicle exhaust emissions contribute significantly to the total emissions of NO_x. However, the contribution of vehicle exhaust emissions to the total emissions of VOCs is less well-understood, with much of the understanding depending on in-laboratory tests or tunnel studies. Whilst these are useful, many of these studies do not represent real-world conditions and measurements from individual vehicles are often limited. Furthermore, vehicle exhaust emissions could be an important source in urban areas, where other VOC sources may not be present. Therefore, it is important that emissions of VOCs directly from the vehicle exhaust are quantified in order to effectively mitigate air quality issues.

A new method of direct exhaust sampling from individual vehicles, point sampling, was carried out by the roadside in Milan, Italy. The point sampling technique involves fast-response measurements from vehicle exhaust plumes at the roadside. Point sampling measurements have been used to derive

emission ratios of NO_x and VOCs for different vehicle categories. We find that motorcycles and mopeds have a NO_x/CO_2 ratio 1.7 times higher than passenger cars and a VOC/CO_2 ratio 5 times higher than passenger cars. The VOC/CO_2 ratio for two stroke (gasoline-oil) vehicles is 6.8 times higher compared to standard gasoline vehicles. We also find that natural gas fuel vehicles also have much higher NO_x and VOC ratios to CO_2 compared to standard fuel vehicles (gasoline and diesel). These vehicle and fuel types may be an important source of NO_x and VOCs in European cities, where there is a significant amount of these vehicle types. They may become more important in low emission zones, where they are typically less stringently regulated than passenger cars, goods vehicles and standard fuel types.

4.2 Introduction

As discussed in Chapter 1, NO_x and VOC emissions play an important role in the formation of O_3 and particulate matter, which contribute to poor air quality in urban areas. It has been well-established that road vehicles are an important source of NO_x in urban areas, being responsible for more than 30% of total NO_x emissions in Europe[207]. NO_x emissions from vehicles are regulated by European emission standards, Euro classes, which limit the emissions of common pollutants, including CO, NO_x and PM, from vehicles. Euro classes are updated every few years and the emission limits become more stringent, information on Euro classes and details surrounding their emission limits are included in Appendix B. The compliance of vehicles with emissions regulations is determined during laboratory tests on chassis dynamometers[208], but, as discussed inSection 1.5, the "Dieselgate" scandal highlighted the need for more real-world measurements due to manufacturers cheating in-laboratory testing[152].

Real-world measurement techniques of NO_x include PEMS (Portable Emission Monitoring System) and remote sensing. PEMS is carried out

by instrumenting individual vehicles and has been used to measure on-road emissions from vehicles over a range of driving conditions[209–211], but PEMS measurements can be time consuming and expensive in order to obtain emissions information from numerous vehicles. Remote sensing is a measurement technique used to produce real-world emissions information from a large number of vehicles, it is also a non-intrusive measurement and therefore emissions testing cannot be optimised for remote sensing measurements[212]. Remote sensing measurements have been used by many studies to highlight trends in emissions of NO_x from road vehicles[208,212,213] and to identify vehicle types, fuel types or certain manufactures that may be high emitters of NO_x[4,154,158,159,162,214].

Whilst emissions of NO_x are well-quantified, emissions of VOCs from road vehicles are less understood. Current understanding of emissions of VOCs from road vehicles is from laboratory or tunnel studies, which can be limited and do not represent real-world conditions[215,216]. Laboratory tests using chassis dynamometers have been used to determine VOC emission source profiles from a variety of vehicles[217], characterise VOC emissions from 2-stroke motorcycles[218] and measure speciated VOC emissions from different fuel type vehicles[219–221]. Laboratory tests of engines have also been used to measure hydrocarbon emissions from different fuel type vehicles[222] and characterise VOC emissions from motorcycles with different emission control devices[151]. Laboratory tests are useful for characterising VOC emissions from vehicles, but it is important that measurements in real-world conditions are carried out.

Tunnel studies have been used to quantify VOC emissions from vehicles and these measurements are carried out in real-world conditions. Tunnel studies have been used to determine source profiles of VOCs from on-road vehicles in China[217], quantify emissions of carbonyls from duty vehicles[223] and quantify exhaust emissions of VOCs from diesel and gasoline vehicles. These studies are useful and are used to produce average emissions of a

vehicle fleet or estimated emissions for a particular vehicle group using vehicle count data. However, tunnel studies cannot be used to obtain emissions information for individual vehicles, which is needed to determine vehicle groups that emit high amounts of VOCs in order to quantify their effect on air quality in urban areas. Other studies have obtained information on emissions of VOCs from vehicles through analysis of ambient VOC measurements[197,224,225] or laboratory measurements of the VOC composition of vehicle fuel samples[129,225].

As discussed in Chapter 2 and Chapter 3, point sampling is a measurement technique for the determination of emissions from on-road vehicles. It has been used for on-road quantification of particulate and gaseous emissions from buses[166,168,176], passenger cars[167] and goods vehicles[177,202]. The point sampling technique offers the potential to broaden the suite of air pollutants, as theoretically any species can be measured, provided the accuracy and response time of the instrument is sufficient to resolve the transient emissions of passing vehicles. More recently the point sampling method was used alongside mass spectrometry for quantification of organic and inorganic gases from heavy-duty trucks[178]. Current point sampling measurement studies highlight the potential of the technique, but have been carried out in controlled conditions with limited influence from other traffic or emission sources, which would be present in urban areas. They also tend to focus on limited vehicle types, typically larger vehicles such as buses, vans and trucks, which produce larger exhaust emission plumes. Therefore, it is important that VOC vehicle emissions in the real-world are quantified for a variety of vehicle types to determine the importance of VOC emissions in urban areas.

In this work, we apply the analysis methods discussed in Section 3.3 to the point sampling measurements carried out in Milan. The work aims to extract combustion-related vehicle plumes from a complex urban background, which is difficult for VOCs as they have a multitude of possible

emission sources. Possible emission sources in urban areas include road transport, evaporative emissions from fuel stations, cooking, residential wood burning, VCP usage and many others. We aim to highlight differences in the emission of NO_x and VOCs by fuel and vehicle type and to identify high emitting vehicles. This work also aims to investigate the speciation of VOC emissions from vehicles and how the results compare to the literature. Furthermore, the emission results extracted from the point sampling measurements will be compared to corresponding results from the EDAR remote sensing instrument to assess the agreement between the two measurement techniques.

4.3 Overview of the vehicle fleet in Milan

As discussed in Section 2.6, vehicle informationganic was obtained using an ANPR camera situated in the window of the Graz/Airyx measurement van behind the WASP (shown in Figure 2.11). There were a total of 9289 vehicle passes that were recorded by the ANPR camera during ~4.5 days of point sampling measurements in Milan. Vehicle characteristics were then obtained from the Italian Ministry of Transportation using the detected number plates, including vehicle type, fuel type, Euro class, emission controls, vehicle weight and many other vehicle characteristics. A summary of selected characteristics of the vehicle fleet, including vehicle type, fuel type and Euro class, captured by the ANPR camera are shown in Figure 4.1.

The vehicle fleet at the point sampling measurement site consisted of a majority of passenger cars (7315 vehicles), with some goods vehicles (1330 vehicles) and a small number of motorcycles and mopeds (402 vehicles). It is likely that the number of motorcycles and mopeds that passed the measurement location is higher as they typically drive closely to other vehicles and therefore their number plates may not have been detected by the ANPR camera. However, it is difficult to say how maw many vehicle passes were

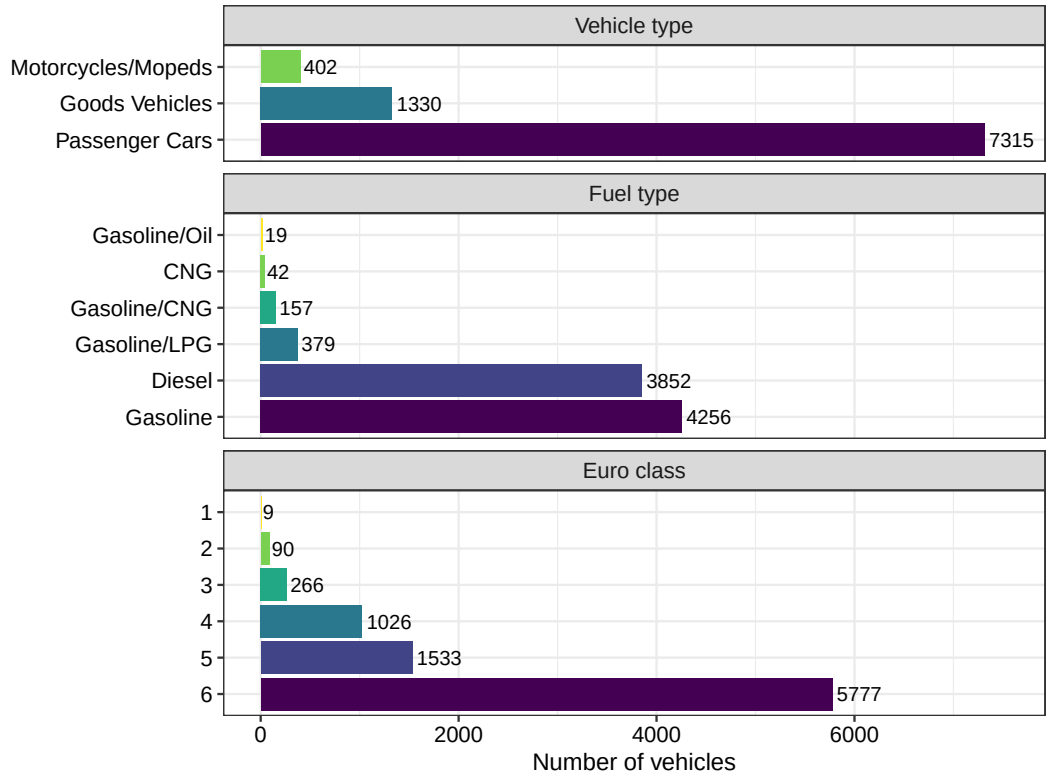

Figure 4.1: A summary of the characteristics of the vehicle fleet recorded by the ANPR camera during roadside point sampling in Milan. The characteristic categories include vehicle type, fuel type and Euro class and the numbers next to each bar correspond to the number of vehicles for each category.

missed as there was no other separate traffic count.

The majority of vehicles were either gasoline (4256 vehicles) or diesel (3852 vehicles) fuel type and there were a small number of other fuel types recorded. 6.2% of vehicles recorded were gas fuel vehicles, which include compressed natural gas (CNG) and gasoline bi-fuels with liquefied petroleum gas (LPG) and CNG. Gasoline/CNG and gasoline/LPG vehicles are bi-fuel vehicles with two separate fuel tanks, where the engine can run on one fuel or the other. LPG is a fuel gas which contains a mixture of hydrocarbon gases, including propane, propylene, butylene, isobutane and n-butane, and it is obtained as a by-product of petroleum refining or natural gas

processing[211,226]. CNG is a fuel gas which contains mainly CH_4 (84%), and smaller amounts of ethane, propane and butane[210] and it is made by compressing natural gas, which is increasingly obtained from shale gas reserves[211,226]. In the EU, CNG and LPG fuel are promoted as an alternative to traditional fossil fuels in order to reduce greenhouse gas emissions. In Italy in 2020, 9% of passenger cars and 4.8% of light goods vehicles were gas fuel vehicles, which is a significant proportion of the total vehicle fleet. Across Europe, the proportion of gas fuel vehicles is slightly lower with 1.8% of passenger cars and 1.1% of light goods vehicles and in the UK less than 1% of vehicles are gas fuel vehicles[227]. During point sampling measurements, there were also a small number of gasoline/oil bi-fuel vehicles (19 vehicles) and this fuel type is associated with 2-stroke engines in motorcycles and mopeds, which require around 3-6% of oil to be added to the fuel due to the absence of a lubricating system.

The majority of the vehicle fleet consisted of Euro class 6 vehicles (5778 vehicles), the most recent Euro class which was introduced in September 2015 for passenger cars. Therefore vehicles of this Euro class should have the lowest emissions as they have the most stringent emission limits. The high proportion of Euro class 6 vehicles could be a result of the point sampling measurement site being located within the low emission zone (LEZ) of Milan. The LEZ is a limited traffic area with no access or an access charge for the most polluting vehicles. Newer vehicles with lower emissions are not charged to use the area and therefore people are encouraged to drive lower emitting vehicles. The possible effect of the measurement location is discussed in subsection 4.3.1.

Figure 4.2 shows a further breakdown of the number of vehicles for each vehicle type, Euro class and fuel type. It is worth noting that Figure 4.2 only includes vehicles that had recorded information for all of the categorical variables and vehicles that were missing information, 374 vehicles, were not included in this plot (but were included in further analysis).

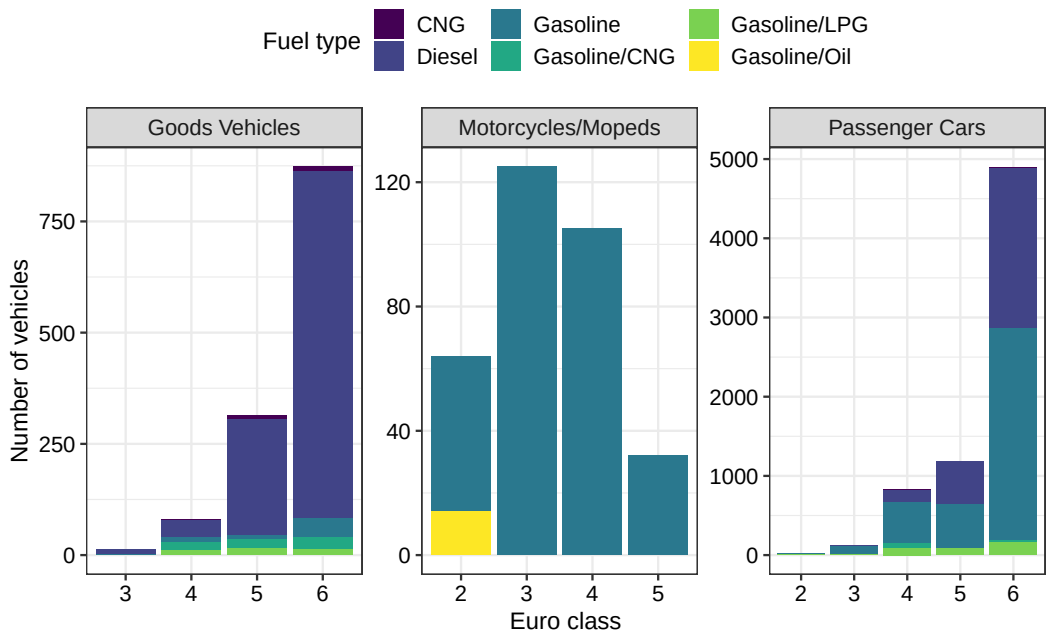

Figure 4.2: A further breakdown of the vehicle fleet recorded by the ANPR camera during roadside point sampling in Milan. The number of vehicles are separated by vehicle type and Euro class and are coloured by the fuel type. Note: the axis scales are different for each vehicle type.

The majority of goods vehicles had a diesel fuel type (82%) with small amounts of gasoline and natural gas fuel types. The goods vehicles were also mainly newer vehicles, with 66% of vehicles being Euro class 6 vehicles. 95% of the goods vehicles were light goods vehicles (pick-up trucks and vans). Motorcycles and mopeds were majority gasoline fuel vehicles (78%), with a small amount of gasoline/oil fuel vehicles, which are used in 2-stroke engines. The most recent Euro class standard for motorcycles and mopeds is Euro class 5, which was introduced in 2020. Only 8% of motorcycles and mopeds were Euro class 5 vehicles, with the majority being older Euro class vehicles. Passenger cars were mainly Euro class 6 vehicles (67%) and the majority were gasoline or diesel fuel type vehicles, with slightly more gasoline vehicles (53% gasoline and 37% diesel). There was also a small percentage of passenger cars with gasoline/gas bi-fuel types (gasoline/LPG

and gasoline/CNG).

The vehicle fleet recorded at the measurement site in Milan had large variety in vehicle type, fuel type and Euro class, with a significant proportion of gas fuel vehicles. The vehicle fleet in Milan could be a contrast to a typical vehicle fleet in UK cities, due to the lack of motorcycles/mopeds and natural gas fuel vehicles. Therefore, the contribution of vehicles to emissions spatially could differ quite drastically and this may be observed during mobile measurements carried out in Milan and UK cities (discussed in Chapter 5).

4.3.1 Representativity of measurement site vehicle fleet in Milan

Additional remote sensing measurements were carried out with the HEAT remote sensing instrument at another location in Milan, directly after the first measurement campaign. The second measurement location was via Francesco Cilea, which is a street located on the north-west side of the outskirts of Milan, outside the low emission zone and 11 km from the Madre Cabrini measurement location (locations of the measurements are shown in Figure B.1). The different vehicle fleets recorded in both locations have been compared to see if the low emission zone affects the composition of the vehicle fleet.

Vehicle fleet information for both of the measurement sites was obtained using the ANPR camera associated with the EDAR measurements. Figure 4.3 shows the comparison between the vehicle fleets recorded at Madre Cabrini and via Cilea. The two measurement sites show a lot of similarities, the majority of vehicles are passenger cars, with a fuel type of gasoline and a Euro class of 6. There is a slightly higher percentage of goods vehicles and diesel vehicles at the Madre Cabrini site and a slightly higher percentage of gas fuel vehicles at the Cilea site.

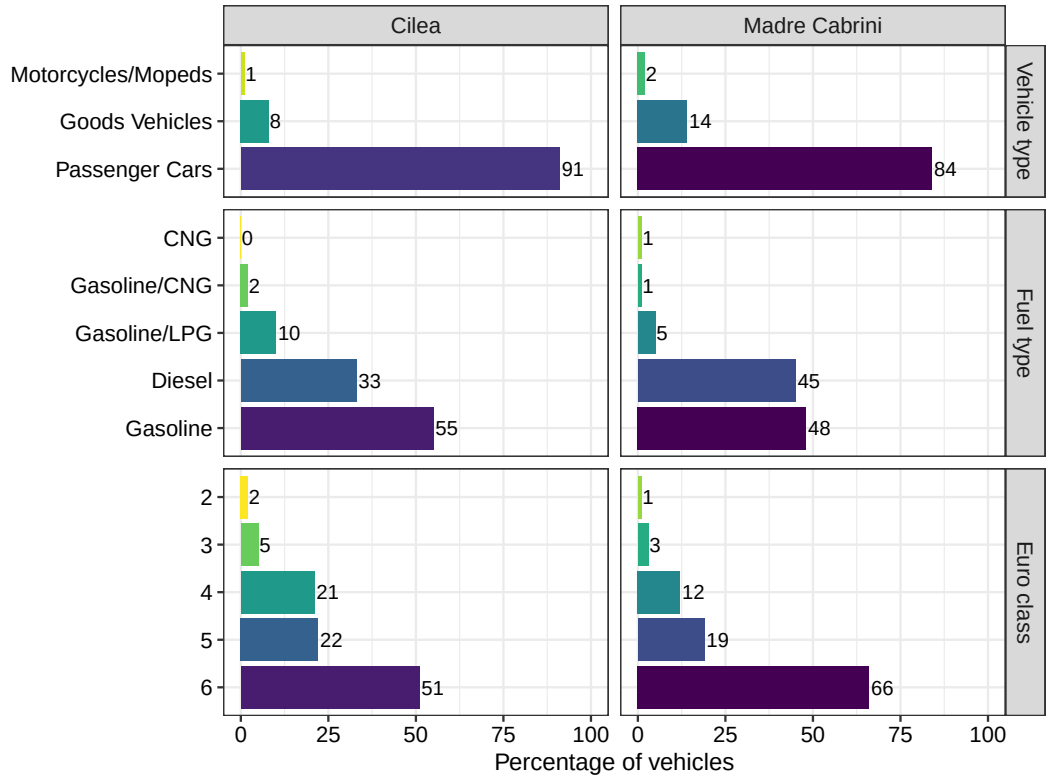

Figure 4.3: A summary of the vehicle fleets recorded by ANPR cameras at the different measurement locations in Milan- Cilea and Madre Cabrini. The numbers next to each bar correspond to the percentage of vehicles for each category, calculated from the total number of vehicles at each site.

Overall, the composition of the vehicle fleets recorded at both measurement locations shows good agreement, therefore suggesting that the low emission zone does not affect vehicle fleet composition. Furthermore, it is likely that the vehicle fleet at the Madre Cabrini measurement site is representative of the vehicle fleet in the area of Milan.

4.4 NO_x emission ratios from point sampling

Emission ratios of NO_x to CO_2 for individual vehicles were calculated using the analysis method described in Section 3.3. Initial investigation of emission ratios calculated from the point sampling measurements focused

on NO_x/CO_2 ratios as NO_x emissions from vehicles are well-quantified by various remote sensing studies[4,158,159,161,162,208,212,213].

NO_x to CO_2 ratios have been extracted and calculated for individual vehicles from point sampling measurements. The ratios have then been grouped by different vehicle categories, including vehicle type, fuel type and Euro class, to give an average NO_x/CO_2 ratio for different vehicle characteristic categories, which is shown in Figure 4.4. NO_x/CO_2 ratios separated by vehicle type, fuel type and Euro class is shown in Figure 4.5.

The vehicle type with the highest average NO_x/CO_2 ratio is goods vehicles. 87% of the goods vehicles were diesel fuel vehicles, which dominate NO_x emissions[161]. Diesel engines emit higher amounts of NO_x due to lean-burn combustion conditions, which is the burning of fuel with an excess of air and in high temperatures[131].

Motorcycles and mopeds are the vehicle type with the second highest average NO_x/CO_2 ratio. The majority of motorcycles and mopeds have a gasoline fuel type and it would therefore be expected that the ratio would be more similar to the ratio of gasoline fuel vehicles. However, the emission standards for motorcycles and mopeds have traditionally been less stringent than for passenger cars. The previous emission standard of motorcycles and mopeds, Euro 4, had NO_x emission limits 1.5 times higher for motorcycles and 2.8 times higher for mopeds when compared to Euro 6 passenger cars (emission limit values included in Appendix B). The introduction of the most recent emission standard for motorcycles and mopeds in 2020, Euro class 5, reduced the emission limit of NO_x to the same value as Euro 6 passenger cars. However, only 12% of the motorcycle and moped extracted from point sampling were associated with Euro 5 emission standards and the majority were associated with older emission standards. Therefore, the relatively older fleet of motorcycles and mopeds are likely to emit higher amounts of NO_x and a higher NO_x/CO_2 ratio is observed. The average NO_x/CO_2 ratio for motorcycles and mopeds is 1.7 times higher than the average ratio for

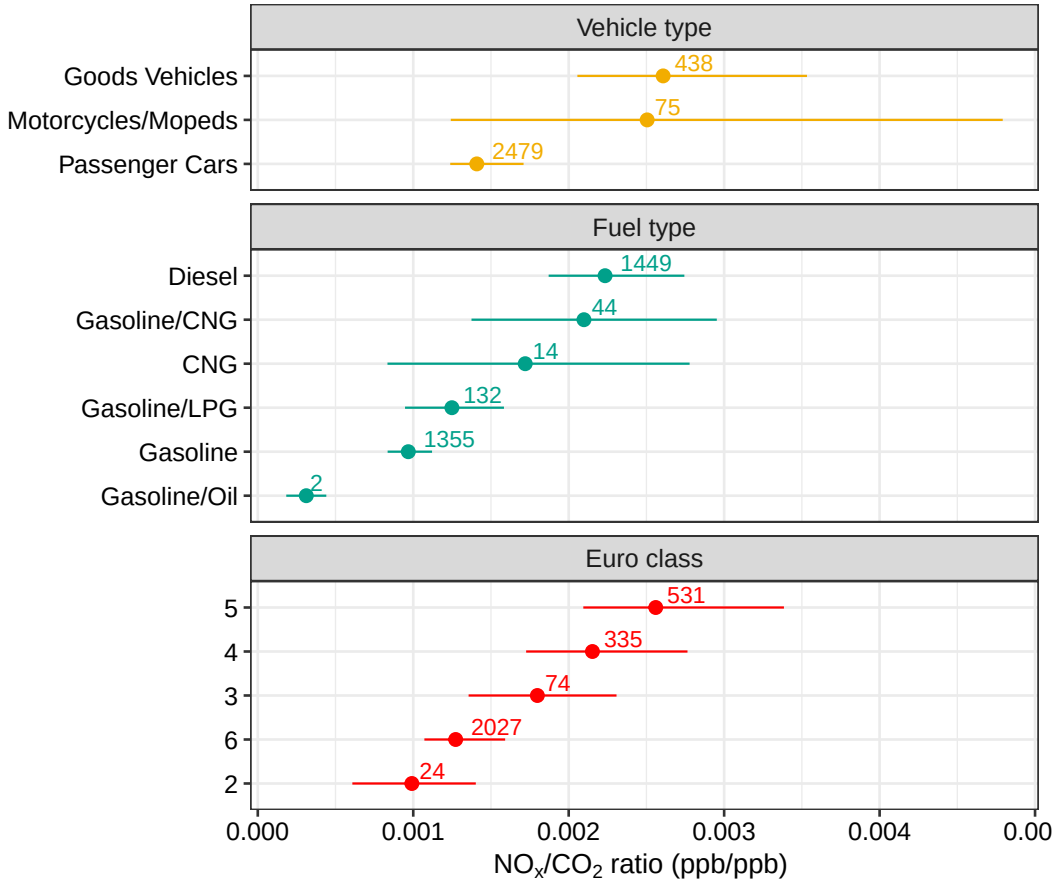

Figure 4.4: Average NO_x/CO_2 ratios (ppb/ppb) calculated for different vehicle characteristic categories, including vehicle type, fuel type and Euro class. The variables in each category are ordered by their corresponding ratio values. The numbers associated with each point represent the number of vehicles used to calculate each average. The error bars represent the 95% confidence interval calculated for each mean value.

passenger cars. This agrees with results from a remote sensing study carried out in Paris, which reported high emissions of NO_x from motorcycles and mopeds[154]. The study reported that fuel specific NO_x emissions of Euro 4 motorcycles and mopeds were more similar to Euro 2 or Euro 3 gasoline passenger cars rather than passenger cars of a similar age (Euro 6)[154]. In this study, the NO_x/CO_2 ratios for Euro 4 motorcycles and mopeds were 4 times higher than Euro class 3 passenger cars and the ratio was similar to

the ratio for Euro 5 diesel goods vehicles (values shown in Figure 4.5).

The LEZ zone in Milan currently limits Euro class 2 motorcycles and mopeds and does not plan to restrict Euro class 4 motorcycles until October 2028[228]. Similar policies are present in LEZs in other European cities, the LEZ in Paris currently limits motorcycles and mopeds only below Euro class 1[229] and the LEZ in London currently limits motorcycles and mopeds below Euro class 3. Therefore motorcycles and mopeds could become a dominating contributor to NO_x emissions whilst other vehicle types, such as passenger cars and goods vehicles, are severely restricted.

Gasoline natural gas bi-fuel and CNG-only fuel vehicles have higher average NO_x/CO_2 ratios than standard gasoline vehicles, but have lower ratios than diesel fuel vehicles. A study using PEMS to measure NO_x emissions from bi-fuel passenger cars revealed that the application of CNG fuel resulted in significantly increased NO_x emissions when compared to gasoline[210]. Higher emissions of NO_x from natural gas fuel vehicles may be a result of higher reported temperatures in the engines of bi-fuel vehicles[230], this indicates elevated combustion temperature and therefore NO_x formation is promoted. Furthermore, when the engine runs on CNG fuel, there is an increased CH_4 conversion efficiency in the catalytic converter and under these conditions, NO_x can only be partially converted and higher amounts of NO_x are emitted[210].

NO_x emissions associated with Euro classes are also shown in Figure 4.4. The NO_x emission would be expected to decrease with increasing Euro class as the emission limits become more stringent, however this is not seen in the average NO_x/CO_2 ratios extracted from point sampling measurements. Euro class 5 shows the highest ratio of all the emission standards. The higher NO_x/CO_2 ratio for Euro 5 could be linked to the "Dieselgate" scandal, which revealed that many manufacturers manipulated software to pass in-laboratory emissions testing of diesel vehicles but on-road emissions were measured to be much higher. The time period of this scandal affected

euro class 5 vehicles and their NO_x emissions were much higher than the emission limits[161]. However, many of these vehicles have now been fixed and Figure 4.5 shows that euro 5 diesel passenger cars have a slightly lower average NO_x/CO_2 ratio than euro 4 diesel passenger cars. Figure 4.5 shows that the high average ratio for euro class 5 vehicles is likely driven by diesel goods vehicles, which have a high NO_x/CO_2 ratio. Euro class 2 has the lowest NO_x/CO_2 ratio and this is likely a result of the ratio being calculated from only passenger cars and motorcycles and mopeds, shown in Figure 4.5. The majority of these vehicles are also gasoline, which are associated with lower NO_x emissions.

Overall, the NO_x/CO_2 ratios extracted from point sampling highlight the importance of motorcycles and mopeds and gas-fuel vehicles as important sources of NO_x. As motorcycles and mopeds have smaller engines and therefore they can emit lower concentrations of CO_2 compared to passenger cars. However, Vasic and Weilenmann [231] evaluated emission results from a number of studies and concluded that absolute emissions of NO_x from motorcycles are still significant compared to passenger cars. Therefore, these vehicle and fuel types are likely to become more important contributors in urban areas as other vehicle and fuel types are more stringently regulated by low emission zones.

Table 4.1 shows a comparison of passenger car NO_x/CO_2 ratios between results from point sampling and a previous study[4]. Measurements from Carslaw and Rhys-Tyler [4] were performed in London in 2012 using remote sensing instrumentation. There is a relatively good agreement between the different vehicle measurements, however all of the diesel NO_x/CO_2 ratios recorded by Carslaw and Rhys-Tyler [4] were higher than the equivalent ratios extracted from point sampling.

It is difficult to say why the diesel vehicle NO_x/CO_2 ratios reported by Carslaw and Rhys-Tyler [4] were higher than point sampling ratios, but the differences could be due to higher congestion in London. During congested

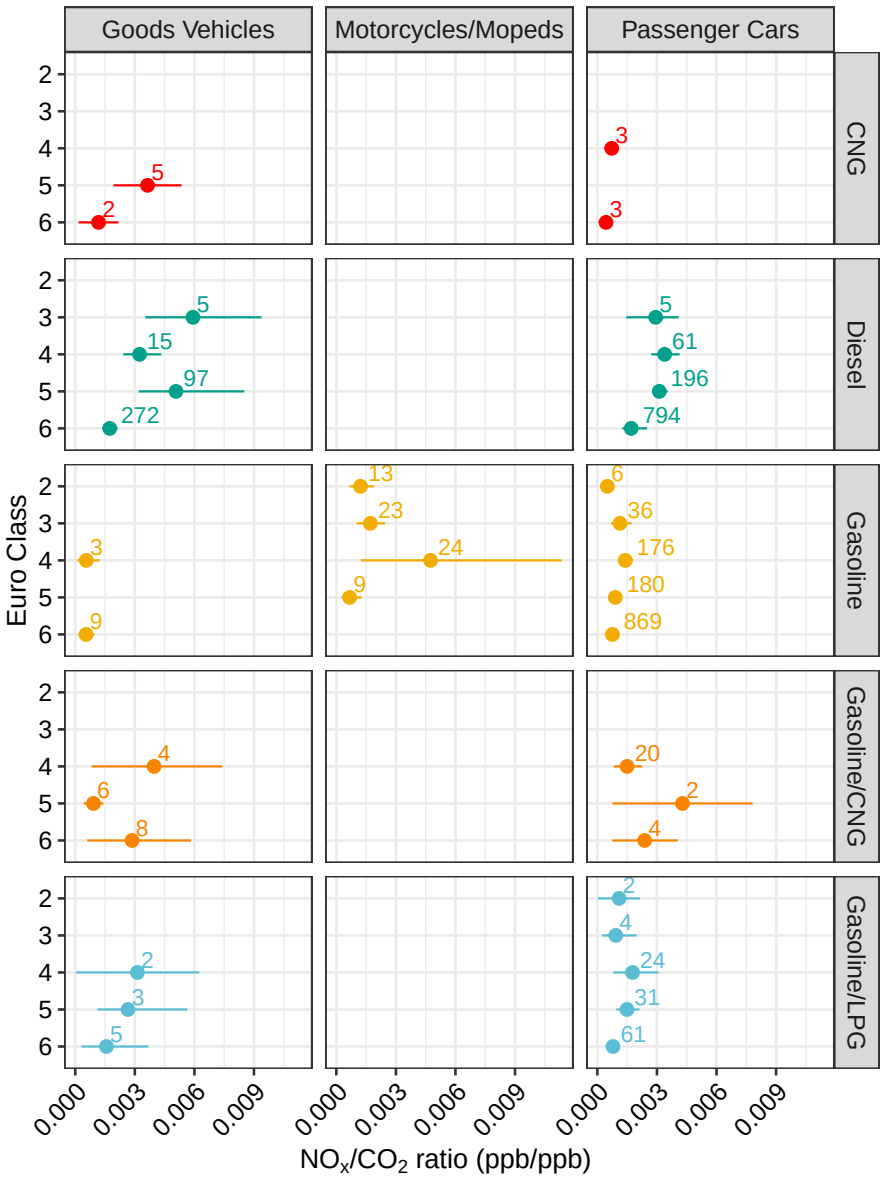

Figure 4.5: Average NO_x/CO_2 ratios (ppb/ppb) calculated for different vehicle characteristic categories, grouped by vehicle type, fuel type and Euro class. The numbers associated with each point represent the number of vehicles used to calculate each average. The error bars represent the 95% confidence interval calculated for each mean value.

traffic conditions, there are lower vehicle speeds and as a result lower engine temperatures. Lower temperatures can negatively affect the performance of catalytic reduction systems, leading to an increase of NO_x emissions[4].

		NO_x/CO_2 ratio (ppb/ppb)	
Fuel type	**Euro class**	**This work**	**Literature**[232]
Petrol	2	0.0005	0.0039
	3	0.0011	0.0015
	4	0.0014	0.0010
	5	0.0009	0.0005
Diesel	3	0.0029	0.0063
	4	0.0033	0.0048
	5	0.0031	0.0050

Table 4.1: A comparison of passenger car NO_x emission ratios (ppb/ppb) extracted from point sampling to literature values (Carslaw and Rhys-Tyler [4]).

4.5 VOC emission measurements and results

Real-world and on-road measurements of VOCs from individual vehicles are limited and in this work we carried out measurements of VOCs from individual passing vehicles using the SIFT-MS during point sampling. Emission ratios of VOCs were then calculated for individual vehicles using the methods described in Section 3.3. The next sections will discuss average VOC/CO_2 ratios extracted from point sampling and highlight important vehicle characteristic categories for VOC emissions. There will also be a discussion on the speciation of VOC emissions from vehicles, as speciated VOCs were measured with the SIFT-MS.

4.5.1 VOC emission ratios from point sampling

Ratios of each VOC to CO_2 were calculated for individual vehicle passes and the combustion-related vehicle plumes were extracted using ΔCO_2 and

p-value filters. The average VOC/CO_2 ratio for each vehicle characteristic category, including vehicle type, Euro class and fuel type, was calculated and this is shown in Figure 4.6. The VOCs that contribute to the average VOC/CO_2 ratio are the compounds shown in Table 2.2, which include acetaldehyde, ethanol, butadiene, benzene, acetone, toluene, C_2−C_4-alkanes and C_2^- and C_3^-alkylbenzenes. VOC/CO_2 ratios separated by vehicle type, fuel type and Euro class is shown in Figure 4.7.

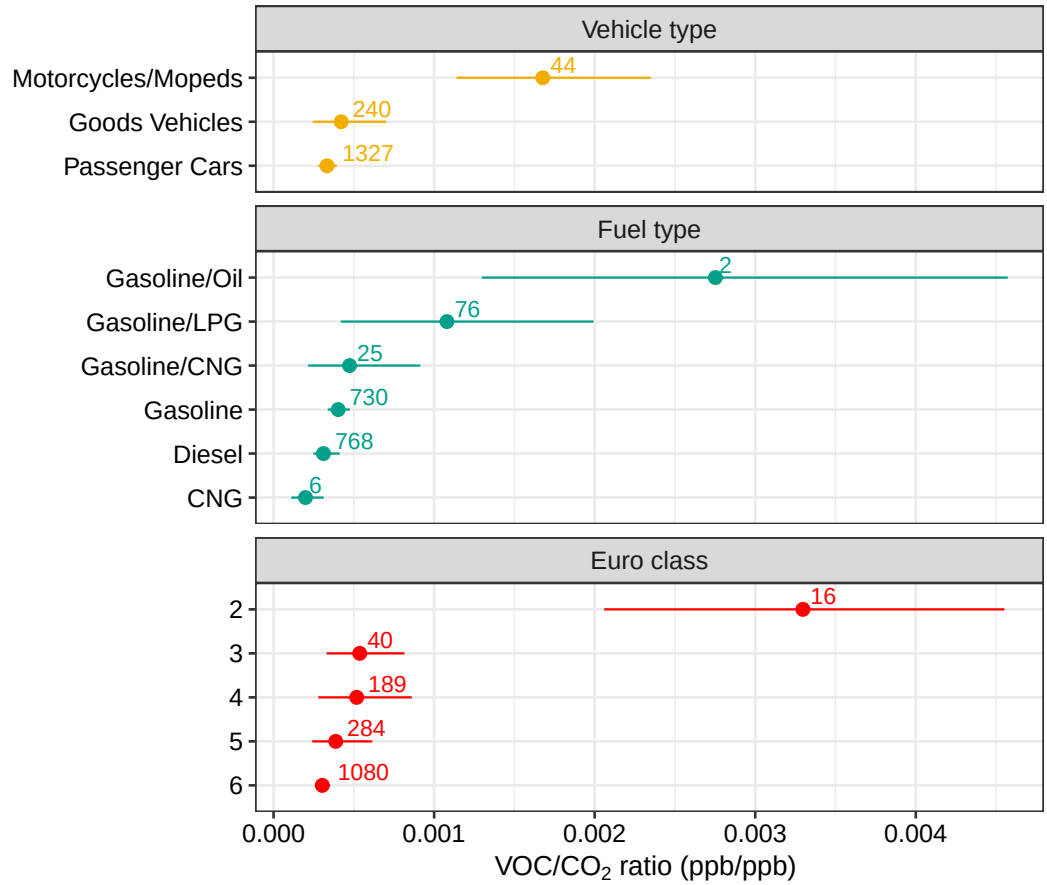

Figure 4.6: Average VOC/CO_2 ratios (ppb/ppb) calculated for different vehicle characteristic categories, including vehicle type, fuel type and Euro class. The variables in each category are ordered by their corresponding ratio values. The numbers associated with each point represent the number of vehicles used to calculate each average. The error bars represent the 95% confidence interval calculated for each mean value.

The vehicle type with the highest average VOC/CO_2 ratio is motorcycles and mopeds. The average VOC/CO_2 ratio for motorcycles and mopeds is approximately 4 times higher than goods vehicles and 5 times higher than passenger cars. The significantly higher ratio for motorcycles and mopeds is likely a result of the composition of the vehicle fleet in Milan as there was a higher proportion of older motorcycles and mopeds compared to passenger cars and goods vehicles. Older vehicles are likely to have higher emissions due to higher emission limits or deterioration of emission controls, such as catalytic converters. Figure 4.7 shows that the VOC/CO_2 ratio for Euro class 2 gasoline motorcycles and mopeds is significantly high and this is likely to influence the average ratio for this vehicle type. However, when euro class 2 gasoline motorcycles and mopeds are removed, the average ratio for gasoline motorcycles and mopeds is 1.6 times higher than gasoline passenger cars and 3.4 times higher than gasoline goods vehicles. As discussed in Section 4.4, emissions from motorcycles and mopeds could become more important in urban areas as they are not typically as strongly regulated as other vehicles types are in low emission zones. These results agree with a study in Paris which analysed VOC measurements of multiple roadside sites and fuel headspace. The study revealed that motorcycles and mopeds were a major driver in the spatial and temporal variability of vehicle-related VOC compounds[225].

The fuel type with the highest average VOC/CO_2 is gasoline/oil vehicles, with the ratio being 6.8 times higher than the average ratio associated with the standard gasoline fuel type. Gasoline/oil bi-fuel is associated with motorcycles and mopeds that are equipped with 2-stroke engines. The design of the engine allows for some of the unburnt fuel/oil mixture to pass directly into the exhaust, therefore resulting in higher VOC emissions[218,233,234]. 2-stroke motorcycles and mopeds also utilise "rich combustion", which is a low-air/fuel ratio and results in increased VOC emissions[234]. Measurements of SOA produced via photochemical reactions of exhaust gas from a 2-stroke

motorcycle/moped in a smog chamber concluded that this vehicle type could dominate urban vehicular pollution despite making up a small fraction of the fleet[234]. It is likely that this engine type will start to be phased out as the design of 2-stroke engines makes it difficult for these vehicles with this engine type to meet new emission limits. However, usage of the 2-stroke engine type could remain important in areas that have a high proportion of these vehicles, possibly more rural areas or developing countries.

Gasoline/LPG fuel type vehicles have an average VOC/CO_2 ratio of 2.8 times higher than the average ratio associated with the standard gasoline fuel type. Similarly, gasoline/CNG also has a slightly higher average ratio than standard gasoline. As discussed in Section 4.3, LPG and CNG fuel consists of a mixture of hydrocarbons, therefore evaporative or unburnt fuel emissions are likely to contribute to higher VOC emissions. C_2-C_4 alkanes were targeted and measured by the SIFT-MS and these compounds are major constituents of both LPG and CNG fuel and have been used as indicators for LPG emissions in other studies[197,224].

Gasoline fuel type vehicles have a slightly higher VOC/CO_2 ratio than diesel, this could be a result of the selected VOC compounds, which were shorter-chain length hydrocarbons and therefore more likely to be emitted from gasoline vehicles. Measurements of VOC compounds from gasoline and diesel samples and source apportionment studies revealed that light alkanes, including toluene and benzene, are prominent in gasoline exhaust emissions, whereas aromatics and heavier alkanes are more prominent in diesel exhaust emissions[129,197,217,220].

Figure 4.6 also shows that the average VOC/CO_2 ratio decreases with increasing Euro class. As new Euro classes are introduced, the emission limits for pollutants, including hydrocarbons, become more stringent, as shown in Appendix B. The most recent Euro class for motorcycles and mopeds, Euro class 5, now has the same hydrocarbon emission limits as Euro 6 gasoline passenger cars. These emission limits are met by introducing new

emissions reductions technology, such as catalytic converters, which convert hydrocarbons into less harmful species, including CO_2 and water. The effect of more stringent emissions limits has been observed as Euro 4 motorcycles and mopeds have a VOC/CO_2 ratio of 1.7 times higher than gasoline Euro 6 passenger cars, which has been reduced to 1.6 times higher for Euro 5 motorcycles and mopeds.

Overall, motorcycles and mopeds and some of the gasoline bi-fuel fuel types could be significant VOC sources in Milan due to their high VOC/CO_2 ratios, which represent a high amount of VOC emitted per unit of fuel burnt. Despite lower emissions of CO_2, motorcycles can represent a significant source of VOCs. Vasic and Weilenmann [231] concluded that emissions of hydrocarbons from motorcycles were significantly higher than passenger cars. Furthermore, emission tests are not carried out on motorcycles and mopeds during road worthiness tests, therefore they could suffer from higher levels of deterioration and emissions could increase even further. The regulation of motorcycles and mopeds and gas fuel vehicles by low emission zones is lagging behind compared with the regulation of other vehicle and fuel types. Therefore, low emission zones may be less effective in reducing VOC emissions and improving air quality. Furthermore, it is likely that the number of motorcycles and mopeds were underestimated as they typically drive close to each other and to other vehicles and therefore may not be captured by the ANPR camera. The spatial effect of vehicle emissions on air pollutant concentrations around Milan will be discussed in Chapter 5.

Table 4.2 shows a comparison of the vehicle fleet average VOC/CO_2 ratios between results from point sampling and a previous study[5]. Ammoura et al. [5] performed measurements of VOCs from vehicles in a tunnel study in Paris. The VOC/CO_2 ratios reported by Ammoura et al. [5] are a factor of 10-100 times higher than corresponding VOCs extracted from point sampling measurements in Milan. The VOC/CO_2 ratios may be much higher during the tunnel measurements due to influences of the differing

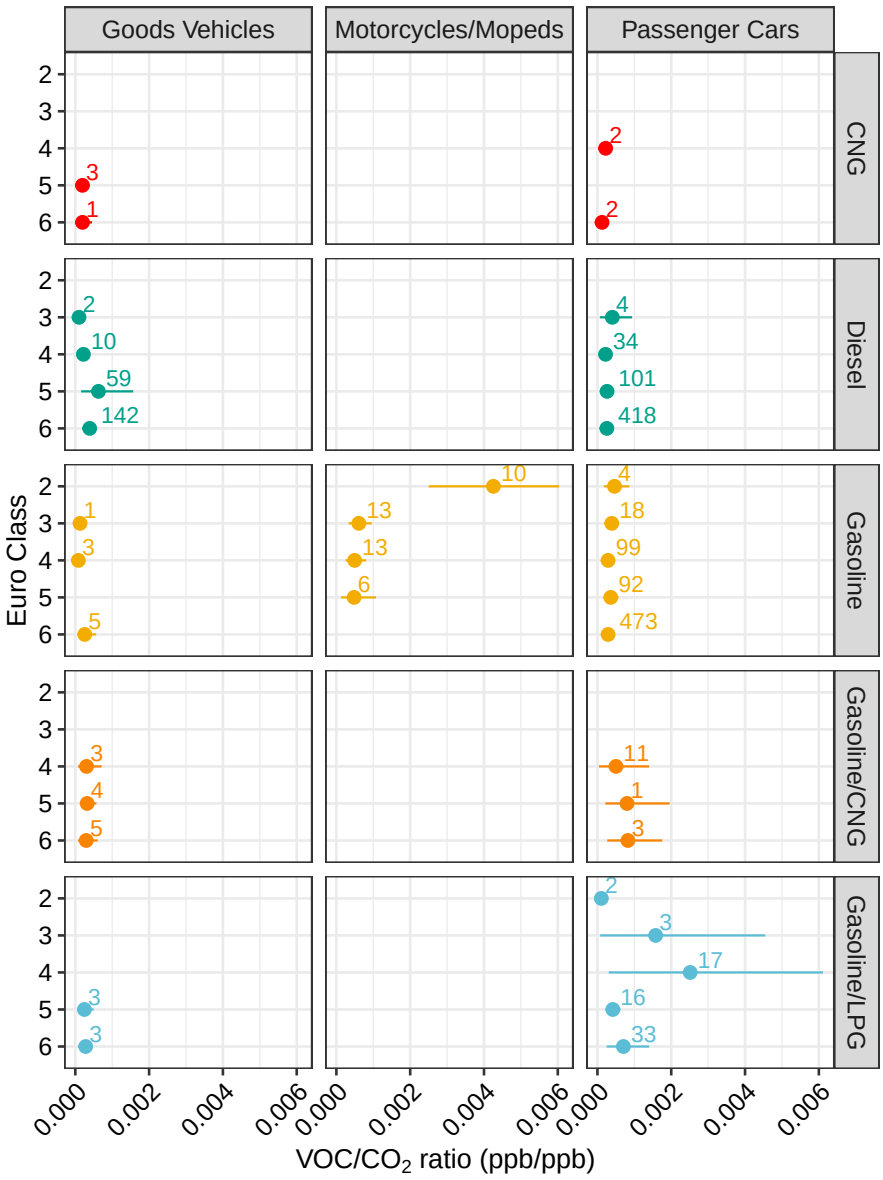

Figure 4.7: Average VOC/CO_2 ratios (ppb/ppb) calculated for different vehicle characteristic categories, grouped by vehicle type, fuel type and euro class. The numbers associated with each point represent the number of vehicles used to calculate each average. The error bars represent the 95% confidence interval calculated for each mean value.

vehicle fleets. The tunnel measurements were carried out 10 years before the Milan point sampling measurements, therefore the vehicle fleet during the tunnel measurements is likely to consist of high-emitting vehicles due

	VOC/CO_2 ratio (ppb/pbb)	
VOC	**This work**	**Literature[5]**
Toluene	0.00021	0.0246
Benzene	0.00014	0.00884
C_2-alkyl benzenes	0.00028	0.00606

Table 4.2: Table comparing VOC emission ratios extracted from point sampling to literature values (Ammoura et al. [5]).

to more lenient emission standards at the time. The tunnel measurements report fleet average VOC emission ratios as they are unable to distinguish between individual vehicles and cannot determine which vehicle categories may be significant high VOC emitters.

4.5.2 Speciated VOC emissions

As discussed in Section 2.6, 9 speciated VOCs were measured by the SIFT-MS during point sampling. The VOC compounds targeted by the SIFT-MS were carefully selected to be representative of vehicle exhaust emissions. However, measured VOC compounds in this work were typically shorter-chain length hydrocarbons, therefore the results might be biased towards gasoline vehicles which emit mainly shorter-chained alkanes due to the fuel composition of gasoline. The majority of selected VOCs had a lifetime of hours to days, due to their short chain-length, therefore their atmospheric concentrations depend on the number and strength of of nearby emission sources[235]. Emission ratios of individual VOCs to CO_2 were calculated for vehicle passes and could then be grouped together by different categories, as is shown in previous sections. This section investigates VOC speciation information for different vehicle and fuel types.

Figure 4.8 shows the average speciated VOC/CO_2 ratios for different

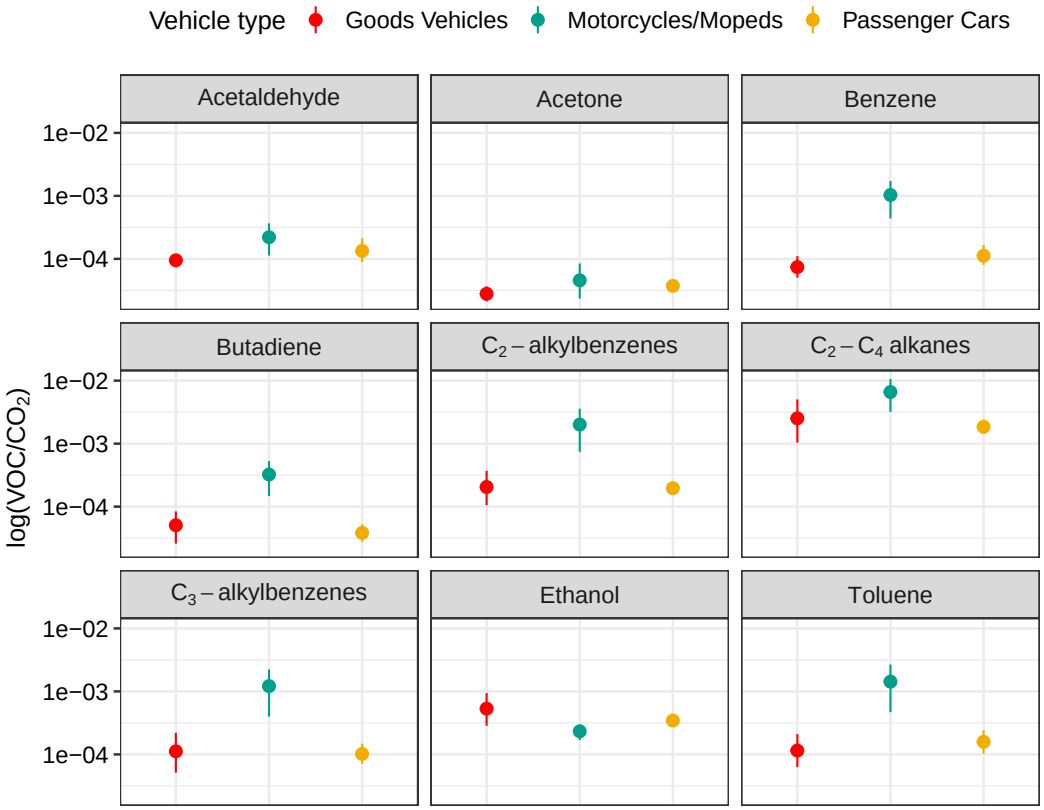

Figure 4.8: Average VOC/CO_2 ratios (ppb/ppb) for speciated VOCs, grouped by vehicle type. The y axis is on a logarithmic scale. The error bars represent the 95% confidence interval calculated for each mean value.

vehicle types. For the majority of the VOCs, motorcycles and mopeds have the highest ratio to CO_2 and this agrees well with Figure 4.6, which also shows that motorcycles and mopeds have the highest average VOC/CO_2 ratio. Benzene, C_2-alkylbenzenes, C_2-C_4 alkanes, C_3-alkylbenzenes and toluene all have visibly higher VOCCO_2 ratios for motorcycles and mopeds. Motorcycles and mopeds have been revealed to be a major contributor to concentrations of these compounds in cities[225,234]. Furthermore, these VOC compounds have been used in many studies as tracers for vehicle exhaust emissions[129,197,225,234].

For all vehicle types, the C_2-C_4 alkanes/CO_2 ratio is the highest, this is likely because this measurement is a combination of 3 compounds- ethane,

propane and butane. However, the measurement of C_2-C_4 alkanes can still be used as a useful tracer for vehicle exhaust emissions. A review of measurements of vehicle emissions of VOCs in China reported that light alkanes were important constituents in the composition of gasoline, diesel and LPG fuel types[217]. Another study which identified tracers for different VOC sources concluded that light alkanes can be used as a tracer for vehicle exhaust emissions[197].

Ethanol is the only VOC that does not have the highest ratio to CO_2 for motorcycles and mopeds. Goods vehicles have the highest ethanol/CO_2 ratio and 82% of goods vehicles are diesel vehicles, which also show slightly higher ethanol/CO_2 ratios in Figure 4.9. Oxygenated VOCs have been found to be an important constituent in exhaust emissions of diesel vehicles during measurements of chassis dynamometer tests[217,220,221]. However, acetaldehyde and acetone had low ratios to CO_2 for all vehicle types, this could possibly be a result of aldehydes and ketones being more reactive in the atmosphere[236] or their emissions from vehicles being too low to detect.

Figure 4.9 shows the average speciated VOC/CO_2 ratios for different fuel types. For the majority of the VOCs including benzene, C_2-alkylbenzenes, C_2-C_4 alkanes, C_3-alkylbenzenes and toluene, the gasoline/oil fuel type has the highest ratio to CO_2. This fuel type is used in 2-stroke motorcycles, which have high emissions of unburnt hydrocarbons due to the engine design which allows for unburnt fuel and oil mixture to pass directly into the exhaust[218,233,234]. As discussed above, the tightening of emissions standards of motorcycles is likely to lead to the decrease of 2-stroke motorcycle usage as they are unlikely to meet emission limits. However, they could remain an important source in areas where usage of older motorcycles is high.

As discussed above, the ethanol/CO_2 ratio is the highest for diesel fuel types. Standard diesel in the EU contains up to 5% biodiesel, which could possibly contribute to ethanol emissions. Chassis dynamometer measurements of VOC emissions from vehicles have shown a high proportion of

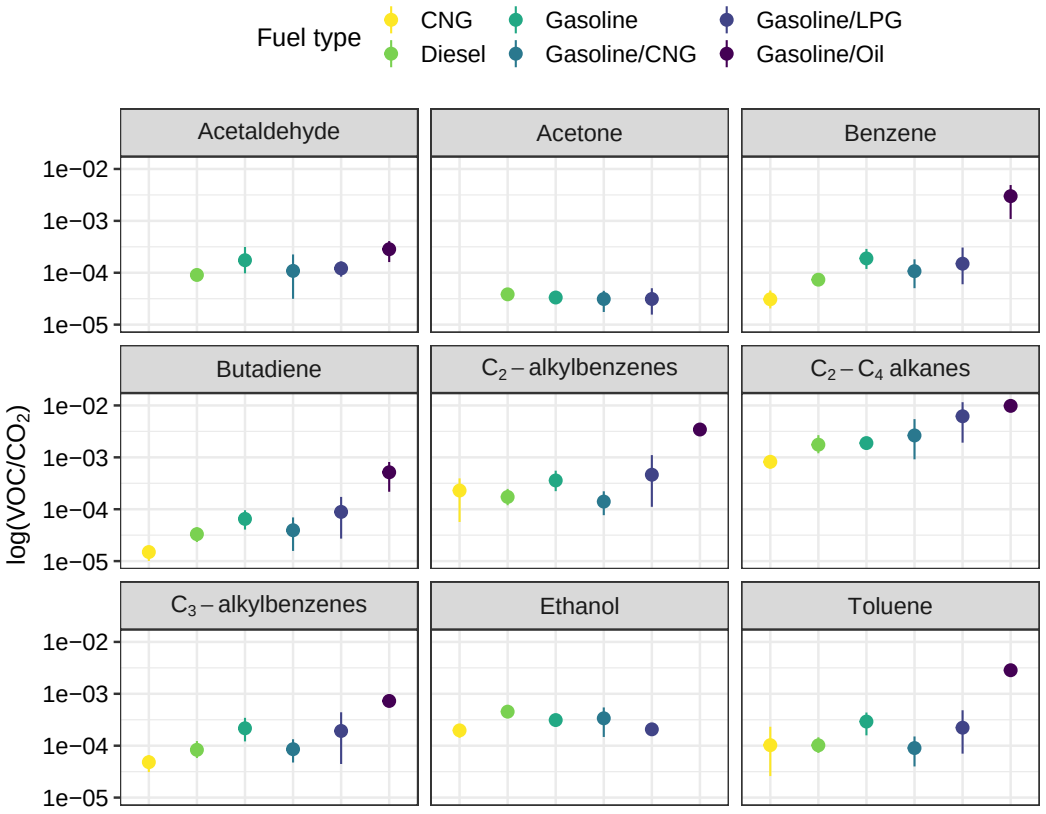

Figure 4.9: Average VOC/CO_2 ratios (ppb/ppb) for speciated VOCs, grouped by fuel type. The y axis is on a logarithmic scale. The error bars represent the 95% confidence interval calculated for each mean value.

oxygenated VOC emissions from diesel exhaust[220,221]. Standard gasoline and gasoline/CNG fuel types also have a slightly higher ethanol/CO_2 ratio and this could be due to the addition of up to 10% ethanol to gasoline fuel in the EU.

Gasoline/CNG and gasoline/LPG also have high ratios of C_2-C_4 alkanes to CO_2, which is a result of C_2-C_4 alkanes being major constituents of natural gas fuels. The ratio of C_2-C_4 alkanes to CO_2 is higher for gasoline/LPG is higher than gasoline/CNG. Other studies have shown that propane and butane contribute a high proportion towards the total VOC in LPG exhaust emissions[197,224,237] and therefore this could explain why gasoline/LPG has higher emissions of C_2-C_4 alkanes.

Overall, speciated VOC emissions are highest for motorcycles and mopeds and gasoline/oil bi-fuels vehicles. This is likely due to an older vehicle fleet of motorcycles and mopeds during point sampling measurements and the use of gasoline/oil bi-fuels in 2-stroke motorcycles which are high emitters of VOCs. Ethanol was observed to be higher for goods vehicles and diesel vehicles, compared to other vehicle and fuel types, which agrees with other studies. Significantly higher ratios to CO_2 were observed for C_2-C_4 alkanes compared to other VOCs measured. This could be a result of the C_2-C_4 alkane measurement representing 3 compounds or that this is an important VOC emitted from vehicles.

4.6 Comparison to EDAR measurements

The emission ratios of species extracted from point sampling measurements and analysis can be compared to the corresponding ratios measured using the EDAR remote sensing instrument. The EDAR instrument uses a laser light source which is placed above the road and the light is swept across the width of the roadway and through the exhaust plume of the vehicle being measured. A reflective strip installed on the roadway reflects this light back to the detector. The light attenuation measured by the detection unit is proportional to the amount of specific pollutants in the vehicle's exhaust plume. The EDAR instrument calculates background corrected ratios of NO_x and total hydrocarbons (HC) to CO_2 directly from the vehicle exhaust[238]. Figure 4.10 and Figure 4.11 show the comparison of the average ratios calculated from the EDAR and point sampling measurements. For the comparison, only the vehicles that were recorded by both the EDAR and Graz ANPR cameras were included, therefore measurements of the same vehicles could be compared.

Figure 4.10 shows the comparison of average NO_x/CO_2 ratios calculated from EDAR and point sampling measurements for vehicle characteristic

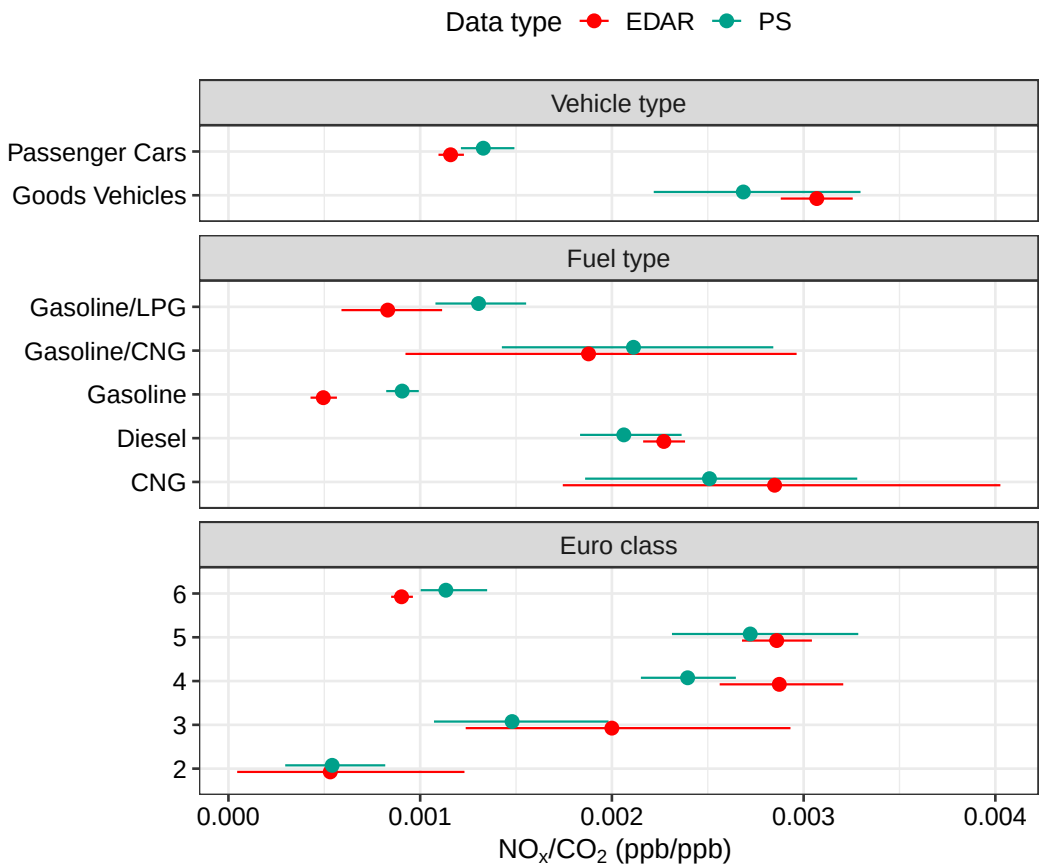

Figure 4.10: Comparison of average NO_x/CO_2 ratios (ppb/ppb) extracted from EDAR remote sensing (red) and point sampling (blue) for vehicle characteristic categories, including vehicle type, fuel type and euro class. The error bars represent the 95% confidence interval calculated for each mean value. The number of vehicles for each category has been filtered for greater than 5.

categories, including vehicle type, fuel type and Euro class. Overall, there is relatively good agreement between the NO_x/CO_2 ratios calculated from the different measurement and analysis methods as the majority of the values are within error divergence. The ratios for the different measurement methods show the same patterns for the vehicle categories, for example goods vehicles and CNG fuel type vehicles have the highest ratio for both measurement methods. The only vehicle categories where differences are not covered by

overlapping error bars are gasoline and euro class 6 vehicles. The error bars associated with the EDAR measurements are higher for most of the average ratios for each vehicle characteristic category, suggesting that the point sampling measurements could be more precise. It is worth noting that motorcycles and mopeds are excluded from this plot as there were only 3 measurements that were recorded for both of the measurement methods. Furthermore, the EDAR measurements had significantly more invalid measurements of motorcycles and mopeds compared to point sampling measurements, although it was difficult to determine what the EDAR measurements classed as a "valid" measurement.

Figure 4.11 shows the comparison of average total HC (EDAR) or VOC (point sampling) to CO_2 ratios calculated from the different measurement methods for vehicle characteristic categories, including vehicle type, fuel type and Euro class. The measurement methods agree well, with all of the values for each vehicle characteristic within the error divergence of the other measurement method. The trends in each vehicle category group also show similar patterns between the two measurement methods, for example motorcycles and mopeds and gasoline/LPG fuel type vehicles have the highest ratios.

The EDAR HC measurement is calibrated against propane and is used as a basis of representing total HCs. Therefore, remote sensing is limited for the measurement of HCs and point sampling can be used to provide a breakdown of individual VOC species. Using the point sampling measurement technique alongside a mass spectrometer is an improvement and it can be used to provide information on speciated VOC emissions. The quantification of speciated VOC emissions is useful for the determination of possible health effects or the O_3 forming potential from vehicular VOC emissions.

Overall, the good agreement between EDAR remote sensing and point sampling indicates that point sampling is a useful measurement technique for determining road vehicular emissions of NO_x and VOCs. An advantage

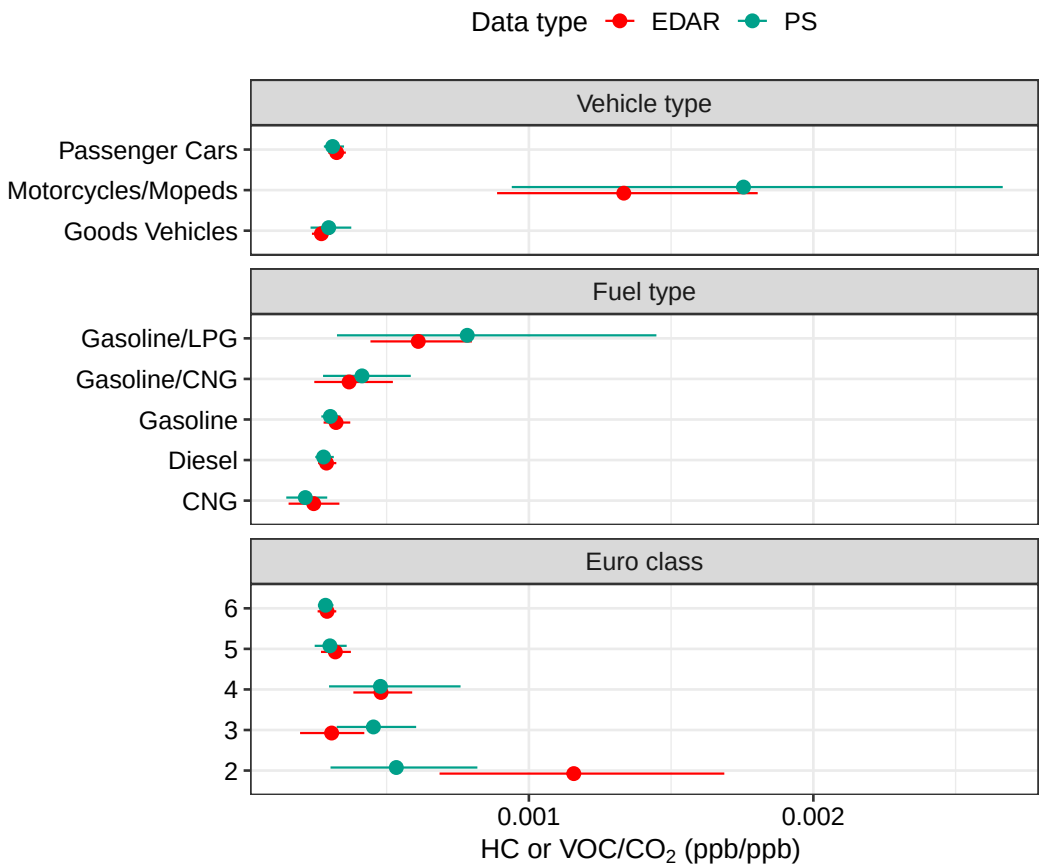

Figure 4.11: Comparison of average total HC or VOC/CO_2 ratios extracted from EDAR remote sensing (red) and point sampling (blue) for vehicle characteristic categories, including vehicle type, fuel type and euro class. The error bars represent the 95% confidence interval calculated for each mean value.

of the point sampling measurement technique compared to remote sensing is that point sampling is less limited in measurement location. A suitable measurement location for point sampling requires a space to park the mobile laboratory, whereas cross-road remote sensing requires a location in which measurements can be performed across the road. A further advantage of point sampling is that targeted measurement compounds can be expanded, provided that measurement of air pollutants can be performed at a high enough time resolution.

4.7 Conclusion

Emission ratios of NO_x and VOCs from individual vehicles have been extracted from point sampling measurements carried out in Milan. Motorcycles and mopeds were shown to have a NO_x/CO_2 ratio 1.7 times higher than passenger cars and a VOC/CO_2 ratio 5 times higher than passenger cars. 2-stroke vehicles which use the gasoline/oil fuel type have a VOC/CO_2 ratio of 6.8 times higher compared to standard gasoline vehicles. Natural gas fuel vehicles also showed much higher NO_x and VOC to CO_2 ratios compared to standard gasoline and diesel fuel type vehicles. These vehicle and fuel types could become an important source of NO_x and VOCs in urban areas, particularly as standard vehicle and fuel types are more highly regulated in low emission zones.

This work has overcome possible challenging conditions of the measurements including emission sources moving in space and time, a mixture of vehicle and fuel types, differing driving conditions and environmental effects, to highlight important vehicle categories for NO_x and VOC emissions. The point sampling measurement technique also shows relatively good agreement with the EDAR remote sensing measurement technique, which supports the accuracy of the point sampling measurement and analysis techniques. This is important as the point sampling measurement technique allows for expansion of the air pollutant species that can be measured and it is likely that point sampling measurements have less constraints related to their set up, when compared to common remote sensing measurement techniques.

Chapter 5

Source apportionment using mobile measurements

5.1 Abstract

Current understanding of air pollutants mostly rely on stationary measurements which are unable to fully represent the spatial variation of pollutants. Mobile laboratories equipped with fast-response instruments have been used to obtain high spatial and temporal measurements of air pollutants and to provide additional information about emission sources in urban areas. In this chapter, we discuss the results from mobile measurement campaigns carried out in York, Manchester and Milan.

Newly-developed analysis techniques have been applied to extract useful emissions information, including the use of a distance weighted regression approach to provide information on the spatial variation of air pollutants or how the intensity of emissions varies spatially. A rolling regression approach has been applied to extract combustion-related dilution events from mobile measurements carried out in Milan, which have been compared to vehicle point measurements to determine the contribution of vehicle emissions towards emissions in urban areas. The temperature dependence of air

pollutant emissions in Manchester has been investigated and we find that NO_x and toluene have strong, but opposite, temperature dependencies.

5.2 Introduction

It is important that emission sources of air pollutants are well understood, in order to combat air quality issues. The current understanding of urban air pollution relies mostly on hourly or daily measurements of a limited number of atmospheric pollutants recorded at fixed monitoring sites. These measurements are unable to fully represent relative contributions of different source types and complex temporal and spatial variations of pollutants.

There is a particular lack of emissions information on sources of VOCs in urban areas. Historically, vehicular emissions of VOCs have been of central importance to air quality issues, such as O_3 and SOA formation. But the composition and sources of these species in urban areas are highly complex, and it is difficult to determine the role played by VOCs from road vehicles relative to other sources. While VOC emissions from vehicle exhaust have been aggressively reduced over the past few decades in Europe through the introduction of technologies such as three-way catalysts on gasoline vehicles, they still present an important source of emissions, accounting for 4% of total UK VOC emissions in 2017[26].

Nevertheless, the reduction in vehicular emissions means it is likely that other sources of emissions, such as volatile chemical products (VCPs), solvent use, cooking, residential wood burning and industry, have become more important. Mass balance analysis by McDonald et al. [24] concluded that emissions from VCPs now account for half of the fossil fuel VOC emissions in industrialised cities. Lewis et al. [26] estimated that in the UK, VOC emissions from solvent use and industrial processes account for 63% of total VOC emissions. This change in the contribution of VOC emissions from different sources is not reflected in current VOC measurements made at

stationary monitoring sites in the UK, which measure only 13 of the 20 most significant VOCs[26] due to set-up taking place 30 years ago when road transport was the dominant VOC emissions source.

To overcome the lack of emissions information, mobile laboratories equipped with fast-response instruments have been used for high spatial and temporal measurements of pollutants and these measurements can be used to increase the understanding of air pollutant emission sources. Mobile measurements have been used in multiple studies for source identification and apportionment. This has been carried out via spatial mapping and hot spot identification of air pollutants. Spatial mapping studies have been used to produce high resolution maps of the spatial variation of gaseous air pollutants, particles and VOCs[105–107,116–119,124,170–172,174]. Spatial mapping studies have used maps of spatial variation of air pollutants to identify important emission sources, including road vehicles[106,170], oil and gas industries[116,118] and VCPs[119,174]. Spatial mapping and hot spot analysis have been used to assess exposure to air pollutants[105,117,172]. Other mobile measurement studies have used complex analysis techniques to identify important emission sources. Richards et al. [195] used principal component analysis to discriminate multiple VOC sources, including road vehicles and industrial operations and Gkatzelis et al. [120] used positive matrix factorisation to determine the contribution of road vehicles and VCPs towards VOC emissions.

These studies highlight how mobile measurements can be used for source apportionment. However, many of the approaches used by other studies have limitations that this work aims to overcome. Current studies that use spatial mapping for source apportionment split the road network into arbitrary segments. In this work, we use the distance-weighted approach discussed in Chapter 3 to investigate the spatial distribution and determine important sources of air pollutants. This work also used pollutant ratios and emission ratios to obtain information on emission sources in urban areas.

This work also aimed to determine the representativity of a point measurement compared to a spatial distribution, by comparing the point sampling and mobile measurements carried out in Milan. Combustion plumes events will be extracted from mobile measurements and the results can be compared to similar results from point sampling, enabling the importance of vehicle emissions on a spatial scale to be determined. The work will, for the first time, investigate any possible temperature dependence of air pollutants, using mobile measurements performed during contrasting seasons in Manchester. The temperature dependence of air pollutants can then be used to provide enhanced information on the characteristics of emission sources. The mobile measurement data sets obtained from different measurement locations are compared to investigate how emissions of air pollutants in different locations vary.

5.3 York results

5.3.1 Summary of measurements

Figure 5.1 shows a statistical summary of the mobile measurements carried out in York, which were performed over 10 days between 30th June to 23rd July 2020 and where 30 repeat drives of the measurement route were made. The plot shows that the mixing ratio of butadiene, isoprene and monoterpenes was consistently below 0.5 ppb and that there was a small amount of variation associated with these compounds. The dominant sources of isoprene and monoterpenes during the time of the measurements is likely to be biogenic emissions due to higher ambient temperatures. There is a larger variation in the mixing ratio of vehicle-emissions related compounds, such as benzene, toluene, C_2- and C_3-alkylbenzenes and NO_2, in addition to other species such as acetaldehyde and ethanol.

The variation in ethanol may be related to emissions from vehicles or

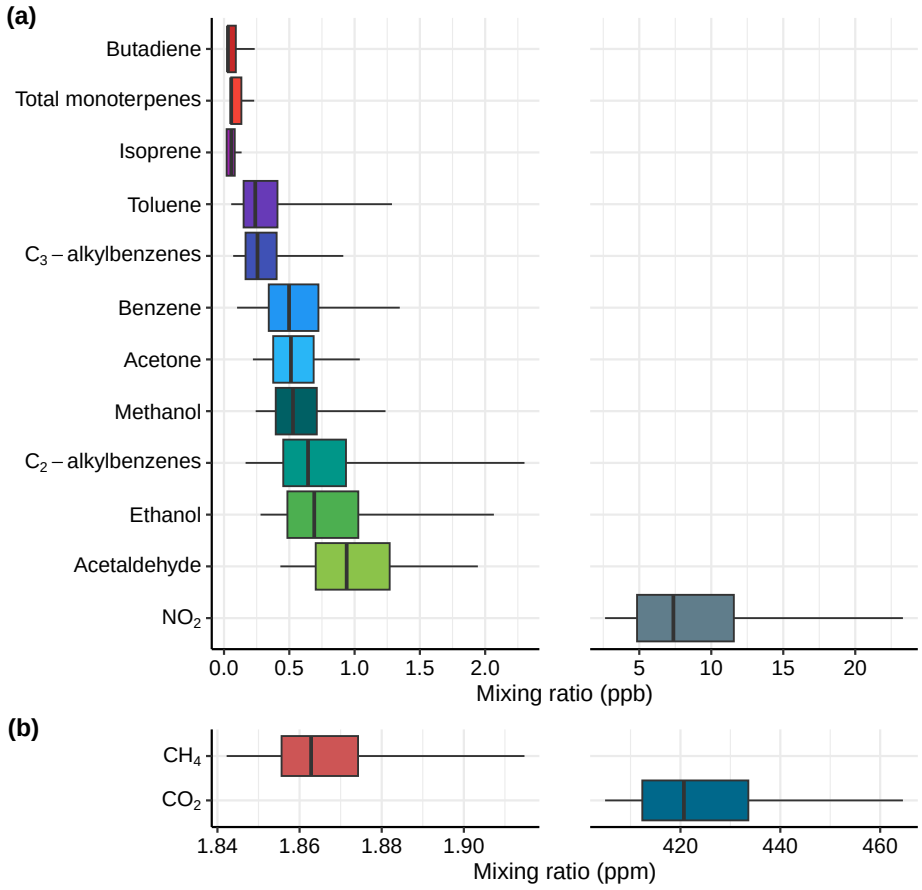

Figure 5.1: Summary of measurements made by a) the SIFT-MS (in ppb) and b) the UGGA (in ppm) during measurements carried out in York over 10 days between 30th June to 23rd July 2020. The box outline contains the 25th to the 75th percentile and the middle line shows the median mixing ratio for each compound. The whiskers represent the 5th and 95th percentile for the mixing ratios of each compound.

fuel evaporation due to bio-ethanol addition in gasoline fuel[26] or from the use of VCPs[120]. A study carried out in London by Dunmore et al. [239] reported that ethanol variation strongly correlated with other road transport-related VOCs, including light alkanes and small aromatics. Lewis et al. [26] estimated that ethanol is the most important VOC emitted by mass in the UK and its variation could also result from domestic solvent use. Acetaldehyde variation may be due to emissions from vehicles as an

oxidation product from gasoline combustion[239] or a secondary product of atmospheric oxidation. It is difficult to say exactly what emission source is responsible for the variation in ethanol and acetaldehyde, but methods such as spatial mapping, correlation between species and ratio analysis can be used to investigate different sources. It is still worth noting that the variation of all of the compounds is still small, which is likely due to Covid-19 restrictions and the resulting reduced economic and traffic activities around York.

5.3.2 Spatial distribution of pollutants

Mean mixing ratios values for pollutants have been spatially mapped using the distance-weighted approach and a σ width of 100 m, as discussed in Section 3.4.

Figure 5.2 shows the mixing ratios of benzene, toluene, ethanol and NO_2 recorded along the York measurement route, as examples of spatial mapping of compounds using the WASP and the SIFT-MS. The plot shows low mixing ratios on Heslington Lane (blue/green at the bottom of Figure 5.2) for all of the compounds. The mixing ratios increase around the city centre where there is higher congestion and vehicle emissions may dominate, but there is also a variety of other possible emission sources.

NO_2 mixing ratios considerably increase in the city centre to above 10 ppb and elevated levels are seen at road junctions, which is expected as NO_2 is strongly indicative of diesel vehicles. Particularly high levels of NO_2 are observed past the train station and on roads with many bus stations (red at the top left of the NO_2 map). Higher NO_2 concentrations are also likely to be influenced by lower dispersion in these areas, as they occur on "canyon" streets, where there are tall buildings on either side and dispersion tends to be lower. Increases in the median benzene and toluene mixing ratios are relatively small, but they show good similarities to each other with some

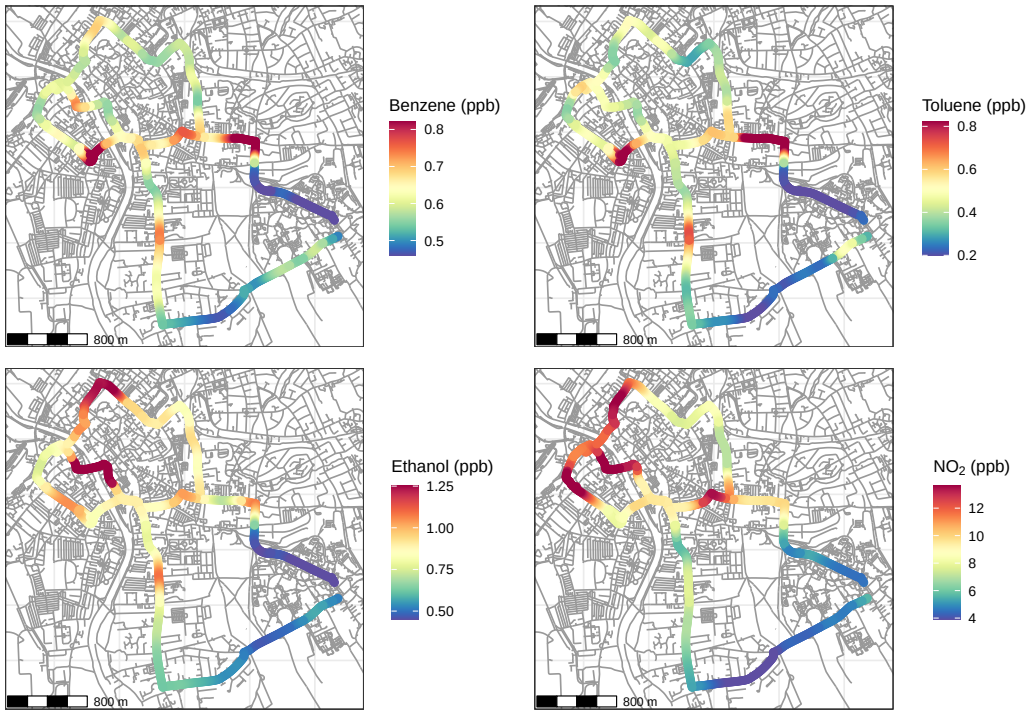

Figure 5.2: Spatial mapping of mean mixing ratios of Benzene (ppb), Toluene (ppb), Ethanol (ppb) and NO_2 (ppb) from mobile measurements around York. Maps created using a σ of 100 m. Legend lower and upper limits represent the 5th and 95th percentile of the pollutant mixing ratio. © OpenStreetMap.

elevated levels at road junctions, which is indicative of emissions from road vehicles. Ethanol is at background levels for the majority of the route, with considerable increases seen in the city centre of above 1 ppb (red in the centre of the ethanol map), which may possibly originate from businesses in the city centre, such as bakeries and breweries. Another possible source of ethanol could be related to hand sanitiser usage in the city centre, which was widely used during the time of measurements due to Covid-19.

5.3.3 Correlation between pollutants

Spatial mapping is useful as it can highlight hotspots of VOCs and trace gases, but they are insufficient in determining and separating emission sources in

urban areas. A method for source apportionment is to consider the correlation between many species over particular roads or areas that measurements have been made. Areas that contain different emission sources should have different correlations, for example an area dominated by vehicle emissions should show strong correlations with VOCs associated with vehicles such as benzene and toluene and these correlations will be different to other sources, such as evaporative emission of solvents. Figure 5.3 shows the Spearman correlation of compounds for all of the measurements made during mobile measurements in York.

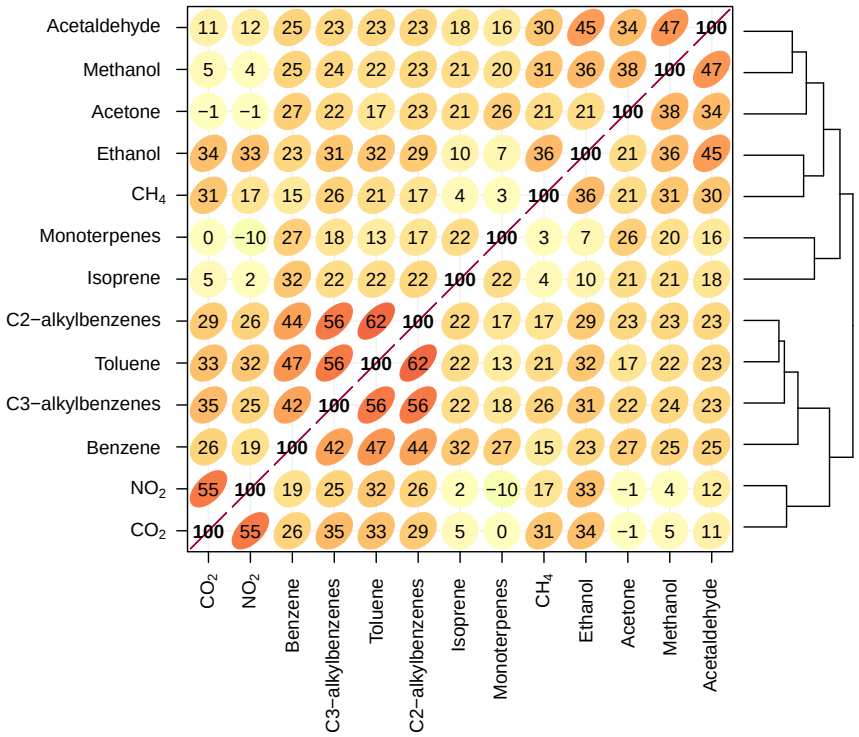

Figure 5.3: Spearman correlation of the compounds measured during measurements in York. A higher correlation coefficient between species is represented by a higher number, a darker red colour and an ellipses shape. The lines on the right-hand side show the hierarchical clustering between compounds and represent clusters of species with similar patterns/behaviours.

Hierarchical clustering is applied to the correlation matrices to group species that are most similar to one another. Hierarchical clustering is an algorithm that groups together similar objects into groups/clusters. For example, benzene, toluene, C_2-alkyl benzenes and C_3-alkyl benzenes appear next to each other in Figure 5.3 and show a clear cluster, indicating similar behaviour. However, there is not a particularly good correlation with NO_2 or CO_2 and therefore it is likely that their emission is from road vehicle fuel evaporation rather than exhaust emissions. There are other clusters of VOCs which are indicative of different source types - for example commons solvents such as acetaldehyde, methanol and acetone are clustered together in linked urban emissions likely emissions from VCPs, rather than relating to road transport. Other trace gases associated with tailpipe emissions also appear in a single cluster, e.g NO_2 and CO_2. Ethanol is equally correlated to species in the vehicle-related cluster (benzene, toluene, C_2-alkyl benzenes and C_3-alkyl benzenes) and species in the non-vehicle related cluster (acetaldehyde, methanol and acetone), indicating that the sources of ethanol in York are complex and that there is not one dominating emission source.

5.3.4 Evaporative source characterisation

Determining the importance of different sources in the emission of atmospheric pollutants is difficult and calculating ratios between compounds can be used as an indicator of dominating emission sources, as discussed in Chapter 3. The toluene to benzene (T/B) ratio has been used in many studies to determine the dominant source of these compounds and it will be applied to mobile measurements from York. Both toluene and benzene are emitted directly from vehicle exhausts and more widely by industry and may also be present due to evaporative emissions from fuels and solvents. Therefore, the T/B ratio is a useful indicator of the relative importance of different sources. A T/B ratio of 1-2 indicates a traffic influence[182,197] and a T/B ratio of over

2 indicates solvent or evaporative influences[197].

A characteristic of mobile measurements is the transient nature of emission sources. For sources such as road vehicle exhaust, the measurements will depend on the traffic conditions, which are inherently variable. With repeat measurements, these variations can be averaged-out to reveal consistent and persistent spatial patterns, which is shown by the spatial maps in Figure 5.2. Some sources can, however, be highly transient such as evaporative emissions from road vehicle fuel stations. The emission source from fuel stations can be highly variable and depends on many variables, for example, the number of vehicles being refuelled. Furthermore, these sources will be intermittently detected due to the prevailing wind direction and it will often be the case that no plume is detected because the wind is from the wrong direction.

In terms of concentration measurements, some source contributions may show as infrequent high concentrations (or ratios of concentrations) that have little or no effect on median values. Using the distance-weighted approach discussed in Section 3.4, the contribution from less frequent, higher concentrations is down-weighted. Calculating a distance-weighted mean is useful when investigating consistent emissions sources, however, there is potentially important information and intermittent sources that can be missed.

As an example, we consider the T/B ratio as being indicative of both road vehicle exhaust and potentially evaporative emissions. The T/B ratio has been calculated for the mobile measurement route driven in York using the distance-weighted regression approach and is shown in Figure 5.4. Figure 5.4 shows hotspots in the T/B ratio of above 3 on Hull Road and Gillygate (both of which are labelled). On Hull Road there are two road vehicle fuel stations and on Gillygate there are a variety of businesses including nail salons, eateries and hairdressers. The increased T/B ratio along these roads is significant as it is continuously high for a large section of the road. These two

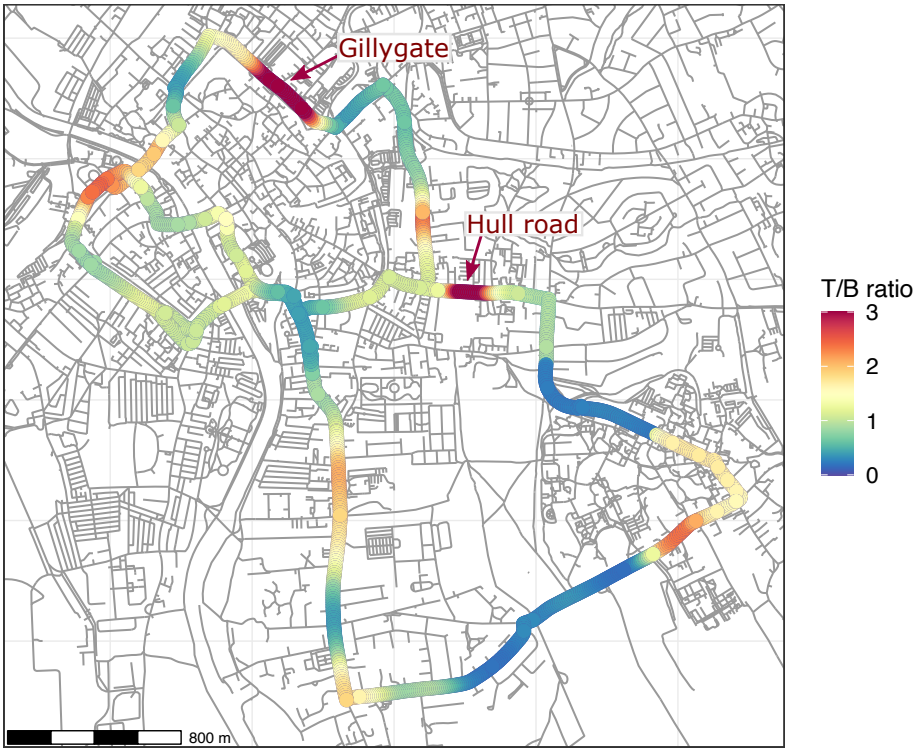

Figure 5.4: A spatial map showing the toluene to benzene (T/B) ratio (ppb/ppb) calculated using ordinary least squares (OLS) regression and weighted by a Gaussian kernel. Map created using a σ of 100 m. © OpenStreetMap.

roads only account for about 5% of the route and may represent an important source of toluene. The use of OLS regression can be used to provide useful emissions information, but it considers the mean response and does not capture the full distribution of relationships that exist between toluene and benzene across all 30 of the repeat drives. To address this issue we adopt quantile regression to provide increased distributional information.

While an OLS regression line minimises the distance of the trend line to each data point, quantile regression attempts to define a line such that a certain proportion of the data is found above and below it and an explanation of quantile regression is included below[240]. For example, the median quantile

regression slope would have 50% of the data either side of it, whereas the slope associated with the 90th percentile would have 90% of the data below and 10% above. Through a quantile regression approach, the influence on the response variable by the predictor variable can be understood at different values of the response variable. The value and/or significance of a slope estimate could significantly vary between different quantiles. For example, a predictor variable may have a large influence on the response variable associated with "average" members of a population, but not those belonging to lower or higher quantiles. In the context of mobile measurements, high quantile values are used to explore the nature of transient evaporative sources that can be difficult to identify through standard linear regression.

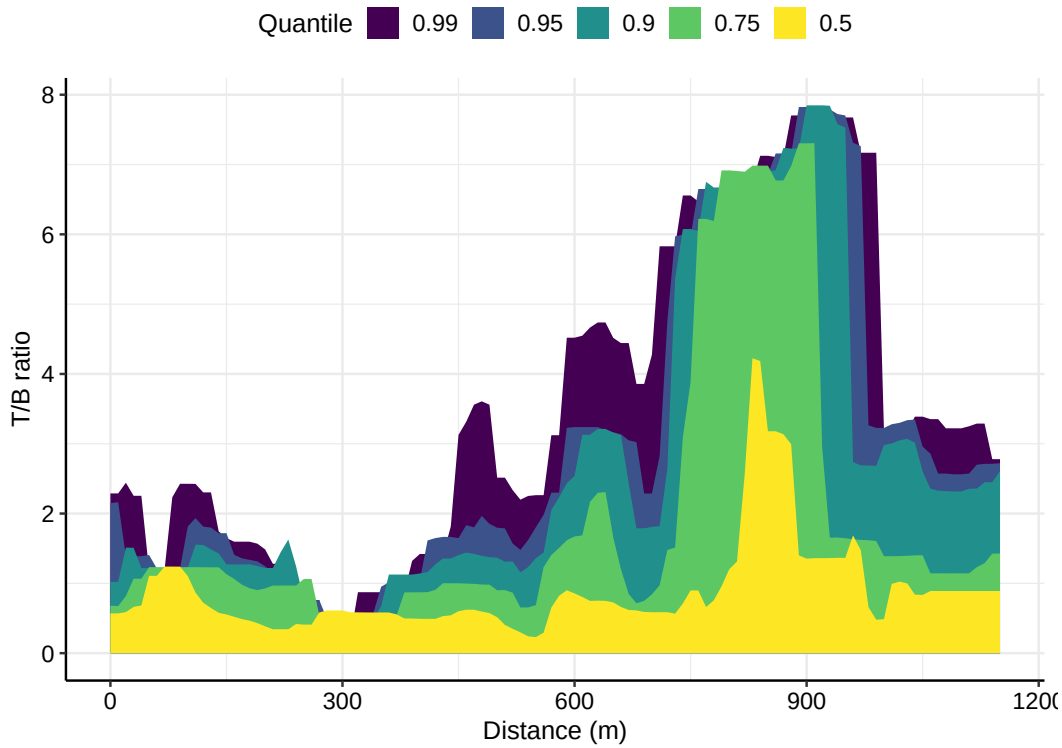

Figure 5.5: Toluene-to-benzene (T/B) ratio along the distance of Hull Road at quantiles of 0.99, 0.95, 0.9, 0.75 and 0.5 calculated using a Gaussian kernel smoother. The large peak at around 860 metres corresponds to a road vehicle fuel station, indicating evaporative emissions from this source.

We use the Gaussian kernel smoother approach discussed in Section 3.4 to provide the T/B ratio calculated at different quantiles along the distance of Hull road, shown in Figure 5.5. The plot shows that as the quantiles increase, so does the T/B ratio. This is significant as the higher quantiles represent intermittent sources that would be missed by considering only the 50th percentile. While the median T/B ratio peak is around 2, the higher quantiles (0.75 to 0.99) converge on a ratio closer to 6 or 7, which will be more representative of the intermittent evaporative source than the median slope value or a standard regression slope. On Hull Road there is a road vehicle fuel station situated at around 860 m, which corresponds to the large increase in the T/B ratio and this is highly likely due to evaporative emissions from the fuel station, due to the absence of other potential sources at this location. Figure 5.5 also shows the spatial extent to which the fuel station has an influence.

Figure 5.6 shows a comparison of the T/B ratio for the roads with a higher T/B ratio (Hull Road and Gillygate, labelled as evaporative) and the remainder of the route. Figure 5.6 shows that at higher quantiles (0.99), the evaporative area has T/B ratio 1.7 times higher than the remainder of the route (6.69 compared to 3.94), which is a significant increase and corresponds to an intermittent evaporative source. Figure 5.6 also shows that at a lower quantiles of 0.5 and 0.75, both of the comparison plots agree well, with similar T/B ratios, representing emissions from vehicle exhausts. These results suggest that on the whole route, there is only a minor contribution of evaporative sources (about 5% of the length) that can clearly be identified in the data.

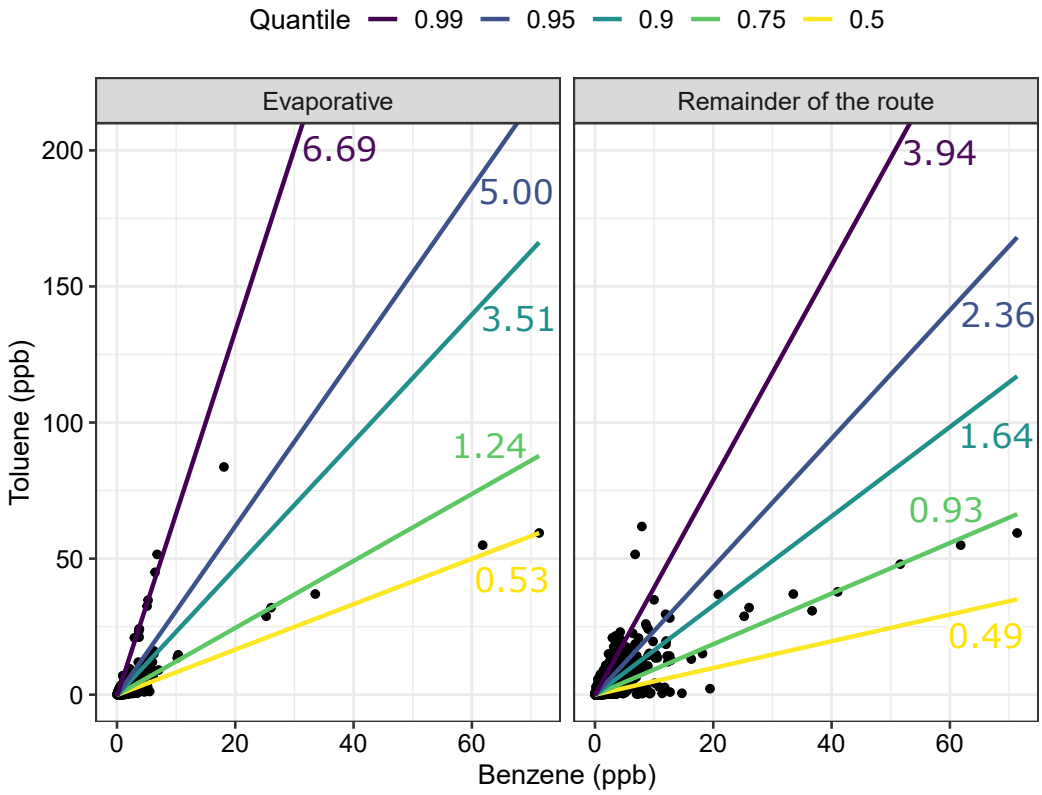

Figure 5.6: The toluene to benzene (T/B) ratio for the evaporative areas (Hull Road and Gillygate) and for the remainder of the route at quantiles of 0.99, 0.95, 0.9, 0.75 and 0.5 with the corresponding slope values also displayed. The toluene and benzene values for each of the comparative figures were produced using data collected from all 30 repeat measurement drives.

5.4 Milan results

5.4.1 Summary of measurements

Figure 5.7 shows a statistical summary of the mobile measurements carried out in Milan between the 30th September to 1st October 2021, during which 7 repeat drives of the measurement route were performed. The plot shows that the mixing ratio of monoterpenes and isoprene was consistently below 0.5 ppb and that there was a small amount of variation for these compounds. For the other compounds there is greater variation in the mixing ratios.

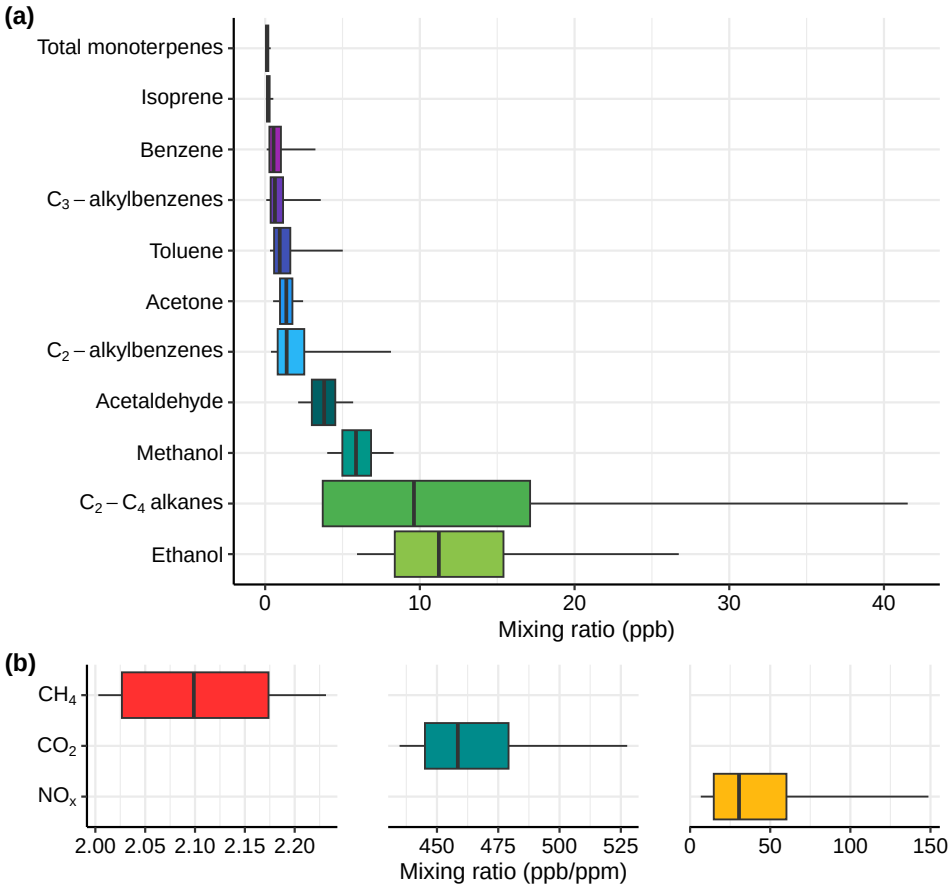

Figure 5.7: Summary of measurements made by a) the SIFT-MS (in ppb) and b) the ICAD and the UGGA (in ppb/ppm) during repeat sampling drives around Milan which were carried between the 30th September and 1st October 2021. The box outline contains the 25th to the 75th percentile and the middle line shows the median mixing ratio for each compound. The whiskers represent the 5th and 95th percentile for the mixing ratios of each compound.

Compounds related to vehicle emissions, including benzene, toluene and C_2- and C_3-alkylbenzenes all show similar median mixing ratios and have similar amounts of variation, which is likely to be influenced from sampling of vehicle exhausts whilst mobile measurements were made. There is a small amount of variation included in acetone and acetaldehyde and these compounds would be expected to be present in the atmosphere as oxidation

products or from VCP usage.

Larger variations in mixing ratio were observed for C_2-C_4 alkanes and ethanol. Ethanol variation may be related to emissions from vehicles or fuel evaporation due to ethanol addition in gasoline fuel[26,239]. Ethanol variation could also result from use of VCPs or solvents[26,120]. The largest variation in mixing ratio is observed for C_2-C_4 alkanes, which are likely to be emitted from vehicle exhausts or from fuel evaporation. C_2-C_4 alkanes could also be emitted due to leakage of natural gas used in residential areas[26]. There is also a large variation in CO_2 and NO_x mixing ratios, which are both related to emissions from vehicle exhausts. Variation in CH_4 could be related to use of natural gas fuel in vehicles or leakage from the natural gas network and may have similar emission sources as C_2-C_4 alkanes. Further analysis, including spatial mapping and comparison of mobile and point sampling results can be used to investigate different emission sources.

5.4.2 Spatial distribution of pollutants

Figure 5.8 shows the distance-weighted mean mixing ratios of toluene, ethanol, NO_x and CO_2 along the Milan mobile measurement route. The maps show some contrasting differences between the different compounds. Toluene mixing ratios are fairly low for the majority of the route, but elevated levels are seen at the top of the road second in from the left (A) and towards the bottom right of the map (B). The elevated levels at the bottom right correspond with elevated levels in CO_2, but only low levels of NO_x, which is indicative of exhaust emissions from road vehicles with lower NO_x emissions, possibly motorcycles or mopeds. However, the other area with an elevated toluene mixing ratio does not seem to correspond to any of the other mapped compounds and the elevated toluene occurs outside of a road vehicle fuelling station, suggesting a possible evaporative emission source.

There is an area towards central Milan (C) which shows elevated levels

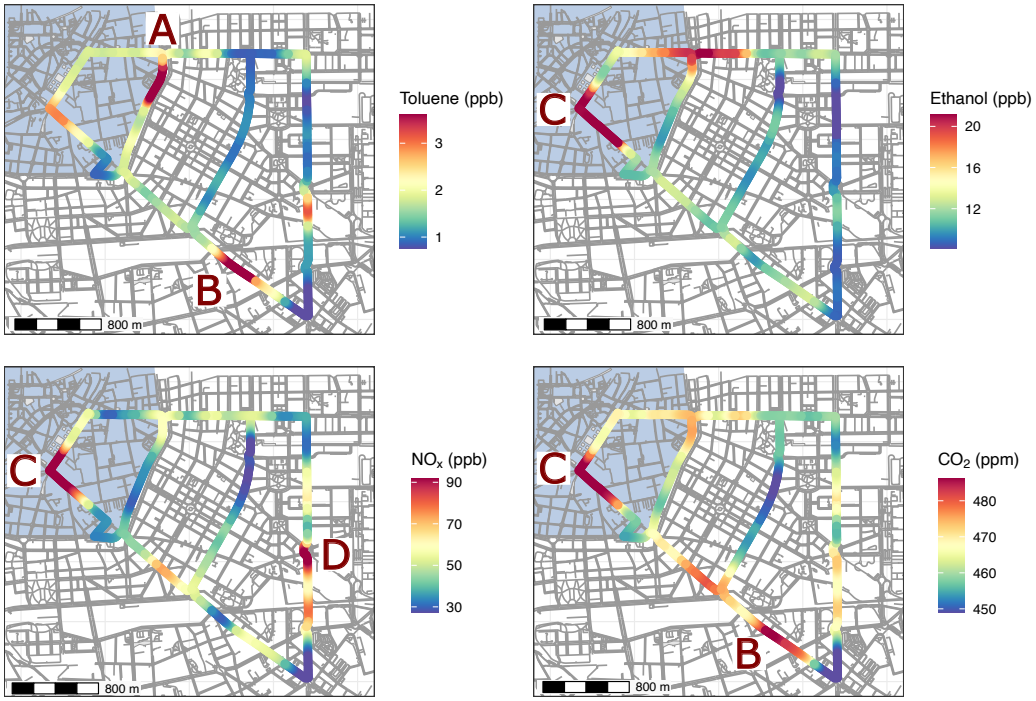

Figure 5.8: Spatial mapping of mean mixing ratios of Toluene (ppb), Ethanol (ppb), NO_x (ppb) and CO_2 (ppm) from mobile measurements around Milan. Maps created using a σ of 100 m and the lower and upper legend limits represent the 5th and 95th percentile of the pollutant mixing ratio. The blue shaded area represents the boundary of the low emission zone. © OpenStreetMap. The letters (A, B, C and D) correspond to hotspot areas of interest.

of ethanol, NO_x and CO_2 (red on the left of the route) and this area has a variety of possible emission sources including hotels, shops, restaurants and bakeries. It is likely that the elevated levels here are due to businesses or from emissions of vehicles that emit low amounts of VOCs, due to lower mixing ratios of toluene which is a good indicator of vehicle emissions.

There is additional area of elevated NO_x observed on the right hand side of the map (D), which occurs near a roundabout on the outer-side of Milan. It is likely that this elevated level is due to vehicle emissions as there are also slightly elevated levels of toluene and CO_2 observed. Higher NO_x mixing

ratios seen in this area could be a result of a higher proportion of high-emitting NO_x vehicles or vehicle operating conditions, such as acceleration from the roundabout.

The next section will further investigate different source type areas observed through spatial mapping to explore different possible emission sources in these areas (inner Milan, outer roundabout and toluene hotspot).

5.4.3 Further investigation of emission source type areas

Figure 5.9 shows a comparison of summary statistics for measurements at the different source type areas revealed by spatial mapping of pollutants. The inner Milan area corresponds to the hotspots of ethanol, NO_x and CO_2 shown towards central Milan, on the left hand side of the spatial mapping (Figure 5.8, C). For the inner Milan area, there are higher mixing ratios observed for acetone, CO_2, ethanol and NO_x, which suggests a mixture of emissions from vehicles and businesses. The mixing ratios of vehicle-related VOCs (benzene, toluene and C_2- and C_3- alkylbenzenes) are fairly low, which suggests emissions from diesel vehicles or passenger cars, which have lower VOC/CO_2 ratios, as shown in Figure 4.6.

The outer roundabout area corresponds to the hotspot of NO_x shown on the outer-right of the NO_x spatial map (Figure 5.8, D). The outer roundabout area shows fairly low mixing ratios for all of the compounds, but there are higher mixing ratios of CO_2 and NO_x. This suggests that the roundabout area may be dominated by emissions from vehicles with lower VOC emissions, such as diesel vehicles or newer passenger cars. The roundabout area is likely to have more free-flow traffic conditions, resulting in lower emissions compared to the inner Milan area which is likely to have higher traffic congestion.

The toluene hotspot area corresponds to higher toluene mixing ratios shown towards the top middle of the toluene spatial map (Figure 5.8, A). The

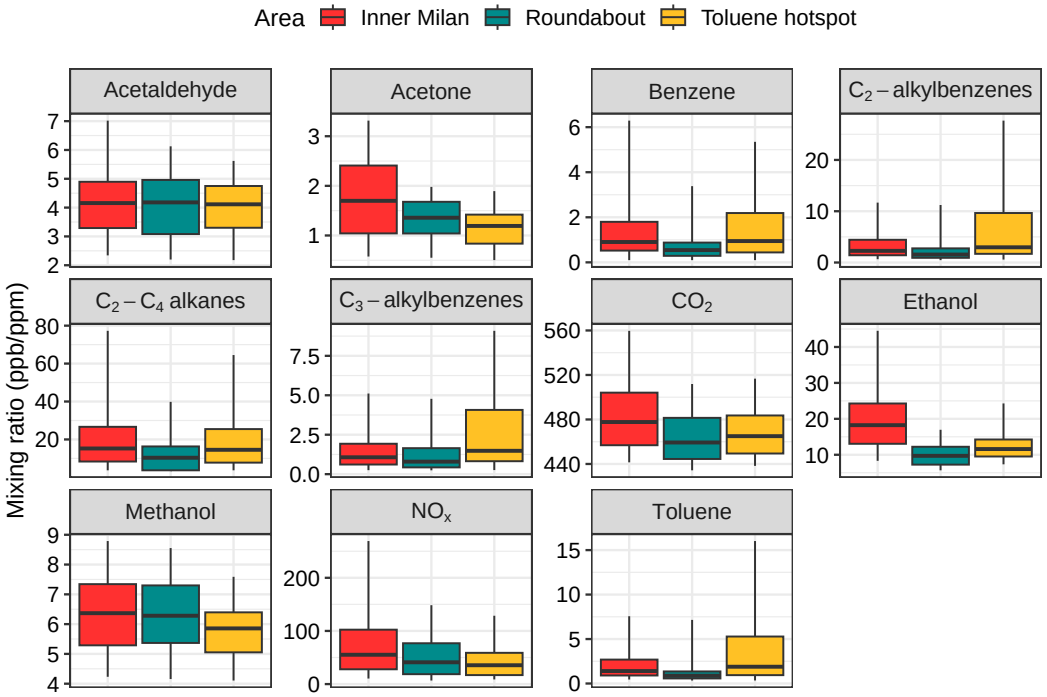

Figure 5.9: A comparison of measurements made during mobile measurements in Milan at different source type areas. The source type areas are inner Milan, the outer roundabout and the toluene hotspot. The box outline contains the 25th to the 75th percentile and the middle line shows the median mixing ratio for each compound. The whiskers represent the 5th and 95th percentile for the mixing ratios of each compound.

toluene hotspot area shows elevated levels of other vehicle-related VOCs including benzene and C_2- and C_3- alkylbenzenes. The area also shows similar levels of CO_2 as the outer roundabout area, but there are fairy low levels of NO_x. This suggests that this area could be dominated by vehicles with lower NO_x and higher VOC emissions, possibly motorcycles and mopeds with a gasoline/oil fuel type or other gasoline vehicles (as shown in Figure 4.4 and Figure 4.6). The higher levels of vehicle-related VOCs could also be a result evaporative emissions from the road vehicle fuel station located near the toluene hotspot.

A spatial map of the distance-weighted calculated NO_x/CO_2 ratio has

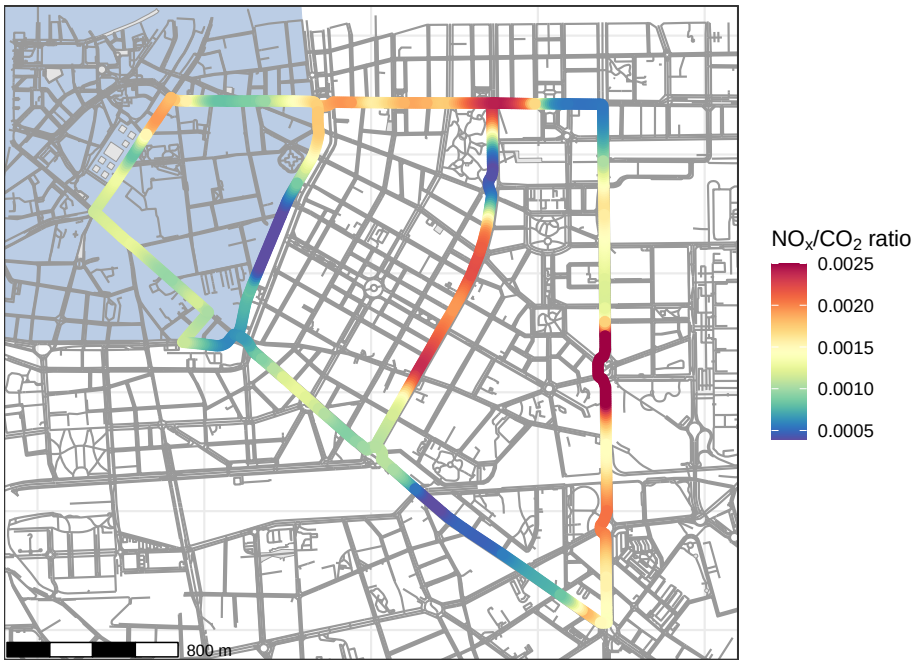

Figure 5.10: A spatial map showing the NO_x/CO_2 ratio (ppb/ppb) calculated using ordinary least squares (OLS) regression and weighted by a Gaussian kernel. Maps created using a σ of 100 m and the lower and upper legend limits represent the 5th and 95th percentile of the ratio. © OpenStreetMap.

also been created for Milan to assist with source characterisation. Figure 5.10 shows the highest NO_x/CO_2 ratio values occur at the outer roundabout area, which agrees with Figure 5.8 and Figure 5.9 and suggests that this area is dominated by high-emitting NO_x vehicle emissions, such as the presence of diesel vehicles or as a result of congestion. The inner Milan area shows lower NO_x/CO_2 ratios, despite showing higher NO_x and CO_2 concentrations in Figure 5.8 and Figure 5.9. This suggests that this area could be dominated by vehicles that emit lower concentrations of NO_x, possibly vehicles that emit higher concentrations of VOCs or newer, cleaner vehicles. There are also some additional areas with higher NO_x/CO_2 ratios, such as traffic junctions,

and this is likely due to increased congestion in these areas.

To further investigate whether areas with low NO_x and high vehicle-related VOCs indicate areas dominated by gasoline vehicles, the relationship between CO_2, NO_x and benzene during mobile measurements has been investigated and is shown in Figure 5.11. The smooth line represents the relationship predicted using a locally weighted regression.

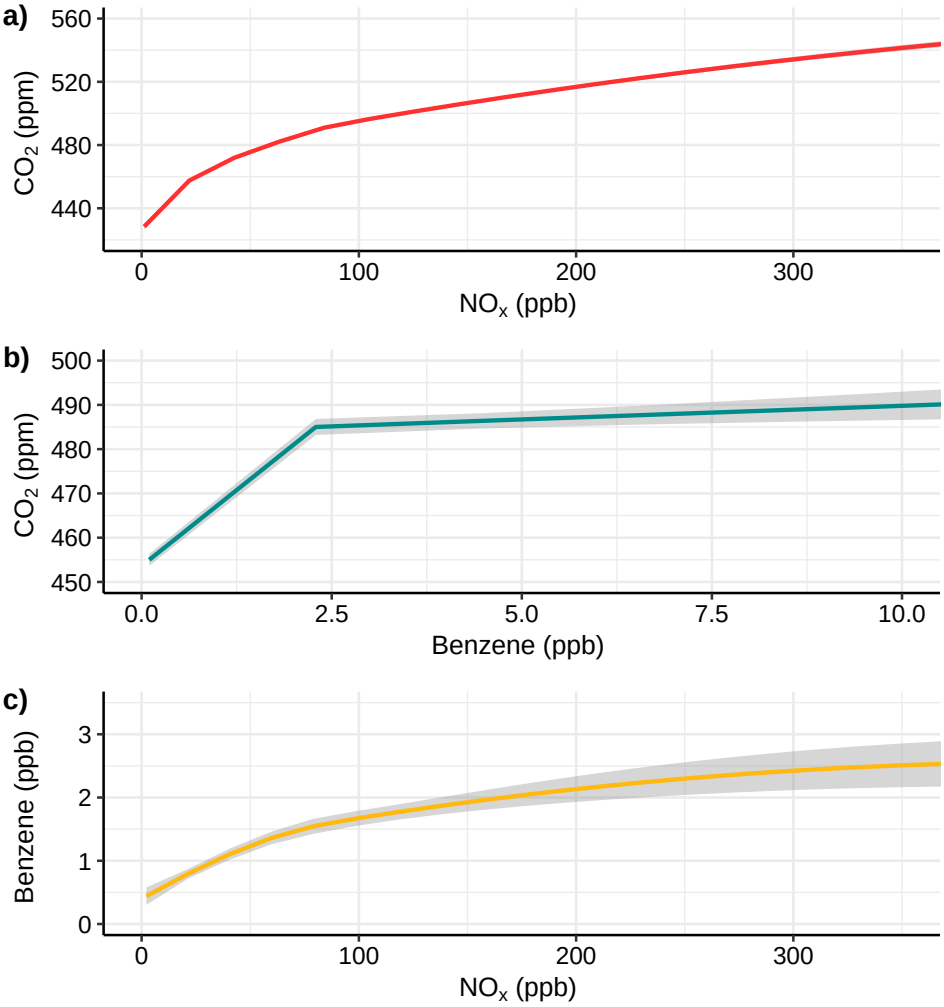

Figure 5.11: Relationship predicted using a locally weighted regression between a) CO_2 and NO_x, b) CO_2 and benzene and c) benzene and NO_x measured during mobile measurements in Milan. Note that the x-axis has been limited by the 99th percentile to remove the influence from outliers.

Figure 5.11 shows the locally weighted regression predicted relationship

between CO_2, NO_x and benzene. These compounds were chosen to examine their relationship with each other and to determine whether NO_x and benzene emissions correlate to combustion emissions (CO_2). Furthermore, investigating the relationship between NO_x and benzene can be used to indicate if these species are co-emitted, likely from vehicles. The relationship between all of the compounds is positive, suggesting that all of the compounds are co-emitted. The relationship between CO_2 and NO_x is the strongest (Figure 5.11a) and it has the smallest associated error divergence. The relationship between CO_2 and benzene is strong until around 2.5 ppb of benzene, where the slope becomes less steep. This could suggest that higher combustion-related emissions of benzene are less common. The relationship between benzene and NO_x has the largest associated error divergence with the regression results, particularly at higher values of NO_x. This suggests that benzene and NO_x may be co-emitted at lower levels of NO_x, but there is less confidence of them being co-emitted at higher NO_x.

5.4.4 Linking point sampling and mobile measurements

Both point sampling and mobile measurements were carried out in Milan, as discussed in Section 2.7. This provides the opportunity for comparison between the two measurement and analysis techniques to determine the spatial representativity of a point measurement and the contribution of vehicle emissions to air quality in an urban area.

Figure 5.12 shows summaries of SIFT-MS measurements of VOCs carried out during point and mobile sampling. For the majority of compounds, the mixing ratios are higher for point sampling than for mobile measurements. This is likely to be a result of the positioning of the sample inlet, which for point sampling was placed at the height of vehicle exhausts and therefore emission plumes were sampled before dilution. Further differences could be a result that point sampling and mobile measurements took place at

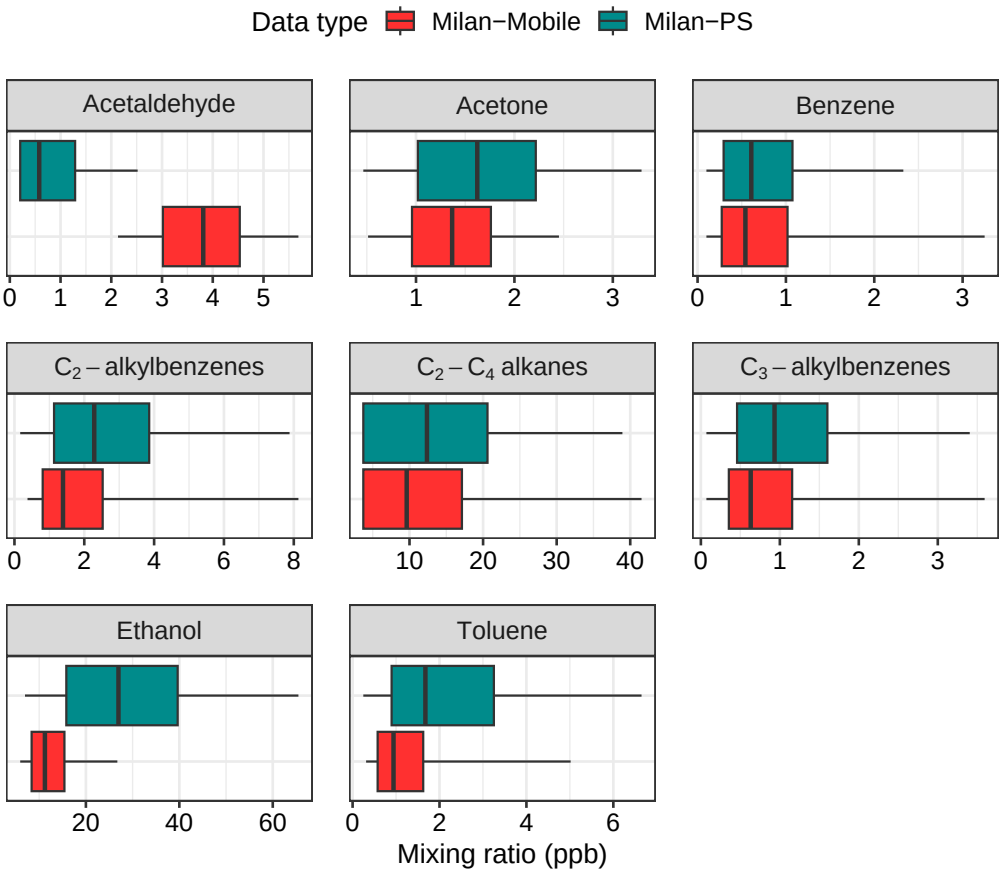

Figure 5.12: Comparison of measurements made by the SIFT-MS during point sampling (in blue) and mobile measurements (in red) carried out in Milan. The box outline contains the 25th to the 75th percentile and the middle line shows the median mixing ratio for each compound. The whiskers represent the 5th and 95th percentile for the mixing ratios of each compound.

different times. Acetaldehyde has a higher median mixing ratio during mobile measurements and can be present in the atmosphere as a product of oxidation processes or directly emitted from cooking[241]. Acetone also has a higher median mixing ratio for the mobile measurements, which is likely due to a variety of possible emission sources in Milan.

Figure 5.13 shows summaries of measurements of CH_4, CO_2 and NO_x carried out during point sampling and mobile measurements. The mixing

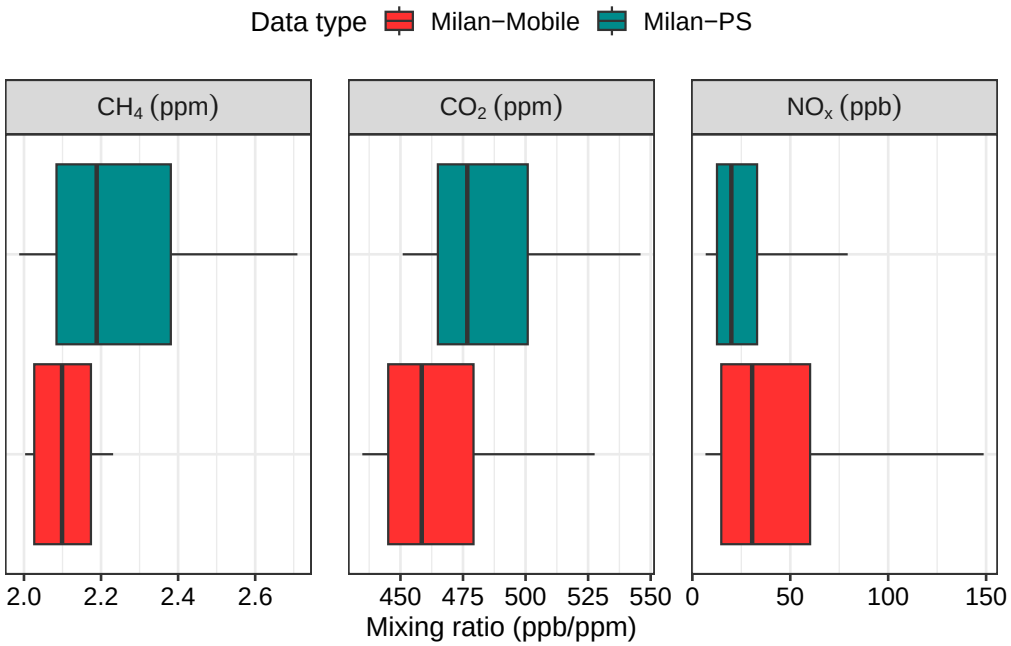

Figure 5.13: Comparison of CH_4, CO_2 and NO_x made during point sampling (in blue) and mobile measurements (in red) carried out in Milan. The box outline contains the 25th to the 75th percentile and the middle line shows the median mixing ratio for each compound. The whiskers represent the 5th and 95th percentile for the mixing ratios of each compound.

ratios for CH_4 and CO_2 are higher for point sampling measurements, but NO_x mixing ratios are higher for mobile measurements. Higher mixing ratios of CO_2 during the point sampling measurements also correspond to higher mixing ratios of the other vehicle-related VOCs during point sampling measurements, which suggests that their emissions are combustion-related. CO_2 and CH_4 are likely to have higher mixing ratios during point sampling because combustion plumes were sampled before dilution. The point sampling location was also influenced by a clear local source of CH_4. During the period that point sampling measurements were performed, there was work being performed on a gas main nearby, which could result in higher CH_4 emissions. Higher mixing ratios of NO_x were observed during mobile measurements,

which is likely the result of more diesel vehicles on the mobile measurement route or more varied driving conditions during mobile measurements which may result in higher NO_x emissions.

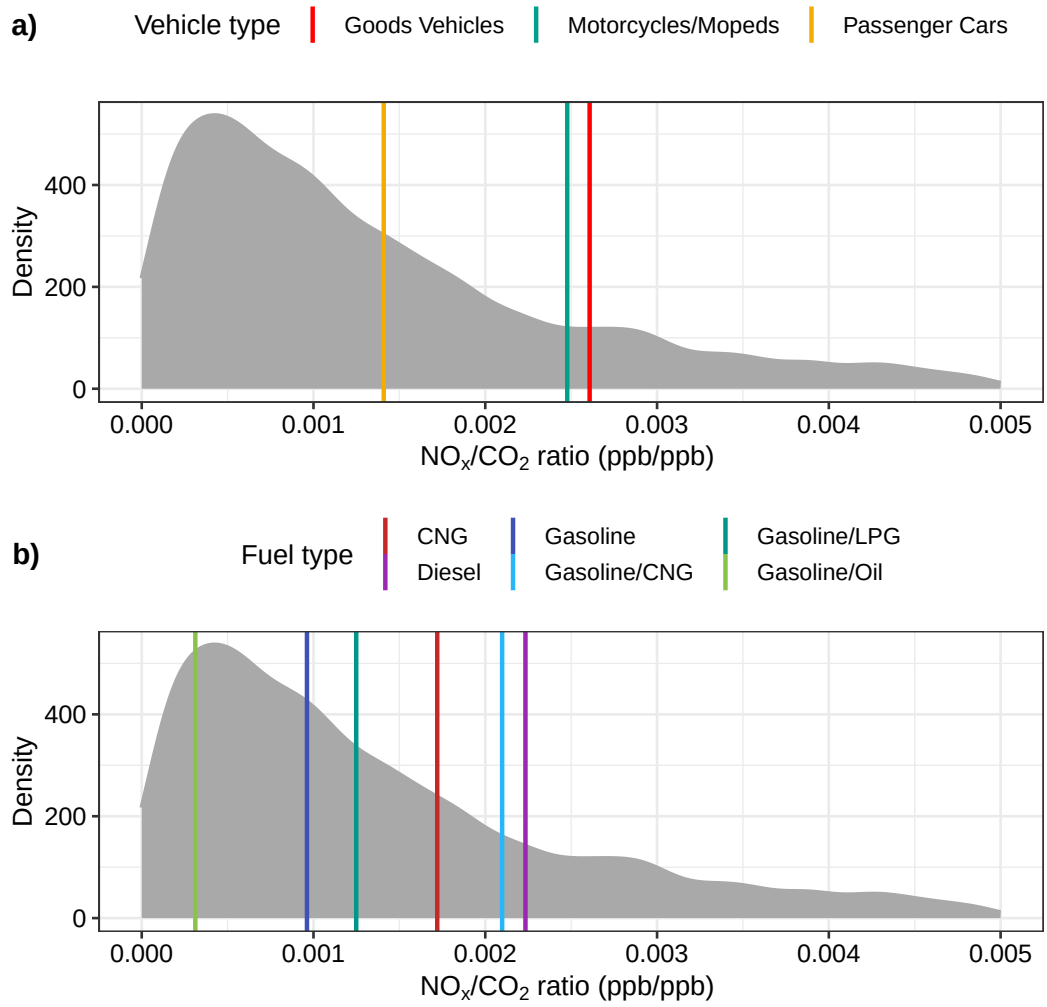

Figure 5.14: Comparison of NO_x/CO_2 ratios (ppb/ppb) extracted from mobile and point sampling measurements carried out in Milan. The density curve shows the distribution of the NO_x/CO_2 ratios extracted from mobile measurements using rolling regression. The vertical lines represent the average NO_x/CO_2 ratios calculated from point sampling for different a) vehicle types and b) fuel types. The x-axis range has been limited for data visualisation.

Combustion-related emission ratios of NO_x and VOCs have been extracted from mobile measurements and then compared to corresponding emission ratios calculated from point sampling. Emission ratios of NO_x and VOCs were extracted using the rolling regression analysis method, which allows for extraction of combustion-related plumes (method described in Section 3.4). Emission ratios from point sampling are also extracted as combustion-related plumes and therefore results from the two measurement methods can be compared.

Figure 5.14 shows the comparison between NO_x/CO_2 ratios extracted from point sampling and mobile measurements. The distribution of NO_x/CO_2 ratios from mobile measurements are shown by the density curve in Figure 5.14 and the vertical lines represent different NO_x/CO_2 ratios for grouped vehicle categories extracted from point sampling. Both Figure 5.14 a and b show that NO_x/CO_2 ratios agree relatively well between the two measurement techniques and that ratios from mobile measurements are slightly higher. The average NO_x/CO_2 ratio extracted from mobile measurements was 1.5 times higher than point sampling ratios. Higher NO_x emissions detected during mobile measurements could be evidence that the sample of vehicles spatially are higher emitters of NO_x. This could be due to higher numbers of vehicles that emit higher amounts of NO_x, such as diesel vehicles or heavy goods vehicles, or that emission control systems are not performing optimally. Furthermore, during mobile measurements a wider variety of driving conditions were sampled compared to point sampling that tended to be free-flowing conditions.

Figure 5.15 shows the comparison of VOC/CO_2 ratios extracted from mobile and point sampling measurements. In both Figure 5.15 a and b the VOC/CO_2 ratios from mobile measurements appear to be lower than the ratios extracted from point sampling. However, the average VOC/CO_2 ratio extracted from mobile measurements was 1.6 times higher than point sampling, which suggests that there are many high concentration emission

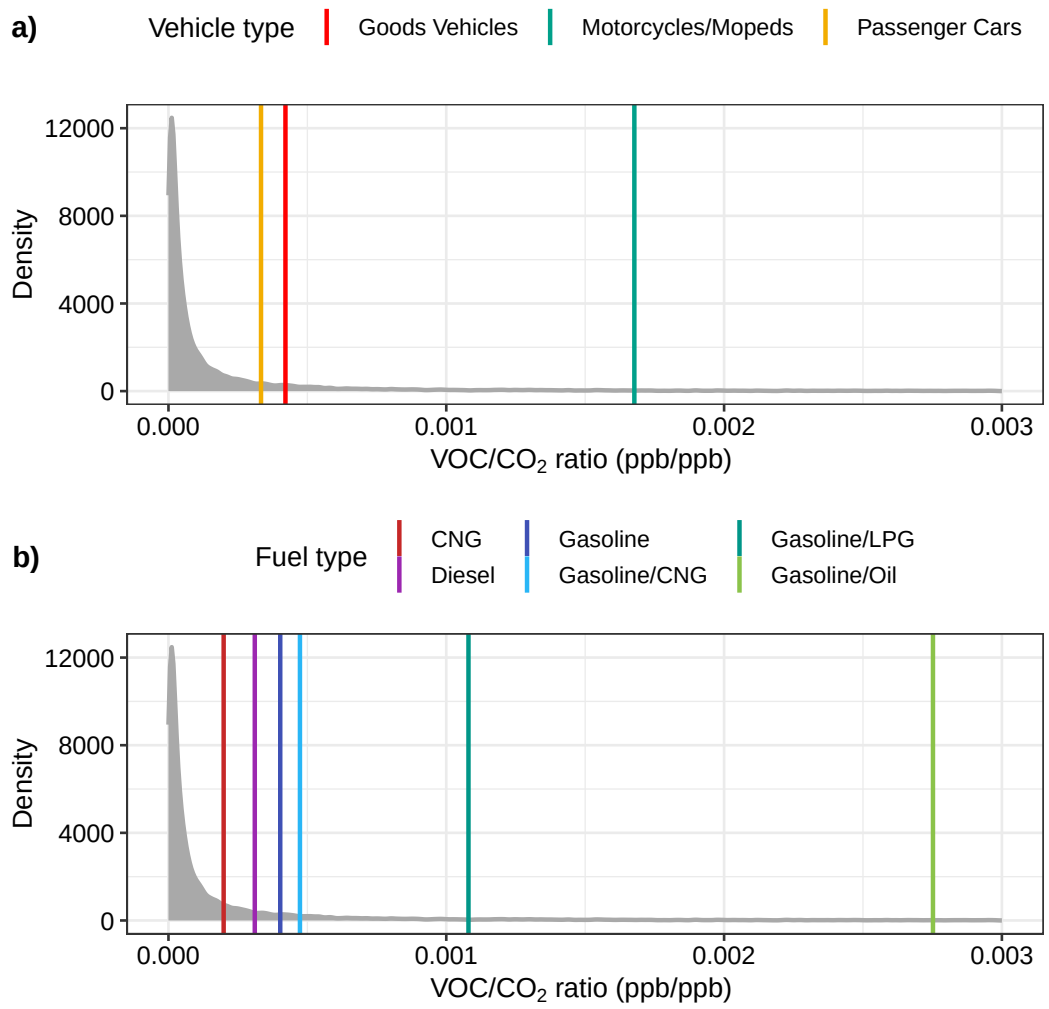

Figure 5.15: Comparison of VOC/CO_2 ratios (ppb/ppb) extracted from mobile and point sampling measurements carried out in Milan. The density curve shows the distribution of the VOC/CO_2 ratios extracted from mobile measurements using rolling regression. The vertical lines represent the average VOC/CO_2 ratios calculated from point sampling for different a) vehicle types and b) fuel types. The x-axis range has been limited for data visualisation.

events which increase the average ratio value. Slightly higher VOC/CO_2 ratios measured during mobile measurements are likely due to sampling of high VOC emitting vehicles, such as motorcycles and mopeds, or greater

variation in driving conditions which cause increased VOC emissions.

Higher average NO_x and VOC emission ratios extracted from mobile measurement compared to point sampling are likely a result of emission events from high-emitting NO_x and VOC vehicles, such as motorcycles and mopeds or natural gas fuel vehicles (as shown in Chapter 4). This indicates that these vehicle types could play an important role in spatial emissions of NO_x and VOCs as there was good agreement in the increase factor of the mobile measurement ratios compared to point sampling (NO_x a factor of 1.5 and VOCs a factor of 1.6). Furthermore, the emission ratios extracted from point sampling are likely to be lower as the vehicle fleet was dominated by Euro class 6 passenger cars, due it being within the low emission zone (Area C) in Milan. Higher emission ratios from mobile measurements could also result from more varied driving conditions of vehicles and influences from vehicular congestion. But, overall the two methods used to extract vehicular emission ratios of NO_x and VOC agree relatively well, showing that both measurement methods can be used to obtain useful information relating to vehicular emissions. Further figures showing the agreement between average point sampling and mobile extracted emission ratios are shown in Appendix C.

Furthermore, emission ratios of NO_x and VOCs extracted from mobile measurements can be spatially mapped, as is shown in Figure 5.16 and Figure 5.17. An advantage of this approach is that local dilution events can be easily extracted from a complex urban environment, which is affected by a multitude of emission sources. Potential emission hotspots of NO_x and VOCs are shown by the red data points on the maps. Hotspots of NO_x and VOC emissions largely occur in areas with high volumes of vehicular traffic, such as congested areas or traffic junctions. Spatial mapping of emission ratios to reveal hotspots can highlight specific areas that could then be further investigated to obtain additional information relating to factors that may affect vehicular emissions, such as traffic congestion levels, vehicle

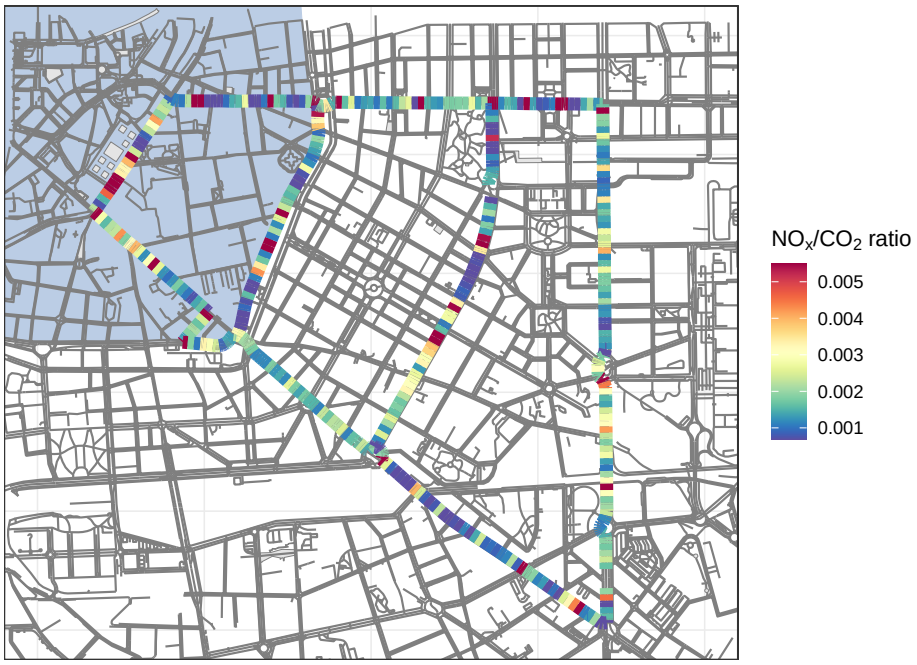

Figure 5.16: Spatial mapping of NO_x/CO_2 ratios (ppb/pbb) from mobile measurements in Milan. The route is divided into 30 m segments and coloured by the mean ratio per segment. The upper and lower limits of the legend represent the 10th and 90th percentile of average 30 m segment ratios. The blue shaded area represents the boundary of the low emission zone. © OpenStreetMap.

fleet composition, and other potential sources of emissions. Therefore, this approach could be used to help to inform policies and design more effective emission reduction strategies.

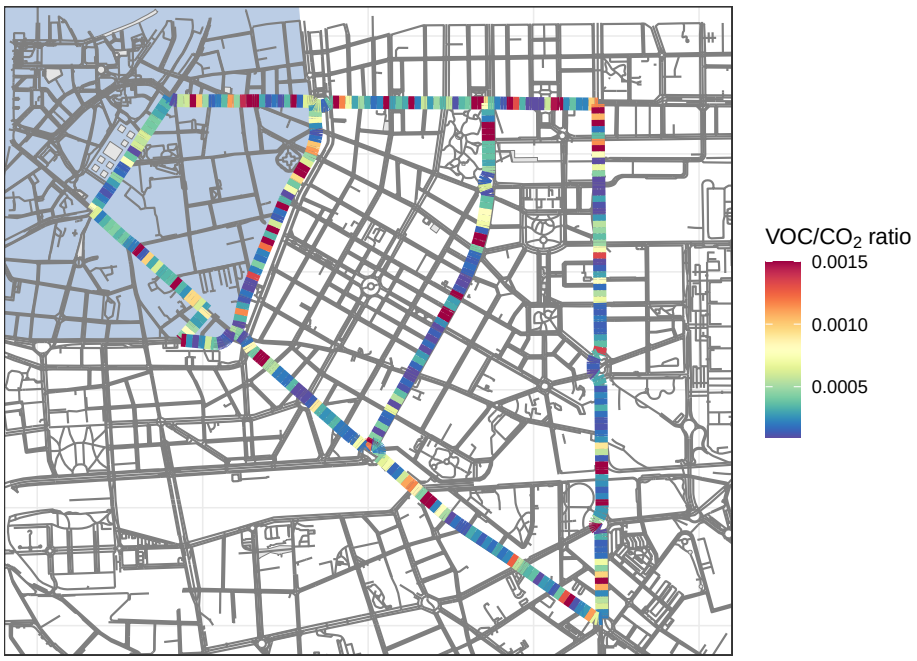

Figure 5.17: Spatial mapping of VOC/CO_2 ratios (ppb/pbb) from mobile measurements in Milan. The route is divided into 30 m segments and coloured by the mean ratio per segment. The upper and lower limits of the legend represent the 10th and 90th percentile of average 30 m segment ratios. The blue shaded area represents the boundary of the low emission zone. © OpenStreetMap.

5.5 Manchester results

5.5.1 Summary of measurements

The mobile measurements in Manchester were carried out during 2 different time periods of the year. The first measurement campaign was carried out in summer (June-July) 2021 and the second campaign was carried out in winter (January) 2022. Both campaigns were carried out in dry weather and the average temperatures were 18 ° C and 5 ° C for summer and winter respect-

ively. Therefore, the measurements took place over contrasting temperature conditions and this allows for investigation into temperature dependence of air pollutant emissions.

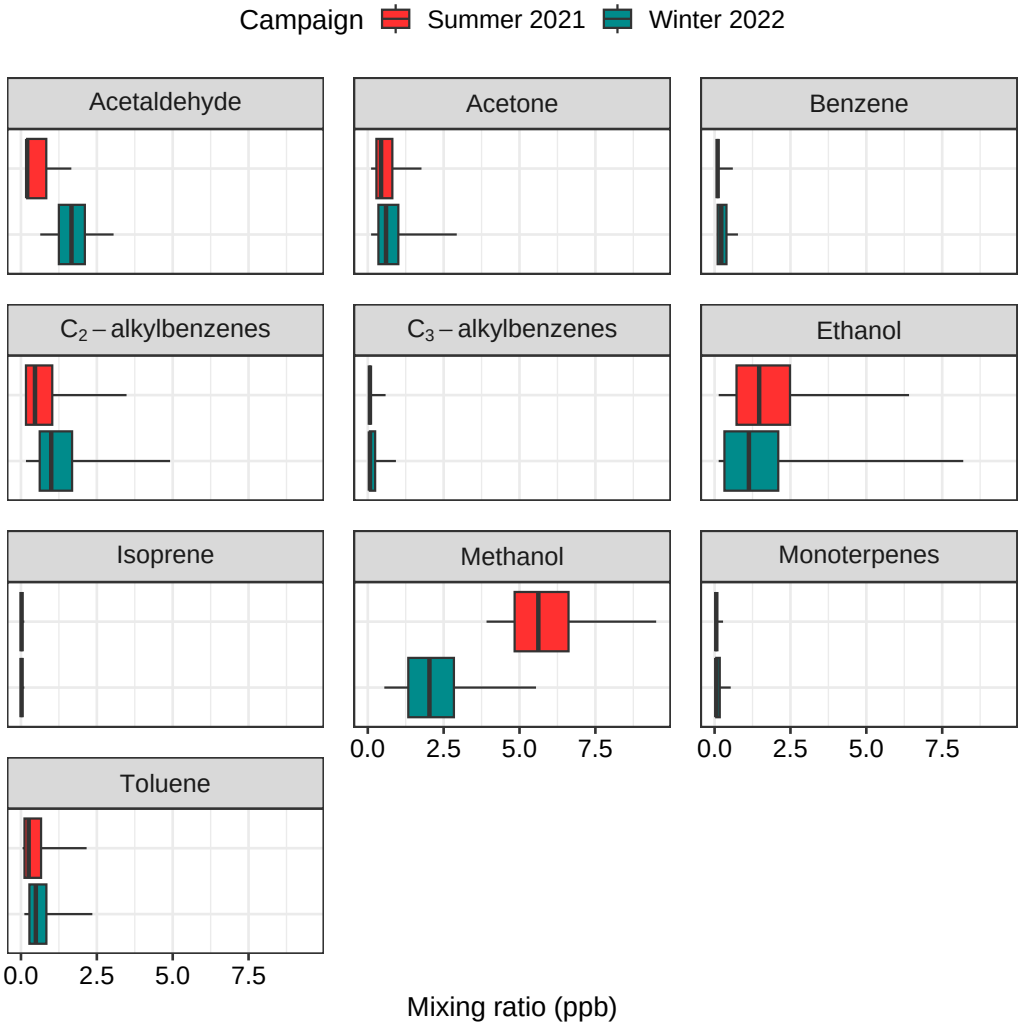

Figure 5.18: Summary of measurements made by the SIFT-MS (in ppb) during repeat sampling drives around Manchester in summer 2021 (June-July, in red) and winter 2022 (January, in blue). The box outline contains the 25th to the 75th percentile and the middle line shows the median mixing ratio for each compound. The whiskers represent the 5th and 95th percentile for the mixing ratios of each compound.

Figure 5.18 shows a statistical summary of the mobile measurements

made by the SIFT-MS, which were carried out in Manchester during summer 2021 and winter 2022. Isoprene and monoterpenes were consistently below 0.5 ppb and the number of measurements below the limit of detection for both species was similar between seasons. Vehicle emission related compounds, including benzene, toluene and C_3-alkylbenzenes, had relatively small variation and higher median mixing ratios were observed in winter, suggesting that vehicle emissions were more important in winter. C_2-alkylbenzenes is also a compound related to vehicle emissions, which had a higher amount of variation and a higher median mixing ratio was also observed in winter. Higher median mixing ratios of VOCs in winter could also result from longer atmospheric lifetimes due to lower photolysis levels and therefore less oxidation from radical species[242]. Analysis of long-term measurements carried out in London by Bohnenstengel et al. [242] reported that winter measurements of benzene had a mixing ratio almost 2 times higher than summer and that other anthropogenic VOCs followed the same trend.

Acetone had a small amount of variation in the mixing ratio and also showed similar mixing ratios in both summer and winter, suggesting that there is a similar amount of production of acetone as an oxidation product in both seasons. The mixing ratio of acetaldehyde has a higher amount of variation in the mixing ratio and a higher median mixing ratio is observed in winter, suggesting possible additional sources in winter. Higher mixing ratios of acetaldehyde in winter could result from direct emissions from vehicles. Dunmore et al. [239] analysed long term measurements in London and suggested that direct acetaldehyde emissions from gasoline and ethanol fuel combustion in road vehicles could be an important emission source of ethanol. However, the study also reported higher production of acetaldehyde in summer due to increased photochemical processing[239], which was not observed during mobile measurements carried out in Manchester.

High amounts of variation in the mixing ratio of methanol and ethanol

are observed for both winter and summer. Higher median mixing ratios are observed for both alcohol compounds in summer, which could be a result of emissions from road vehicles or evaporative emissions from vehicle fuel or VCPs. The 95th percentile mixing ratios of ethanol show a higher value in winter, which could be a result of the introduction of E10 gasoline (up to 10% ethanol) in November 2021. Therefore, higher amounts of ethanol could be measured from vehicle exhausts or evaporative emissions from vehicles and fuel stations. Dunmore et al. [239] reported that ethanol measured in winter correlated with vehicle emission-related VOC species, suggesting a road vehicle emission source.

Figure 5.19 shows a statistical summary of the mobile measurements made by the ICAD (CO_2 and NO_x), the UGGA (CH_4) and the O_3 analyser, which were carried out in Manchester during summer 2021 and winter 2022. Higher median mixing ratios of CO_2 were observed in winter, which is likely related to less plant coverage and therefore reduced plant take-up of CO_2. NO_x also shows higher median mixing ratios in winter and many studies have shown a temperature dependence of NO_x emissions from vehicles, which increase as temperature decreases[214]. For CH_4, CO_2 and NO_x an important factor will be the meteorological conditions where dispersion is less efficient in wintertime, along with increased combustion of fuels. The median mixing ratio of O_3 is higher in summer and this is a result of increased oxidation of VOCs in summer and therefore higher levels of O_3 production[239,242].

In addition to different emission sources between the two season, mixing ratios of air pollutants can be affected by meteorological conditions including boundary layer height. The boundary layer (BL) is the lowest layer of the troposphere and the height of the BL determines the extent to which atmospheric emissions can disperse and mix. In the winter, the BL height is lower due to lower temperatures which generate more stable atmospheric conditions[243,244]. Additionally, dilution in winter is reduced due to lower temperatures and wind speed and therefore emissions are trapped close to

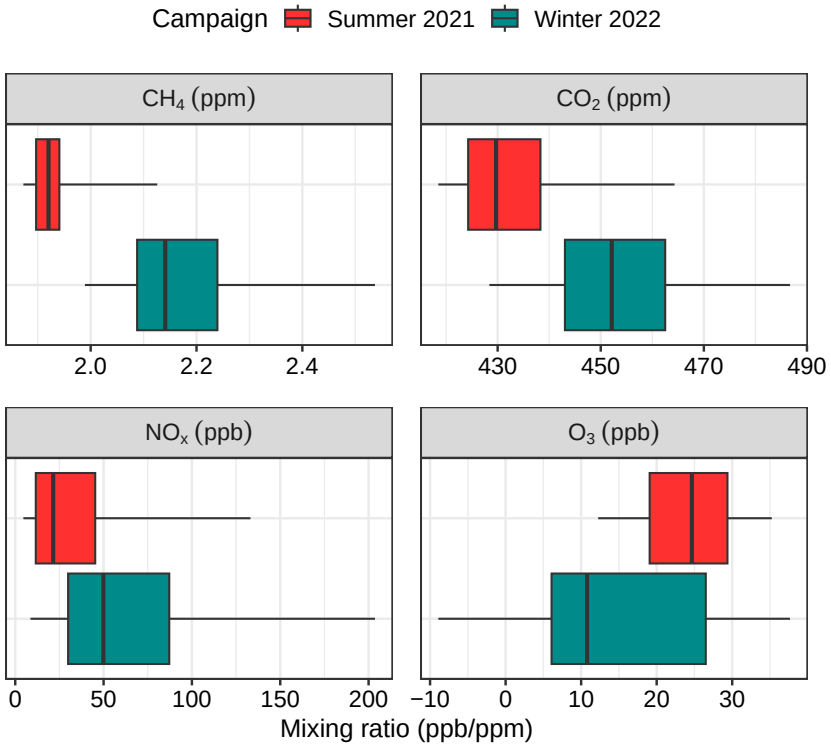

Figure 5.19: Summary of measurements made by the ICAD, UGGA and O_3 analyser (in ppb/ppm) during repeat sampling drives around Manchester in summer 2021 (June-July, in red) and winter 2022 (January, in blue). The box outline contains the 25th to the 75th percentile and the middle line shows the median mixing ratio for each compound. The whiskers represent the 5th and 95th percentile for the mixing ratios of each compound.

the surface[245]. Lower BL heights, temperatures and wind speed in winter could therefore explain higher mixing ratios for the majority of measured air pollutants in winter.

5.5.2 Spatial distribution of pollutants

Figure 5.20 and Figure 5.21 shows spatial mapping of the distance-weighted mean mixing ratios for toluene, ethanol, NO_x and CO_2 separated by season (summer and winter). As shown in Figure 5.18 the median mixing ratio of ethanol was slightly higher during the summer measurements, but the

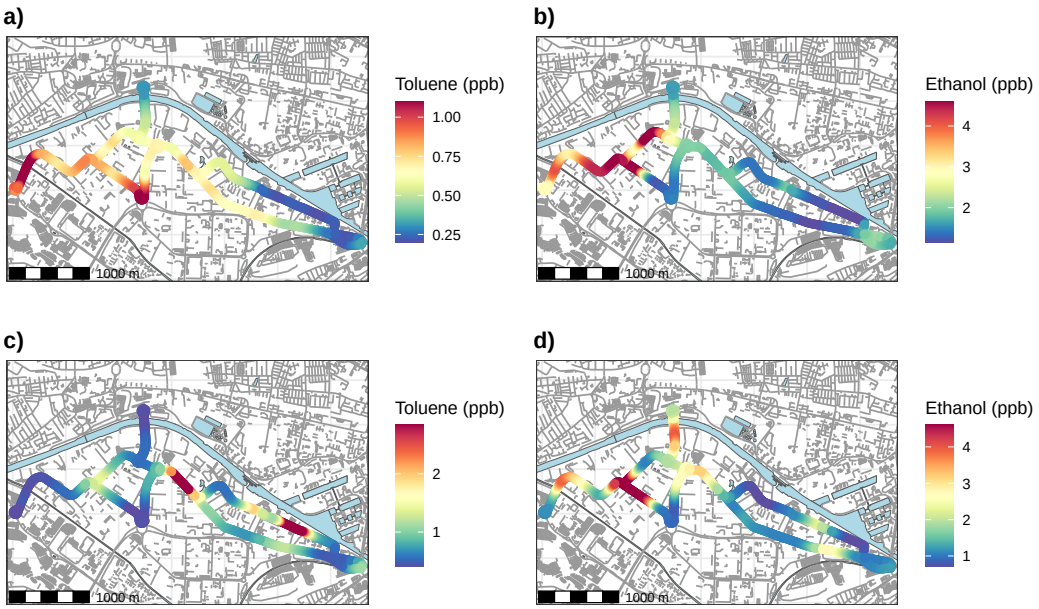

Figure 5.20: Spatial mapping of mean mixing ratios of a) summer toluene (ppb), b) summer ethanol (ppb), c) winter toluene (ppb) and d) winter ethanol (ppb) from mobile measurements around Manchester. Maps created using a σ of 100 m. Legend lower and upper limits represent the 5th and 95th percentile of the pollutant mixing ratio. © OpenStreetMap.

median mixing ratio of toluene was slightly higher in winter.

The maps of toluene (a and c) show that there is a different spatial distribution of toluene between the 2 seasons. The map of toluene in summer (Figure 5.20a) shows hotspots towards the bottom of the maps which are also seen in maps of CO_2 and NO_x (Figure 5.21). The hotspots are near two roundabouts and the correlation between ethanol, NO_x and CO_2 indicates emissions from road vehicles. The map of toluene in winter (Figure 5.20c) does not have the same clear hotspots near the roundabouts and instead has hotspots in the middle and on the right of the map. The area with the toluene hotspot in the middle of the map has a variety of possible emission sources including food manufacturers and vehicle repair shops, therefore it is possible that higher toluene mixing ratios resulted as evaporative emissions.

The maps of ethanol (b and d) show some similarities in the spatial distribution between the two seasons. They both have lower mixing ratios to the right hand side of the map, but the left of the map shows higher mixing ratios. The hotspot of ethanol which is observed in both of the maps (left/middle of the map) occurs in an area of concentrated and various industrial businesses, including vehicle garages, waste management, a tank container depot, alongside a variety of others, suggesting possible emissions directly from these businesses. The map of ethanol in summer (Figure 5.20b) also shows some additional hotspots which could result from evaporative emissions from road vehicles or industry due to higher ambient temperatures during the summer measurements. The hotspot of ethanol in summer towards the middle/left of the map correlates slightly with elevated levels of CO_2, which suggests a vehicle-related emission.

Figure 5.21 shows spatial mapping of the distance-weighted mean mixing ratios for NO_x and CO_2, separated by season (summer and winter). The maps for NO_x and CO_2 for both of the seasons show a similar spatial distribution for both of the pollutants. Furthermore the hotspots for NO_x and CO_2 are present in the maps for both seasons, which suggests that the emission sources of NO_x and CO_2 do not vary with temperature. Hotspots of NO_x and CO_2 are observed at roundabouts or at junctions, which are areas that typically have higher volumes of road vehicles and higher levels of congestion. Furthermore, similar spatial patterns between NO_x and CO_2 are observed, with elevated mixing ratios of NO_x occurring at the same area as elevated mixing ratios of CO_2, suggesting that they are emitted from the same source, likely to be exhaust emissions from road vehicles. The mixing ratios of NO_x and CO_2 measured in the winter were higher than in the summer, possibly due to increased traffic flow and reduced dispersion in the winter. NO_x may also have a vehicular temperature dependence-related emission, which will be investigated in subsection 5.5.3.

Some of the elevated levels of toluene and ethanol measured in summer

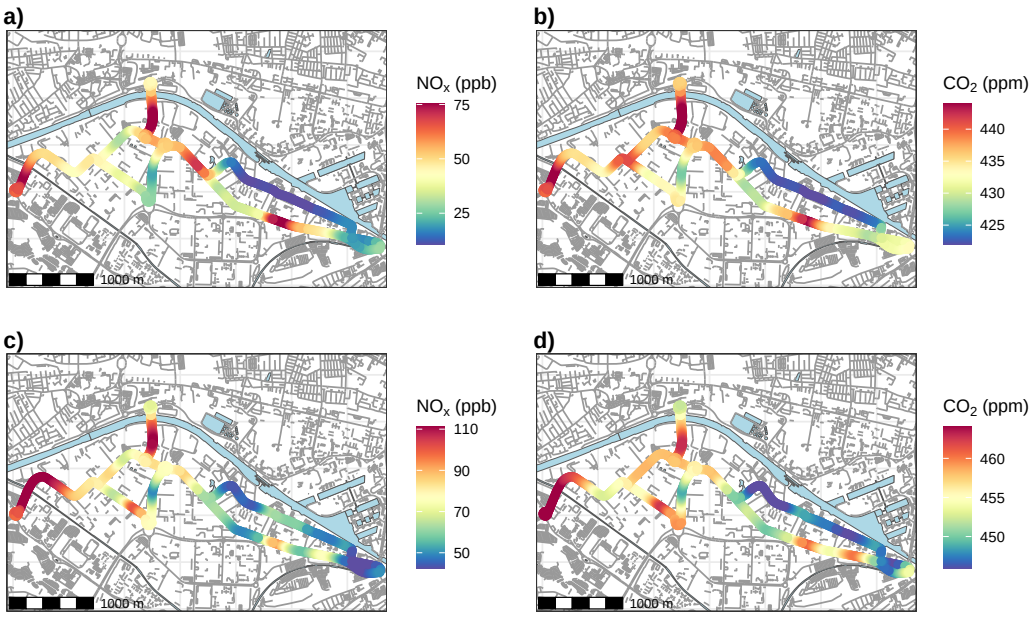

Figure 5.21: Spatial mapping of median values of a) summer NO_x (ppb), b) summer CO_2 (ppm), c) winter NO_x (ppb) and d) winter CO_2 (ppm) from mobile measurements around Manchester. Maps created using a σ of 100 m. Legend lower and upper limits represent the 5th and 95th percentile of the pollutant mixing ratio. © OpenStreetMap.

also correlate with elevated levels of NO_x and CO_2, particularly around the left-hand roundabout. This suggests that this area of the measurement route in summer may have been dominated by road vehicle emissions. However, other hotspots of ethanol and toluene in summer and all hotspots in winter have low agreement with NO_x and CO_2, suggesting that they are not related to emissions from vehicles.

A spatial map of the distance-weighted calculated NO_x/CO_2 ratio has also been created for summer and winter in Manchester to assist with source characterisation. Figure 5.22 shows that there are some similarities in the spatial variation in the NO_x/CO_2 ratio between the two seasons, but there are also some differences. In both summer and winter, there are low NO_x/CO_2 ratios in the middle of both maps and high ratios on the top right-hand road.

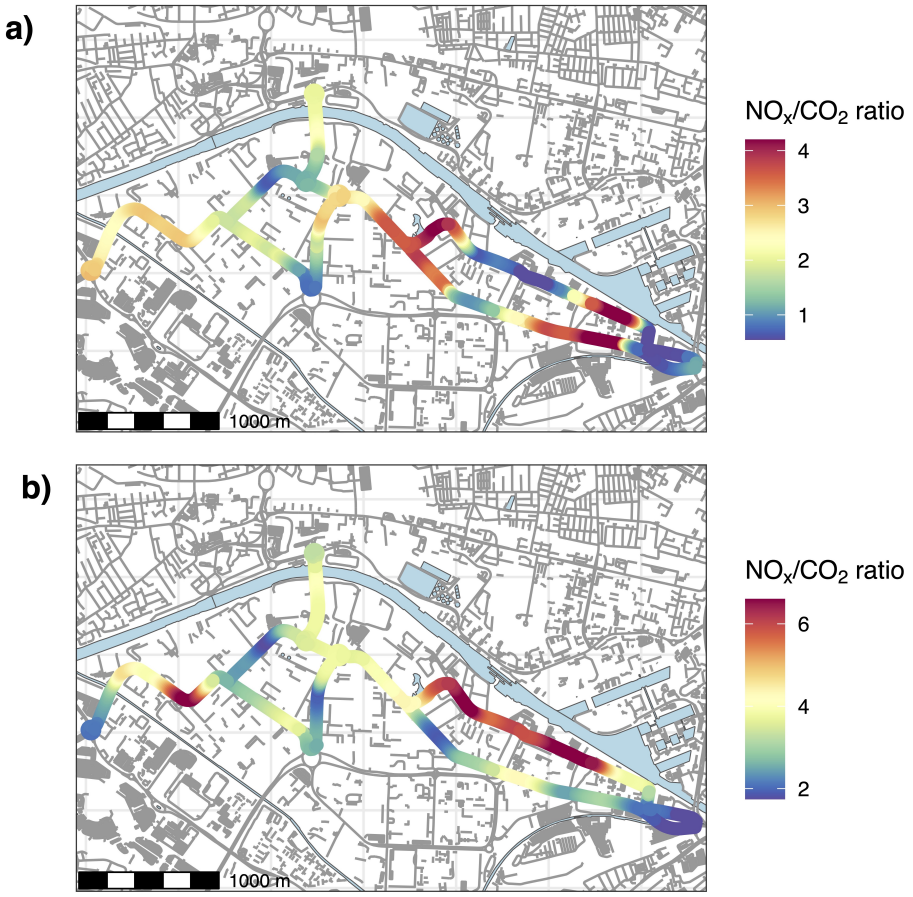

Figure 5.22: A spatial map showing the NO_x/CO_2 ratio (ppb/ppb) for a) summer and b) winter in Manchester calculated using ordinary least squares (OLS) regression and weighted by a Gaussian kernel. Legend lower and upper limits represent the 5th and 95th percentile of the ratio. Map created using a σ of 100 m. © OpenStreetMap.

However, in winter there is an additional hotspot in the ratio on the left-hand side of the map, due to a high-emitting NO_x source, such as diesel vehicles or a temperature dependent source. Also in winter there is an extended area of a high NO_x/CO_2 on the top right-hand road that is not present in summer, indicating a temperature dependent emission along this road. In summer, the areas of high NO_x/CO_2 ratios appear around road junctions and therefore increased ratios are likely a result of increased NO_x emissions from

congestion. Overall, Figure 5.22 shows a possible temperature dependence of NO_x emissions and this will be investigated in the next section.

5.5.3 Temperature dependence

The Manchester mobile measurements were carried out during two different seasons, summer and winter, and this provides the opportunity to investigate the effects of ambient temperature on emissions. To quantify the influence of ambient temperature on emission ratios we study the marginal effects, which are used when the effect of one variable depends on the value of another variable (the moderator). Marginal effects are computed by including an interaction term in the regression model, which describes how the outcome variable changes when a specific independent variable changes. Models with interaction terms can be used to explore the relationship between the dependent and independent variables at various values of the moderator.

Equation 5.1 shows the equation for the regression model with ambient temperature (T) included as an interaction term, where β_1 and β_2 are the regression coefficients and X and Y represent the pollutant species. The emissions intensity is found by taking the partial derivative of Equation 5.1 with respect to the X variable to give Equation 5.2. The derivative is a function of temperature, meaning there is no unique effect of the X variable on the Y variable, it is dependent on the value of temperature.

$$Y = \beta_1 X + \beta_2 XT \tag{5.1}$$

$$\frac{\partial Y}{\partial X} = \beta_1 + \beta_2 T \tag{5.2}$$

The regression models were used to make adjusted predictions of the Y variable using the independent variable at discrete values of temperature. The emission ratios were obtained from the gradient of the linear fit of the

X and Y variables. The calculations were conducted using the **ggeffects** R package[246].

In the linear models used here the interaction term is a single, constant value multiplied by the temperature (Equation 5.2). Therefore only linear relationships can accurately be modelled in this way. Previous studies investigating the temperature dependence of vehicular NO_x emissions suggests that it is close to linear between -13 and +13 ° C[247] and approximately linear between 0 ° C and 25 ° C for light duty diesel vehicles[214]. The measurements in Manchester were made over a temperature range of 0.5-20.6 ° C, therefore a linear approximation is sensible. To avoid using the models in conditions they had not been developed under, where the linear assumption may be violated, predictions were only made for air temperatures within the observational range.

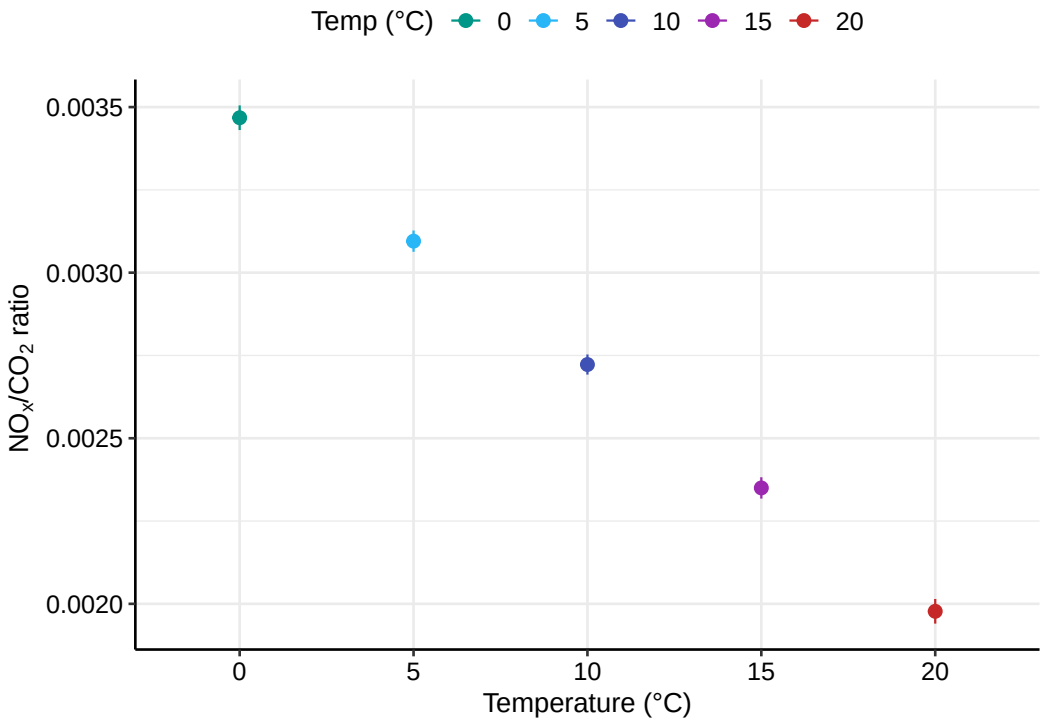

Figure 5.23: Predicted NO_x/CO_2 ratios (ppb/ppb) from mobile measurements in Manchester at temperatures between 0 ° C and 20 ° C.

Figure 5.23 shows the NO_x/CO_2 emission ratio predicted at different temperatures. It shows that the NO_x/CO_2 ratio is strongly dependent on ambient temperature, as the NO_x/CO_2 ratio is 1.8 times higher at 0 ° C compared to 20 ° C. Temperature dependence of NO_x calculated using this approach is consistent with other studies. Grange et al. [214] reported an increase of 1.6-2 at 0 ° C compared to to 20 ° C for light duty diesel passenger vehicles using on-road remote sensing. Gasoline vehicles showed little evidence of temperature dependent NO_x emissions, suggesting the effect is strongly linked to the performance of diesel emission control technologies[214]. Wærsted et al. [247] reported an increase of 2.1 in NO_x emissions over 0 ° C to 20 ° C, which were estimated for a vehicle fleet using ambient measurements in Norway. This compares favourably with a factor of 1.8 which has been derived from mobile measurements over the same temperature range (0 ° C to 20 ° C). While the specific details of the vehicle fleet in both this study and Wærsted et al. [247] are not known, it would be expected that both locations will be strongly influenced by light and heavy duty vehicle diesel NO_x emissions, which dominate European vehicle emissions of NO_x. There are many unknown relevant factors preventing the complete explanation of the observed trends in the mobile data, but it is clear that higher emissions of NO_x occur at lower temperatures, which may have implications regarding winter time exposure from a public health perspective.

Figure 5.24 shows the T/B emission ratio predicted at different temperatures. It shows that the T/B ratio is dependent on temperature and the T/B ratio is 1.2 times higher at 20 ° C compared to 0 ° C. T/B ratios of over 2 can be indicative of evaporative emissions[197]. Schnitzhofer et al. [248] reported a temperature dependence of toluene during long-term measurements carried out at a motorway location in Austria and an increase in the T/B ratio by a factor of 2 over the temperature range of -15 ° C to 20 ° C. The T/B ratio increase reported by Schnitzhofer et al. [248] is larger than the increase of 1.2 derived from mobile measurements. However, the temperature range

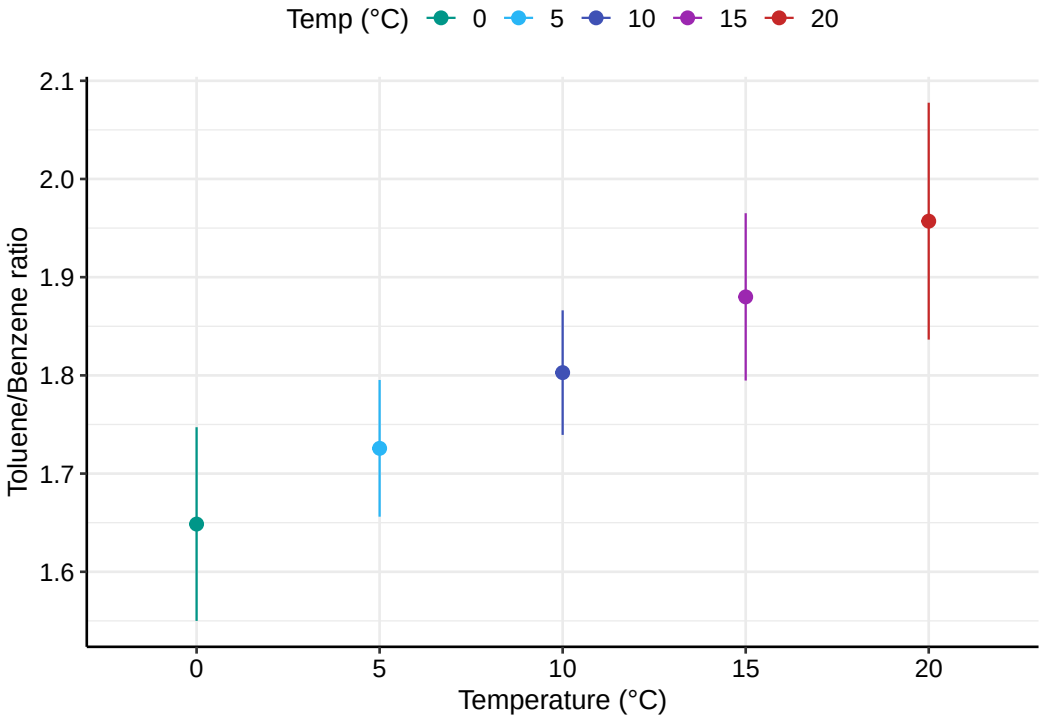

Figure 5.24: Predicted toluene/benzene (T/B) ratios (ppb/ppb) from mobile measurements in Manchester at temperatures between 0 ° C and 20 ° C.

that occurred during mobile measurements is much smaller than the range reported by Schnitzhofer et al. [248], 0 ° C and 20 ° C and -15 ° C and 20 ° C respectively. The increase in the T/B ratio with temperature indicates that toluene has a temperature dependent evaporative source, whereas benzene is dominated by non-temperature dependent vehicular emissions[248].

5.6 Comparison of mobile measurements- Manchester and Milan

The mobile measurements carried out in Manchester and Milan took place in contrasting locations with different emission sources. The measurements in Manchester were carried out in the Trafford Park industrial area, which is an area with a wide variety of industrial premises. Whereas, the measurements

in Milan were carried out in a complex urban environment with a mixture of different emission sources. Furthermore, the two measurement locations are likely to have contrasting vehicle fleets. Milan has a high usage of natural gas fuel vehicles and motorcycles and mopeds, but the Trafford Park area is likely to have a high proportion of goods vehicles and diesel-fuel vehicles, due to the area being dominated by industry. Therefore, the different measurement locations could have distinct compositions and intensities of emissions. The mobile measurements in Milan have been compared to contrasting measurements carried out in Manchester in summer (June-July 2021), the summer measurements were chosen as a comparison as the measurements took place during similar temperature conditions (around 20 ° C). A possible limitation of this comparison is that there may have been varying meteorology in the different measurement locations and that it is likely that Milan had more traffic than Manchester.

Figure 5.25 shows a comparison of the measurements made by the SIFT-MS during repeat mobile sampling in Manchester and Milan. For all of the compounds, the median mixing ratios were higher in Milan, suggesting that there is a higher emissions intensity in Milan. This could be a result of a greater variety of emission sources in Milan, which emit higher amounts of VOCs. It is also likely that there is a higher contribution from vehicles to total emissions, due to much higher mixing ratios of vehicle-related VOCs (benzene, toluene and C_2- and C_3-alkylbenzenes). A higher contribution of vehicular emissions to VOC mixing ratios in Milan is likely a result of a more varied vehicle fleet in Milan, with high usage of natural gas fuel vehicles and motorcycles and mopeds, which were measured to have high VOC/CO_2 ratios.

Figure 5.26 shows a comparison of the measurements made by the ICAD, the UGGA and the O_3 analyser during repeat mobile sampling in Manchester and Milan. For all of the compounds, the median mixing ratios were higher in Milan, which suggests a higher emissions intensity in Milan. CH_4 mixing

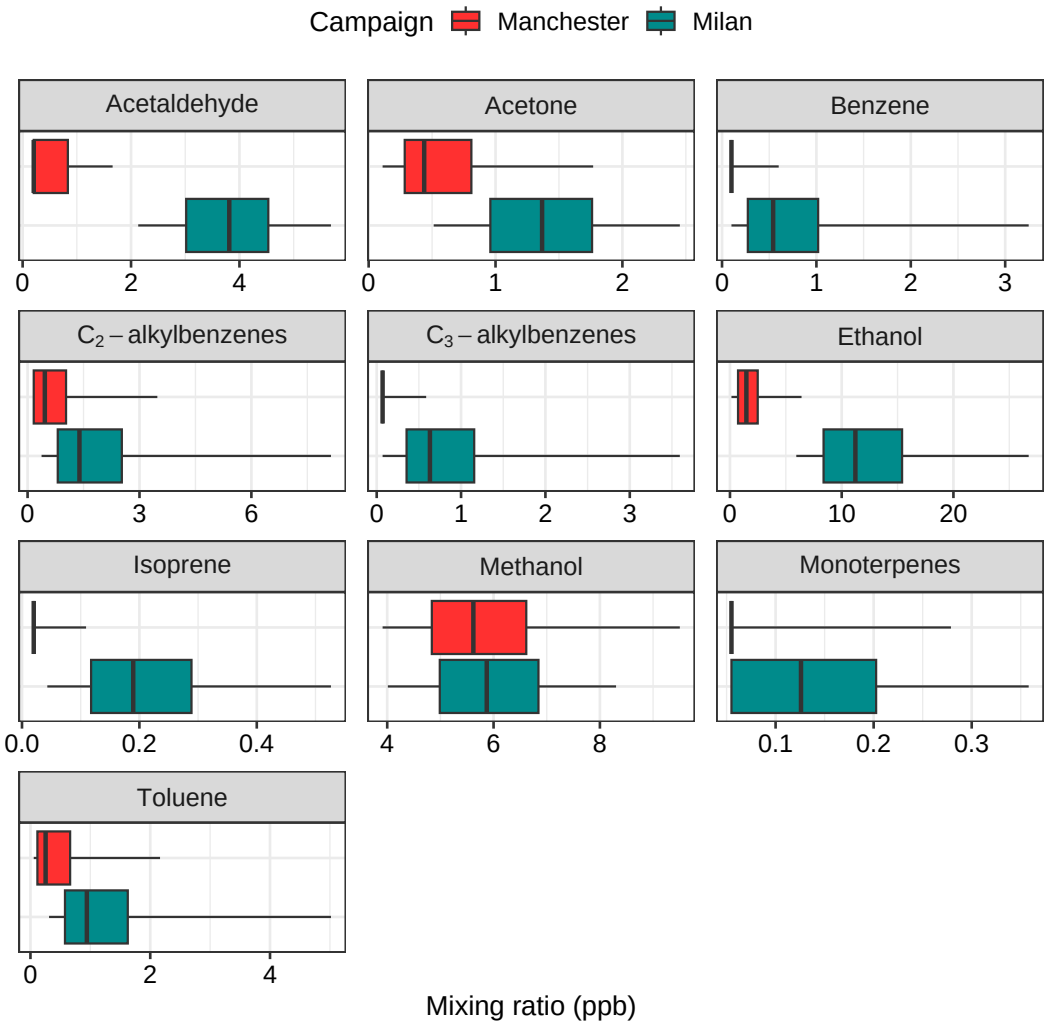

Figure 5.25: Summary of measurements made by the SIFT-MS (in ppb) during mobile measurements carried out in Manchester and Milan. The box outline contains the 25th to the 75th percentile and the middle line shows the median mixing ratio for each compound. The whiskers represent the 5th and 95th percentile for the mixing ratios of each compound.

ratios are significantly higher in Milan than Manchester, which could be a result of high usage of natural gas fuel vehicles in Milan or gas work that was ongoing near the measurement site. CO_2 mixing ratios in Milan are much higher than Manchester, but a smaller difference is seen in NO_x mixing ratios, which could be a result of a higher proportion of high-emitting NO_x

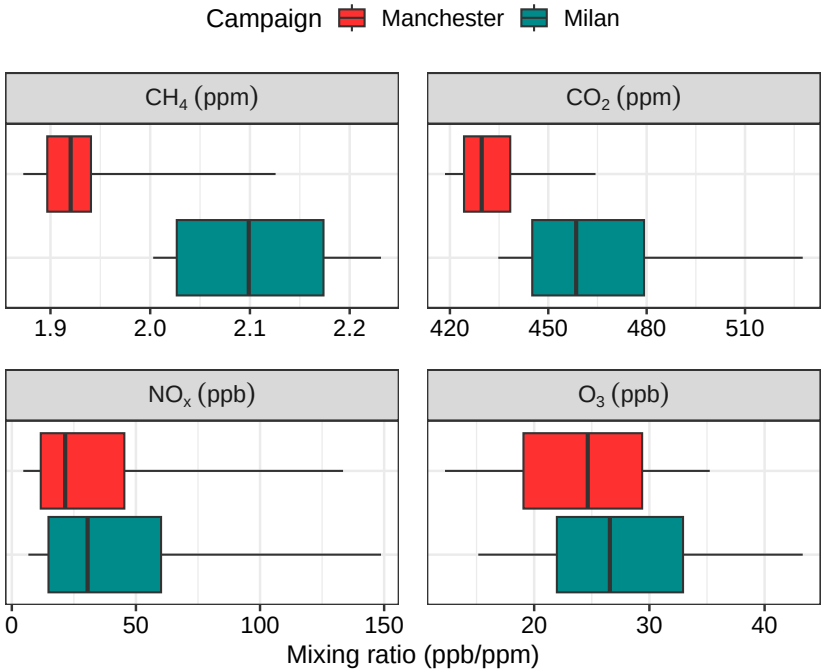

Figure 5.26: Summary of measurements made by the ICAD, the UGGA and the O_3 analyser (in ppb/ppm) during mobile measurements carried out in Manchester and Milan. The box outline contains the 25th to the 75th percentile and the middle line shows the median mixing ratio for each compound. The whiskers represent the 5th and 95th percentile for the mixing ratios of each compound.

diesel vehicles in Manchester. O_3 mixing ratios are higher in Milan, which is likely to a result of higher mixing ratios of VOCs and NO_x in Milan, which play an important role in the formation of O_3.

To investigate further the possible contributions of vehicles to air pollutant emissions, the relationship between NO_x, CO_2 and benzene for Manchester and Milan has been explored and is shown in Figure 5.27. The relationship between NO_x and CO_2 for both of the measurement locations is shown to be similar (Figure 5.27a), with a strong relationship. However, the relationship between NO_x and CO_2 for Milan is much stronger due to a steeper slope and higher CO_2 values, which suggests a higher emissions intensity of

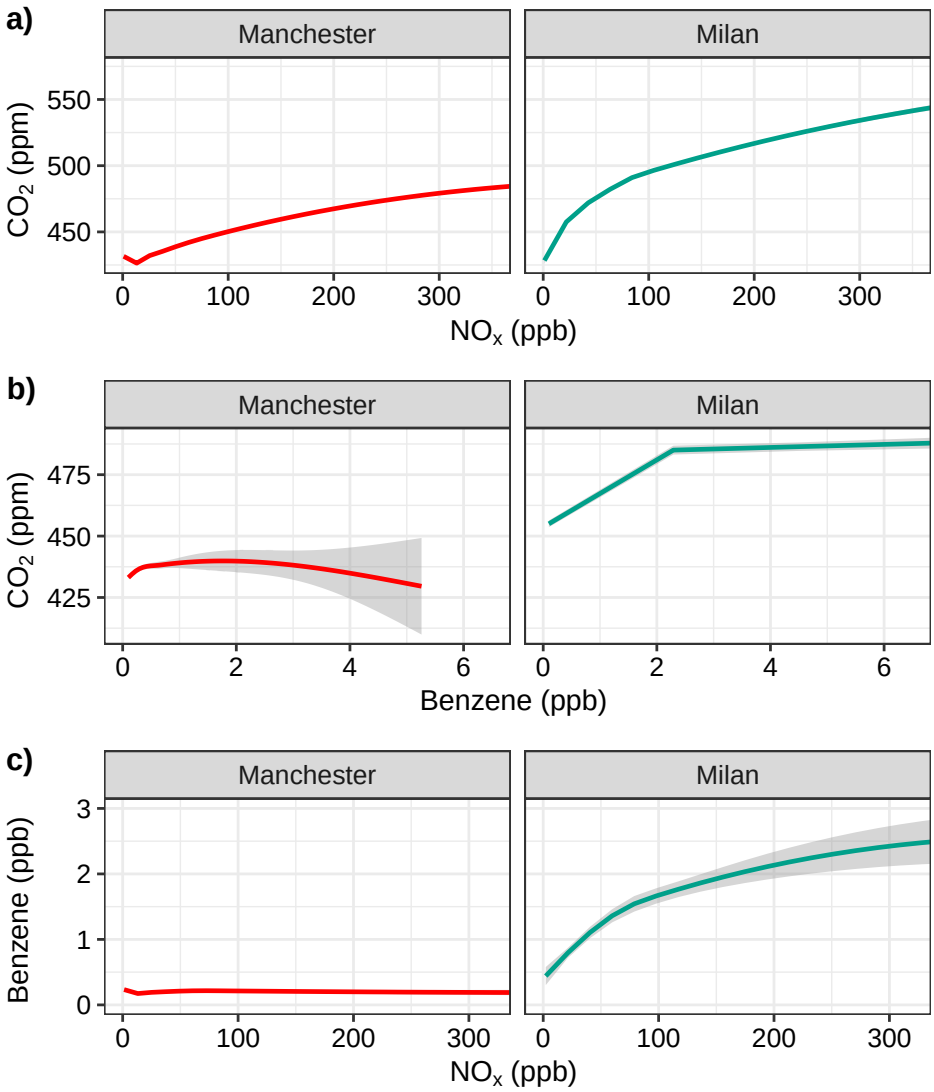

Figure 5.27: A comparison of the relationship predicted by a locally weighted regression between NO_x (ppb), CO_2 (ppm) and benzene (ppb) during mobile measurements in Manchester and Milan. Note that the x-axis has been limited by the 99th percentile to remove the influence from outliers.

NO_x and CO_2 in Milan compared to Manchester. Furthermore, a stronger relationship between NO_x and CO_2 in Milan suggests that the species are co-emitted, likely from combustion emission sources. The relationships between CO_2 and benzene are contrasting for the measurement locations. The relationship between CO_2 and benzene observed in Manchester is weak

and anti-correlated at higher benzene concentrations, whereas for Milan the relationship is positive. Furthermore, much lower concentrations of benzene were present in Manchester than Milan. This is likely a result of the differing vehicle fleets in the two measurement locations, as the vehicle fleet in Milan is composed of a higher proportion of vehicles which emit a higher amount of VOCs, such as motorcycles and mopeds and therefore the benzene measurements are likely to be combustion-related. However, in Manchester the vehicle fleet is likely to be composed of a higher proportion of diesel vehicles, which emit a lower amount of VOCs. Furthermore, in Manchester as benzene increases, CO_2 decreases, which suggests that higher concentration emissions of benzene are not combustion-related and are likely emitted from other sources, such as evaporative emissions. The relationship between benzene and NO_x for the two measurement locations is also contrasting. Measurements from Milan show a positive relationship between NO_x and benzene, whereas in Manchester there seems to be no relationship. As suggested above, this could be due to contrasting vehicle fleets and indicative of a higher proportion of diesel vehicles in Manchester, which emit high amounts of NO_x and low amounts of VOCs.

Overall, the emissions intensity in Milan was observed to be much higher than in Manchester, with higher mixing ratios of all compounds in Milan. This is likely a result of a more varied source type area of Milan, which includes a varied vehicle fleet and a highly complex urban area with many possible emission sources.

5.7 Conclusion

Current understanding of measurements rely on point measurements, typically made at single points. In this work we have shown that it is feasible to carry out fast response mobile measurements in order to obtain useful information about emission sources of air pollutants. New analysis methods

have been used to reveal emission sources of air pollutants in urban areas. The distance-weighted approach has been used to calculate mean mixing ratios and ratios between pollutants, which can then be spatially mapped to reveal persistent emissions and hotspot features. This approach was used to identify evaporative emissions in York and different emission source type areas in Milan.

Combustion dilution events were extracted from the mobile measurements carried out in Milan and the results compared to results from point sampling results. This allowed for the determination of the spatial representativity of point measurements, which can be used to determine the importance of vehicle emissions in an urban area.

The temperature dependence of air pollutant emissions was investigated through analysis of mobile measurements carried out during different seasons in Manchester. The influence of ambient temperature on emission ratios was studied and a strong, but opposite, temperature dependence of NO_x and toluene was reported, which agrees well with other studies. This approach could be applied with the distance-weighted regression approach to assess the temperature dependence of emissions across a road network and provide useful information on spatial emission sources.

Overall, the use of mobile measurements can be used to provide information on the spatial distribution of air pollutants, which would be impossible to obtain from current air quality monitoring networks in urban areas. This information can be used to determine the importance of emission source types in urban areas, which is useful for combating air quality issues. Mobile measurements can also be used to extract combustion dilution events from vehicle plumes, which allows for the quantification of vehicle emissions in an urban area.

Chapter 6

Summary and conclusions

Poor air quality is the leading environmental threat to human health, being responsible for 6.7 million premature deaths worldwide. Important air pollutants from a health and environmental perspective are ozone (O_3) and fine particulate matter ($PM_{2.5}$), which are both dominated by secondary formation. Nitrogen oxides (NO_x) and volatile organic compounds (VOCs) play an important role in the secondary atmospheric formation of O_3 and PM. VOC emission sources are highly complex and it is difficult to determine important sources from current stationary measurements. Furthermore, vehicles may represent an important VOC source, but there are a limited number of studies that determine VOC emissions from individual vehicles. Therefore, new measurement methods have been developed to investigate and develop the understanding of emissions of NO_x and VOCs, including mobile measurements and vehicle point sampling.

This thesis shows the development of a mobile laboratory for high temporal and spatial measurements of a variety of air pollutants. Also shown is the application of the mobile laboratory to mobile measurements and vehicle point sampling techniques in order to obtain useful information relating to air pollutant emission sources. There is a strong focus on VOC emissions due to limited knowledge on their emission sources, particularly in complex

urban areas. Furthermore, there is also a focus on vehicular VOC emissions in real world driving conditions in order to increase the understanding of VOC emissions from road vehicles.

Chapter 2 considered the installation and application of a selected-ion flow-tube mass spectrometer (SIFT-MS) into a mobile laboratory for high temporal and spatial VOC measurements. To our knowledge, a SIFT-MS instrument had not been used for mobile measurements before, therefore much of the work involved ensuring that the SIFT-MS was suitable for these types of measurements. An important advantage of the SIFT-MS instrument used in this work is that provides easy to use software and does not require considerable experience compared to other mass spectrometry instruments, therefore enabling a variety of users. Furthermore, the SIFT-MS can be used with the careful selection of target VOC compounds to ensure that emission sources are investigated at an appropriate time resolution.

Chapter 3 presents the development of new analysis methods to be applied to vehicle point sampling and mobile measurement data. The vehicle point sampling analysis method presents a data processing method to overcome any possible challenges by ensuring the time alignment of pollutants, identification of a combustion plume and then the calculation of emission ratios. Air pollutants are aligned to give the best correlation to CO_2 in order to remove possible effects from differing instrument response times or meteorological conditions. Combustion-related vehicle emissions were extracted through the use of a CO_2 filter, allowing for vehicular emissions to be extracted from a complex urban background. Furthermore, this allows for emission ratios to be calculated without the need for background determination.

The mobile measurement analysis method uses regression-based approaches to ensure that a variety of emissions can be extracted from spatial measurements. A novel aspect of the approach is the adoption of a distance-weighting to determine the spatial variation of air pollutants and avoids

arbitrarily splitting up of the road network, ensuring that important emissions information is not missed. Furthermore, a rolling regression method to extract combustion-related emissions from a complex urban environment is also developed as a new way in which complex, mobile measurements can be analysed. The rolling regression approach enables vehicular emissions to be quantified spatially. Finally, different regression based approaches were evaluated and the importance of including measurement errors in regression calculations (e.g. for emission ratios) considered.

Chapter 4 presents the results from the point sampling measurement campaign in Milan. Measurements of vehicular emissions can be affected by a multitude of vehicular characteristics, including vehicle type, fuel type, emission reduction technologies and driving conditions, and also by other external factors including meteorological conditions. Furthermore, the nature of vehicular emissions itself can be problematic as the emission source of interest is moving in space and time. Therefore, the aim of the chapter was to determine whether it is feasible to measure NO_x and VOCs from individual vehicles, using the point sampling measurement technique, in order to develop the understanding of VOC emissions from vehicles. Furthermore, another aim was to determine any differences in emissions behaviour as a result of different vehicle and fuel types, which is helpful for development of air quality policies. A key development for this chapter was the measurement of individual VOCs from individual vehicles under real driving conditions. This approach is analogous to vehicle emission remote sensing, but extends remote sensing capabilities to allow speciated exhaust plume composition measurements to be made. Using the analysis methods detailed in Chapter 3 to determine emission ratios, motorcycles and mopeds were highlighted as possible significant sources of VOCs and NO_x, compared to other vehicle types. In typical low emission zones, high-emitting NO_x diesel vehicles are heavily targeted and the regulations of motorcycles and mopeds in the same area are less stringent. Therefore, motorcycles and

mopeds could play an important role in air quality in urban areas if they are not as strongly regulated and could become particularly important for O_3 formation, if NO_x is reduced but VOCs are kept relatively constant.

Chapter 5 presents the results from mobile measurement campaigns carried out in York, Milan and Manchester. The aim of the chapter was to examine whether it was feasible to obtain useful information about a variety of emission sources using fast response measurements. Persistent sources and emissions have been revealed by spatial mapping using the distance weighted regression approach, which is useful to determine exposure to air pollutants. The experimental design of multiple repeats of the same circuit ensures that emission features revealed through spatial mapping are persistent and not transient in nature. Mobile measurements can be further analysed to calculate spatial emission ratios, which can indicate emission intensities on a spatial scale. Combustion-related emission ratios were calculated from mobile measurements in Milan and compared to corresponding results from vehicle point sampling, in order to examine the spatial representativity of point measurements and to quantify the effect of vehicle emissions spatially.

Overall, both of the measurement techniques in Milan agreed well, with the mobile-calculated emission ratios slightly higher than point sampling-calculated emission ratios, likely due to increased variation in vehicular operating conditions during mobile measurements. The point sampling measurement technique has an associated practical constraint as the measurement site has to be suitable. Mobile measurements overcome this constraint and measurements can be carried out on any suitable road, but there is an added spatial complexity to mobile measurements. However, the analysis methods developed in Chapter 3 deal with this spatial complexity to ensure that useful emissions information can still be extracted from mobile measurements.

Finally, in a new application of mobile measurements, the ambient temperature dependence of air pollutants was considered through emis-

sion ratios predicted at different temperatures, using measurements from Manchester during two contrasting seasons (summer and winter). This work shows the potential of a dedicated campaign which could cover a range of temperature conditions to further develop temperature dependence emissions of VOCs, for which there is a lack of information. An advantage of mobile measurements is the amount of data that can be obtained in a relatively short time frame. The high temporal and spatial resolution nature of mobile measurements results in a large amount of information that would take a long time to gather with a fixed site. For example, the same amount of information obtained from hours of mobile measurements could take years if a fixed monitoring site was used.

Overall, the point sampling and mobile analysis and measurement approaches represent useful techniques which were used to generate new and important insights surrounding air pollutant emission sources, with a particular emphasis on road vehicle emissions. Furthermore, both approaches are able to provide information that cannot be obtained from stationary sites and the mobile measurement approach is particularly useful for quantifying emission sources spatially. Both techniques can be expanded to quantify a wide range of air pollutants and emission sources, which is particularly important as it is likely that air pollutant emissions will undergo large changes over the coming decades.

This thesis presents emission ratios of VOCs from individual vehicles, which were extracted using the point sampling measurement method. Also presented is the use of mobile measurements to extract a variety of information surrounding emission sources of VOCs and NO_x in urban areas.

6.1 Future directions

It is important that the emission sources of PM and O_3 precursors, including NO_x and VOCs, are fully understood if related health and environmental

issues are to be solved. This thesis presents new measurement and analysis approaches to develop the understanding surrounding NO_x and VOC emission sources, with a particular focus on vehicular emissions. The work presented in this thesis could be extended in a number of ways and future directions of the work will be discussed below.

Chapter 4 focuses on emission ratios calculated for fairly broad vehicle characteristic groups, including vehicle type, fuel type and euro class. Some of the vehicle characteristic groups consist of a limited number of observations and therefore the emission ratios associated with these groups could be biased. To overcome this possible limitation of the work, a longer measurement campaign could be carried out to enable measurements of an increased number of vehicles. This would enable vehicle characteristic groups to be investigated even further, such as further investigating the effects of euro classes or manufacturers. Vehicle point sampling could also be carried out in different locations, so that a variety of vehicle fleets and driving conditions were sampled.

The measurement location for point sampling has to be carefully selected and possible locations are limited. There has to be a compromise in the traffic flow in order for there to be enough vehicles to obtain a large enough sample fleet, but not too busy so that individual vehicle plumes are not distinguishable. However, the analysis method presented in Chapter 3 showed that accounting for distinguishable plumes does not affect overall grouped ratios by a significant amount. Furthermore, point sampling could be used to quantify other non-exhaust related vehicular emissions. In the coming decades, combustion-related emissions are likely to become less important through the electrification of the vehicle fleet. Therefore, point sampling could be used to quantify evaporative emissions from vehicles or particulate emissions from tyre and brake wear, all that is required is a fast response measurement and an understanding of tracer species for a particular emission source.

The work presented in Chapter 5 highlights the limited knowledge of the emission sources in urban areas and despite thorough analysis, it is still difficult in some areas to say exactly where or what a particular emission source is. For example, it is difficult to determine where emissions are from in the highly complex area of Milan compared to Hull Road in York, where emissions are highly likely to result from a fuel station. Therefore, a future direction of this work would be to update emission inventories and have more detailed emissions information for a variety of sources on an urban/city-scale level. This would make investigating emission sources much easier and would help to make emission inventories more accurate. Also presented is the comparison of combustion- and vehicle-related emissions from mobile measurements and point sampling. A development to this work would be to link the emission ratios from mobile measurements to vehicle-specific data. This could include linking mobile measurements to individual vehicles, using a camera to obtain number plate information, or to traffic data, which could indicate areas with higher traffic volumes. Linking the mobile measurements to vehicle specific data would help to develop the application of mobile measurements to investigate vehicle emissions.

Future directions for both point sampling and mobile measurements would be the development of emission ratios into emission factors. For point sampling this would involve the calculation of distance-based emission factors. Therefore, emission factors could be compared to current inventory estimates, which are typically based on old measurements and are limited. It is important that emission inventories are well-quantified and reflect real-world emissions as accurately as possible as they are used for air quality modelling and predictions, which are used to develop air pollution reduction strategies. Both point sampling and mobile measurement techniques could be expanded to a broad range of air pollutants as long as a suitable measurement instrument with a sufficient time resolution is available. This would be useful to target ever-changing air pollutants of interest as emission

reduction policies and technologies are successful. For example, an air pollutant of interest in the future could be NH_3 as emerging evidence suggests that vehicular emissions could be an important source of NH_3 in urban areas.

6.2 Final remarks

It is still difficult to determine the emission sources of air pollutants, particularly VOCs, in urban areas when relying only on limited stationary measurements and laboratory measurements that do not reflect real-world conditions. It is likely that over the coming decades emission sources will go through a vast amount of change due to policies which aim to combat climate change and improve air quality. The effect of such policies is already being observed with the electrification of vehicle fleets and decreasing fossil fuel burning, particularly in developed countries. However, the point sampling and mobile measurement approaches described in this thesis are well suited to provide important emissions information on a variety of air pollutants and their sources in order to increase the understanding surrounding new atmospheric problems that may arise in the future.

Appendix A

Supporting Information for Chapter 2

The purpose of this appendix is to provide further details about the SIFT-MS measurements, including the uncertainty calculation and quantification of the product ions.

A.1 Syft standard details

A.2 Calculation of SIFT-MS uncertainties

Uncertainties for the calibrated SIFT-MS measurements were calculated using the following (taken from Reimann et al. [192]):

$$u\chi^2_{sample} = u\chi^2_{prec} + u\chi^2_{sampling} \tag{A.1}$$

$$u\chi^2_{prec} = (\chi_{sample} * \sigma RSD)^2 + (\frac{\chi_D}{3})^2 \tag{A.2}$$

$$u\chi_{cal} = (RSE\ of\ slope)^2 + (u_{gas})^2 + (u_{blender})^2 \tag{A.3}$$

Species	**MM**
Ethylene	28
Isobutane	58
Benzene	78
Toluene	92
Ethylbenzene	106
Tetrafluorobenzene	150
Hexafluorobenzene	186
Octafluorotoluene	236

Table A.1: Compounds and their molecular masses (MM, g mol^{-1}) in the Syft 2ppm standard gas, which was used to generate the daily instrument calibration factor (ICF).

where

- $u\chi_{prec}$ is the error associated with the measurement
- $u\chi_{cal}$ is the error associated with the calibration
- chi_{sample} is the error associated with the concentration
- σRSD is the relative standard deviation of at least 6 calibrations
- χ_D is the limit of detection
- RSE is the relative standard error of the calibration slope
- u_{gas} is the uncertainty of the gas standard = 5%
- $u_{blender}$ is the uncertainty of the gas blender = 1%

Uncertainties for SIFT-MS measurement compounds that are not calibrated for are determined by the systematic errors, which total ±35%. Equation 2.1 can be expanded to give the following equation:

$$[A] = \frac{[P^+]\, ICF_i + \sum\limits_{all\ ki} ([P_{ki}]\, ICF_{ki})}{t_r\ br_i \sum\limits_{all\ j} (k_j\, [R_j^+]\, ICF_j)} \tag{A.4}$$

where

- k has an error of ±15%
- ICF has an error of ±10%
- b_r has an error of ±10%

A.3 Further SIFT-MS details

Details on the product ion masses targeted by the SIFT-MS are shown in Table A.2, including branching ratio, rate constant and the molecular formula. The branching ratio is the relative abundance of a product ion formed from the reaction of a certain reagent ion with the target compound. The rate constant (k) is the rate of the reaction between the reagent ion and the target compound. The product formula is the molecular formula of the product ion formed through the reaction of the reagent ion and the target compound.

Species	**Ratio**	**k**	**Formula**
Acetaldehyde (NO^+)	1	6.0×10^{-10}	CH_3CO^+
Acetaldehyde (H_3O^+)	1	3.7×10^{-9}	$C_2H_5O^+$
Acetone	1	1.2×10^{-9}	$NO^+.C_3H_6O$
Benzene	0.76	1.75×10^{-9}	$C_6H_6{}^+$
1,3-Butadiene (NO^+)	1	1.2×10^{-9}	$C_4H_6{}^+$
1,3-Butadiene (H_3O^+)	1	1.4×10^{-9}	$C_4H_7{}^+$
C_2-alkyl benzenes	1	1.9×10^{-9}	$C_8H_{10}{}^+$
C_2-C_4-alkanes	0.25	1.0×10^{-12}	$C_2H_4{}^+$
C_3-alkyl benzenes	1	1.9×10^{-9}	$C_9H_{12}{}^+$
Ethanol (NO^+)	1	1.2×10^{-9}	$C_2H_5O^+$
Ethanol (H_3O^+)	1	2.7×10^{-9}	$C_2H_7O^+$
Isoprene	1	1.7×10^{-9}	$C_5H_8{}^+$
Methanol (H_3O^+)	1	2.7×10^{-9}	CH_5O^+
Monoterpenes	0.88	2.2×10^{-9}	$C_{10}H_{16}{}^+$
NO_2	1	6.2×10^{-10}	$NO_2{}^+$
Toluene	1	1.7×10^{-9}	$C_7H_8{}^+$

Table A.2: The branching ratio, rate constant (k) and product formula for the product ion masses the SIFT-MS was targeting during measurements.

Appendix B

Supporting Information for Chapter 4

The purpose of this appendix is to provide further details for Chapter 4, including the location of the EDAR sampling sites and European emission standards.

Figure B.1: Map of the EDAR remote sensing sampling sites- Via Madre Cabrini and Via Francesco Cilea (© Google). Visualised by the *ggmap* R package [3].

		Distance-Specific Emission (g/km)				
Stage	**Date**	**CO**	**HC+NO_x**	**HC**	**NO_x**	**PM**
Petrol						
Euro 1	07/1992	2.72	0.97	—	—	—
Euro 2	01/1996	2.20	0.50	—	—	—
Euro 3	01/2000	2.30	—	0.20	0.15	–
Euro 4	01/2005	1.00	—	0.10	0.08	—
Euro 5	09/2009	1.00	—	0.10	0.06	0.005
Euro 6	09/2014	1.00	—	0.10	0.06	0.005
Diesel						
Euro 1	07/1992	2.72	0.97	—	—	0.14
Euro 2	01/1996	1.00	0.70	—	—	0.08
Euro 3	01/2000	0.64	0.56	—	0.50	0.05
Euro 4	01/2005	0.50	0.30	—	0.25	0.025
Euro 5	09/2009	0.50	0.23	—	0.18	0.0045
Euro 6	09/2014	0.50	0.17	—	0.08	0.0045

Table B.1: European emission standards for passenger cars.

		Distance-Specific Emission (g/km)			
Stage	**Date**	**CO**	**HC**	**NO_x**	**PM**
Euro 1	1999	13.0	3.0	0.3	—
Euro 2	2003	5.5	1.0	0.3	—
Euro 3	2006	2.0	0.3	0.15	—
Euro 4	2016	1.14	0.17	0.09	—
Euro 5	2020	1.00	0.10	0.06	0.0045

Table B.2: European emission standards for motorcycles and mopeds.

Appendix C

Supporting Information for Chapter 5

The purpose of this chapter is to provide further details for Chapter 5, including some further figures comparing point sampling and mobile emission ratios.

Figure C.1 and Figure C.2 shows the average emission ratios of NO_x and VOCs extracted from point sampling and mobile measurements. The top two figures show the average ratios calculated for different vehicle types and fuel types from point sampling measurements and the bottom figure shows the ratios extracted using rolling regression performed on mobile measurements. Both figures show a good agreement between the point sampling and mobile calculated emission ratios for both NO_x and VOCs with the mobile ratios being on the magnitude and within error divergence of the point sampling ratios.

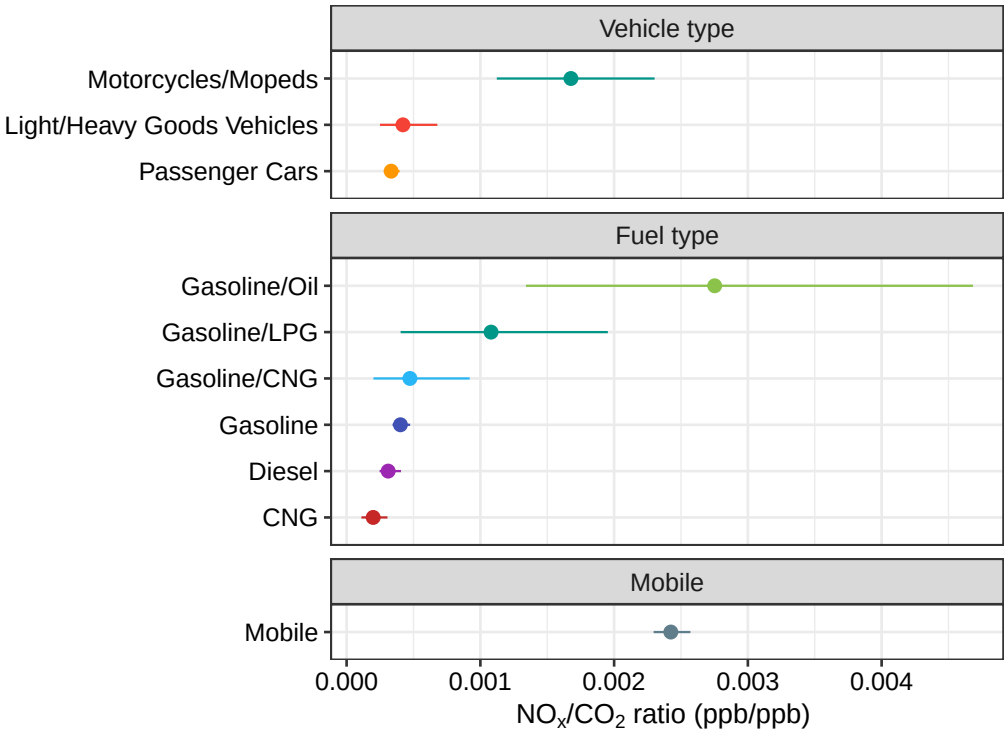

Figure C.1: Average NO_x/CO_2 ratios (ppb/ppb) calculated from point sampling and mobile measurements. The error bars represent the 95% confidence interval calculated for each mean value.

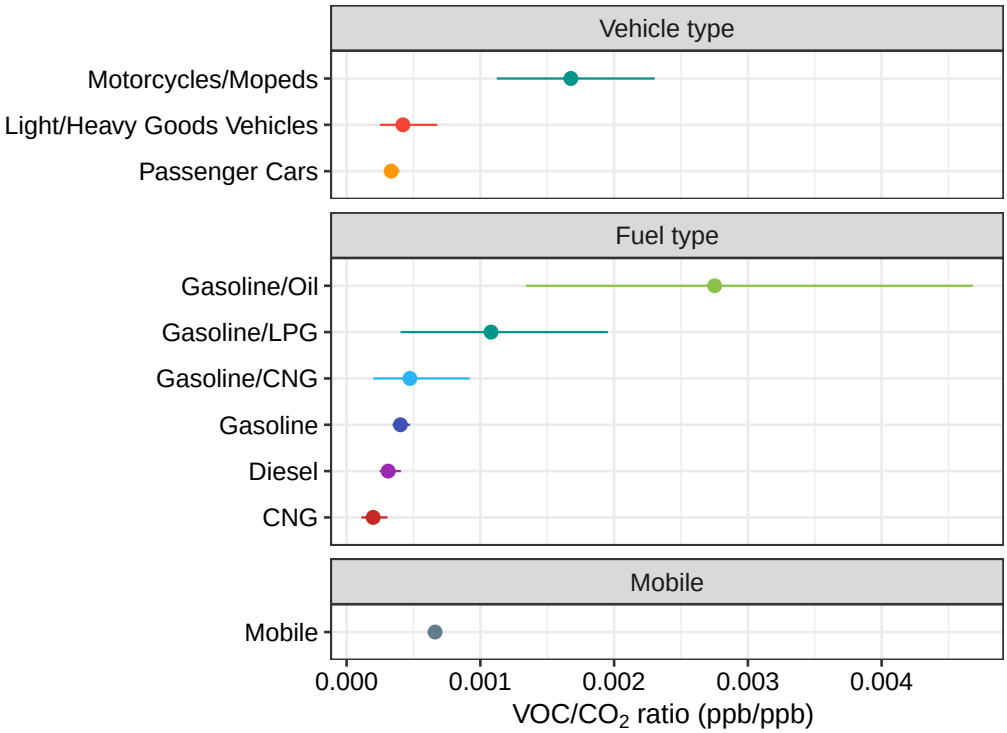

Figure C.2: Average VOC/CO_2 ratios (ppb/ppb) calculated from point sampling and mobile measurements. The error bars represent the 95% confidence interval calculated for each mean value

Bibliography

[1] Monks, P. S. Gas-phase radical chemistry in the troposphere. *Chemical Society Reviews* 34.5 (2005), pp. 376–395. URL: https://doi.org/10.1039/B307982C.

[2] Wu, C. and Zhen Yu, J. Evaluation of linear regression techniques for atmospheric applications: the importance of appropriate weighting. *Atmos. Meas. Tech* 11 (2018), pp. 1233–1250. URL: https://doi.org/10.5194/amt-11-1233-2018.

[3] Kahle, D. and Wickham, H. ggmap: Spatial Visualization with ggplot2. *The R Journal* 5.1 (2013), pp. 144–161. URL: https://journal.r-project.org/archive/2013-1/kahle-wickham.pdf.

[4] Carslaw, D. C. and Rhys-Tyler, G. New insights from comprehensive on-road measurements of NOx, NO2 and NH3 from vehicle emission remote sensing in London, UK. *Atmospheric Environment* 81 (2013), pp. 339–347. URL: https://doi.org/10.1016/j.atmosenv.2013.09.026.

[5] Ammoura, L., Xueref-Remy, I., Gros, V., Baudic, A., Bonsang, B., Petit, J.-E., Perrussel, O., Bonnaire, N., Sciare, J. and Chevallier, F. Atmospheric measurements of ratios between CO 2 and co-emitted species from traffic: a tunnel study in the Paris megacity. *Atmos. Chem. Phys* 14 (2014), pp. 12871–12882. URL: https://doi.org/10.5194/acp-14-12871-2014.

[6] Abbafati, C. et al. Global burden of 369 diseases and injuries in 204 countries and territories, 1990–2019: a systematic analysis for the Global Burden of Disease Study 2019. *The Lancet* 396.10258 (2020), pp. 1204–1222. URL: https://doi.org/10.1016/S0140-6736(20)30925-9.

[7] Health Effects Institute. State of Global Air 2020. Special Report (2020), pp. 1–28. URL: https://www.stateofglobalair.org/.

[8] Klepac, P., Locatelli, I., Korošec, S., Künzli, N. and Kukec, A. Ambient air pollution and pregnancy outcomes: A comprehensive review and identification of environmental public health challenges. *Environmental Research* 167 (2018), pp. 144–159. URL: https://doi.org/10.1016/j.envres.2018.07.008.

[9] Chen, H., Kwong, J. C., Copes, R., Hystad, P., Donkelaar, A. van, Tu, K., Brook, J. R., Goldberg, M. S., Martin, R. V., Murray, B. J., Wilton, A. S., Kopp, A. and Burnett, R. T. Exposure to ambient air pollution and the incidence of dementia: A population-based cohort study. *Environment International* 108 (2017), pp. 271–277. URL: https://doi.org/10.1016/j.envint.2017.08.020.

[10] World Bank. The Global Health Cost of PM2.5 Air Pollution: A Case for Action Beyond 2021. *International Development in Focus* (2022). URL: https://doi.org/10.1596/978-1-4648-1816-5.

[11] HEI Panel on the Health Effects of Long-Term Exposure to Traffic-Related Air Pollution. Systematic Review and Meta-analysis of Selected Health Effects of Long-Term Exposure to Traffic-Related Air Pollution. Special Report 23 (2022). URL: https://www.healtheffects.org/publications.

[12] Barnes, J. H., Chatterton, T. J. and Longhurst, J. W. Emissions vs exposure: Increasing injustice from road traffic-related air pollution in the United Kingdom. *Transportation Research Part D: Transport and Environment* 73 (2019), pp. 56–66. URL: https://doi.org/10.1016/j.trd.2019.05.012.

[13] Pénard-Morand, C. and Annesi-Maesano, I. Air pollution: from sources of emissions to health effects. *Breathe* 1.2 (2004), pp. 108–119. URL: https://breathe.ersjournals.com/content/1/2/108.

[14] Ashfaq, A. and Sharma, P. Environmental effects of air pollution and application of engineered methods to combat the problem. *Journal of Industrial Pollution Control* 29.1 (2012). URL: https://www.icontrolpollution.com/articles/environmental-effects-of-air-pollution-and-application-of-engineered-methods-to-combat-the-problem-.php?aid=45739%20.

[15] Shindell, D., Bréon, F.-m., Collins, W., Fuglestvedt, J., Huang, J., Koch, D., Lamarque, J.-f., Lee, D., Mendoza, B., Nakajima, T., Robock, A., Stephens, G., Takemura, T., Zhang, H., Qin, D., Plattner, G.-k., Tignor, M., Allen, S., Boschung, J., Nauels, A., Xia, Y., Bex, V. and Midgley, P. Anthropogenic and Natural Radiative Forcing. In: Climate Change 2013: The Physical Science Basis. Contribution of Working Group I. Cambridge University Press, 2013.

[16] Shuai, J., Kim, S., Ryu, H., Park, J., Lee, C. K., Kim, G. B., Ultra, V. U. and Yang, W. Health risk assessment of volatile organic compounds exposure near Daegu dyeing industrial complex in South Korea. *BMC Public Health* 18.1 (2018), p. 528. URL: https://doi.org/10.1186/s12889-018-5454-1.

[17] Kampa, M. and Castanas, E. Human health effects of air pollution. *Environmental Pollution* 151.2 (2008), pp. 362–367. URL: https://doi.org/10.1016/j.envpol.2007.06.012.

[18] Liu, N., Bu, Z., Liu, W., Kan, H., Zhao, Z., Deng, F., Huang, C., Zhao, B., Zeng, X., Sun, Y., Qian, H., Mo, J., Sun, C., Guo, J., Zheng, X., Weschler, L. B. and Zhang, Y. Health effects of exposure to indoor volatile organic compounds from 1980 to 2017: A systematic review and meta-analysis. *Indoor Air* 32.5 (2022), e13038. URL: https://doi.org/10.1111/ina.13038.

[19] Zhang, J. J., Wei, Y. and Fang, Z. Ozone pollution: A major health hazard worldwide. *Frontiers in Immunology* (2019), p. 2518. URL: https://doi.org/10.3389/fimmu.2019.02518.

[20] Kourtchev, I., Giorio, C., Manninen, A., Wilson, E., Mahon, B., Aalto, J., Kajos, M., Venables, D., Ruuskanen, T., Levula, J., Loponen, M., Connors, S., Harris, N., Zhao, D., Kiendler-Scharr, A., Mentel, T., Rudich, Y., Hallquist, M., Doussin, J. F., Maenhaut, W., Bäck, J., Petäjä, T., Wenger, J., Kulmala, M. and Kalberer, M. Enhanced volatile organic compounds emissions and organic aerosol mass increase the oligomer content of atmospheric aerosols. *Scientific Reports* 6.1 (2016), pp. 1–9. URL: https://doi.org/10.1038/srep35038.

[21] Zhang, R., Wang, G., Guo, S., Zamora, M. L., Ying, Q., Lin, Y., Wang, W., Hu, M. and Wang, Y. Formation of Urban Fine Particulate Matter. *Chemical Reviews*

115.10 (2015), pp. 3803–3855. URL: https://doi.org/10.1021/acs.chemrev.5b00067.

[22] Wu, K., Yang, X., Chen, D., Gu, S., Lu, Y., Jiang, Q., Wang, K., Ou, Y., Qian, Y., Shao, P. and Lu, S. Estimation of biogenic VOC emissions and their corresponding impact on ozone and secondary organic aerosol formation in China. *Atmospheric Research* 231 (2020), p. 104656. URL: https://doi.org/10.1016/j.atmosres.2019.104656.

[23] *Pollutant information: Non methane VOC - NAEI, UK*. URL: https://naei.beis.gov.uk/overview/pollutants?pollutant_id=9.

[24] McDonald, B. C., De Gouw, J. A., Gilman, J. B., Jathar, S. H., Akherati, A., Cappa, C. D., Jimenez, J. L., Lee-Taylor, J., Hayes, P. L., McKeen, S. A., Cui, Y. Y., Kim, S. W., Gentner, D. R., Isaacman-VanWertz, G., Goldstein, A. H., Harley, R. A., Frost, G. J., Roberts, J. M., Ryerson, T. B. and Trainer, M. Volatile chemical products emerging as largest petrochemical source of urban organic emissions. *Science* 359.6377 (2018), pp. 760–764. URL: https://doi.org/10.1126/science.aaq0524.

[25] Pennington, E. A., Seltzer, K. M., Murphy, B. N., Qin, M., Seinfeld, J. H. and Pye, H. O. Modeling secondary organic aerosol formation from volatile chemical products. *Atmospheric Chemistry and Physics* 21.24 (2021), pp. 18247–18261. URL: https://doi.org/10.5194/acp-21-18247-2021.

[26] Lewis, A. C., Hopkins, J. R., Carslaw, D. C., Hamilton, J. F., Nelson, B. S., Stewart, G., Dernie, J., Passant, N. and Murrells, T. An increasing role for solvent emissions and implications for future measurements of volatile organic compounds: Solvent emissions of VOCs. *Philosophical Transactions of the Royal Society A: Mathematical, Physical and Engineering Sciences* 378.2183 (2020). URL: https://doi.org/10.1098/rsta.2019.0328.

[27] National Atmospheric Emissions Inventory (NAEI UK). *NAEI Data*. URL: https://naei.beis.gov.uk/data/.

[28] Manisalidis, I., Stavropoulou, E., Stavropoulos, A. and Bezirtzoglou, E. Environmental and Health Impacts of Air Pollution: A Review. *Frontiers in Public Health* 8 (2020), p. 14. URL: https://doi.org/10.3389/fpubh.2020.00014.

[29] Singh, A. and Agrawal, M. Acid rain and its ecological consequences. *Journal of Environmental Biology* (2008).

[30] Finlayson-Pitts, B. J. and Pitts, J. N. Atmospheric chemistry of tropospheric ozone formation: Scientific and regulatory implications. *Air and Waste* 43.8 (1993), pp. 1091–1100. URL: https://doi.org/10.1080/1073161X.1993.10467187.

[31] Thunis, P., Clappier, A., Beekmann, M., Putaud, J. P., Cuvelier, C., Madrazo, J. and De Meij, A. Non-linear response of PM2.5 to changes in NOx and NH3 emissions in the Po basin (Italy): Consequences for air quality plans. *Atmospheric Chemistry and Physics* 21.12 (2021), pp. 9309–9327. URL: https://doi.org/10.5194/acp-21-9309-2021.

[32] Delmas, R., Serça, D. and Jambert, C. Global inventory of NOx sources. *Nutrient Cycling in Agroecosystems* 48.1-2 (1997), pp. 51–60. URL: https://doi.org/10.1023/A:1009793806086.

[33] *Pollutant information: Nitrogen Oxides - NAEI, UK*. URL: https://naei.beis.gov.uk/overview/pollutants?pollutant_id=6.

[34] Nuvolone, D., Petri, D. and Voller, F. The effects of ozone on human health. *Environmental Science and Pollution Research* 25.9 (2018), pp. 8074–8088. URL: https://doi.org/10.1007/s11356-017-9239-3.

[35] Grulke, N. E. and Heath, R. L. Ozone effects on plants in natural ecosystems. *Plant Biology* 22.S1 (2020), pp. 12–37. URL: https://doi.org/10.1111/plb.12971.

[36] McDuffie, E., Martin, R., Yin, H. and Brauer, M. Global Burden of Disease from Major Air Pollution Sources (GBD MAPS): A Global Approach. Research Report 210. Boston, MA: Health Effects Institute, 2021. URL: https://www.healthdata.org/sites/default/files/files/policy_report/2021/PolicyReport_GBD-MAPS_Research-Report-210_2021.pdf.

[37] Feng, S., Gao, D., Liao, F., Zhou, F. and Wang, X. The health effects of ambient PM2.5 and potential mechanisms. *Ecotoxicology and Environmental Safety* 128 (2016), pp. 67–74. URL: https://doi.org/10.1016/j.ecoenv.2016.01.030.

[38] Peters, A. Ambient air pollution and Alzheimer's disease: the role of the composition of fine particles. *Proceedings of the National Academy of Sciences* 120.3 (2023), e2220028120. URL: https://doi.org/10.1073/pnas.2220028120.

[39] Harrison, R. M. Airborne particulate matter. *Philosophical Transactions of the Royal Society A* 378.20190319 (2020). URL: https://doi.org/10.1098/rsta.2019.0319.

[40] Harrison, R. M. and Beddows, D. C. Efficacy of Recent Emissions Controls on Road Vehicles in Europe and Implications for Public Health. *Scientific Reports 2017 7:1* 7.1 (2017), pp. 1–5. URL: https://doi.org/10.1038/s41598-017-01135-2.

[41] Erisman, J. and Schaaph, M. The need for ammonia abatement with respect to secondary PM reductions in Europe. *Environmental Pollution* 129 (2004), pp. 159–163. URL: https://doi.org/10.1016/j.envpol.2003.08.042.

[42] Fine, P. M., Sioutas, C. and Solomon, P. A. Secondary particulate matter in the United states: Insights from the particulate matter supersites program and related studies. *Journal of the Air and Waste Management Association* 58.2 (2008), pp. 234–253. DOI: 10.3155/1047-3289.58.2.234. URL: https://www.tandfonline.com/action/journalInformation?journalCode=uawm20.

[43] Yin, J., Cumberland, S. A., Harrison, R. M., Allan, J., Young, D. E., Williams, P. I. and Coe, H. Receptor modelling of fine particles in southern England using CMB including comparison with AMS-PMF factors. *Atmospheric Chemistry and Physics* 15.4 (2015), pp. 2139–2158. URL: https://doi.org/10.5194/acp-15-2139-2015.

[44] Fowler, D., Brimblecombe, P., Burrows, J., Heal, M. R., Grennfelt, P., Stevenson, D. S., Jowett, A., Nemitz, E., Coyle, M., Lui, X., Chang, Y., Fuller, G. W., Sutton, M. A., Klimont, Z., Unsworth, M. H. and Vieno, M. A chronology of global air quality. *Philosophical Transactions of the Royal Society A* 378.2183 (2020). URL: https://doi.org/10.1098/rsta.2019.0314.

[45] Bell, M. L. and Davis, D. L. Reassessment of the lethal London fog of 1952: novel indicators of acute and chronic consequences of acute exposure to air

pollution. *Environmental Health Perspectives* 109.SUPPL. 3 (2001), pp. 389–394. URL: https://doi.org/10.1289/ehp.01109s3389.

[46] *Clean Air Act 1956*. URL: https://www.legislation.gov.uk/ukpga/Eliz2/4-5/52/enacted.

[47] WHO global air quality guidelines: Particulate matter (PM2.5 and PM10), ozone, nitrogen dioxide, supfur dioxide and cabon monoxide. World Health Organisation, 2021. URL: https://www.who.int/publications/i/item/9789240034228.

[48] Department for Environment Food and Rural Affairs (Defra). *UK Air Quality Policy Context- Defra, UK*. URL: https://uk-air.defra.gov.uk/air-pollution/uk-eu-policy-context.

[49] *Air quality strategy: framework for local authority delivery*. URL: https://www.gov.uk/government/publications/the-air-quality-strategy-for-england/air-quality-strategy-framework-for-local-authority-delivery#annex-a-tables-of-pollutants-and-limits.

[50] *National air quality objectives and European Directive limit and target values for the protection of human health*. URL: https://uk-air.defra.gov.uk/assets/documents/Air_Quality_Objectives_Update.pdf.

[51] *Directive 2008/50/EC of the European Parliament and of the council of 21 May 2008 on ambient air quality and cleaner air for Europe*. 2008. URL: https://eur-lex.europa.eu/LexUriServ/LexUriServ.do?uri=OJ:L:2008:152:0001:0044:en:PDF.

[52] *Press release: Environment: Commission takes action against UK for persistent air pollution problems*. 2014. URL: https://ec.europa.eu/commission/presscorner/detail/en/IP_14_154.

[53] *Judgment of the Court (Seventh Chamber) of 4 March 2021. European Commission v United Kingdom of Great Britain and Northern Ireland. Case C-664/18.* 2021. URL: https://eur-lex.europa.eu/legal-content/EN/TXT/?uri=CELEX%3A62018CJ0664.

[54] Smith, L. Brexit and air quality- Briefing paper. *2019*. House of Commons Library. URL: www.parliament.uk/commons-library%7Cintranet.parliament.uk/commons-library%7Cpapers@parliament.uk%7C@commonslibrary.

[55] *The National Emission Ceilings Regulations 2018*. 2018. URL: https://www.legislation.gov.uk/uksi/2018/129/contents/made.

[56] *National Emissions Ceilings Regulations (NECR) - NAEI, UK*. URL: https://naei.beis.gov.uk/about/why-we-estimate?view=necr.

[57] Stone, D., Whalley, L. K. and Heard, D. E. Tropospheric OH and HO2 radicals: field measurements and model comparisons. *Chemical Society Reviews* 41.19 (2012), pp. 6348–6404. URL: https://doi.org/10.1039/C2CS35140D.

[58] Alicke, B., Geyer, A., Hofzumahaus, A., Holland, F., Konrad, S., Pätz, H. W., Schäfer, J., Stutz, J., Volz-Thomas, A. and Platt, U. OH formation by HONO photolysis during the BERLIOZ experiment. *Journal of Geophysical Research: Atmospheres* 108.D4 (2003), pp. 3–1. URL: https://doi.org/10.1029/2001JD000579.

[59] Dusanter, S., Vimal, D., Stevens, P. S., Volkamer, R., Molina, L. T., Baker, A., Meinardi, S., Blake, D., Sheehy, P., Merten, A., Zhang, R., Zheng, J., Fortner, E. C., Junkermann, W., Dubey, M., Rann, T., Eichinger, B., Lewandowski, P., Prueger, J. and Holder, H. Measurements of OH and HO2 concentrations during the MCMA-2006 field campaign - Part 2: Model comparison and radical budget. *Atmospheric Chemistry and Physics* 9.18 (2009), pp. 6655–6675. URL: https://doi.org/10.5194/acp-9-6655-2009.

[60] Zhang, W., Tong, S., Jia, C., Wang, L., Liu, B., Tang, G., Ji, D., Hu, B., Liu, Z., Li, W., Wang, Z., Liu, Y., Wang, Y. and Ge, M. Different HONO Sources for Three Layers at the Urban Area of Beijing. *Environmental Science and Technology* 54.20 (2020), pp. 12870–12880. URL: https://doi.org/10.1021/acs.est.0c02146.

[61] Song, M., Zhao, X., Liu, P., Mu, J., He, G., Zhang, C., Tong, S., Xue, C., Zhao, X., Ge, M. and Mu, Y. Atmospheric NOx oxidation as major sources for nitrous acid (HONO). *npj Climate and Atmospheric Science 2023 6:1* 6.1 (2023), pp. 1–8. URL: https://doi.org/10.1038/s41612-023-00357-8.

[62] Jacob, D. J. The oxidizing power of the atmosphere. Cambridge, MA: Harvard University, 2003.

[63] Mohnen, V., Chameides, W., Penkett, S., Demerijan, K., Platt, U., Lenschow, D., Schurath, U., Logan, J., Silva Dias, P. da and McNeal, R. Chapter 4- Tropospheric Chemistry: Processes controlling ozone and hydroxyl radical. *Tropospheric Atmospheric Ozone 1985: Assessment of Our Understanding of the Processes Controlling Its Present Distribution and Change- Volume 1*. World Meteorological Organisation, 1985.

[64] Geyer, A., Alicke, B., Konrad, S., Schmitz, T., Stutz, J. and Platt, U. Chemistry and oxidation capacity of the nitrate radical in the continental boundary layer near Berlin. *Journal of Geophysical Research: Atmospheres* 106.D8 (2001), pp. 8013–8025. URL: https://doi.org/10.1029/2000JD900681.

[65] Ball, S. Atmospheric chemistry at night. *ECG Environmental Briefs* 3 (2014). URL: https://www.envchemgroup.com/eb3-atmospheric-chemistry-at-night.html.

[66] Wang, Y., Hu, B., Tang, G., Ji, D., Zhang, H., Bai, J., Wang, X. and Wang, Y. Characteristics of ozone and its precursors in Northern China: A comparative study of three sites. *Atmospheric Research* 132-133 (2013), pp. 450–459. DOI: 10.1016/j.atmosres.2013.04.005.

[67] Ghosh, B., Papanastasiou, D. K., Talukdar, R. K., Roberts, J. M. and Burkholder, J. B. Nitryl chloride (ClNO2): UV/vis absorption spectrum between 210 and 296 K and O(3P) quantum yield at 193 and 248 nm. *Journal of Physical Chemistry A* 116.24 (2012), pp. 5796–5805. URL: https://doi.org/10.1021/jp207389y.

[68] Le Breton, M., Hallquist, Å. M., Kant Pathak, R., Simpson, D., Wang, Y., Johansson, J., Zheng, J., Yang, Y., Shang, D., Wang, H., Liu, Q., Chan, C., Wang, T., Bannan, T. J., Priestley, M., Percival, C. J., Shallcross, D. E., Lu, K., Guo, S., Hu, M. and Hallquist, M. Chlorine oxidation of VOCs at a semi-rural site in Beijing: Significant chlorine liberation from ClNO2 and subsequent gas- and particle-phase Cl-VOC production. *Atmospheric Chemistry and Physics* 18.17

(2018), pp. 13013–13030. URL: https://doi.org/10.5194/acp-18-13013-2018.

[69] Zhou, W., Zhao, J., Ouyang, B., Mehra, A., Xu, W., Wang, Y., Bannan, T. J., Worrall, S. D., Priestley, M., Bacak, A., Chen, Q., Xie, C., Wang, Q., Wang, J., Du, W., Zhang, Y., Ge, X., Ye, P., Lee, J. D., Fu, P., Wang, Z., Worsnop, D., Jones, R., Percival, C. J., Coe, H. and Sun, Y. Production of N2O5 and ClNO2 in summer in urban Beijing, China. *Atmospheric Chemistry and Physics* 18.16 (2018), pp. 11581–11597. DOI: 10.5194/ACP-18-11581-2018.

[70] Riedel, T. P., Wolfe, G. M., Danas, K. T., Gilman, J. B., Kuster, W. C., Bon, D. M., Vlasenko, A., Williams, E. J., Lerner, B. M., Veres, P. R., Roberts, J. M., Holloway, J. S., Lefer, B., Brown, S. S. and Thornton, J. A. An MCM modeling study of nitryl chloride (ClNO2) impacts on oxidation, ozone production and nitrogen oxide partitioning in polluted continental outflow. *Atmospheric Chemistry and Physics* 14.8 (2014), pp. 3789–3800. URL: https://doi.org/10.5194/acp-18-11581-2018.

[71] Keene, W. C., Stutz, J., Pszenny, A. A. P., Maben, J. R., Fischer, E. V., Smith, A. M., Von Glasow, R., Pechtl, S., Sive, B. C., Varner, R. K., Keene, W. C., Stutz, J., Pszenny, A. A. P., Maben, J. R., Fischer, E. V., Smith, A. M., Von Glasow, R., Pechtl, S., Sive, B. C. and Varner, R. K. Inorganic chlorine and bromine in coastal New England air during summer. *Journal of Geophysical Research: Atmospheres* 112.D10 (2007). URL: https://doi.org/10.1029/2006JD007689.

[72] Riedel, T. P., Bertram, T. H., Crisp, T. A., Williams, E. J., Lerner, B. M., Vlasenko, A., Li, S. M., Gilman, J., De Gouw, J., Bon, D. M., Wagner, N. L., Brown, S. S. and Thornton, J. A. Nitryl chloride and molecular chlorine in the coastal marine boundary layer. *Environmental Science and Technology* 46.19 (2012), pp. 10463–10470. URL: https://doi.org/10.1021/es204632r.

[73] Wang, X., Jacob, D. J., Eastham, S. D., Sulprizio, M. P., Zhu, L., Chen, Q., Alexander, B., Sherwen, T., Evans, M. J., Lee, B. H., Haskins, J. D., Lopez-Hilfiker, F. D., Thornton, J. A., Huey, G. L. and Liao, H. The role of chlorine in global tropospheric chemistry. *Atmospheric Chemistry and Physics* 19.6 (2019), pp. 3981–4003. URL: https://doi.org/10.5194/acp-19-3981-2019.

[74] Priestley, M., Le Breton, M., Bannan, T. J., Worrall, S. D., Bacak, A., Smedley, A. R., Reyes-Villegas, E., Mehra, A., Allan, J., Webb, A. R., Shallcross, D. E., Coe, H. and Percival, C. J. Observations of organic and inorganic chlorinated compounds and their contribution to chlorine radical concentrations in an urban environment in northern Europe during the wintertime. *Atmospheric Chemistry and Physics* 18.18 (2018), pp. 13481–13493. URL: https://doi.org/10.5194/acp-18-13481-2018.

[75] Bannan, T. J., Murray Booth, A., Bacak, A., Muller, J. B., Leather, K. E., Le Breton, M., Jones, B., Young, D., Coe, H., Allan, J., Visser, S., Slowik, J. G., Furger, M., Prévôt, A. S., Lee, J., Dunmore, R. E., Hopkins, J. R., Hamilton, J. F., Lewis, A. C., Whalley, L. K., Sharp, T., Stone, D., Heard, D. E., Fleming, Z. L., Leigh, R., Shallcross, D. E. and Percival, C. J. The first UK measurements of nitryl chloride using a chemical ionization mass spectrometer in central London in the summer of 2012, and an investigation of the role of Cl atom oxidation. *Journal of Geophysical Research: Atmospheres* 120.11 (2015), pp. 5638–5657. URL: https://doi.org/10.1002/2014JD022629.

[76] Finlayson-Pitts, B. J. and Pitts, J. N. Tropospheric Air Pollution: Ozone, Airborne Toxics, Polycyclic Aromatic Hydrocarbons, and Particles. *Science* 276.5315 (1997), pp. 1045–1052. URL: https://doi.org/10.1126/science.276.5315.1045.

[77] Atkinson, R. Atmospheric chemistry of VOCs and NOx. *Atmospheric Environment* 34.12-14 (2000), pp. 2063–2101. URL: https://doi.org/10.1016/S1352-2310(99)00460-4.

[78] Perring, A. E., Pusede, S. E. and Cohen, R. C. An observational perspective on the atmospheric impacts of alkyl and multifunctional nitrates on ozone and secondary organic aerosol. *Chemical Reviews* 113.8 (2013), pp. 5848–5870. URL: https://doi.org/10.1021/cr300520x.

[79] Kley, D. Tropospheric chemistry and transport. *Science* 276.5315 (1997), pp. 1043–1045. URL: https://doi.org/10.1126/science.276.5315.1043.

[80] Sillman, S. The relation between ozone, NOx and hydrocarbons in urban and polluted rural environments. *Atmospheric Environment* 33.12 (1999), pp. 1821–1845. URL: https://doi.org/10.1016/S1352-2310(98)00345-8.

[81] National Research Council. *Rethinking the Ozone Problem in Urban and Regional Air Pollution: 6- VOCs and NOx*. Washington, DC: The National Academies Press, 1991. URL: https://doi.org/10.17226/1889.

[82] Ziemann, P. J. and Atkinson, R. Kinetics, products, and mechanisms of secondary organic aerosol formation. *Chem. Soc. Rev* 41 (2012), pp. 6582–6605. URL: https://doi.org/10.1039/C2CS35122F.

[83] Calvert, J. G., Derwent, R. G., Orlando, J. J., Tyndall, G. S. and Wallington, T. J. *Mechanisms of Atmospheric Oxidation of the Alkanes*. Oxford University Press, 2008.

[84] Calvert, J. G., Mellouki, A., Orlando, J., Pilling, M. and Wallington, T. *The mechanisms of atmospheric oxidation of the oxygenates*. Oxford University Press, 2011.

[85] Long, B., Bao, J. L. and Truhlar, D. G. Atmospheric Chemistry of Criegee Intermediates: Unimolecular Reactions and Reactions with Water. *Journal of the American Chemical Society* 138.43 (2016), pp. 14409–14422. URL: https://doi.org/10.1021/jacs.6b08655.

[86] Calvert, J. G., Atkinson, R., Becker, K. H., Kamens, R. M., Seinfeld, J. H., Wallington, T. H. and Yarwood, G. *The Mechanisms of Atmospheric Oxidation of the Aromatic Hydrocarbons*. 2002.

[87] Kroll, J. H. and Seinfeld, J. H. Chemistry of secondary organic aerosol: Formation and evolution of low-volatility organics in the atmosphere. *Atmospheric Environment* 42.16 (2008), pp. 3593–3624. URL: https://doi.org/10.1016/j.atmosenv.2008.01.003.

[88] Kanakidou, M., Seinfeld, J. H., Pandis, S. N., Barnes, I., Dentener, F. J., Facchini, M. C., Van Dingenen, R., Ervens, B., Nenes, A., Nielsen, C. J., Swietlicki, E., Putaud, J. P., Balkanski, Y., Fuzzi, S., Horth, J., Moortgat, G. K., Winterhalter, R., Myhre, C. E. L., Tsigaridis, K., Vignati, E., Stephanou, E. G. and Wilson,

J. Organic aerosol and global climate modelling: a review. *Atmos. Chem. Phys* 5 (2005), pp. 1053–1123. URL: https://doi.org/10.5194/acp-5-1053-2005.

[89] Zhang, Q., Jimenez, J. L., Canagaratna, M. R., Allan, J. D., Coe, H., Ulbrich, I., Alfarra, M. R., Takami, A., Middlebrook, A. M., Sun, Y. L., Dzepina, K., Dunlea, E., Docherty, K., DeCarlo, P. F., Salcedo, D., Onasch, T., Jayne, J. T., Miyoshi, T., Shimono, A., Hatakeyama, S., Takegawa, N., Kondo, Y., Schneider, J., Drewnick, F., Borrmann, S., Weimer, S., Demerjian, K., Williams, P., Bower, K., Bahreini, R., Cottrell, L., Griffin, R. J., Rautiainen, J., Sun, J. Y., Zhang, Y. M. and Worsnop, D. R. Ubiquity and dominance of oxygenated species in organic aerosols in anthropogenically-influenced Northern Hemisphere midlatitudes. *Geophysical Research Letters* 34.13 (2007). URL: https://doi.org/10.1029/2007GL029979.

[90] Ding, X., Wang, X.-M., Gao, B., Fu, X.-X., He, Q.-F., Zhao, X.-Y., Yu, J.-Z., Zheng, M., Wang, ..-M., Gao, B., Fu, X.-X., He, Q.-F., Zhao, X.-Y., Yu, J.-Z. and Zheng, M. Tracer-based estimation of secondary organic carbon in the Pearl River Delta, south China. *Journal of Geophysical Research: Atmospheres* 117.D5 (2012), p. 5313. URL: https://doi.org/10.1029/2011JD016596.

[91] Gentner, D. R., Jathar, S. H., Gordon, T. D., Bahreini, R., Day, D. A., El Haddad, I., Hayes, P. L., Pieber, S. M., Platt, S. M., De Gouw, J., Goldstein, A. H., Harley, R. A., Jimenez, J. L., Prévôt, A. S. and Robinson, A. L. Review of Urban Secondary Organic Aerosol Formation from Gasoline and Diesel Motor Vehicle Emissions. *Environmental Science and Technology* 51.3 (2017), pp. 1074–1093. URL: https://doi.org/10.1021/acs.est.6b04509.

[92] *Brief history - Defra, UK*. URL: https://uk-air.defra.gov.uk/networks/brief-history.

[93] *Details of Award- Air quality supersite triplets (UK-AQST)*. URL: https://gotw.nerc.ac.uk/list_full.asp?pcode=NE%2FV017624%2F1&cookieConsent=A.

[94] *EU Standard Methods for monitoring and UK Approach - Defra, UK*. URL: https://uk-air.defra.gov.uk/networks/monitoring-methods?view=eu-standards.

[95] *Automatic Hydrocarbon Network - Defra, UK*. URL: https://uk-air.defra.gov.uk/networks/network-info?view=hc.

[96] Automatic Urban and Rural Network (AURN) LSO Manual-Essential Background Reading (2021). URL: www.gov.uk/environment-agency.

[97] Dunlea, E. J., Herndon, S. C., Nelson, D. D., Volkamer, R. M., San Martini, F., Sheehy, P. M., Shorter, J. H., Wormhoudt, J. C., Lamb, B. K., Allwine, E. J., Gaffney, J. S., Marley, N. A., Grutter, M., Marquez, C., Blanco, S., Cardenas, B., Retama, A., Ramos Villegas, C. R., Kolb, C. E., Molina, L. T. and Molina, M. J. *Evaluation of nitrogen dioxide chemiluminescence monitors in a polluted urban environment*. Tech. rep. 2007, pp. 2691–2704. URL: www.atmos-chem-phys.net/7/2691/2007/.

[98] Lee, J. D., Drysdale, W. S., Finch, D. P., Wilde, S. E. and Palmer, P. I. UK surface NO2 levels dropped by 42% during the COVID-19 lockdown: Impact on surface O3. *Atmospheric Chemistry and Physics* 20.24 (2020), pp. 15743–15759. URL: https://doi.org/10.5194/acp-20-15743-2020.

[99] James Dernie and Peter Dumitrean. UK Hydrocarbon Network Annual Report for 2012 (2013). URL: https://uk-air.defra.gov.uk/library/reports?report_id=771.

[100] Langley, G. J., Cancho-Gonzalez, S. and Herniman, J. M. Different detectors used with SFC. *Separation Science and Technology (New York)* 14 (2022), pp. 299–324. DOI: 10.1016/B978-0-323-88487-7.00002-4.

[101] Martin, R. V., Brauer, M., Donkelaar, A. van, Shaddick, G., Narain, U. and Dey, S. No one knows which city has the highest concentration of fine particulate matter. *Atmospheric Environment: X* 3 (2019), p. 100040. URL: https://doi.org/10.1016/j.aeaoa.2019.100040.

[102] Pirjola, L., Parviainen, H., Hussein, T., Valli, A., Hämeri, K., Aaalto, P., Virtanen, A., Keskinen, J., Pakkanen, T. A., Mäkelä, T. and Hillamo, R. E. "Sniffer" - A novel tool for chasing vehicles and measuring traffic pollutants. *Atmospheric Environment* 38.22 (2004), pp. 3625–3635. URL: https://doi.org/10.1016/j.atmosenv.2004.03.047.

[103] Pirjola, L., Pajunoja, A., Walden, J., Jalkanen, J. P., Rönkkö, T., Kousa, A. and Koskentalo, T. Mobile measurements of ship emissions in two harbour areas in Finland. *Atmospheric Measurement Techniques* 7.1 (2014), pp. 149–161. URL: https://doi.org/10.5194/amt-7-149-2014.

[104] Wu, F. C., Xie, P. H., Li, A., Chan, K. L., Hartl, A., Wang, Y., Si, F. Q., Zeng, Y., Qin, M., Xu, J., Liu, J. G., Liu, W. Q. and Wenig, M. Observations of SO2 and NO2 by mobile DOAS in the Guangzhou eastern area during the Asian Games 2010. *Atmospheric Measurement Techniques* 6.9 (2013), pp. 2277–2292. URL: https://doi.org/10.5194/amt-6-2277-2013.

[105] Bush, S. E., Hopkins, F. M., Randerson, J. T., Lai, C. T. and Ehleringer, J. R. Design and application of a mobile ground-based observatory for continuous measurements of atmospheric trace gas and criteria pollutant species. *Atmospheric Measurement Techniques* 8.8 (2015), pp. 3481–3492. URL: https://doi.org/10.5194/amt-8-3481-2015.

[106] Apte, J. S., Messier, K. P., Gani, S., Brauer, M., Kirchstetter, T. W., Lunden, M. M., Marshall, J. D., Portier, C. J., Vermeulen, R. C. and Hamburg, S. P. High-Resolution Air Pollution Mapping with Google Street View Cars: Exploiting Big Data. *Environmental Science and Technology* 51.12 (2017), pp. 6999–7008. URL: https://doi.org/10.1021/acs.est.7b00891.

[107] Ars, S., Vogel, F., Arrowsmith, C., Heerah, S., Knuckey, E., Lavoie, J., Lee, C., Pak, N. M., Phillips, J. L. and Wunch, D. Investigation of the spatial distribution of methane sources in the greater Toronto area using mobile gas monitoring systems. *Environmental Science and Technology* 54.24 (2020), pp. 15671–15679. URL: https://doi.org/10.1021/acs.est.0c05386.

[108] Vojtisek-Lom, M., Arul Raj, A. F., Jindra, P., Macoun, D. and Pechout, M. On-road detection of trucks with high NOx emissions from a patrol vehicle with on-board FTIR analyzer. *Science of the Total Environment* 738 (2020), p. 139753. URL: https://doi.org/10.1016/j.scitotenv.2020.139753.

[109] Saarikoski, S., Timonen, H., Carbone, S., Kuuluvainen, H., Niemi, J. V., Kousa, A., Rönkkö, T., Worsnop, D., Hillamo, R. and Pirjola, L. Investigating the chemical species in submicron particles emitted by city buses. *Aerosol Sci-*

ence and Technology 51.3 (2017), pp. 317–329. URL: https://doi.org/10.1080/02786826.2016.1261992.

[110] Popovici, I. E., Goloub, P., Podvin, T., Blarel, L., Loisil, R., Unga, F., Mortier, A., Deroo, C., Victori, S., Ducos, F., Torres, B., Delegove, C., Choël, M., Pujol-Söhne, N. and Pietras, C. Description and applications of a mobile system performing on-road aerosol remote sensing and in situ measurements. *Atmospheric Measurement Techniques* 11.8 (2018), pp. 4671–4691. URL: https://doi.org/10.5194/amt-11-4671-2018.

[111] Alas, H. D. C., Weinhold, K., Costabile, F., Di Ianni, A., Müller, T., Pfeifer, S., Di Liberto, L., Turner, J. R. and Wiedensohler, A. Methodology for high-quality mobile measurement with focus on black carbon and particle mass concentrations. *Atmospheric Measurement Techniques* 12.9 (2019), pp. 4697–4712. URL: https://doi.org/10.5194/amt-12-4697-2019.

[112] Marshall, A. G. and Hendrickson, C. L. High-Resolution Mass Spectrometers. *Annual Review of Analytical Chemistry* 1.1 (2008), pp. 579–599. URL: https://doi.org/10.1146/annurev.anchem.1.031207.112945.

[113] Haag, A. M. Mass analyzers and mass spectrometers. *Advances in Experimental Medicine and Biology* 919 (2016), pp. 157–169. URL: https://doi.org/10.1007/978-3-319-41448-5_7.

[114] Kolb, C. E., Herndon, S. C., Mcmanus, J. B., Shorter, J. H., Zahniser, M. S., Nelson, D. D., Jayne, J. T., Canagaratna, M. R. and Worsnop, D. R. Mobile laboratory with rapid response instruments for real-time measurements of urban and regional trace gas and particulate distributions and emission source characteristics. *Environmental Science and Technology* 38.21 (2004), pp. 5694–5703. URL: https://doi.org/10.1021/es030718p.

[115] Herndon, S. C., Jayne, J. T., Zahniser, M. S., Worsnop, D. R., Knighton, B., Alwine, E., Lamb, B. K., Zavala, M., Nelson, D. D., McManus, J. B., Shorter, J. H., Canagaratna, M. R., Onasch, T. B. and Kolb, C. E. Characterization of urban pollutant emission fluxes and ambient concentration distributions using a mobile laboratory with rapid response instrumentation. *Faraday Discussions* 130.0 (2005), pp. 327–339. URL: https://doi.org/10.1039/B500411J.

[116] Knighton, W. B., Herndon, S. C., Wood, E. C., Fortner, E. C., Onasch, T. B., Wormhoudt, J., Kolb, C. E., Lee, B. H., Zavala, M., Molina, L. and Jones, M. Detecting fugitive emissions of 1,3-butadiene and styrene from a petrochemical facility: An application of a mobile laboratory and a modified proton transfer reaction mass spectrometer. *Industrial and Engineering Chemistry Research* 51.39 (2012), pp. 12706–12711. URL: https://doi.org/10.1021/ie202794j.

[117] Yacovitch, T. I., Herndon, S. C., Roscioli, J. R., Floerchinger, C., Knighton, W. B. and Kolb, C. E. Air Pollutant Mapping with a Mobile Laboratory during the BEE-TEX Field Study. *Environmental Health Insights* 9.Suppl 4 (2015), p. 7. URL: https://doi.org/10.4137/EHI.S15660.

[118] Warneke, C., Geiger, F., Edwards, P. M., Dube, W., Pétron, G., Kofler, J., Zahn, A., Brown, S. S., Graus, M., Gilman, J. B., Lerner, B. M., Peischl, J., Ryerson, T. B., De Gouw, J. A. and Roberts, J. M. Volatile organic compound emissions from the oil and natural gas industry in the Uintah Basin, Utah: Oil and gas well pad emissions compared to ambient air composition. *Atmospheric Chemistry and Physics* 14.20 (2014), pp. 10977–10988. URL: https://doi.org/10.5194/acp-14-10977-2014.

[119] Coggon, M. M., McDonald, B. C., Vlasenko, A., Veres, P. R., Bernard, F., Koss, A. R., Yuan, B., Gilman, J. B., Peischl, J., Aikin, K. C., Durant, J., Warneke, C., Li, S. M. and De Gouw, J. A. Diurnal Variability and Emission Pattern of Decamethylcyclopentasiloxane (D5) from the Application of Personal Care Products in Two North American Cities. *Environmental Science and Technology* 52.10 (2018), pp. 5610–5618. URL: https://doi.org/10.1021/acs.est.8b00506.

[120] Gkatzelis, G. I., Coggon, M. M., McDonald, B. C., Peischl, J., Aikin, K. C., Gilman, J. B., Trainer, M. and Warneke, C. Identifying Volatile Chemical Product Tracer Compounds in U.S. Cities. *Environmental Science and Technology* 55.1 (2021), pp. 188–199. URL: https://doi.org/10.1021/acs.est.0c05467.

[121] Gkatzelis, G. I., Coggon, M. M., Mcdonald, B. C., Peischl, J., Gilman, J. B., Aikin, K. C., Robinson, M. A., Canonaco, F., Prevot, A. S., Trainer, M. and Warneke, C. Observations Confirm that Volatile Chemical Products Are a

Major Source of Petrochemical Emissions in U.S. Cities. *Environmental Science and Technology* 55 (2021), p. 4343. URL: https://doi.org/10.1021/acs.est.0c05471.

[122] Shah, R. U., Coggon, M. M., Gkatzelis, G. I., McDonald, B. C., Tasoglou, A., Huber, H., Gilman, J., Warneke, C., Robinson, A. L. and Presto, A. A. Urban Oxidation Flow Reactor Measurements Reveal Significant Secondary Organic Aerosol Contributions from Volatile Emissions of Emerging Importance. *Environmental Science and Technology* 54.2 (2020), pp. 714–725. URL: https://doi.org/10.1021/acs.est.9b06531.

[123] Stockwell, C., Coggon, M., Gkatzelis, G., Ortega, J., McDonald, B., Peischl, J., Aikin, K., Gilman, J., Trainer, M. and Warneke, C. Volatile organic compound emissions from solvent- and water-borne coatings: compositional differences and tracer compound identifications. *Atmospheric Chemistry and Physics* 21 (2021), pp. 6005–6022. URL: https://doi.org/10.5194/acp-21-6005-2021.

[124] Yuan, B., Coggon, M. M., Koss, A. R., Warneke, C., Eilerman, S., Peischl, J., Aikin, K. C., Ryerson, T. B. and De Gouw, J. A. Emissions of volatile organic compounds (VOCs) from concentrated animal feeding operations (CAFOs): Chemical compositions and separation of sources. *Atmospheric Chemistry and Physics* 17.8 (2017), pp. 4945–4956. URL: https://doi.org/10.5194/acp-17-4945-2017.

[125] Coggon, M. M., Veres, P. R., Yuan, B., Koss, A., Warneke, C., Gilman, J. B., Lerner, B. M., Peischl, J., Aikin, K. C., Stockwell, C. E., Hatch, L. E., Ryerson, T. B., Roberts, J. M., Yokelson, R. J. and Gouw, J. A. de. Emissions of nitrogen-containing organic compounds from the burning of herbaceous and arboraceous biomass: Fuel composition dependence and the variability of commonly used nitrile tracers. *Geophysical Research Letters* 43.18 (2016), pp. 9903–9912. URL: https://doi.org/10.1002/2016GL070562.

[126] *2021 UK Greenhouse Gas Emissions, Final Figures*. Department for Business, Energy and Industrial Strategy, 2023. URL: https://www.gov.uk/government/statistics/final-uk-greenhouse-gas-emissions-national-statistics-1990-to-2021.

[127] Dey, S. and Chandra Dhal, G. Controlling carbon monoxide emissions from automobile vehicle exhaust using copper oxide catalysts in a catalytic converter. *Materials Today Chemistry* 17 (2020), p. 100282. URL: https://doi.org/10.1016/j.mtchem.2020.100282.

[128] Streets, D. G., Gupta, S., Waldhoff, S. T., Wang, M. Q., Bond, T. C. and Yiyun, B. Black carbon emissions in China. *Atmospheric Environment* 35.25 (2001), pp. 4281–4296. URL: https://doi.org/10.1016/S1352-2310(01)00179-0.

[129] Suppajariyawat, P., Andrade, A. F. B. D., Elie, M., Baron, M. and Gonzalez-Rodriguez, J. The Use of Chemical Composition and Additives to Classify Petrol and Diesel Using Gas Chromatography-Mass Spectrometry and Chemometric Analysis: A UK Study. *Open Chemistry* 17.1 (2019), pp. 183–197. URL: https://doi.org/10.1515/chem-2019-0021.

[130] Cames, M. and Helmers, E. Critical evaluation of the European diesel car boom - Global comparison, environmental effects and various national strategies. *Environmental Sciences Europe* 25.1 (2013), pp. 1–22. URL: https://doi.org/10.1186/2190-4715-25-15.

[131] Heywood, J. B. *Internal Combustion Engine Fundamentals*. McGraw-Hill Education, 2018. Chap. 2, pp. 64–65.

[132] Hasan Shahariar, G. M., Sajjad, M., Suara, K. A., Jahirul, M. I., Chu-Van, T., Ristovski, Z., Brown, R. J. and Bodisco, T. A. On-road CO2 and NOx emissions of a diesel vehicle in urban traffic. *Transportation Research Part D: Transport and Environment* 107 (2022), p. 103326. DOI: 10.1016/J.TRD.2022.103326.

[133] Resitolu, I. A., Altinisik, K. and Keskin, A. The pollutant emissions from diesel-engine vehicles and exhaust aftertreatment systems. *Clean Technologies and Environmental Policy* 17.1 (2015), pp. 15–27. URL: https://doi.org/10.1007/s10098-014-0793-9.

[134] Van Setten, B. A., Makkee, M. and Moulijn, J. A. Science and technology of catalytic diesel particulate filters. *Catalysis Reviews* 43.4 (2007), pp. 489–564. URL: https://doi.org/10.1081/CR-120001810.

[135] Calvert, J. G., Heywood, J. B., Sawyer, R. F. and Seinfeld, J. H. Achieving acceptable air quality: Some reflections on controlling vehicle emissions. *Science* 261.5117 (1993), pp. 37–45. DOI: 10.1126/SCIENCE.261.5117.37.

[136] Small, K. A. and Kazimi, C. *On the Costs of Air Pollution from Motor Vehicles*. Tech. rep. 1. 1995, pp. 7–32.

[137] Dornoff, J. Position brief: How to make Euro 7 more effective: An analysis of the European Commission's proposal for light- and heavy-duty vehicles. *The International Council on Clean Transportation* (2023). URL: https://theicct.org/publication/euro7-analysis-recommendations-jan23/.

[138] Holman, C., Harrison, R. and Querol, X. *Review of the efficacy of low emission zones to improve urban air quality in European cities*. 2015. DOI: 10.1016/j.atmosenv.2015.04.009.

[139] *Ultra Low Emission Zone - Transport for London*. URL: https://tfl.gov.uk/modes/driving/ultra-low-emission-zone.

[140] *Inner London Ultra Low Emission Zone- One Year Report*. Tech. rep. Mayor of London, 2023.

[141] York, A. and Tsolakis, A. Cleaner Vehicle Emissions. *Encyclopedia of Materials: Science and Technology* (2010), pp. 1–7. URL: https://doi.org/10.1016/B978-008043152-9.02253-3.

[142] Schlatter, J. C. and Mitchell, P. J. Three-Way Catalyst Response to Transients. *Industrial and Engineering Chemistry Product Research and Development* 19.3 (1980), pp. 288–293. URL: https://doi.org/10.1021/i360075a002.

[143] Farren, N. J., Davison, J., Rose, R. A., Wagner, R. L. and Carslaw, D. C. Underestimated ammonia emissions from road vehicles. *Environmental Science and Technology* 54.24 (2020), pp. 15689–15697. URL: https://doi.org/10.1021/acs.est.0c05839.

[144] Farren, Naomi J, Davison, Jack, Rose, Rebecca A, Wagner, Rebecca L, Carslaw and David C. Characterisation of ammonia emissions from gasoline and gasoline hybrid passenger cars (2021). URL: https://doi.org/10.1016/j.aeaoa.2021.100117.

[145] Suarez-Bertoa, R. and Astorga, C. Isocyanic acid and ammonia in vehicle emissions. *Transportation Research Part D: Transport and Environment* 49 (2016), pp. 259–270. URL: https://doi.org/10.1016/j.trd.2016.08.039.

[146] Asman, W. A., Sutton, M. A. and Schjørring, J. K. Ammonia: emission, atmospheric transport and deposition. *New Phytologist* 139.1 (1998), pp. 27–48. URL: https://doi.org/10.1046/j.1469-8137.1998.00180.x.

[147] Henningsen, S. Air Pollution from Large Two-Stroke Diesel Engines and Technologies to Control It. *Handbook of Air Pollution From Internal Combustion Engines* (1998), pp. 477–534. URL: https://doi.org/10.1016/B978-012639855-7/50053-3.

[148] Schaefer, M., Hofmann, L., Girot, P. and Rohe, R. Investigation of NOx- and PM-reduction by a Combination of SCR-catalyst and Diesel Particulate Filter for Heavy-duty Diesel Engine. *International Journal of Fuels and Lubricants* 2.1 (2009), pp. 386–398. URL: https://doi.org/10.4271/2009-01-0912.

[149] He, J., Chen, K. and Xu, J. Urban Air Pollution and Control. *Encyclopedia of Sustainable Technologies* (2017), pp. 243–257. URL: https://doi.org/10.1016/B978-0-12-409548-9.10182-4.

[150] Majewski, W. A. DieselNet Technology Guide: Diesel Particulate Filters (2020). URL: www.DieselNet.com..

[151] Dhital, N. B., Yang, H. H., Wang, L. C., Hsu, Y. T., Zhang, H. Y., Young, L. H. and Lu, J. H. VOCs emission characteristics in motorcycle exhaust with different emission control devices. *Atmospheric Pollution Research* 10.5 (2019), pp. 1498–1506. URL: https://doi.org/10.1016/j.apr.2019.04.007.

[152] Brand, C. Beyond 'Dieselgate': Implications of unaccounted and future air pollutant emissions and energy use for cars in the United Kingdom. *Energy Policy* 97 (2016), pp. 1–12. URL: https://doi.org/10.1016/j.enpol.2016.06.036.

[153] Giechaskiel, B., Clairotte, M., Valverde-Morales, V., Bonnel, P., Kregar, Z., Franco, V. and Dilara, P. Framework for the assessment of PEMS (Portable Emissions Measurement Systems) uncertainty. *Environmental Research*

166.June (2018), pp. 251–260. URL: https://doi.org/10.1016/j.envres.2018.06.012.

[154] Dallmann, T., Bernard, Y., Tietge, U. and Muncrief, R. Remote sensing of motor vehicle emissions in Paris. *The International Council on Clean Transportation* (2019). URL: https://theicct.org/publication/remote-sensing-of-motor-vehicle-emissions-in-paris/.

[155] Bishop, G. A., Starkey, J. R., Ihlenfeldt, A., Williams, W. J. and Stedman, D. H. IR long-path photometry: A remote sensing tool for automobile emissions. *Analytical Chemistry* 61.10 (1989). URL: https://doi.org/10.1021/ac00185a746.

[156] Bishop, G. A. and Stedman, D. H. Measuring the Emissions of Passing Cars. *Accounts of Chemical Research* 29.10 (1996), pp. 489–495. URL: https://doi.org/10.1021/ar950240x.

[157] Burgard, D. A., Bishop, G. A., Stadtmuller, R. S., Dalton, T. R. and Stedman, D. H. Spectroscopy Applied to On-Road Mobile Source Emissions. *Applied Spectroscopy* 60.5 (2006), 135A–148A. URL: https://doi.org/10.1366/000370206777412185.

[158] Davison, J., Rose, R. A., Farren, N. J., Wagner, R. L., Murrells, T. P. and Carslaw, D. C. Verification of a National Emission Inventory and Influence of On-road Vehicle Manufacturer-Level Emissions. *Environmental Science and Technology* 55.8 (2021), pp. 4452–4461. URL: https://doi.org/10.1021/acs.est.0c08363.

[159] Carslaw, D. C., Beevers, S. D., Tate, J. E., Westmoreland, E. J. and Williams, M. L. Recent evidence concerning higher NOx emissions from passenger cars and light duty vehicles. *Atmospheric Environment* 45.39 (2011), pp. 7053–7063. URL: https://doi.org/10.1016/j.atmosenv.2011.09.063.

[160] Carslaw, D. C., Farren, N. J., Vaughan, A. R., Drysdale, W. S., Young, S. and Lee, J. D. The diminishing importance of nitrogen dioxide emissions from road vehicle exhaust. *Atmospheric Environment: X* 1 (2019), p. 100002. URL: https://doi.org/10.1016/j.aeaoa.2018.100002.

[161] Grange, S. K., Grange, S. K., Farren, N. J., Vaughan, A. R., Davison, J. and Carslaw, D. C. Post-Dieselgate: Evidence of NOxEmission Reductions Using On-Road Remote Sensing. *Environmental Science and Technology Letters* 7.6 (2020), pp. 382–387. URL: https://doi.org/10.1021/acs.estlett.0c00188.

[162] Davison, J., Rose, R. A., Farren, N. J., Wagner, R. L., Wilde, S. E., Wareham, J. V. and Carslaw, D. C. Gasoline and diesel passenger car emissions deterioration using on-road emission measurements and measured mileage. *Atmospheric Environment: X* 14 (2022), p. 100162. URL: https://doi.org/10.1016/j.aeaoa.2022.100162.

[163] Franco, V., Kousoulidou, M., Muntean, M., Ntziachristos, L., Hausberger, S. and Dilara, P. Road vehicle emission factors development: A review. *Atmospheric Environment* 70 (2013), pp. 84–97. URL: https://doi.org/10.1016/j.atmosenv.2013.01.006.

[164] Pöhler, D., Engel, T., Roth, U., Reber, J., Horbanski, M., Lampel, J. and Platt, U. NOx RDE measurements with Plume Chasing-Validation, detection of high emitters and manipulated SCR systems. *23rd Transport and Air Pollution Conference* (2019). URL: https://www.et.co.uk/assets/resources/files/rde-plume-chasing-paper-pohler-et-al.pdf.

[165] Pöhler, D. Heavy Duty Vehicle (HDV) NOx emission measurement with mobile remote sensing (Plume Chasing) and subsequent inspection of high emitters (2020).

[166] Jayaratne, E. R., Morawska, L., Ristovski, Z. D. and He, C. Rapid identification of high particle number emitting on-road vehicles and its application to a large fleet of diesel buses. *Environmental Science and Technology* 41.14 (2007), pp. 5022–5027. URL: https://doi.org/10.1021/es063020v.

[167] Hak, C. S., Hallquist, M., Ljungström, E., Svane, M. and Pettersson, J. B. A new approach to in-situ determination of roadside particle emission factors of individual vehicles under conventional driving conditions. *Atmospheric Environment* 43.15 (2009), pp. 2481–2488. URL: https://doi.org/10.1016/j.atmosenv.2009.01.041.

[168] Hallquist, M., Jerksjö, M., Fallgren, H., Westerlund, J. and Sjödin, Å. Particle and gaseous emissions from individual diesel and CNG buses. *Atmos. Chem. Phys* 13 (2013), pp. 5337–5350. URL: https://doi.org/10.5194/acp-13-5337-2013.

[169] Hu, S., Paulson, S. E., Fruin, S., Kozawa, K., Mara, S. and Winer, A. M. Observation of elevated air pollutant concentrations in a residential neighborhood of Los Angeles California using a mobile platform. *Atmospheric Environment* 51 (2012), pp. 311–319. URL: https://doi.org/10.1016/j.atmosenv.2011.12.055.

[170] Tan, Y., Lipsky, E. M., Saleh, R., Robinson, A. L. and Presto, A. A. Characterizing the spatial variation of air pollutants and the contributions of high emitting vehicles in Pittsburgh, PA. *Environmental Science and Technology* 48.24 (2014), pp. 14186–14194. URL: https://doi.org/10.1021/es5034074.

[171] Miller, D. J., Actkinson, B., Padilla, L., Griffin, R. J., Moore, K., Lewis, P. G. T., Gardner-Frolick, R., Craft, E., Portier, C. J., Hamburg, S. P. and Alvarez, R. A. Characterizing Elevated Urban Air Pollutant Spatial Patterns with Mobile Monitoring in Houston, Texas. *Environmental Science and Technology* 54.4 (2020), pp. 2133–2142. URL: https://doi.org/10.1021/acs.est.9b05523.

[172] Cummings, L. E., Stewart, J. D., Reist, R., Shakya, K. M. and Kremer, P. Mobile Monitoring of Air Pollution Reveals Spatial and Temporal Variation in an Urban Landscape. *Frontiers in Built Environment* 7 (2021), p. 68. URL: https://doi.org/10.3389/fbuil.2021.648620.

[173] Jordan, A., Haidacher, S., Hanel, G., Hartungen, E., Märk, L., Seehauser, H., Schottkowsky, R., Sulzer, P. and Märk, T. D. A high resolution and high sensitivity proton-transfer-reaction time-of-flight mass spectrometer (PTR-TOF-MS). *International Journal of Mass Spectrometry* 286.2-3 (2009), pp. 122–128. DOI: 10.1016/j.ijms.2009.07.005.

[174] Coggon, M. M., Gkatzelis, G. I., McDonald, B. C., Gilman, J. B., Schwantes, R. H., Abuhassan, N., Aikin, K. C., Arendd, M. F., Berkoff, T. A., Brown, S. S., Campos, T. L., Dickerson, R. R., Gronoff, G., Hurley, J. F., Isaacman-Vanwertz, G., Koss, A. R., Li, M., McKeen, S. A., Moshary, F., Peischl, J., Pospisilova, V.,

Ren, X., Wilson, A., Wu, Y., Trainer, M. and Warneke, C. Volatile chemical product emissions enhance ozone and modulate urban chemistry. *Proceedings of the National Academy of Sciences of the United States of America* 118.32 (2021), e2026653118. URL: https://doi.org/10.1073/pnas.2026653118.

[175] Edie, R., Robertson, A. M., Soltis, J., Field, R. A., Snare, D., Burkhart, M. D. and Murphy, S. M. Off-Site Flux Estimates of Volatile Organic Compounds from Oil and Gas Production Facilities Using Fast-Response Instrumentation. *Environmental Science and Technology* 54.3 (2020), pp. 1385–1394. URL: https://doi.org/10.1021/acs.est.9b05621.

[176] Watne, Å. K., Psichoudaki, M., Ljungström, E., Le Breton, M., Hallquist, M., Jerksjö, M., Fallgren, H., Jutterström, S. and Hallquist, Å. M. Fresh and Oxidized Emissions from In-Use Transit Buses Running on Diesel, Biodiesel, and CNG. *Environmental Science and Technology* 52.14 (2018), pp. 7720–7728. URL: https://doi.org/10.1021/acs.est.8b01394.

[177] Zhou, L., Liu, Q., Lee, B. P., Chan, C. K., Hallquist, Å. M., Sjödin, Å., Jerksjö, M., Salberg, H., Wängberg, I., Hallquist, M., Salvador, C. M., Gaita, S. M. and Mellqvist, J. A transition of atmospheric emissions of particles and gases from on-road heavy-duty trucks. *Atmospheric Chemistry and Physics* 20.3 (2020), pp. 1701–1722. URL: https://doi.org/10.5194/acp-20-1701-2020.

[178] Zhou, L., Salvador, C. M., Priestley, M., Hallquist, M., Liu, Q., Chan, C. K. and Hallquist, Å. M. Emissions and Secondary Formation of Air Pollutants from Modern Heavy-Duty Trucks in Real-World Traffic- Chemical Characteristics Using On-Line Mass Spectrometry. *Environmental Science and Technology* 55.21 (2021), pp. 14515–14525. URL: https://doi.org/10.1021/acs.est.1c00412.

[179] Lehnert, A. S., Behrendt, T., Ruecker, A., Pohnert, G. and Trumbore, S. E. SIFT-MS optimization for atmospheric trace gas measurements at varying humidity. *Atmospheric Measurement Techniques* 13.7 (2020), pp. 3507–3520. URL: https://doi.org/10.5194/amt-13-3507-2020.

[180] Španěl, P. and Smith, D. Quantification of trace levels of the potential cancer biomarkers formaldehyde, acetaldehyde and propanol in breath by SIFT-MS.

Journal of Breath Research 2.4 (2008), p. 046003. URL: https://doi.org/10.1088/1752-7155/2/4/046003.

[181] Castada, H. Z. and Barringer, S. A. Online, real-time, and direct use of SIFT-MS to measure garlic breath deodorization: a review. *Flavour and Fragrance Journal* 34.5 (2019), pp. 299–306. URL: https://doi.org/10.1002/ffj.3503.

[182] Langford, V. S., Padayachee, D., McEwan, M. J. and Barringer, S. A. Comprehensive odorant analysis for on-line applications using selected ion flow tube mass spectrometry (SIFT-MS). *Flavour and Fragrance Journal* 34.6 (2019), pp. 393–410. URL: https://doi.org/10.1002/ffj.3516.

[183] Yeoman, A. M., Shaw, M., Carslaw, N., Murrells, T., Passant, N. and Lewis, A. C. Simplified speciation and atmospheric volatile organic compound emission rates from non-aerosol personal care products. *Indoor Air* 30.3 (2020), pp. 459–472. URL: https://doi.org/10.1111/ina.12652.

[184] Prince, B. J., Milligan, D. B. and McEwan, M. J. Application of selected ion flow tube mass spectrometry to real-time atmospheric monitoring. *Rapid Communications in Mass Spectrometry* 24.12 (2010), pp. 1763–1769. URL: https://doi.org/10.1002/rcm.4574.

[185] Crilley, L. R., Kramer, L. J., Ouyang, B., Duan, J., Zhang, W., Tong, S., Ge, M., Tang, K., Qin, M., Xie, P., Shaw, M. D., Lewis, A. C., Mehra, A., Bannan, T. J., Worrall, S. D., Priestley, M., Bacak, A., Coe, H., Allan, J., Percival, C. J., Popoola, O. A., Jones, R. L. and Bloss, W. J. Intercomparison of nitrous acid (HONO) measurement techniques in a megacity (Beijing). *Atmospheric Measurement Techniques* 12.12 (2019), pp. 6449–6463. URL: https://doi.org/10.5194/amt-12-6449-2019.

[186] Smith, D. and Spanel, P. The novel selected-ion flow tube approach to trace gas analysis of air and breath. *Rapid Communications in Mass Spectrometry* 10.10 (1996), pp. 1183–1198. URL: https://doi.org/10.1002/(SICI)1097-0231(19960731)10:10%3C1183::AID-RCM641%3E3.0.CO;2-3.

[187] Smith, D. and Španěl, P. Selected ion flow tube mass spectrometry (SIFT-MS) for on-line trace gas analysis. *Mass Spectrometry Reviews* 24.5 (2005), pp. 661–700. DOI: 10.1002/mas.20033. URL: https://onlinelibrary.wiley.com/doi/

full/10.1002/mas.20033%20https://onlinelibrary.wiley.com/doi/abs/10.1002/mas.20033%20https://onlinelibrary.wiley.com/doi/10.1002/mas.20033.

[188] Horbanski, M., Pöhler, D., Lampel, J. and Platt, U. The ICAD (iterative cavity-enhanced DOAS) method. *Atmospheric Measurement Techniques* 12.6 (2019), pp. 3365–3381. URL: https://doi.org/10.5194/amt-12-3365-2019.

[189] Gupta, M. Cavity-Enhanced Laser Absorption Spectrometry for Industrial Applications. *Gases & Instrumentation International* June (2012), pp. 23–29. URL: http://www.lgrinc.net/documents/Cavity-Enhanced%20Laser%20Absorption%20Spectrometry%20for%20Industrial%20Applications%20May_June%202012.pdf.

[190] Tan, Z. and Long, X. Off-axis integrated cavity output spectroscopy and its application. *Optics Communications* 283.7 (2010), pp. 1406–1409. URL: https://doi.org/10.1016/j.optcom.2009.11.081.

[191] *COVID-19: Stringency Index*. URL: https://ourworldindata.org/grapher/covid-stringency-index?tab=chart&country=~GBR.

[192] Reimann, S., Wegener, R., Claude, A. and Sauvage, S. ACTRIS-2 WP3 - Deliverable 3.17. Updated Measurement Guideline for NOx and VOCs (2018), pp. 59–62. URL: https://www.actris.eu/sites/default/files/inline-files/WP3_D3.17_M42_0.pdf.

[193] Syft Technolgies. *Syft Technologies Tech Talks #10. Calibration Approaches for Real-Time Analysis*. URL: https://www.syft.com/syft-technologies-tech-talks-10-calibration-approaches-for-real-time-analysis.

[194] Giskeodegard Guro, F. and Lydersen, S. *Measurements below the detection limit*. URL: https://tidsskriftet.no/en/2022/09/medicine-and-numbers/measurements-below-detection-limit.

[195] Richards, L. C., Davey, N. G., Gill, C. G. and Krogh, E. T. Discrimination and geo-spatial mapping of atmospheric VOC sources using full scan direct mass spectral data collected from a moving vehicle. *Environmental Science: Processes and Impacts* 22.1 (2020), pp. 173–186. URL: https://doi.org/10.1039/C9EM00439D.

[196] Langford, B., Davison, B., Nemitz, E. and Hewitt, C. N. Mixing ratios and eddy covariance flux measurements of volatile organic compounds from an urban canopy (Manchester, UK). *Atmos. Chem. Phys* 9.6 (2009), pp. 1971–1987. URL: https://doi.org/10.5194/acp-9-1971-2009.

[197] Simpson, I. J., Blake, D. R., Blake, N. J., Meinardi, S., Barletta, B., Hughes, S. C., Fleming, L. T., Crawford, J. H., Diskin, G. S., Emmons, L. K., Fried, A., Guo, H., Peterson, D. A., Wisthaler, A., Woo, J.-H., Barré, J., Gaubert, B., Kim, J., Kim, M. J., Kim, Y., Knote, C., Mikoviny, T., Pusede, S. E., Schroeder, J. R., Wang, Y., Wennberg, P. O. and Zeng, L. Characterization, sources and reactivity of volatile organic compounds (VOCs) in Seoul and surrounding regions during KORUS-AQ. *Elementa: Science of the Anthropocene* 8 (2020). URL: https://doi.org/10.1525/elementa.434.

[198] Parrish, D. D., Stohl, A., Forster, C., Atlas, E. L., Blake, D. R., Goldan, P. D., Kuster, W. C. and Gouw, J. A. de. Effects of mixing on evolution of hydrocarbon ratios in the troposphere. *Journal of Geophysical Research: Atmospheres* 112.D10 (2007), pp. 10–34. URL: https://doi.org/10.1029/2006JD007583.

[199] Roberts, J. M., Fehsenfeld, F. C., Liu, S. C., Bollinger, M. J., Hahn, C., Albritton, D. L. and Sievers, R. E. Measurements of aromatic hydrocarbon ratios and NOx concentrations in the rural troposphere: Observation of air mass photochemical aging and NOx removal. *Atmospheric Environment (1967)* 18.11 (1984), pp. 2421–2432. URL: https://doi.org/10.1016/0004-6981(84)90012-X.

[200] Shona Wilde. *mobilemeasr: A package to facilitate the analysis of mobile air quality data*. 2022. URL: https://github.com/shonawilde/mobilemeasr.

[201] Padilla, L. E., Ma, G. Q., Peters, D., Dupuy-Todd, M., Forsyth, E., Stidworthy, A., Mills, J., Bell, S., Hayward, I., Coppin, G., Moore, K., Fonseca, E., Popoola, O. A., Douglas, F., Slater, G., Tuxen-Bettman, K., Carruthers, D., Martin, N. A., Jones, R. L. and Alvarez, R. A. New methods to derive street-scale spatial patterns of air pollution from mobile monitoring. *Atmospheric Environment* 270 (2022), p. 118851. URL: https://doi.org/10.1016/j.atmosenv.2021.118851.

[202] Farren, N. J., Schmidt, C., Juchem, H., Pöhler, D., Wilde, S. E., Wagner, R. L., Wilson, S., Shaw, M. D. and Carslaw, D. C. Emission ratio determination from road vehicles using a range of remote emission sensing techniques. *Science of The Total Environment* 875 (2023), p. 162621. URL: https://doi.org/10.1016/j.scitotenv.2023.162621.

[203] Ayers, G. P. Comment on regression analysis of air quality data. *Atmospheric Environment* 35.13 (2001), pp. 2423–2425. URL: https://doi.org/10.1016/S1352-2310(00)00527-6.

[204] York, D. Least-Squares Fitting of a Straight Line. *Canadian Journal of Physics* 44.5 (1966), pp. 1079–1086. URL: https://doi.org/10.1139/p66-090.

[205] York, D., Evensen, N. M., Martinez, M. L. and Delgado, J. D. B. Unified equations for the slope, intercept, and standard errors of the best straight line. *American Journal of Physics* 72.3 (2004), p. 367. URL: https://doi.org/10.1119/1.1632486.

[206] Wagner, R. L., Farren, N. J., Davison, J., Young, S., Hopkins, J. R., Lewis, A. C., Carslaw, D. C. and Shaw, M. D. Application of a mobile laboratory using a selected-ion flow-tube mass spectrometer (SIFT-MS) for characterisation of volatile organic compounds and atmospheric trace gases. *Atmospheric Measurement Techniques* 14.9 (2021), pp. 6083–6100. URL: https://doi.org/10.5194/amt-14-6083-2021.

[207] European Environment Agency. *Explaining road transport emissions: A non-technical guide*. 2016. URL: https://data.europa.eu/doi/10.2800/71804.

[208] Bernard, Y., Tietge, U., German, J. and Muncrief, R. Determination of real-world emissions from passenger vehicles using remote sensing data. *The International Council on Clean Transportation* (2018). URL: https://theicct.org/publication/determination-of-real-world-emissions-from-passenger-vehicles-using-remote-sensing-data/.

[209] May, J., Favre, C., Bosteels, D., Andersson, J., Clarke, D. and Heaney, M. On-Road Testing and PEMS Data Analysis for two Euro 6 Diesel Vehicles. *20th International Transport and Air Pollution Conference* (2014).

[210] Dimaratos, A., Toumasatos, Z., Triantafyllopoulos, G., Kontses, A. and Samaras, Z. Real-world gaseous and particle emissions of a Bi-fuel gasoline/CNG Euro 6 passenger car. *Transportation Research Part D: Transport and Environment* 82 (2020), p. 102307. URL: https://doi.org/10.1016/j.trd.2020.102307.

[211] Giechaskiel, B., Lähde, T., Clairotte, M., Suarez-Bertoa, R., Valverde, V., Melas, A. D., Selleri, T. and Bonnel, P. Emissions of Euro 6 Mono- and Bi-Fuel Gas Vehicles. *Catalysts 2022, Vol. 12, Page 651* 12.6 (2022), p. 651. URL: https://doi.org/10.3390/catal12060651.

[212] Borken-Kleefeld, J., Dallmann, T., Berlin, B. |., Brussels, |., San, |. and Washington, F. |. Remote sensing of motor vehicle exhaust emissions. *The International Council on Clean Transportation* (2018). URL: https://theicct.org/publication/remote-sensing-of-motor-vehicle-exhaust-emissions/.

[213] Bishop, G. A. and Stedman, D. H. A decade of on-road emissions measurements. *Environmental Science and Technology* 42.5 (2008), pp. 1651–1656. URL: https://doi.org/10.1021/es702413b.

[214] Grange, S. K., Farren, N. J., Vaughan, A. R., Rose, R. A. and Carslaw, D. C. Strong Temperature Dependence for Light-Duty Diesel Vehicle NOx Emissions. *Environmental Science and Technology* 53.11 (2019), pp. 6587–6596. URL: https://doi.org/10.1021/acs.est.9b01024.

[215] Wang, M., Zhu, R., Zhang, R., Li, S. and Bao, X. On-Road Emission Characteristics of Volatile Organic Compounds from Light-Duty Diesel Trucks Meeting Different Emission Standards. *Johnson Matthey Technology Review* 65.3 (2021), pp. 404–417. URL: https://doi.org/10.1595/205651320X15900542621515.

[216] Huang, H., Hu, H., Zhang, J. and Liu, X. Characteristics of volatile organic compounds from vehicle emissions through on–road test in Wuhan, China. *Environmental Research* 188 (2020), p. 109802. DOI: 10.1016/J.ENVRES.2020.109802.

[217] Hong-li, W., Sheng-ao, J., Sheng-rong, L., Qing-yao, H., Li, L., Shi-kang, T., Cheng, H., Li-ping, Q. and Chang-hong, C. Volatile organic compounds (VOCs) source profiles of on-road vehicle emissions in China. *Science of The*

Total Environment 607-608 (2017), pp. 253–261. URL: https://doi.org/10.1016/j.scitotenv.2017.07.001.

[218] Martini, G., Astorga, C., Adam, T., Bonnel, P., Farfaletti, A., Junninen, H., Manfredi, U., Montero, L., Müller, A., Krasenbrink, A., Larsen, B., Rey, M. and De Santi, G. Physical & Chemical Characterization of emissions from 2-Stroke motorcycles Comparison with 4-stroke engines. *JRC Scientific and Technical Report* (2009). DOI: 10.2788/38196. URL: https://publications.jrc.ec.europa.eu/repository/handle/JRC53779.

[219] Suarez-Bertoa, R., Zardini, A. A., Keuken, H. and Astorga, C. Impact of ethanol containing gasoline blends on emissions from a flex-fuel vehicle tested over the Worldwide Harmonized Light duty Test Cycle (WLTC). *Fuel* 143 (2015), pp. 173–182. URL: https://doi.org/10.1016/j.fuel.2014.10.076.

[220] Marques, B., Kostenidou, E., Martinez Valiente, A., Vansevenant, B., Sarica, T., Fine, L., Temime-Roussel, B., Tassel, P., Perret, P., Liu, Y., Sartelet, K., Ferronato, C. and D'anna, B. Detailed Speciation of Non-Methane Volatile Organic Compounds in Exhaust Emissions from Diesel and Gasoline Euro 5 Vehicles Using Online and Offline Measurements (2022). URL: https://doi.org/10.3390/toxics10040184.

[221] Wang, S., Yuan, B., Wu, C., Wang, C., Li, T., Huangfu, Y., Qi, J., Li, X., Zheng, J., Zhu, M., Lou, S., Wang, H., Karl, T., Graus, M. and Shao, M. Oxygenated VOCs as significant but varied contributors to VOC emissions from vehicles. *Atmos. Chem. Phys. Discuss* [preprint, (2022). URL: https://doi.org/10.5194/acp-22-9703-2022.

[222] Tabar, A. R., Hamidi, A. A. and Ghadamian, H. Experimental investigation of CNG and gasoline fuels combination on a 1.7 L bi-fuel turbocharged engine. *International Journal of Energy and Environmental Engineering* 8.1 (2017), pp. 37–45. URL: https://doi.org/10.1007/s40095-016-0223-3.

[223] Grosjean, D., Grosjean, E. and Gertler, A. W. On-Road Emissions of Carbonyls from Light-Duty and Heavy-Duty Vehicles. *Environmental Science and Technology* 35.1 (2000), pp. 45–53. URL: https://doi.org/10.1021/es001326a.

[224] Lai, C. H., Chang, C. C., Wang, C. H., Shao, M., Zhang, Y. and Wang, J. L. Emissions of liquefied petroleum gas (LPG) from motor vehicles. *Atmospheric Environment* 43.7 (2009), pp. 1456–1463. URL: https://doi.org/10.1016/j.atmosenv.2008.11.045.

[225] Salameh, T., Sauvage, S., Locoge, N., Gauduin, J., Perrussel, O. and Borbon, A. Spatial and temporal variability of BTEX in Paris megacity: Two-wheelers as a major driver. *Atmospheric Environment: X* 1 (2019), p. 100003. URL: https://doi.org/10.1016/j.aeaoa.2018.100003.

[226] Bae, C. and Kim, J. Alternative fuels for internal combustion engines. *Proceedings of the Combustion Institute* 36.3 (2017), pp. 3389–3413. URL: https://doi.org/10.1016/j.proci.2016.09.009.

[227] Díaz, S., Rajon Bernard, M., Bernard, Y., Bieker, G., Lee, K., Mock, P., Mulholland, E., Ragon, P.-L., Rodriguez, F., Tietge, U. and Wappelhorst, S. *European vehicle market statistics 2020/2021*. Tech. rep. ICCT, 2021. URL: http://eupocketbook.theicct.org.

[228] *Urban Access Regulations in Europe- Milano LEZ Area B*. URL: https://urbanaccessregulations.eu/countries-mainmenu-147/italy-mainmenu-81/milano-lez-area-b.

[229] *Urban Access Regulations in Europe- Paris*. URL: https://urbanaccessregulations.eu/countries-mainmenu-147/france/paris.

[230] Ghorbanian, J. and Ahmadi, M. Experimental thermal analysis of cylinder block and head of a bi-fuel turbocharged engine. *Meccanica* 47.8 (2012), pp. 1987–2004. URL: https://doi.org/10.1007/s11012-012-9569-7.

[231] Vasic, A.-M. and Weilenmann, M. Comparison of Real-World Emissions from Two-Wheelers and Passenger Cars. *Environmental Science & Technology* 40.1 (2006), pp. 149–154. URL: https://doi.org/10.1021/es0481023.

[232] Carslaw, D. and Rhys-Tyler, G. Remote sensing of NO2 exhaust emissions from road vehicles: A report to the City of London Corporation and London Borough of Ealing (2013). URL: https://uk-air.defra.gov.uk/assets/documents/reports/cat05/1307161149_130715_DefraRemoteSensingReport_Final.pdf.

[233] Spezzano, P., Picini, P. and Cataldi, D. Contribution of unburned lubricating oil and gasoline-derived n-alkanes to particulate emission from non-catalyst and catalyst -equipped two-stroke mopeds operated with synthetic lubricating oil. *Journal of Environmental Monitoring* 10.10 (2008), pp. 1202–1210. URL: https://doi.org/10.1039/B809519A.

[234] Platt, S. M., Haddad, I. E., Pieber, S. M., Huang, R. J., Zardini, A. A., Clairotte, M., Suarez-Bertoa, R., Barmet, P., Pfaffenberger, L., Wolf, R., Slowik, J. G., Fuller, S. J., Kalberer, M., Chirico, R., Dommen, J., Astorga, C., Zimmermann, R., Marchand, N., Hellebust, S., Temime-Roussel, B., Baltensperger, U. and Prévôt, A. S. Two-stroke scooters are a dominant source of air pollution in many cities. *Nature Communications 2014 5:1* 5.1 (2014), pp. 1–7. URL: https://doi.org/10.1038/ncomms4749.

[235] Katzenstein, A. S., Doezema, L. A., Simpson, I. J., Blake, D. R. and Rowland, F. S. Extensive regional atmospheric hydrocarbon pollution in the southwestern United States. *Proceedings of the National Academy of Sciences* 100.21 (2003), pp. 11975–11979. URL: https://doi.org/10.1073/pnas.1635258100.

[236] Mellouki, A., Wallington, T. J. and Chen, J. Atmospheric Chemistry of Oxygenated Volatile Organic Compounds: Impacts on Air Quality and Climate. *Chemical Reviews* 115.10 (2015), pp. 3984–4014. URL: https://doi.org/10.1021/cr500549n.

[237] Wang, M., Li, S., Zhu, R., Zhang, R., Zu, L., Wang, Y. and Bao, X. On-road tailpipe emission characteristics and ozone formation potentials of VOCs from gasoline, diesel and liquefied petroleum gas fueled vehicles. *Atmospheric Environment* 223 (2020), p. 117294. URL: https://doi.org/10.1016/j.atmosenv.2020.117294.

[238] *EDAR | HEAT*. URL: https://www.heatremotesensing.com/edar.

[239] Dunmore, R. E., Whalley, L. K., Sherwen, T., Evans, M. J., Heard, D. E., Hopkins, J. R., Lee, J. D., Lewis, A. C., Lidster, R. T., Rickard, A. R. and Hamilton, J. F. Atmospheric ethanol in London and the potential impacts of future fuel formulations. *Faraday Discussions* 189.0 (2016), pp. 105–120. URL: https://doi.org/10.1039/C5FD00190K.

[240] Koenker, R. *quantreg: Quantile Regression*. 2021. URL: https://cran.r-project.org/package=quantreg.

[241] Peng, C. Y., Lan, C. H., Lin, P. C. and Kuo, Y. C. Effects of cooking method, cooking oil, and food type on aldehyde emissions in cooking oil fumes. *Journal of Hazardous Materials* 324 (2017), pp. 160–167. URL: https://doi.org/10.1016/j.jhazmat.2016.10.045.

[242] Bohnenstengel, S. I., Belcher, S. E., Aiken, A., Allan, J. D., Allen, G., Bacak, A., Bannan, T. J., Barlow, J. F., Beddddows, D. C., Blossss, W. J., Booth, A. M., Chemel, C., Coceal, O., Di Marco, C. F., Dubey, M. K., Faloon, K. H., Flemiming, Z. L., Furger, M., Gietl, J. K., Graves, R. R., Green, D. C., Grimmimmimmond, C. S., Halios, C. H., Hamiamiamilton, J. F., Harrisison, R. M., Heal, M. R., Heard, D. E., Helfter, C., Herndon, S. C., Holmes, R. E., Hopkins, J. R., Jones, A. M., Kelly, F. J., Kotthaus, S., Langford, B., Lee, J. D., Leigh, R. J., Lewisis, A. C., Lidsidsidster, R. T., Lopez-Hilfiker, F. D., McQuaidaid, J. B., Mohr, C., Monks, P. S., Nemimitz, E., Ng, N. L., Percival, C. J., Prévôt, A. S., Ricketts, H. M., Sokhi, R., Stone, D., Thornton, J. A., Tremper, A. H., Valach, A. C., Vissisisser, S., Whalley, L. K., Williamsiamsiamsiams, L. R., Xu, L., Young, D. E. and Zotter, P. Meteorology, air quality, and health in London: The ClearfLo project. *Bulletin of the American Meteorological Society* 96.5 (2015), pp. 779–804. URL: https://doi.org/10.1175/BAMS-D-12-00245.1.

[243] Zhao, H., Che, H., Xia, X., Wang, Y., Wang, H., Wang, P., Ma, Y., Yang, H., Liu, Y., Wang, Y., Gui, K., Sun, T., Zheng, Y. and Zhang, X. Climatology of mixing layer height in China based on multi-year meteorological data from 2000 to 2013. *Atmospheric Environment* 213 (2019), pp. 90–103. URL: https://doi.org/10.1016/j.atmosenv.2019.05.047.

[244] Li, Q., Zhang, H., Cai, X., Song, Y. and Zhu, T. The impacts of the atmospheric boundary layer on regional haze in North China. *npj Climate and Atmospheric Science 2021 4:1* 4.1 (2021), pp. 1–10. URL: https://doi.org/10.1038/s41612-021-00165-y.

[245] Miao, Y., Liu, S., Guo, J., Huang, S., Yan, Y. and Lou, M. Unraveling the relationships between boundary layer height and PM2.5 pollution in China based

on four-year radiosonde measurements. *Environmental Pollution* 243 (2018), pp. 1186–1195. URL: https://doi.org/10.1016/j.envpol.2018.09.070.

[246] Lüdecke, D. ggeffects: Tidy Data Frames of Marginal Effects from Regression Models. *Journal of Open Source Software* 3.26 (2018), p. 772. DOI: 10.21105/JOSS.00772.

[247] Wærsted, E. G., Sundvor, I., Denby, B. R. and Mu, Q. Quantification of temperature dependence of NOx emissions from road traffic in Norway using air quality modelling and monitoring data. *Atmospheric Environment: X* 13 (2022), p. 100160. URL: https://doi.org/10.1016/j.aeaoa.2022.100160.

[248] Schnitzhofer, R., Beauchamp, J., Dunkl, J., Wisthaler, A., Weber, A. and Hansel, A. Long-term measurements of CO, NO, NO2, benzene, toluene and PM10 at a motorway location in an Austrian valley. *Atmospheric Environment* 42.5 (2008), pp. 1012–1024. URL: https://doi.org/10.1016/j.atmosenv.2007.10.004.